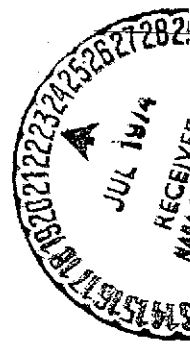

THE CRYOGENIC WIND TUNNEL FOR HIGH REYNOLDS NUMBER TESTING

by

Robert Ashworth Kilgore

Ph.D.

February 1974

CONTENTS

ABSTRACT

FACULTY OF ENGINEERING AND APPLIED SCIENCE

AERONAUTICS AND ASTRONAUTICS

Doctor of Philosophy

THE CRYOGENIC WIND TUNNEL FOR HIGH REYNOLDS NUMBER TESTING

by Robert Ashworth Kilgore

Theoretical considerations indicate that cooling the wind-tunnel test gas to cryogenic temperatures will provide a large increase in Reynolds number with no increase in dynamic pressure while reducing the tunnel drive-power requirements. Studies have been made of the variations of Reynolds number and other parameters over wide ranges of Mach number, pressure, and temperature with due regard to the avoidance of liquefaction of the test gas.

Experiments performed at the N.A.S.A. Langley Research Center in a cryogenic low-speed continuous-flow tunnel and in a cryogenic transonic continuous-flow pressure tunnel have demonstrated the predicted changes in Reynolds number, drive power, and fan speed with temperature, while operating with nitrogen as the test gas. The experiments have also demonstrated that cooling to cryogenic temperatures by spraying liquid nitrogen directly into the tunnel circuit is practical and that tunnel temperature can be controlled within very close limits.

The independent control of temperature, pressure, and Mach number available in a pressurized cryogenic tunnel will allow for the first time the independent determination of the effects of Reynolds number, aeroelasticity, and Mach number on the aerodynamic characteristics of a model.

The consequences of the thermal and caloric imperfections of the test gas under cryogenic conditions have been examined and found to be insignificant for operating pressures up to 5 atmospheres.

Whereas most types of wind tunnel could operate with advantage at cryogenic temperatures, the continuous-flow fan-driven tunnel is particularly well suited to take full advantage of operating at these temperatures. A continuous-flow fan-driven cryogenic tunnel to satisfy current requirements for test Reynolds number can be constructed and operated using existing techniques. Both capital and operating costs appear acceptable.

ACKNOWLEDGEMENTS

Many people have made contributions to the research which is the subject of this thesis. I would like to express my thanks to:

The members of the team at the Langley Research Center who, by their skill and dedication, made possible the development of the transonic cryogenic tunnel;

My co-workers in the Stability and Dynamics Branch of the High-Speed Aircraft Division who have contributed greatly to the successful operation of the transonic cryogenic tunnel. In particular, acknowledgement is made to Mr. Jerry B. Adcock for his assistance with the design of the transonic tunnel as well as with the computer work related to the real-gas studies;

My Supervisors, Dr. M. Goodyer and Dr. M. Judd. They have been a constant source of inspiration, help, and encouragement.

SUMMARY

A theoretical investigation published by Smelt in 1945 indicated that the use of air at temperatures in the cryogenic range, that is below about 172 K (-150°F), would permit large reductions of wind-tunnel size and power requirements in achieving a given Reynolds number. Lack of suitable cooling techniques and suitable structural materials precluded application of this cryogenic wind-tunnel concept at the time of Smelt's work. Because of the recent advances in cryogenic engineering and structural materials and the current interest, both in this country and in Europe, in the development of high Reynolds number transonic tunnels, a program has been initiated recently at the NASA Langley Research Center to extend the analyses of Smelt and to study the feasibility of the application of the cryogenic wind-tunnel concept to transonic testing. Studies have been made of the variations of Reynolds number and other parameters over a wide range of Mach number, pressure, and temperature with due regard to avoiding liquefaction. The consequences of the thermal and caloric imperfections of the test gas under cryogenic conditions have been examined and found to be insignificant for operating pressures up to 5 atmospheres.

The results of this work to date indicate that cryogenic subsonic, transonic, and supersonic wind tunnels can offer significant increases of test Reynolds number without increase of aerodynamic loads. As a result of the decreased velocity of sound as temperature is lowered, the drive-power requirements for cryogenic tunnels are considerably lower than for normal tunnels. The independent control of temperature, pressure, and Mach number which is available in a cryogenic pressure tunnel will allow for the first time the independent determination of the effects of Reynolds number, aeroelasticity, and Mach number on the aerodynamic characteristics of a model.

Experiments performed at the NASA Langley Research Center in a cryogenic low-speed continuous-flow tunnel and in a cryogenic transonic continuous-flow pressure tunnel have demonstrated the predicted changes in Reynolds number, drive power, and fan speed with temperature, while operating with nitrogen as the test gas. The experiments have also demonstrated that cooling to cryogenic temperatures by spraying liquid nitrogen directly into the tunnel circuit is practical and that tunnel temperature can be controlled within close limits.

Based on this theoretical and experimental work, the cryogenic concept appears very promising. Whereas most types of wind tunnel could operate with advantage at cryogenic temperatures, the continuous-flow fan-driven tunnel is particularly well suited to take full advantage of operating at cryogenic temperatures. A continuous-flow fan-driven cryogenic tunnel to satisfy current requirements for test Reynolds number can be constructed and operated using existing techniques. Both capital and operating costs appear acceptable.

1. Introduction.

Contents:

1.1 The Need for High Reynolds Number Wind Tunnels.

The discovery during the development of many high-subsonic-speed transports that the flow simulation provided by existing wind tunnels was inadequate, coupled with present interest in the development of transonic aircraft, transports and fighters, has resulted in a review of the problems of flow simulation in transonic wind tunnels. Among the more serious problems are those associated with wall interference, model support interference (including model distortion and the dynamic characteristics of the support system), geometric and elastic differences between the model and the full-scale aircraft, propulsion system simulation (including inlet and nozzle flows), stream nonuniformities (Mach number gradient, flow angularity, turbulence, and noise), and problems related to inadequate test Reynolds number. The results of most wind tunnel tests are compromised to some degree by one or more of these problems. The problem of inadequate test Reynolds number and a potential solution to the problem comprise the subject of this thesis.

The need for increased testing capability in terms of Reynolds number has been well documented, for example in references 1 and 2. A major problem is that of scale effect on boundary-layer

shock-wave interaction. Not only is aircraft performance affected by the interaction, but other characteristics such as loads and load distribution, stability, buffeting, and maneuverability are also affected.

The C-141 airplane developed for the U. S. Air Force provided one of the first indications of large discrepancies between wind-tunnel and flight data which could be directly attributed to Reynolds number effect. According to reference 3, the C-141 airplane came close to failure because of the inadequate Reynolds number capability of existing transonic wind tunnels.

The possibility of simulating high values of Reynolds number in wind tunnels has not been overlooked and many devices for causing boundary layer transition are in use in the various aeronautical laboratories. However, as noted in reference 4, fixing the location of boundary layer transition is in itself seldom sufficient to duplicate the flow associated with full-scale Reynolds number.

Recognition of such problems has resulted in a consensus, both in the United States and in Europe, that there is an urgent need for wind tunnels having greatly improved Reynolds number capability. The need is especially acute at transonic speeds where, because of the large power requirements of transonic tunnels, economic forces have dictated the use of relatively small tunnels. With ever increasing aircraft size, the existing transonic tunnels are becoming even more inadequate in test Reynolds number capability.

The inadequate Reynolds number capability of existing tunnels was the underlying theme of many of the papers presented at the Fluid Dynamics Panel Specialists' Meeting, held at Göttingen, Germany in 1971. One of the fundamental difficulties is to define the level of Reynolds number which is required for valid transonic testing. Evans and Taylor in reference 5 conclude that for transonic

flow over swept wings, testing over a range of chord Reynolds number from 15 to 25 million should give adequate information to allow extrapolation to any higher Reynolds number. Based on a study of shock position on an airfoil as a function of Reynolds number, Igoe and Baals, in reference 6 have found an apparent plateau of shock position versus Reynolds number to exist for chord Reynolds numbers of the order of 20 to 50 million. In support of the need for this general level, after reviewing the probable requirements, several of the papers presented at the Göttingen meeting (references 4, 7, and 8) proposed new wind tunnel facilities which would be capable of providing a Reynolds number at transonic speeds of at least 40×10^6 based on the mean chord of a typical swept-wing aircraft. Although there is some lack of agreement as to the exact level of Reynolds number which must be realized for valid testing, there is complete agreement that test Reynolds numbers much higher than those currently available are urgently needed. The complete agreement as to the need for higher Reynolds numbers contrasts sharply with the lack of agreement as how best to meet the need.

1.2 Methods Available for Increasing Reynolds Number.

At a given Mach number, the Reynolds number may be increased by using a heavy gas rather than air as the test gas, by increasing the size of the tunnel and model, by increasing the operating pressure of the tunnel, and by reducing the test temperature. The method chosen to increase Reynolds number will, in general, also affect dynamic pressure, mass flow rate, and the power consumption of the tunnel per unit of run time.

1.2.1 Using a heavy gas

The use of a heavy gas is a well known method of achieving high Reynolds number. According to reference 9, because it is stable

and inert chemically, inexpensive, and readily available, Freon-12 is one of the most suitable of the heavy gases for use in a wind tunnel. However, the ratio of specific heats, γ, for Freon-12 is considerably different from that for air (γ = 1.40 and 1.13 for air and Freon-12 respectively at standard conditions). Because of this difference, as reported in reference 10, data obtained in Freon-12 does not agree with data obtained in air when compressibility effects become significant in transonic and supersonic flow.

1.2.2 Increasing size

One of the most straightforward methods of achieving high Reynolds number is to increase the size of the tunnel and model. However, if stagnation pressure and temperature remain constant, both mass flow rate and drive power increase as the square of the size. Design studies, such as reported in reference 4, for large high Reynolds number wind tunnels which are capable of continuous running at normal temperatures and moderate pressure (5 atmospheres or less) show them to be very costly and also to make heavy demands on power. The increase in capital and operating costs are serious problems associated with this method of achieving near full-scale Reynolds number. An additional nontrivial problem associated with testing in very large tunnels is the cost of models as well as the cost of modifying models during a test program.

1.2.3 Increasing pressure

From the point of view of capital and operating costs it is better to increase Reynolds number by increasing pressure rather than size. However, the increase in dynamic pressure will produce increases in model, balance, and sting loads with accompanying increase in aeroelastic and support interference problems.

The maximum operating pressure which can be used and still obtain satisfactory data is not firmly established. The pressure limit depends upon the type of model being tested as well as the amount of model distortion and sting interference that can be accepted.

The tunnel designer is thus faced with a serious dilemma in trying to design a conventional tunnel capable of achieving high Reynolds numbers. In order to avoid excessive model and sting loads he must have a large tunnel which, from the economic point of view, he can neither afford to build nor operate. Historically, this dilemma has forced the tunnel designer to abandon the conventional continuous flow tunnel with all of its technical advantages and adopt some form of intermittent tunnel using energy storage techniques. The degree to which tunnel designers have abandoned the continuous flow tunnel is illustrated by the title of reference 8, "High Reynolds Number Wind Tunnels - Blowdown or Ludwieg Tube?" The wind tunnel user would like to have a continuous flow tunnel. When he is forced to use an intermittent tunnel, whatever the type, he is being forced away from an ideal situation to a compromised situation, simply by economics.

The two ideals, a continuous (or near-continuous) tunnel, together with economic feasibility, are both required. The achievement of both ideals can be realized when full advantage is taken of the increase in Reynolds number resulting from a reduction in test temperature.

1.2.4 Reducing test temperature

A theoretical investigation by Smelt in reference 11 in 1945 indicated that the use of air at temperatures in the cryogenic range, that is, below about 172K ($-150^{\circ}F$), would permit large reductions of wind-tunnel size and power requirements in comparison

with a wind tunnel operated at normal temperature and at the same pressure, Mach number, and Reynolds number. The lack of a practical means of cooling a wind tunnel to cryogenic temperatures and the unavailability of suitable structural materials precluded application of this cryogenic wind-tunnel concept at the time of Smelt's work.

The first practical application of the cryogenic concept was a low temperature test rig for centrifugal compressors as reported by Rush in reference 12. The test rig consisted of a single-stage compressor pumping air through a closed circuit containing an air-liquid nitrogen heat exchanger which cooled the air to about 125K. By operating at very low temperatures, dynamic similarity was achieved with a substantial reduction in both rotational speed and the power required to drive the compressor. In this application of the cryogenic concept, the main interest was in the reduction of rotational speed and the attendant reduction in impeller loading which allowed development tests to be conducted with impellers of easily machined materials.

In the autumn of 1971, while studying ways of increasing test Reynolds number of tunnels of modest size using magnetic-suspension and balance systems, Goodyer (reference 13) suggested the use of cryogenic test temperatures. Theoretically, such an approach is ideally suited for this application since for a given size tunnel operating at constant stagnation pressure there is realized a large increase in Reynolds number with no increase in dynamic pressure or model loads. Further study quickly indicated that the advances which have been made in recent years in the field of cryogenic engineering and structural materials have been such that a cryogenic wind tunnel appears practical and should be given serious consideration.

1.3 The Research and Development Program Related to the Cryogenic Concept.

Following a theoretical investigation started in October 1971 and aimed at extending the analysis of Smelt, an experimental program was initiated with the objective of verifying some of the theoretical predictions and to expose and solve the practical problems of using a cryogenic wind tunnel. The experimental program consisted of building and operating two fan-driven cryogenic wind tunnels. The first was a low-speed atmospheric tunnel. The second was a pressurized transonic tunnel.

This thesis contains the major results of the theoretical and experimental studies of the cryogenic concept. Based on the results of these studies, a section is included giving the anticipated design features and operational characteristics of cryogenic tunnels capable of achieving full-scale Reynolds number.

2. Methods of Increasing Reynolds Number.

There are several methods available for increasing the Reynolds number of model tests in a wind tunnel. In this chapter the methods which have been exploited in the past are reviewed and their principal characteristics outlined briefly in order to allow comparisons to be made between these methods and the use of a low temperature test gas as a means of increasing Reynolds number.

Contents:

2.1 Introduction.

In a comparison of methods for increasing test Reynolds number, in all cases except perhaps in tests at low subsonic speeds it is proper to adopt a value of test Mach number which is representative of the range required from the tunnel. Therefore for transonic testing any proposed method of increasing Reynolds number has to exclude contributions from a change of Mach number. At a fixed but representative Mach number, the Reynolds number of model tests in a wind tunnel may be increased, relative to some datum value in air, either by using a heavy test gas or mixtures of gases other than air, by increasing the size of the tunnel and model, by increasing the operating pressure of the tunnel, or by reducing the test temperature. The method chosen to increase Reynolds number will, in general, also affect dynamic pressure, mass flow rate, and drive power. In this

chapter, expressions are presented for Reynolds number, dynamic pressure, mass flow rate, and drive power which allow comparisons to be made between the various methods of increasing Reynolds number. The comparisons are then made between the various methods but with the assumption of a constant temperature of the test gas. Additional comparisons are made in Chapter 3 where the use of low test temperature is introduced as a method for increasing test Reynolds number.

2.2 Basic Relations.

2.2.1 Reynolds number

Reynolds number, R, is defined as

$$R \equiv \frac{\rho V \ell}{\mu} \qquad \text{---- 2.1}$$

where ρ = density, V = velocity, μ = viscosity } at free-stream conditions

ℓ = measure of model or test section linear dimension

The equation of state for a perfect gas is

$$\rho = \frac{m\,P}{\mathcal{R}\,T}$$

where m = molecular weight of the gas

P = static pressure

$\mathcal{R}$ = universal gas constant

T = static temperature

The free-stream Mach number, M, is given by

$$M = \frac{V}{a}$$

where a is the speed of sound.

For a perfect gas

$$V = Ma = M\sqrt{\gamma \frac{R}{m} T}$$

where γ is the ratio of specific heats.

Upon substitution of V and ρ from the above expressions into equation 2.1, one can write

$$R = \frac{PM\ell}{\mu}\sqrt{\frac{m\gamma}{RT}} \qquad \text{---- 2.2}$$

It is convenient to compare the various techniques in terms of stagnation rather than static values, and therefore equation 2.2 is now modified to allow stagnation values to appear by first invoking the usual static-to-stagnation temperature and pressure expressions for isentropic flow of a perfect gas

$$\frac{T}{T_t} = \frac{2}{2 + (\gamma - 1)M^2}$$

and

$$\frac{P}{P_t} = \left(\frac{2}{2 + (\gamma - 1)M^2}\right)^{\frac{\gamma}{\gamma-1}}$$

where the subscript t denotes stagnation conditions.

Also, for any given gas μ is a function of temperature alone, to the first order. If μ varied as $T^{1.0}$, the value of μ corresponding to static temperature conditions would be proportional to the stagnation value, μ_t, for a given Mach number. Since μ does vary nearly as $T^{1.0}$, little error is introduced in the following

analysis by making the simplifying assumption that $\mu \propto \mu_t$ for a given Mach number.

Hence, following the assumption of constant Mach number for the purposes of comparison, equation 2.2 may be rewritten in the form

$$R \propto \frac{P_t \ell}{\mu_t} \sqrt{\frac{m\gamma}{T_t}} \qquad \text{---- 2.3}$$

2.2.2 Dynamic pressure

Dynamic pressure is defined as

$$q \equiv \frac{1}{2} \rho V^2$$

Upon substitution of ρ and V from the equations given above, for constant Mach number this becomes

$$q \propto \gamma P_t \qquad \text{---- 2.4}$$

2.2.3 Mass flow

The mass flow rate through the test section is given by

$$\dot{m} = \rho V A_e$$

where A_e is the effective flow area of the test section. Following substitution for V and ρ, the adoption of constant Mach number, and the assumption that the ratio of effective area, A_e, to the geometrical flow area, A, remains sensibly constant, this becomes

$$\dot{m} \propto P_t A \sqrt{\frac{m\gamma}{T_t}}$$

2.2.4 Drive power

The ratio of the power input to the fan to the rate of flow of kinetic energy in the test section free stream is usually defined as the power factor η.

Thus

$$\text{Power} = \eta q V A_e$$

For a given tunnel geometry η is a function of Reynolds number and Mach number. With constant Mach number and ratio A_e/A, and neglecting as insignificant the variation of η with Reynolds number, one can write

$$\text{Power} \propto \gamma^{3/2} A P_t \sqrt{\frac{T_t}{m}} \qquad \text{—— 2.5}$$

The expressions derived for Reynolds number, dynamic pressure, mass flow rate, and power are tabulated below showing the terms through which they are influenced by changes in the test gas, tunnel size, stagnation pressure, and stagnation temperature. Constant Mach number is assumed. For the case where stagnation temperature is the independent variable, the simplifying assumption is made that, for any given gas,

$$\mu \propto \mu_t \propto T_t^{0.9}$$

For the case where tunnel size is the variable, it is assumed that

$$A \propto \ell^2$$

TABLE 2.1.

Influence of test gas, tunnel size, and stagnation pressure and temperature on Reynolds number, dynamic pressure, mass flow rate, and drive power with constant test Mach number.

Property / Variable	$R \propto \frac{P_t \ell}{\mu_t}\sqrt{\frac{m\gamma}{T_t}}$	$q \propto \gamma P_t$	$\dot{m} \propto P_t A\sqrt{\frac{m\gamma}{T_t}}$	Power $\propto \gamma^{3/2} A P_t \sqrt{\frac{T_t}{m}}$
Test Gas	$\frac{\sqrt{m\gamma}}{\mu_t}$	γ	$\sqrt{m\gamma}$	$\frac{\gamma^{3/2}}{\sqrt{m}}$
Tunnel Size, ℓ	ℓ		ℓ^2	ℓ^2
Stagnation Pressure, P_t	P_t	P_t	P_t	P_t
Stagnation Temperature, T_t	$\frac{1}{T_t^{1.4}}$		$\frac{1}{\sqrt{T_t}}$	$\sqrt{T_t}$

2.3 Using a Heavy Gas.

The use of a heavy gas is a well-known method of achieving high Reynolds number. After toxic gases and gases which have high condensation temperatures have been eliminated, one of the most suitable of those remaining is Freon-12 ($C\ Cl_2\ F_2$) which has been used with good results in subsonic tests. The relations in Table 2.1 may be used to assess the changes in R, q, $\dot{m}$, and drive power when Freon-12 rather than air is used as the test gas. The relevant properties of Freon-12 compared with those of air are as follows:

molecular weight	$m_F \approx 4.17\ m_{AIR}$
ratio of specific heats	$\gamma_F \approx 0.81\ \gamma_{AIR}$
viscosity	$\mu_F \approx 0.69\ \mu_{AIR}$

Assuming tunnel size, stagnation pressure, and stagnation temperature are held constant, the above values with the expressions of Table 2.1 give the following:

$$R_F \approx 2.66 R_{AIR}$$

$$q_F \approx 0.81 q_{AIR}$$

$$\dot{m}_F \approx 1.84 \dot{m}_{AIR}$$

$$\text{Power}_F \approx 0.36\ \text{Power}_{AIR}$$

Thus, the use of Freon-12 as a test gas rather than air can result in a significant increase in test Reynolds number while reducing both dynamic pressure and drive power. However, the ratio of specific heats, γ, for Freon-12 is considerably different from that for air (γ = 1.40 and 1.13 for air and Freon-12 respectively at standard conditions). Apparently the consequences of this are small in subsonic flow, and where effects do exist there are techniques for correcting wind-tunnel data. However, as reported in reference 10,

data obtained in Freon-12 does not agree with data obtained in air when compressibility effects become significant.

An important example of the differences between the behavior of Freon-12 and air is the pressure change in a shock wave. The relation between the static pressure upstream and downstream of a shock wave normal to the stream is given by

$$\frac{P_2}{P_1} = \frac{2\gamma}{\gamma + 1} M_1^2 - \frac{\gamma - 1}{\gamma + 1}$$

The ratio of the pressure rise across the shock, $\Delta P = P_2 - P_1$, to upstream static pressure is

$$\frac{\Delta P}{P_1} = \frac{P_2 - P_1}{P_1} = \frac{P_2}{P_1} - 1$$

or

$$\frac{\Delta P}{P_1} = \frac{2\gamma}{\gamma + 1} \left(M_1^2 - 1 \right)$$

For the same values of upstream Mach number and static pressure, the ratio $\frac{\Delta P}{P_1}$ is 10 percent higher in air than in Freon-12 because of the differences in γ. In flow fields in which the stability of the position of the shock is sensitive to the interaction between the shock wave and boundary layer, significant differences could exist in the shock position, and hence, in the aerodynamic data between tests made in air and Freon-12.

Mixtures of gases can be chosen which offer advantages over air, while maintaining γ for the mixture close to that for air. One such mixture is Freon-12 with argon, but it has been shown in reference 14 that the advantages in wind-tunnel design that would

result from the use of this mixture would be relatively small.

2.4 Increasing Size.

One of the most straightforward methods of increasing test Reynolds number is to increase the size of the model. However, if ℓ is taken to be a measure of model linear dimension, the test section area, A, must increase as ℓ^2 if tunnel wall interference effects are to be kept constant. Assuming a given test gas and holding stagnation pressure and stagnation temperature constant, the expressions of Table 2.1 show that Reynolds number increases linearly with increasing size, dynamic pressure is independent of size, and both mass flow rate and drive power increase as the square of the size.

The increases in capital and operating costs are serious problems associated with this method of increasing Reynolds number. These problems can be illustrated by citing as an example a semi-continuous transonic tunnel proposed in reference 4. The tunnel would have a test section 6.1 m (20 feet) square, operate at a stagnation pressure of 5 atmospheres, and provide a Reynolds number at Mach 1 of 40×10^6 based on 0.61 m (2 feet). The estimated capital cost of this hydraulic drive pumped-storage tunnel, capable of running for 15 minutes every 4 hours, was in excess of $100,000,000. The total hydraulic power was estimated as 447MW (600,000 horsepower). The estimated annual electrical charges ranged from $935,000 to $1,500,000. According to reference 4, should such a tunnel be powered by large electric drive motors connected directly to the electrical network, the annual electrical charges for making twenty 15 minute runs per week would vary from $3,640,000 for "off-peak" operation to $10,230,000 for "on-peak" operation.

In addition to the high operating and capital investment costs for large tunnels, the cost of models as well as the cost of modifying models during a test program increases with model size.

2.5 Increasing Pressure.

From the relations shown in Table 2.1 it can be seen that Reynolds number, dynamic pressure, mass-flow rate, and power all increase linearly with increasing pressure. From the point of view of capital and operating costs it is therefore better to increase Reynolds number by increasing pressure rather than by increasing size. However, the accompanying increase in dynamic pressure will produce, in relation to a low pressure tunnel, increases in balance and model loads and stresses, reductions in test lift coefficient capability, increases in support sting interference and aft fuselage distortion, and a reduced stress margin for use in aeroelastic matching. At transonic speeds, as noted in reference 3, stagnation pressures in excess of about 5 atmospheres are not practical for developmental type testing of large aspect ratio models due to excessive wing deformation. If in the order of 5 atmospheres is a practical upper limit on stagnation pressure, then a test section about 6.1 m (20 feet) square will be required to provide a Reynolds number at Mach 1 of 40×10^6. These are the same characteristics as those of the semi-continuous tunnel proposed in reference 4, a tunnel which is clearly too costly to build or operate.

2.6 Discussion.

At normal operating temperatures in the continuous flow tunnel there is no practical way to increase test Reynolds number to the 40 or 50×10^6 range (based on mean aerodynamic chord) which is generally considered to be the minimum required for the broad spectrum of current and near-future transonic testing.

The technical problems associated with the use of a heavy gas at transonic speeds are not likely to be overcome. The financial problems associated with increasing tunnel size are obvious. The maximum operating pressure which can be used while obtaining satisfactory

data is not firmly established. The pressure limit depends upon the type of model being tested as well as the amount of compromise one is willing to accept in areas such as sting interference and model distortion.

This dilemma has forced the tunnel designer to abandon the continuous flow moderate pressure transonic tunnel with all of its technical advantages and adopt some form of intermittent tunnel using energy storage techniques. Intermittent tunnels such as those considered in reference 8 introduce serious technical problems associated with very short run times and/or high operating pressures.

A possible solution to the dilemma does, however, exist. In the next chapter the use of low test temperatures in tunnels of modest size and operating at modest pressure is studied as an alternative approach to the methods of increasing Reynolds number examined in this chapter.

2.7 List of Symbols Used in Chapter 2.

Symbol	Meaning
a	speed of sound
A	test-section area, $A \propto \ell^2$
ℓ	measure of model or test section linear dimension
m	molecular weight
$\dot{m}$	mass flow rate
M	free-stream Mach number
P	pressure
q	dynamic pressure
R	Reynolds number
$\mathcal{R}$	universal gas constant
T	temperature

V	velocity
ρ	density
μ	viscosity
γ	ratio of specific heats
η	power factor

Subscripts

e	effective
t	stagnation conditions
AIR	air
F	Freon-12

3. Increasing Reynolds Number by Reducing Test Temperature.

Increasing Reynolds number by the use of a low temperature test gas is described in this chapter. Comparisons are made between this method of increasing Reynolds number and the methods which have been used in the past as described in Chapter 2.

Contents:

3.1 Introduction.

The use of low temperatures in wind tunnels was first proposed by Smelt in reference 11 as a means of reducing tunnel drive power requirements at constant values of test Mach number, Reynolds number, and pressure. Studies have been made which show that a significant increase in Reynolds number may be realized at Mach numbers up to about 3 by operating at cryogenic temperatures. In this chapter the changes in Reynolds number, dynamic pressure, test-section mass flow rate, and tunnel drive power due to changes in temperature are described. Consideration is then given to the limits on the minimum operating temperatures which may be set by condensation and by real gas effects. Finally, in relation to the alternative methods which are available, some of the advantages of increasing Reynolds number by the use of low test temperatures are described.

3.2 Effects of Reducing Temperature.

The relations presented in Table 2.1 are used in the following sections to illustrate the effect of reducing test temperature in a given gas with constant values of tunnel size, stagnation pressure, and Mach number.

For comparison purposes, it is assumed that the test gas is air. A stagnation temperature for normal tunnels of 322K (120°F) is here assumed as a datum. Figure 3.1 shows the variation of several flow parameters in the tunnel test section as the stagnation temperature is reduced from this datum. With decreasing temperature, viscosity, μ, is reduced, density, ρ, is increased, and because of a reduction of the speed of sound, a, with decreasing temperature and the assumption of constant test section Mach number, the velocity, V, is reduced.

3.2.1 Reynolds number

The effect of the changes in the flow parameters is a variation in Reynolds number approximately in accordance with the relation

$$R \propto \frac{1}{T_t^{1.4}}$$

As can be seen in Figure 3.1, the relative variation of viscosity with stagnation temperature, T_t, is a weak function of the assumed Mach number, and therefore the relative change of Reynolds number with temperature is also a weak function of Mach number. Curves are shown for several free-stream Mach numbers.

3.2.2 Dynamic pressure

The aerodynamic loads which act on a particular model with a fixed orientation relative to the flow vary strongly with dynamic pressure at a fixed test Mach number, with, under normal circumstances, a small influence of Reynolds number. With these constraints the stresses and deflections within a model, as noted in reference 15, vary

in direct proportion to q. This is conditional on the effects of changes of Reynolds number, if any, being small. From Table 2.1 it is seen that as the test temperature is reduced there is no change of dynamic pressure. Therefore, by reducing temperature, an increase of Reynolds number is achieved without increase of aerodynamic loads except as introduced by the change of Reynolds number. Note that changes of aerodynamic loading from this source are common by definition to all methods of increasing Reynolds number and are normally second-order effects. Problems that might arise from aeroelastic distortion of the model or its supports due to increase of dynamic pressure therefore do not arise, in contrast with the case of increasing Reynolds number by increasing stagnation pressure. This constant dynamic pressure feature of the cryogenic tunnel is extremely important, particularly with regard to isolating Reynolds number effects from aeroelastic effects as will be discussed more fully in a later chapter. An increase of Reynolds number is therefore achieved with lower aerodynamic loads compared with the same increase by pressure. Some advantages associated with the reduced loads include reduced support interference, and a reduction in the severity of afterbody modification, both of which arise from the need for a smaller size of sting.

Alternatively, or additionally, the reduced loads could allow an increase in the load-limited maximum lift coefficient, or allow the model to be designed for improved aeroelastic matching.

3.2.3 Test-section mass flow rate

For constant tunnel size, stagnation pressure, and Mach number, test-section mass flow rate increases with decreasing temperature in accordance with the relation

$$\dot{m} \propto \frac{1}{\sqrt{T_t}}$$

Thus, for example, when operating at temperatures near 100K, the mass flow rate is increased by about a factor of 1.8 over the mass flow rate at ambient conditions. For certain modes of cryogenic operation of blowdown or injector-driven tunnels considered in Chapter 5, the increase in mass flow rate will reduce run time when operating from a fixed size of air storage tank. In general, however, the increase of mass flow rate is of no consequence.

3.2.4 Drive power

For constant tunnel size and pressure, the relation between drive power and temperature is

$$\text{Drive power} \propto \sqrt{T_t}$$

The variations of drive power, as Reynolds number is increased from the datum, is shown on Figure 3.2 for the three methods of increasing Reynolds number in air.

If Reynolds number is increased just by enlarging the wind tunnel and model, power will increase as the square of the size, curve A on Figure 3.2. If Reynolds number is increased just by increasing the stagnation pressure, power will increase in direct proportion to the increase in pressure, curve B. However, as Reynolds number is increased by means of a reduction of test temperature in a particular size of wind tunnel, the drive power is reduced, curve C.

The power economy of the cryogenic wind tunnel has a significant impact on operating costs and on total energy consumption, as will be discussed later.

3.3 The Operational Limits Set by the Saturation Boundary.

The minimum stagnation temperature which can conceivably be used in a cryogenic wind tunnel depends on several factors. It has been assumed that liquefaction must be avoided under the most adverse conditions to be met on the model. The test gas is most likely to begin to condense in localized low-pressure regions adjacent to the model. The local pressures in turn depend on the shape and orientation of the model, and on the test Mach number and stagnation pressure. In order to compute likely conditions in these regions, variations of maximum local Mach number $M_{L,max}$, with free-stream Mach number M_∞, have been assumed and are shown on Figure 3.3. The curves shown on this figure were constructed from inspections of pressure distributions over typical wing sections.* In order to compute the minimum temperatures that may be utilized the assumptions have been made that the test gas expands isentropically as an ideal gas from the tunnel settling chamber through to the localized high Mach number regions and that the saturation boundary for the test gas should not be crossed. It is believed that some of these assumptions are biased toward the conservative. For example, based on 2-D airfoil tests results described in Chapter 7, it appears that several degrees of supersaturation can occur without adverse effects on the test results. In addition, the maximum local Mach numbers shown on Figure 3.3 may be higher than those realized in many tests.

In Chapter 4 are presented the stagnation temperatures which cause the test gas to reach the saturation boundary at these local conditions, the temperatures therefore represent minima. The minimum temperatures for air and nitrogen have been calculated for a range of Mach numbers and pressures up to 7 atmospheres. The data from Chapter 4 is used in the following sections to demonstrate the operational

*Airfoils having peaky pressure distributions were not included.

limits set by the saturation boundaries for testing in air or nitrogen.

3.3.1 Testing in air

For sonic tests in a cryogenic wind tunnel using air as the test gas, the permissible minimum stagnation temperature, T_t, and the Reynolds number relative to datum (at T_t = 322K = 120°F) are given in the table presented below for stagnation pressures, P_t, up to 5 atmospheres. The stagnation temperatures have been chosen such that the saturation boundary is reached at $M_{L,max} = 1.4$.

TESTING IN AIR, $M_\infty = 1$, $M_{L,max} = 1.4$

P_t, Atm	1	2	3	4	5
T_t, K	98.7	107.3	112.3	116.0	119.0
Reynolds number relative to datum (T_t = 322K)	5.33	4.71	4.40	4.20	4.04

As can be seen, cryogenic operation is effective in increasing Reynolds number even at elevated pressures. Thus, where tunnel size is restricted or where economies in drive power are required, Reynolds number can be increased by combining the advantages of cryogenic operation with moderate increases in pressure.

3.3.2 Testing in nitrogen

The following table for sonic tests in nitrogen shows the permissible minimum operating temperatures and relative Reynolds number in nitrogen and is based on the same assumptions and is directly comparable with the table for air presented above.

TESTING IN NITROGEN, $M_\infty = 1$, $M_{L,max} = 1.4$

P_t, Atm	1	2	3	4	5
T_t, K	95.7	102.5	107.0	110.4	113.3
Reynolds number relative to datum (T_t = 322K)	5.59	5.05	4.75	4.53	4.37

As can be seen, lower test temperatures can be used for nitrogen than for air because the saturation temperature of nitrogen is lower than the dewpoint for air. In addition to the increased Reynolds number available in nitrogen, there are other advantages to using nitrogen rather than air as the test gas.

3.4 Nitrogen as a Test Gas.

Recent advances in cryogenic technology and the availability of liquid nitrogen in large quantities at low cost have eliminated many of the problems of cooling a wind tunnel to cryogenic temperatures which formerly existed. Evaporating liquid nitrogen offers an attractive alternative to mechanical refrigeration. Once the use of nitrogen as the test gas is accepted, the particularly simple cooling technique is available of injecting and evaporating liquid nitrogen inside the tunnel circuit. As might be expected, the properties of air and nitrogen are similar since air is about 78-percent nitrogen by volume.

The advantage of the nitrogen cryogenic tunnel over tunnels using air at conventional temperatures is shown on Figure 3.4.

As can be seen, useful increases of Reynolds number are obtainable over a wide range of Mach number and pressure. Corresponding operating temperatures are shown on Figure 3.5, the temperatures

assumed for the datum tunnels but set by the saturation boundary for the cryogenic tunnels.

Based on the 2-D airfoil test results described in Chapter 7, it appears that under some circumstances several degrees of local supersaturation can occur without adverse effects on the test results. If supersaturation is permissible, the operating temperatures shown on Figure 3.5 can be lowered with corresponding increase in the test Reynolds number.

3.5 Other Factors Limiting Test Conditions.

The limits on the ranges of pressure and temperature which can be used in a cryogenic wind tunnel, maxima and minima, could be dictated by many factors. These may include loading considerations in the tunnel structure, model and sting loads and deflections, available power, economic consideration, condensation of the test gas, real gas effects, and perhaps others.

The limitations imposed by condensation of the test gas were considered briefly in the preceeding sections and are considered in more detail in the next chapter. The possible limitations imposed by other real gas effects are also considered in the next chapter. Other possible limitations, less fundamental than these two, will first be mentioned.

There will be a need in any future large cryogenic high Reynolds number tunnel not only to test at high values of Reynolds number but to test over a range of Reynolds number which might extend upwards from the maximum achievable in present-day tunnels. Furthermore, because high Reynolds number testing will be expensive, it is anticipated that much of the development work will be done at low Reynolds number in conventional ambient temperature tunnels with only final development and verification testing being done at high

Reynolds numbers. Therefore the test-section of the cryogenic tunnel will need to be about the same size as the more widely used conventional tunnels. Following recognition of this constraint, design studies introduced later suggest that in order to span the range of Reynolds number required, both high and low temperature operation of the tunnel is needed.

A possible limitation on operating at high temperatures could arise from restrictions on drive power and on fan rotational speed. As Reynolds number is reduced by raising the test temperature (pressure and Mach number being held constant) the required drive power and fan speed increase. In any tunnel design both will be limited and the limitations could possibly dictate a bound on the maximum useable temperature. The problem of matching the motor power and fan speed characteristics to the tunnel requirements over a wide range of temperature can be mitigated by using a variable pitch fan and/or variable gearing in the drive system.

A non-fundamental limitation on maximum pressure arises from considerations of the increasing effect of support interference and model distortion with increasing pressure. As noted in Chapter 2, section 2.5, stagnation pressures in excess of about 5 atmospheres are not practical for developmental type testing of large aspect ratio models due to excessive wing deformation.

3.6 Discussion.

The problems associated with increasing Reynolds number by using heavy gases, by increasing size, or by increasing pressure are avoided when Reynolds number is increased by using low temperatures. The use of low test temperatures in tunnels of modest size (with test sections similar to those in many existing tunnels, around 3 m square) and operating at modest pressure (stagnation pressure less than 5 atm.) offers the only viable method of achieving Reynolds

numbers in the 40 or 50 $\times 10^6$ range in continuous flow tunnels. Many of the limitations on test conditions have been briefly mentioned in this chapter. In order to better define the possible limitations imposed either by the saturation boundary of the test gas or by other real gas effects, these two areas are studied in more detail in the next chapter before proceeding to a more detailed examination of cryogenic tunnels in subsequent chapters.

3.7 List of Symbols Used in Chapter 3.

Symbol	Meaning
a	speed of sound
$\dot{m}$	mass flow rate
M_∞	free-stream Mach number
$M_{L,max}$	maximum local Mach number
P	pressure
q	dynamic pressure
R	Reynolds number
T	temperature
V	velocity
ρ	density
μ	viscosity

Subscript

t	stagnation conditions

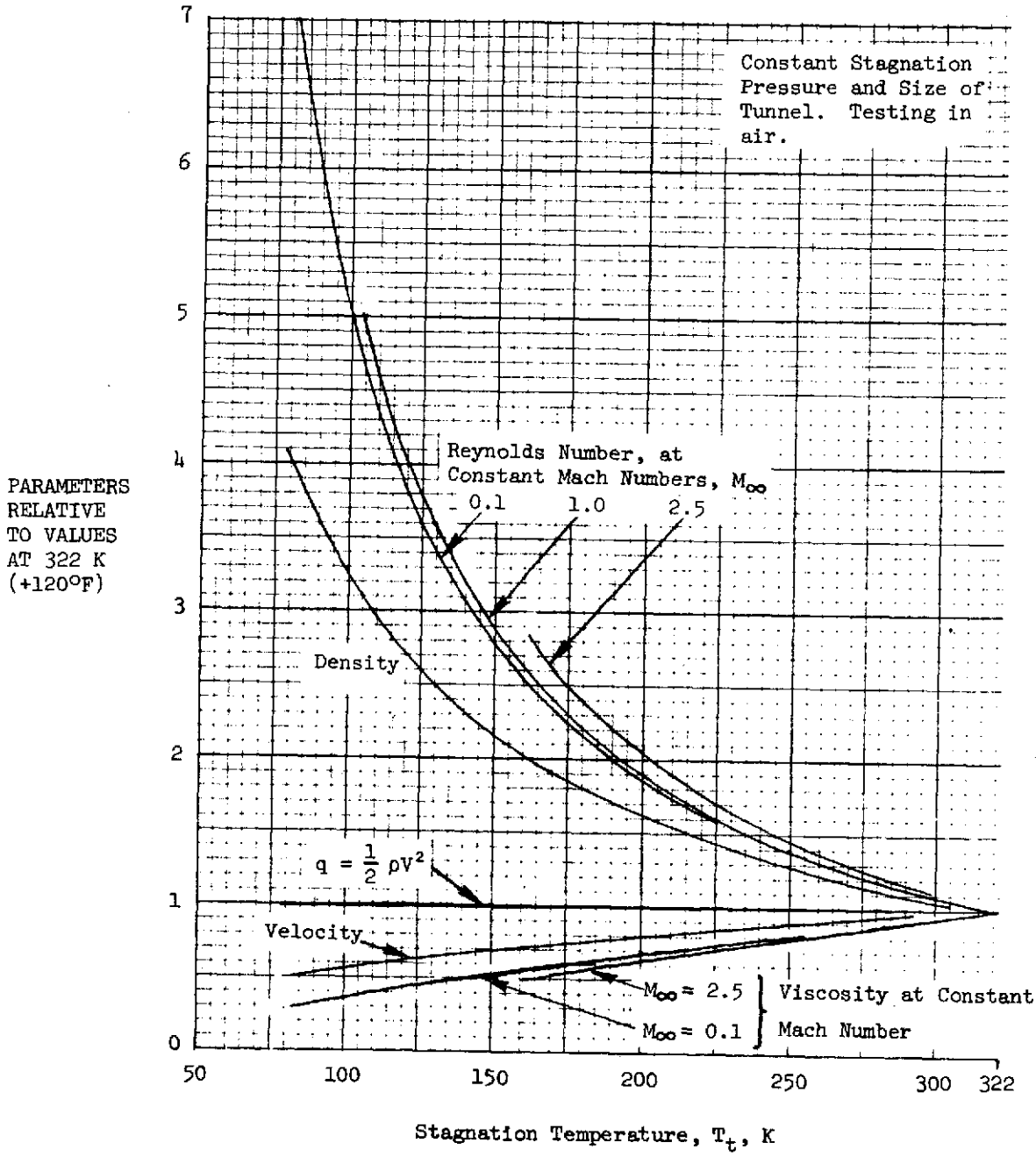

Figure 3.1 Variation of test section flow parameters with temperature.

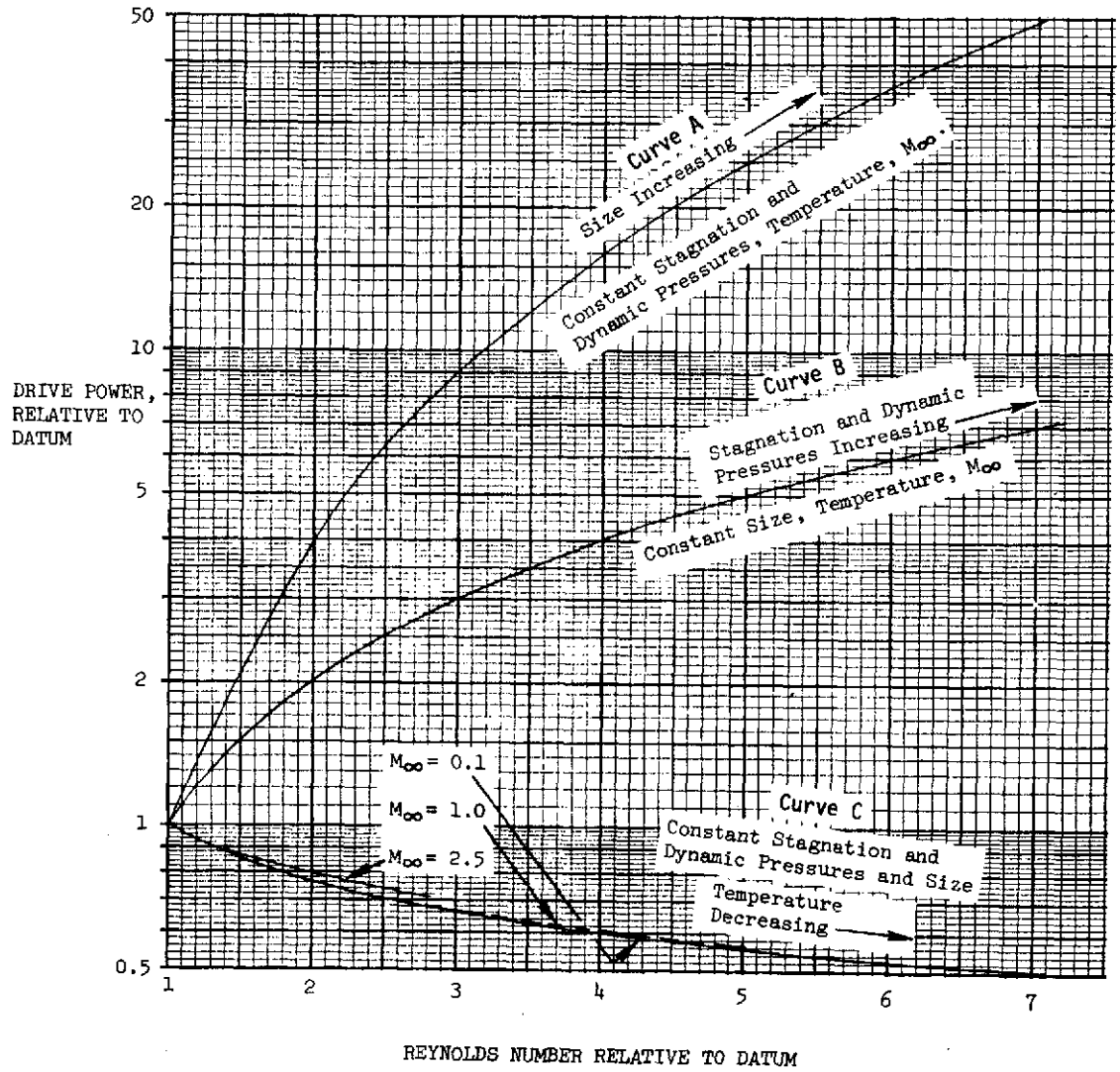

Figure 3.2 Variation of drive power for three methods of increasing Reynolds number.

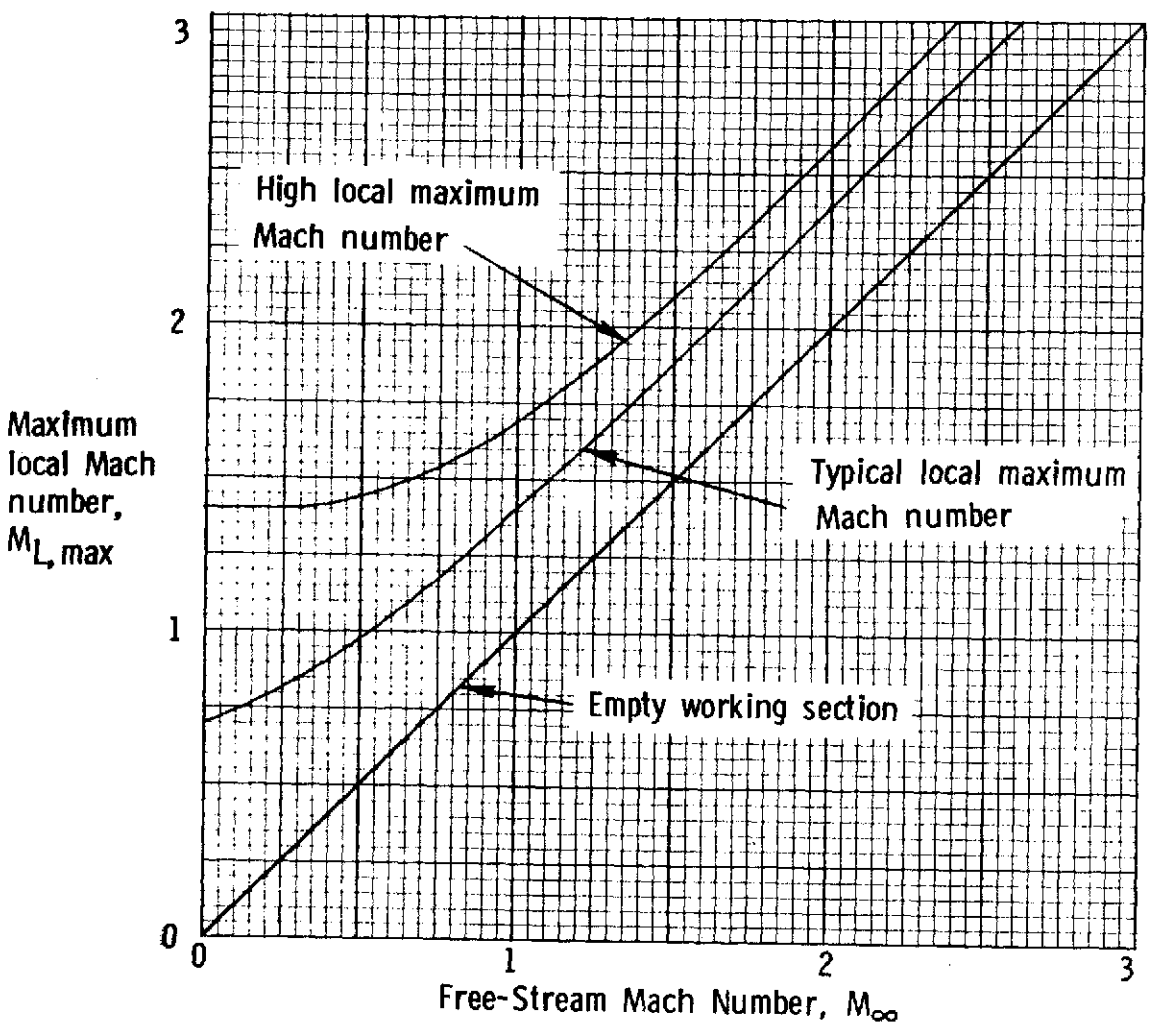

Figure 3.3 Assumed local Mach number as a function of free-stream Mach number.

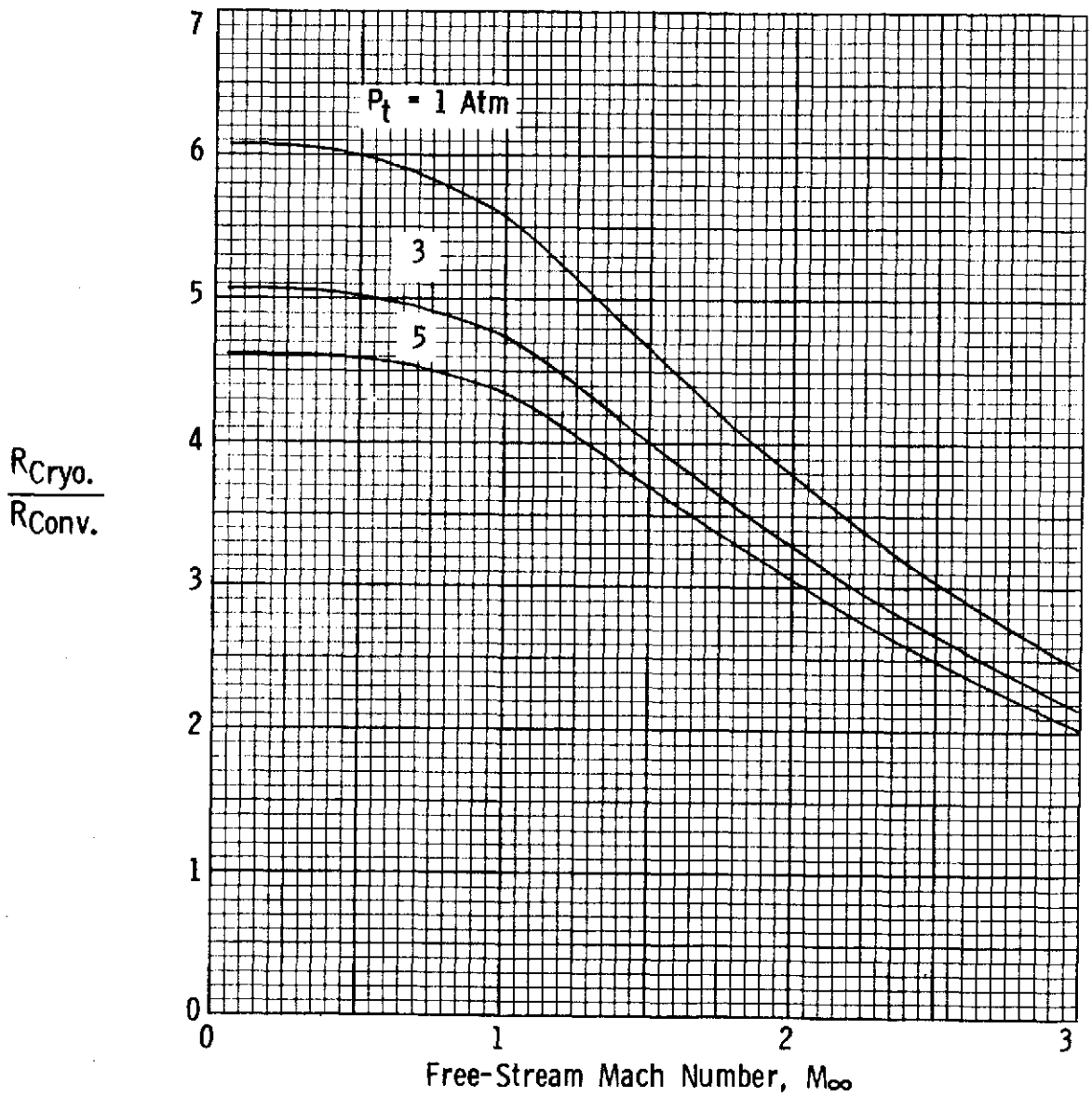

Figure 3.4 Reynolds number in cryogenic nitrogen tunnel relative to Reynolds number in conventional tunnel of same size as a function of free-stream Mach number and stagnation pressure.

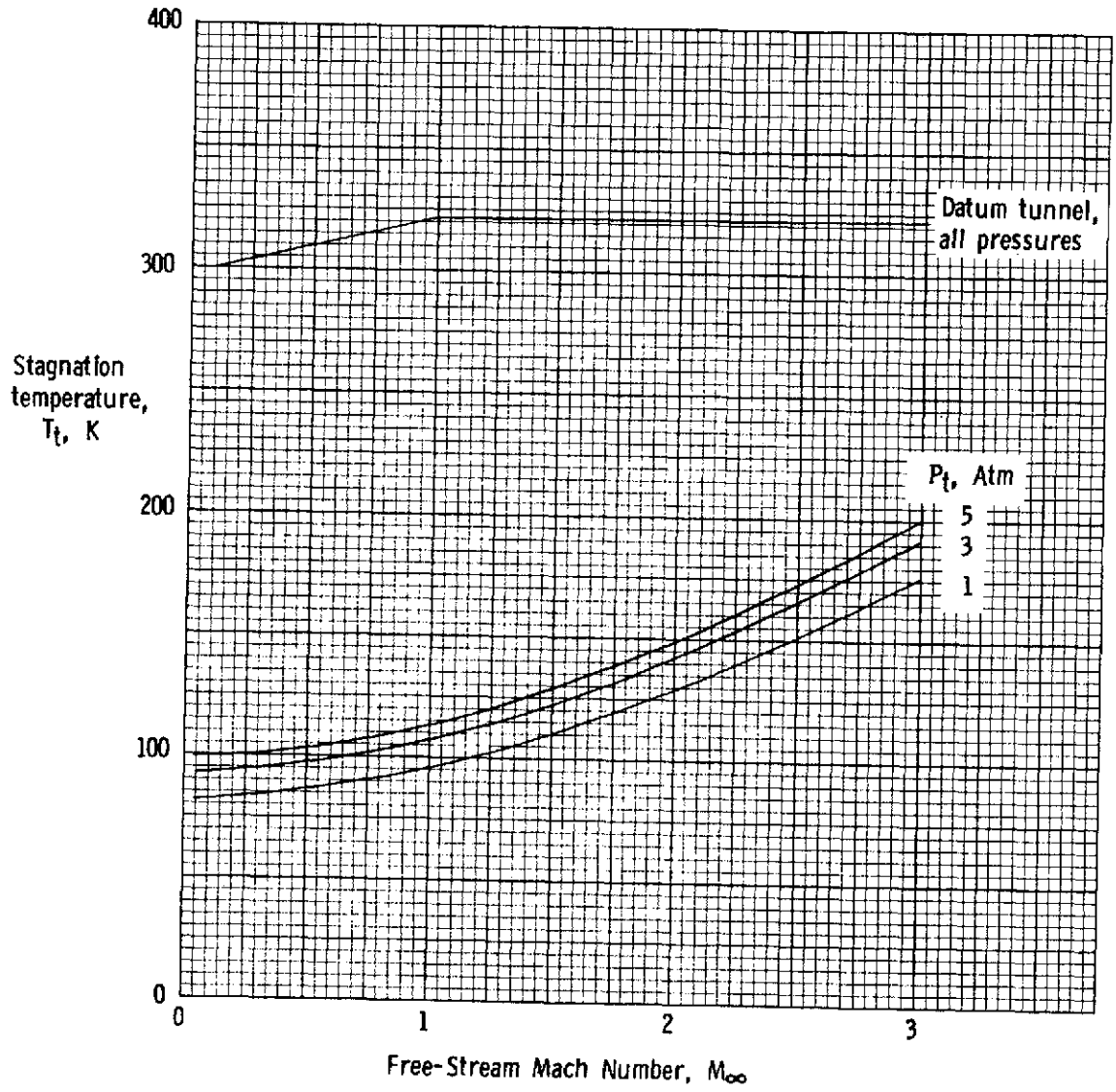

Figure 3.5 Assumed stagnation temperature in datum tunnel and minimum stagnation temperature in cryogenic nitrogen tunnel as a function of free-stream Mach number and stagnation pressure.

4. Real-Gas Considerations for High Reynolds Number Tunnels.

In this chapter some of the consequences of departures of the test gas from equilibrium perfect gas behavior are considered.

Contents:

4.1 Introduction.

In the cryogenic tunnels which have been built to date, the circuit is cooled, and the heat added to the stream by the drive fan is balanced, by the evaporation of liquid nitrogen directly in the tunnel circuit. Thus the test gas is nitrogen rather than air. Since air is about 78-percent nitrogen and 21-percent oxygen by volume and both nitrogen and oxygen are diatomic molecules having nearly the same molecular weights, there is little doubt that at ambient temperatures any test results obtained in nitrogen would be the same as results obtained in air. However, since at cryogenic temperatures the behavior of the gas, air or nitrogen, departs significantly from that of a perfect gas, the magnitude of any real-gas effects must be determined together with the possible operational limits which they might impose. The real-gas effects studied include liquefaction, thermal imperfection, and caloric imperfection. Operating limits set by the saturation boundaries of nitrogen and air are presented, and the consequences of the thermal and caloric imperfections on both isentropic flow and the flow across

a normal shock in nitrogen have been studied over wide ranges of temperature and pressure.

4.2 Saturation Boundaries.

As noted in Chapter 3, section 3.3, the test gas is most likely to condense in localized low-pressure regions adjacent to the model. If it is assumed that the test gas expands isentropically as an ideal gas from the settling chamber to these localized high Mach number regions, the value of local Mach number uniquely determines the ratio of local static to tunnel stagnation conditions. It will be shown in section 4.3 that, for all practical purposes, isentropic expansions of nitrogen at cryogenic temperatures and pressures up to 5 atmospheres give the same stagnation to static pressure and temperature ratios as would be obtained with a thermally and calorically perfect gas. This statement is valid providing the gas does not begin to condense.

Therefore, in sections 4.2.1 to 4.2.3 which follow, gas properties are calculated as though the gas were ideal. The temperature and pressure ratios for an ideal gas having $\gamma = 1.4$ and flowing at Mach number M are

$$\frac{T}{T_t} = \frac{5}{5 + M^2} \qquad \text{---- 4.1}$$

and

$$\frac{P}{P_t} = \left(\frac{5}{5 + M^2}\right)^{7/2} \qquad \text{---- 4.2}$$

4.2.1 Testing in nitrogen

Using the vapor pressure equation for nitrogen from reference 16, the minimum usable stagnation temperatures have been

calculated from equations 4.1 and 4.2 for a range of Mach numbers and stagnation pressures. The minimum stagnation temperature is assumed to be that value which, in combination with the assumed maximum local Mach number on the model, $M_{L,max}$, results in the gas just reaching the saturation boundary at the static conditions obtaining at $M_{L,max}$. The results are shown in Figure 4.1 for Mach number $M_{L,max}$ up to 2 and stagnation pressures up to 7 atmospheres.

Figure 4.2 illustrates the restrictions which are imposed on stagnation temperature when testing in a sonic free stream. The restrictions are set by the gas reaching the saturation boundary at three different values of local Mach number M_L for various values of stagnation pressure. At a given stagnation pressure, the Reynolds number which can be obtained is reduced as the maximum local Mach number, $M_{L,max}$, is increased since the saturation boundary and thus the possibility of liquefaction is determined by the local values of temperature and pressure rather than the free-stream values. The range of local Mach number shown on this figure covers the range of maximum values likely to be met on any model at $M_\infty = 1.0$. With a knowledge of the maximum local Mach number expected or achieved during a test, the permissible test conditions are well defined and any possibility of liquefaction of the test gas can easily be avoided.

4.2.2 Testing in air

Using the saturated vapor (dew) temperature data for air from reference 17, the minimum stagnation temperatures which can be used to avoid condensation by the same criteria but with air as the test gas have been calculated from equations 4.1 and 4.2. The results are shown in Figure 4.3 for maximum local Mach numbers up to 2 and stagnation pressures up to 7 atmospheres.

Comparison of the minimum operating temperatures for air, Figure 4.3, with those for nitrogen, Figure 4.1, show that significantly lower temperatures can be used with nitrogen when testing at the same values of maximum local Mach number and stagnation pressure. The ability to test at lower temperatures results in significantly increased test Reynolds numbers, because of the strong rate of chance of Reynolds number with temperature at low temperatures, illustrated on Figure 3.1.

4.2.3 Testing in Air-Nitrogen Mixtures

In Chapter 5 the cryogenic operation of various types of non-fan-driven tunnels is considered. In some of these tunnels, high pressure air is cooled to the desired operating temperature by mixing it directly with liquid nitrogen. Under these conditions the test gas is a mixture of air and nitrogen. For the purposes of this analysis, this mixture is considered to be a mixture of the two gases oxygen and nitrogen. The liquefaction point may be calculated from the following relation taken from reference 18.

$$P = \frac{P_O P_N}{P_O - (P_O - P_N)F_O} \qquad \text{—— } 4.3$$

where

P = total pressure in atmospheres

P_O = vapor pressure of oxygen

P_N = vapor pressure of nitrogen

and

F_O = mol fraction of oxygen in the mixture

The values of P_O and P_N may be calculated to sufficient accuracy from the following empirical expression from reference 19.

$$\log_{10} P_O = 4.06295 - \frac{366.523}{T} \qquad \text{____ 4.4}$$

and

$$\log_{10} P_N = 3.93352 - \frac{304.494}{T} \qquad \text{____ 4.5}$$

where

P = vapor pressure, atmospheres

and

T = temperature, K

When operating a tunnel with an air-nitrogen mixture, minimum permissible stagnation temperatures can be obtained by using equations 4.4 and 4.5 in equation 4.3. The mol fraction of oxygen F_O will range from zero for tests in pure nitrogen to 0.23 for tests in air, and may be calculated from the particular air-nitrogen ratio which is in use to sufficient accuracy with the following equation

$$F_O = \frac{0.23\dot{m}_{AIR}}{\dot{m}_{t.s.}} \qquad \text{____ 4.6}$$

where

$\dot{m}_{AIR}$ = Mass flow rate of air

$\dot{m}_{t.s.}$ = Test section mass flow rate

It is assumed that air is 23-percent oxygen by weight, and that all of the liquid nitrogen is vaporized.

Once the variation of vapor pressure with temperature has been found, equations 4.1 and 4.2 may again be used to establish the minimum useable stagnation temperature as a function of test Mach number and operating pressure.

The analysis of this section may be regarded as a generalization of the preceeding two sections. The operating temperatures presented for N_2 and air on Figures 4.1 and 4.3 are particular cases in the generalization, the two extremes between which lie operating temperatures for N_2 - air mixtures. Some examples of tunnels which could utilize such mixtures are discussed in Chapter 5.

4.3 Isentropic Expansion Relations.

The need to give consideration to the effects of thermal and caloric imperfections on flow characteristics at cryogenic temperatures is apparent from Figure 4.4 where the compressibility factor, Z, and the ratio of specific heats, γ, for nitrogen are shown at a constant pressure of 5 atmospheres over a range of temperatures. Departure of Z from unity is designated a thermal imperfection, and departure of γ from 1.4 a caloric imperfection. At 5 atmospheres, both parameters depart from their ideal-gas values by about 6 or 7-percent at the lower temperatures.

During the period when cryogenic tunnels were first being considered at the Langley Research Center, preliminary calculations of the effects of caloric imperfections had been made by simply using the real-gas value of the ratio of specific heats, γ, in the ideal gas equations which describe isentropic flow processes such as equations 4.1 and 4.2. These calculations (see ref. 20) indicated a strong effect of γ on the isentropic flow process, and were leading to the choice of test conditions which gave advantages in terms of Reynolds number over conventional tunnels markedly less attractive than those attainable in a cryogenic tunnel in which test conditions were limited solely by the saturation boundary. Therefore there was a strong inducement to choose test conditions where γ was appreciably different from 1.4, but at the same time there was a need to properly

understand the consequences of the choice. Along isentropes extending from stagnation conditions through free stream and beyond to the localized low pressure regions on the model there are changes in the local value of γ. An attempt was therefore made to determine "effective" or average values for γ. More properly in this context the term γ should be replaced by an expression such as "isentropic expansion coefficient". While using a thermodynamic chart to extract effective isentropic expansion coefficients it was discovered that coefficients derived in this manner were all remarkably close to the ideal expansion coefficient of 1.4. It was decided to investigate this phenomenon more rigorously by using the best available data on the real-gas properties of nitrogen and using analytical methods where possible in place of the graphical method. Both isentropic flows and normal shock flows were investigated because of their importance in transonic flow fields.

The thermodynamic properties for nitrogen were obtained from a National Bureau of Standards computer program (see reference 21) based in part on the work by Jacobsen reported in reference 16. Obtainable from the NBS program were values for Z and γ. The program was first modified to allow computation of isentropic expansions. The variations of gas properties such as pressure and temperature through the expansion process were calculated using real-gas values of Z and γ and then compared with values for the same gas properties derived from ideal-gas equations with constant (ideal) values of compressibility factor, $Z = 1$, and ratio of specific heats, $\gamma = 1.4$. Calculations have been made over a wide range of stagnation pressures and temperatures. An example of the results is presented in Figure 4.5 where the ratio of the "real" and "ideal" pressure ratios necessary to expand isentropically to $M_\infty = 1$ is presented as a function of tunnel stagnation temperature and pressure.

As can be seen, the real-gas effects are extremely small.

This discovery has allowed lower test temperatures to be considered in tunnel designs. A design is considered in Appendix II intended to generate a Reynolds number in sonic flow of 50×10^6 based on the mean chord of $0.1 \sqrt{\text{test-section area}}$ adopted as a basis for comparison. The cryogenic tunnel would have a 3m × 3m test section and operate at about 2-1/2 atmospheres. Under these conditions the real-gas static to stagnation pressure ratio differs from the ideal-gas pressure ratio by only about two-tenths of one percent. Also shown for comparison is the equivalent Reynolds number point for the same size test section but normal temperature operation. It is interesting to note that the real-gas effect in the cryogenic temperature tunnel is actually less than in the ambient temperature tunnel where a considerably higher stagnation pressure is required to obtain this Reynolds number.

A comparison is made on Figure 4.6 between the results obtained from the modified National Bureau of Standards program and the results obtained when just one of the two relevant real-gas effects is considered in isolation. For the purposes of illustration it is assumed that the compressibility factor is constant, but the actual values of the ratio of specific heats are used in the ideal pressure ratio equation (equation 4.2). As can be seen, very misleading results are obtained when the incorrect approach is taken.

The ratios of "real" to "ideal" static to stagnation temperature and density ratios for isentropic expansion to $M_\infty = 1$ in nitrogen are presented in Figures 4.7 and 4.8 respectively. As can be seen, the real-gas ratios again differ from the corresponding ideal-gas ratios by very small amounts for stagnation pressures up to about 5 atmospheres even at the lowest values of stagnation temperature.

Additional information on the influences of real-gas

effects on flow properties is given on Figure 4.9 where the variations of the "real" to "ideal" pressure, temperature, and density ratios are plotted as functions of the Mach number to which isentropic expansions proceed. Constant values of stagnation pressure and temperature of 4 atmospheres and 120K, respectively, were used for these calculations. These test conditions correspond to a Reynolds number at $M_\infty = 1$ of 216×10^6 per meter (66×10^6 per foot).

As can be seen, the real-gas ratios which describe the isentropic expansion in nitrogen differ little from the corresponding ideal-gas ratios. Except for the most exacting experimental work it is most probable that the ideal-gas ratios could be used with acceptable accuracy. Where sufficiently accurate instrumentation is available, even the small residual errors could be eliminated in some circumstances by using the real-gas ratios, for example in setting tunnel Mach number by pressure ratio. However, errors of this small magnitude are of the same order as the usual uncertainty in pressure and other measurements and would be considered insignificant in most wind-tunnel work.

4.4 Normal-Shock Relations.

The NBS program was also modified so that the various conventional ratios of properties which describe normal shock flow could be calculated using the real-gas properties and compared with the corresponding ideal-gas ratios. Calculations have been made over wide ranges of stagnation pressures and temperatures. An example of the results is presented in Figure 4.10 where the ratio of the "real" and "ideal" static pressure ratios across a normal shock having an upstream-side flow Mach number M_1 of 1.4 is presented as a function of tunnel stagnation temperature and pressure. As in the case of isentropic processes, the real-gas effects are extremely small. For the same tunnel design example

the real-gas static pressure ratio differs from the ideal-gas ratios by only about two-tenths of one percent. The other real-gas ratios (density and static temperature) associated with normal shock flow also differ from the ideal ratios by approximately the same percentage. As in the case of isentropic processes, in those situations where the real-gas equations cannot be used the errors which would be introduced would usually be considered insignificant.

4.5 Conclusions from the Studies of Real-Gas Effects.

1. The saturation boundary is well defined and therefore any possible effects of liquefaction of the test gas can easily be avoided provided that the maximum local Mach number on the model is known.
2. The use of real values of the ratio of specific heats in the ideal isentropic equations gives results which are generally in error by an unacceptable amount. Both the thermal and the caloric imperfections must be taken into account.
3. For stagnation pressures up to about 5 atmospheres, the isentropic expansion and the normal shock relations calculated from the real-gas properties of nitrogen differ by a maximum of about 0.4-percent (depending on test conditions) from the corresponding relations calculated from ideal diatomic gas properties and ideal gas equations.
4. For most purposes it would be satisfactory to adopt ideal gas equations in the analysis of wind-tunnel test data taken in a cryogenic nitrogen wind tunnel at any stagnation pressure up to about 5 atmospheres.

4.6 List of Symbols Used in Chapter 4.

Symbol	Meaning
$\bar{c}$	reference chord, 0.1 $\sqrt{\text{Test-section area}}$
F_O	mol fraction of oxygen in oxygen-nitrogen mixture
$\dot{m}$	mass flow rate
M	Mach number
P	pressure
$R_{\bar{c}}$	Reynolds number based on $\bar{c}$
R	gas constant
T	temperature, kelvin
V	volume
Z	compressibility factor
γ	ratio of specific heats
ρ	density

Subscripts

1	conditions upstream of normal shock
2	conditions downstream of normal shock
max	maximum value
min	minimum value
AIR	air
L	local conditions
N	nitrogen
O	oxygen
t	stagnation conditions
∞	free-stream conditions

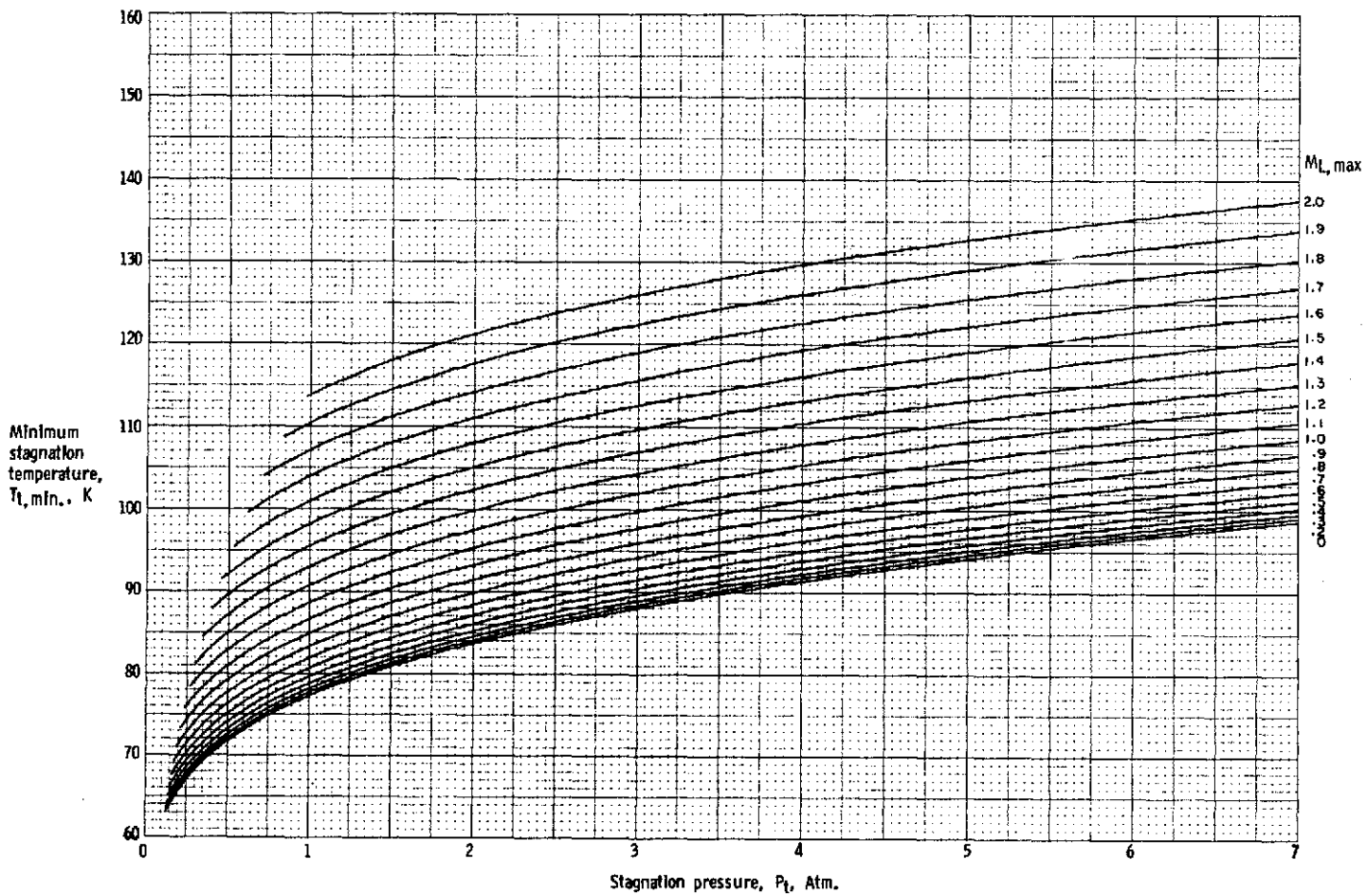

Figure 4.1 Variation of minimum stagnation temperature, $T_{t,min}$, with stagnation pressure and maximum local Mach number for testing in nitrogen.

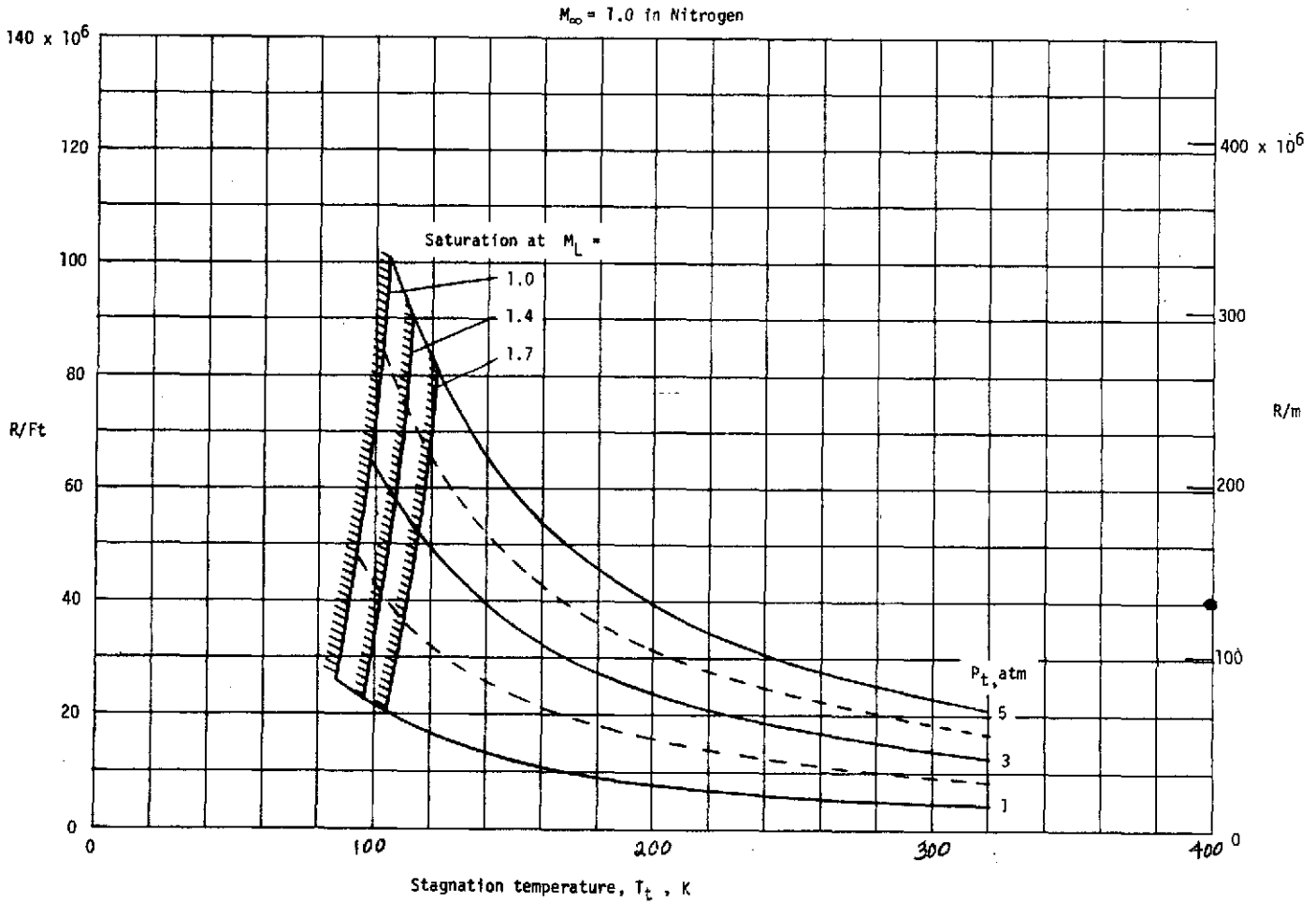

Figure 4.2 Restrictions imposed on stagnation temperature and Reynolds number due to saturation as a function of stagnation pressure and maximum local Mach number.

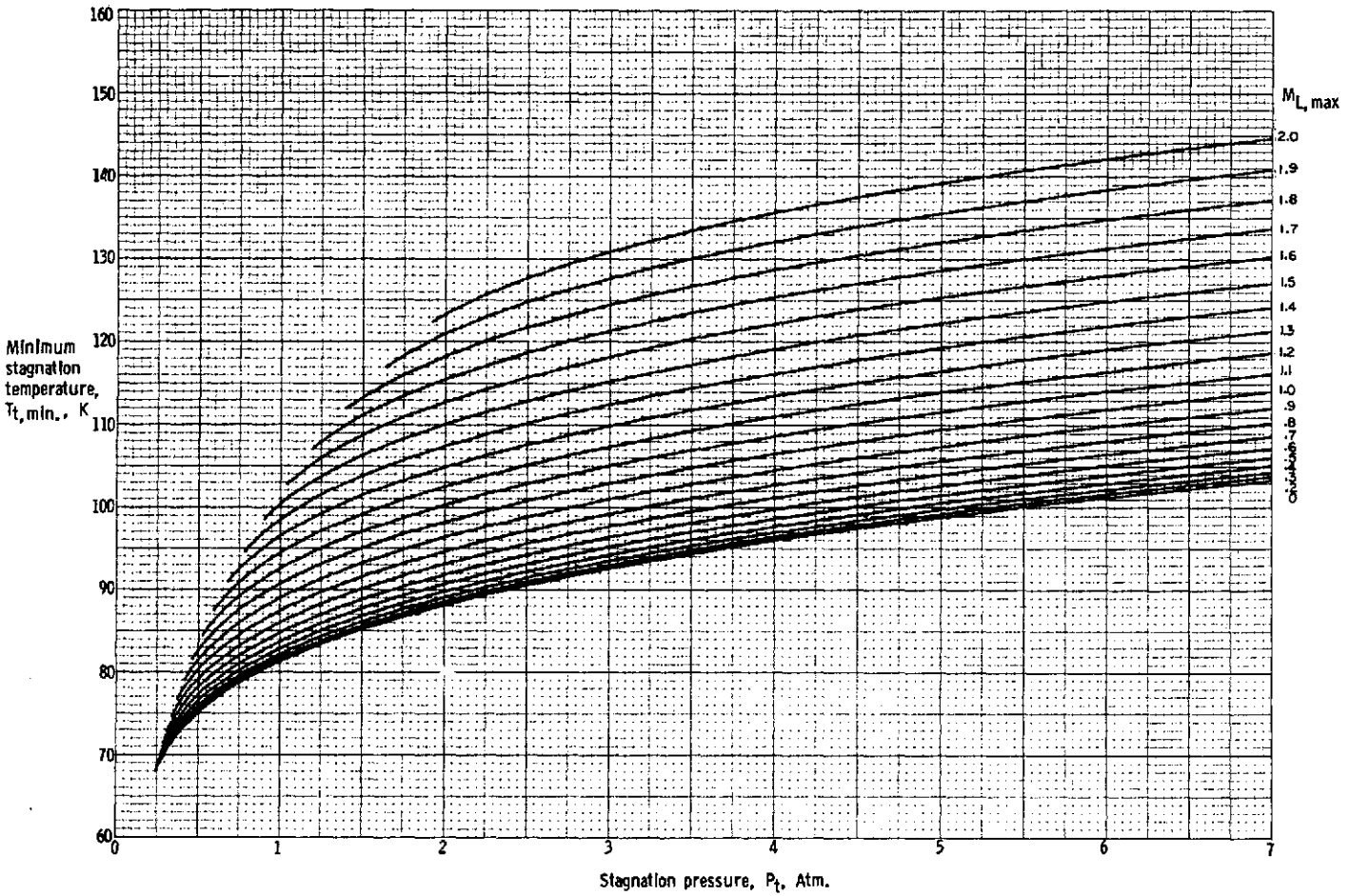

Figure 4.3 Variation of minimum stagnation temperature, $T_{t,min}$, with stagnation pressure and maximum local Mach number for testing in air.

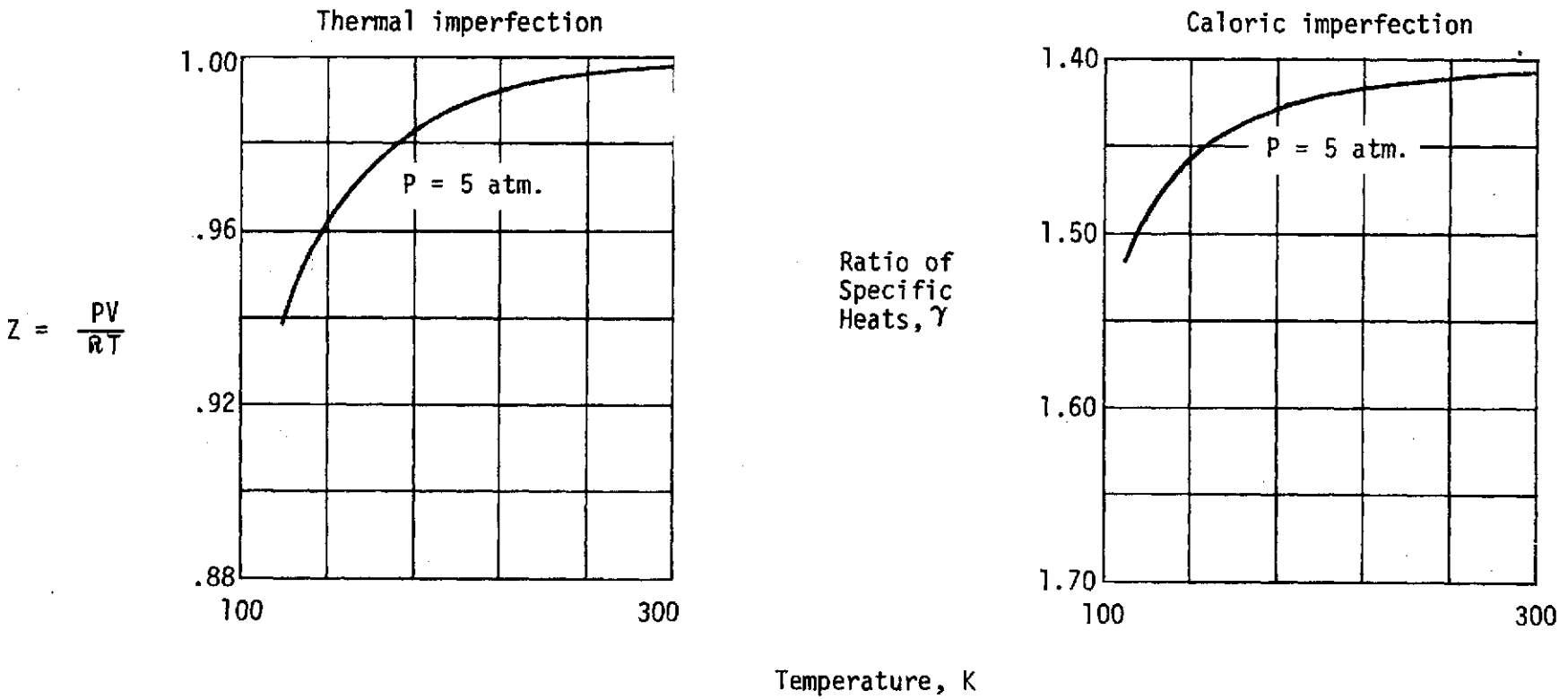

Figure 4.4 Compressibility factor, Z, and ratio of specific heats, γ, for nitrogen as a function of temperature.

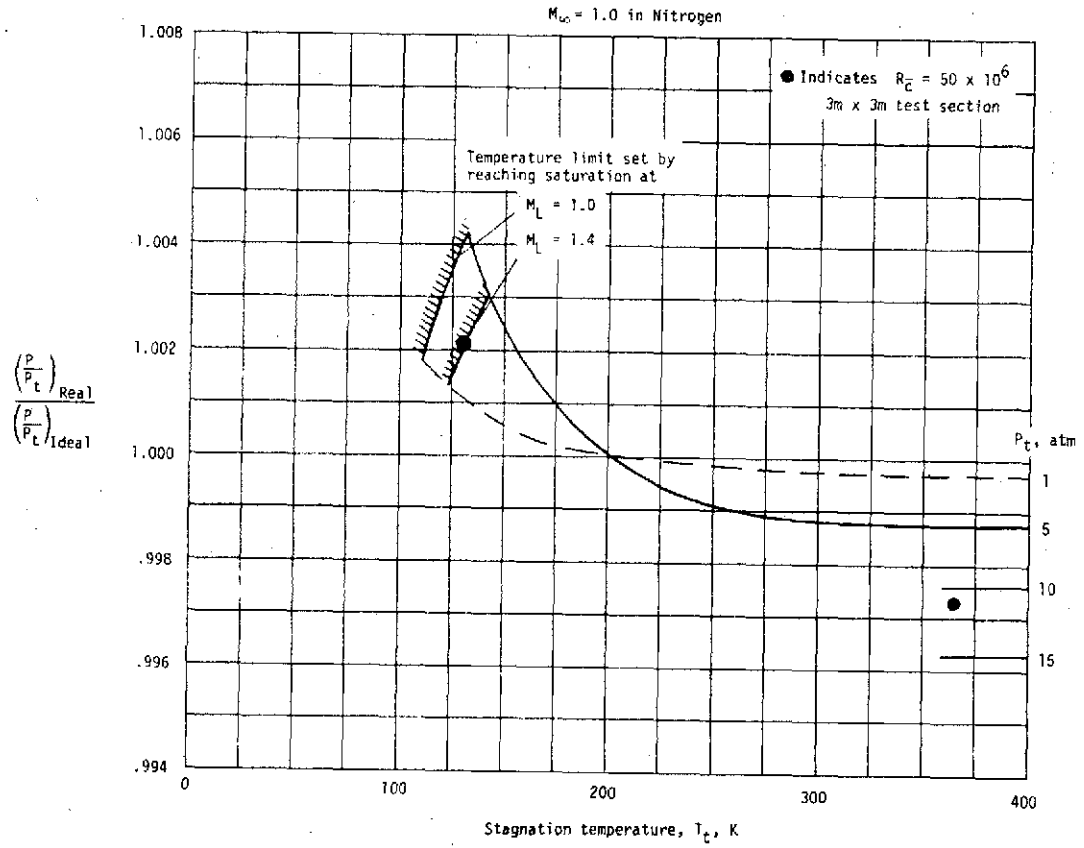

Figure 4.5 Ratio of real-gas to ideal-gas pressure ratios necessary to expand isentropically to $M_\infty = 1$ in nitrogen as a function of temperature and pressure. Solid symbol indicates conditions needed for $R_{\bar{c}} = 50 \times 10^6$ in a 3m x 3m test section.

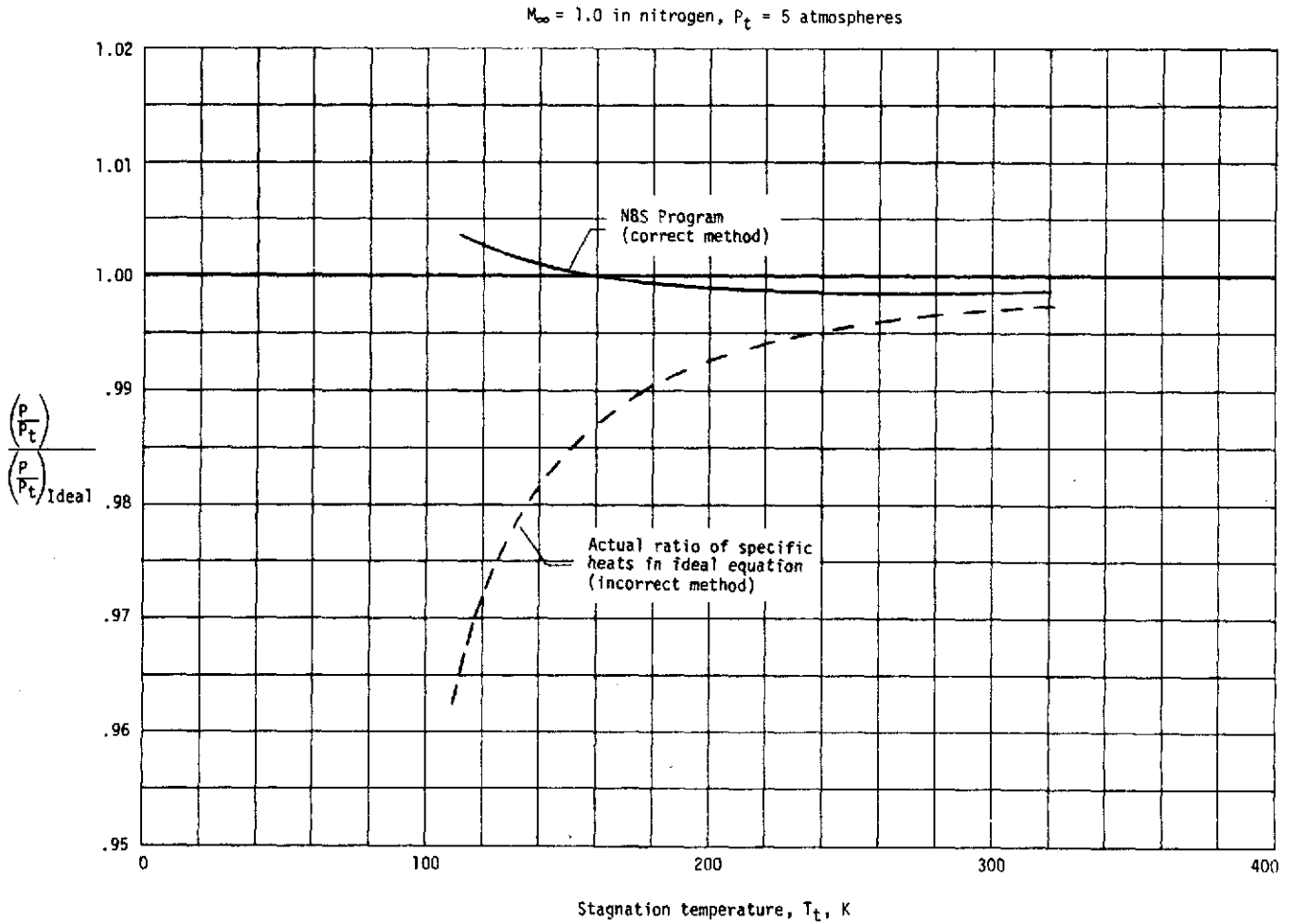

Figure 4.6 Comparison of methods used to calculate the pressure ratio necessary to expand isentropically to $M_\infty = 1$ in nitrogen from a stagnation pressure of 5 atmospheres as a function of stagnation temperature.

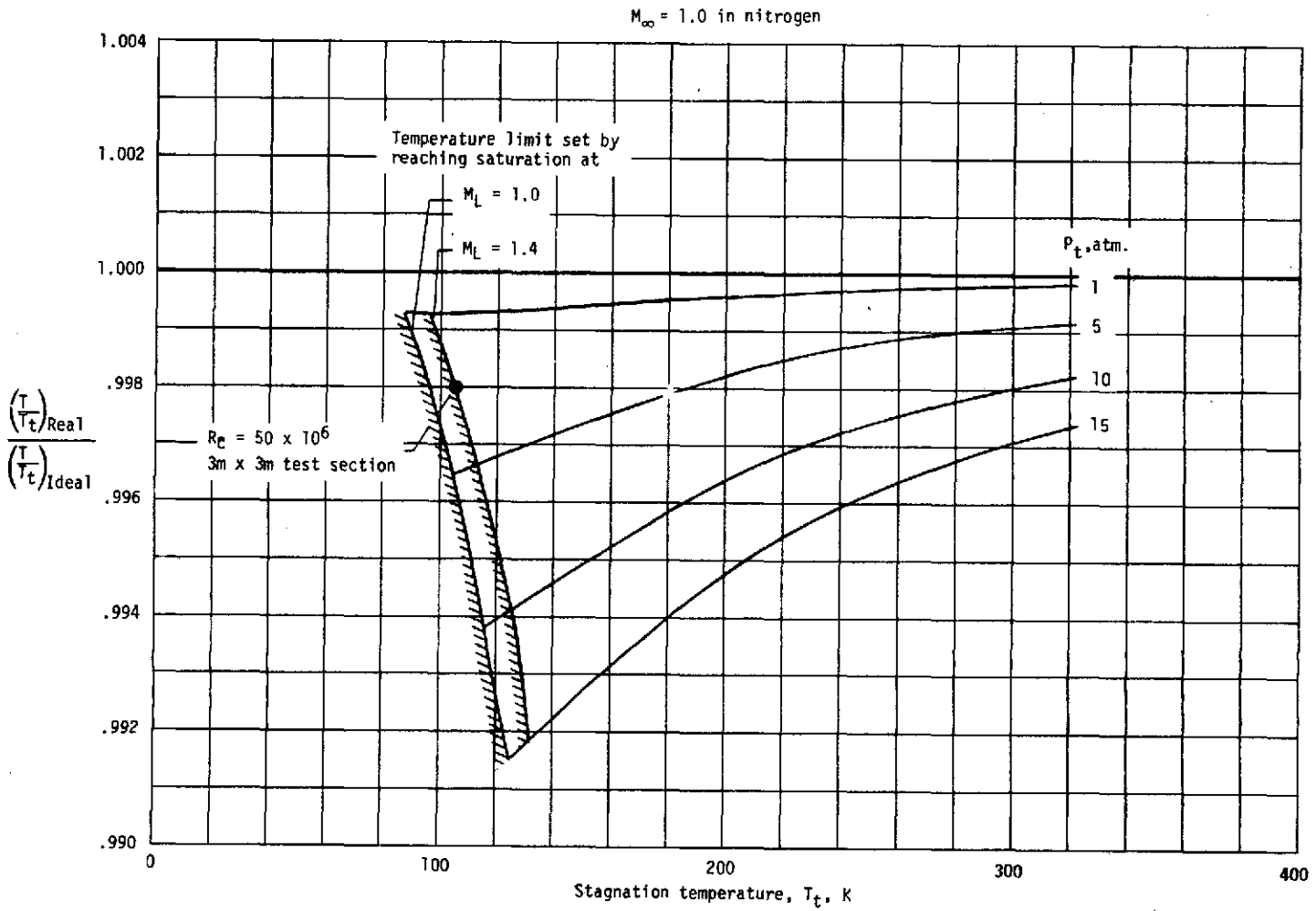

Figure 4.7 Ratio of real-gas to ideal-gas temperature ratios for isentropic expansion to M_∞ = 1.0 in nitrogen as a function of stagnation temperature and pressure.

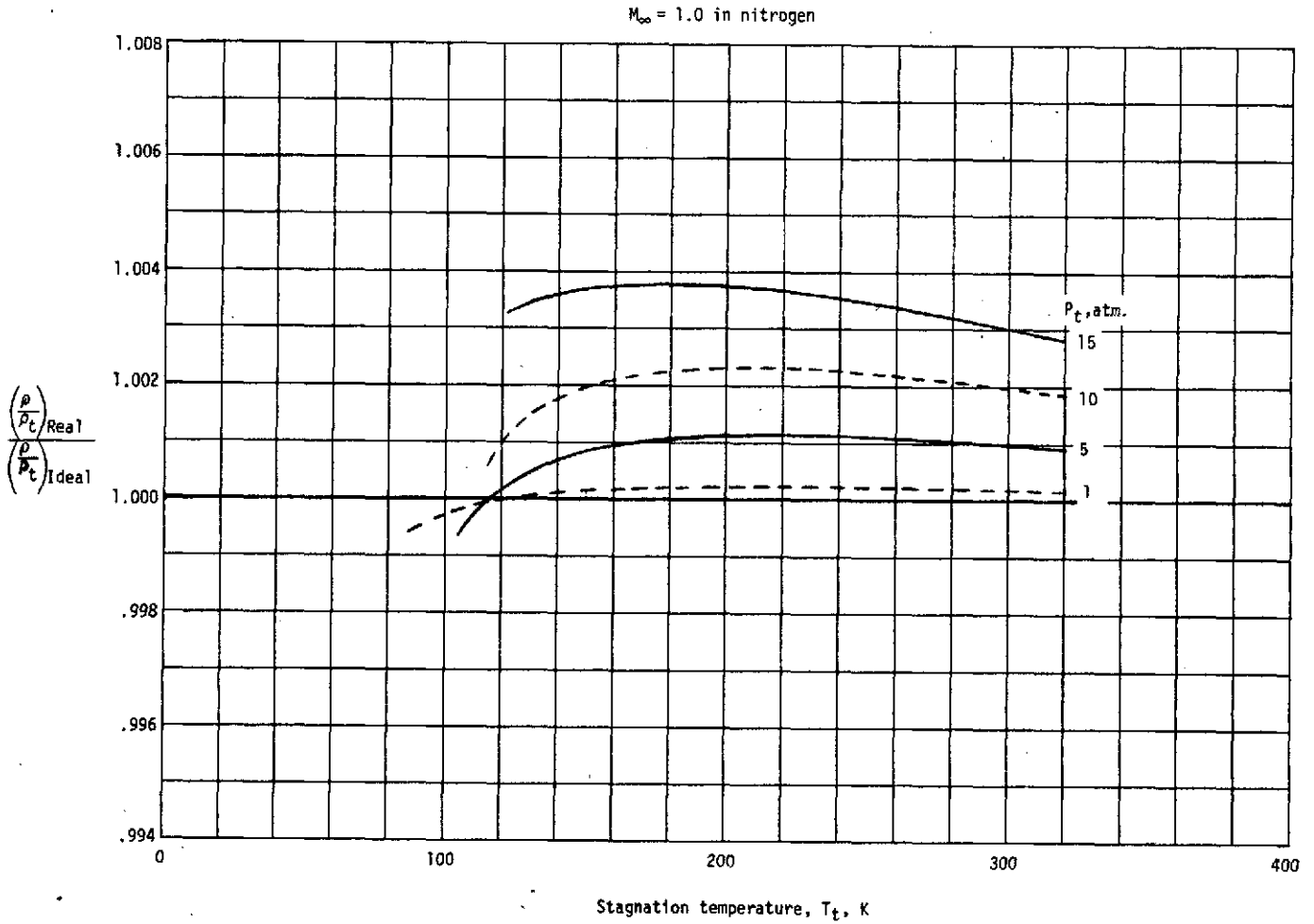

Figure 4.8 Ratio of real-gas to ideal-gas density ratios for isentropic expansion to $M_\infty = 1$ in nitrogen as a function of stagnation temperature and pressure.

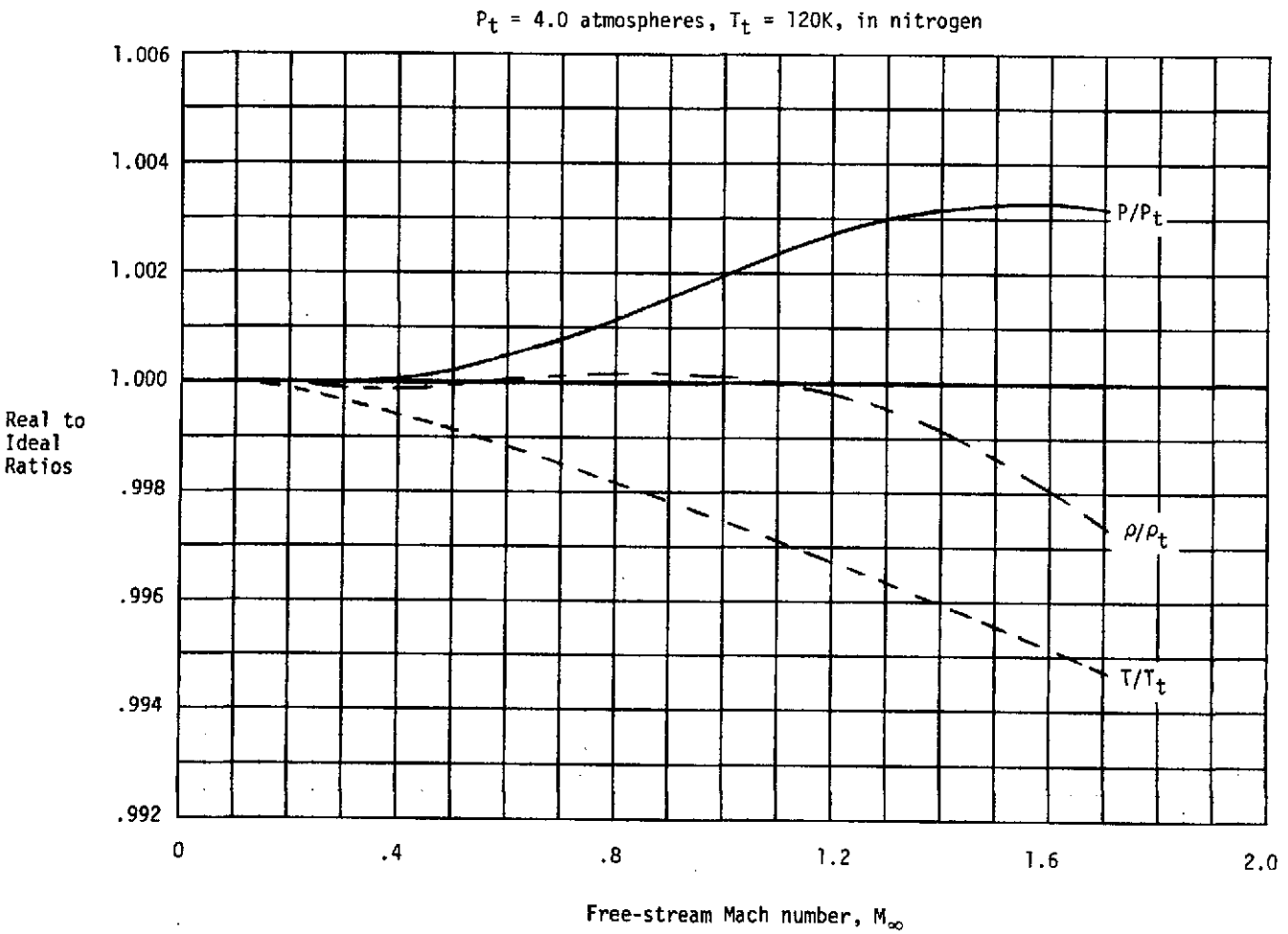

Figure 4.9 Variations of real-gas to ideal-gas pressure, temperature, and density ratios in nitrogen as a function of the Mach number to which the isentropic expansion is made.

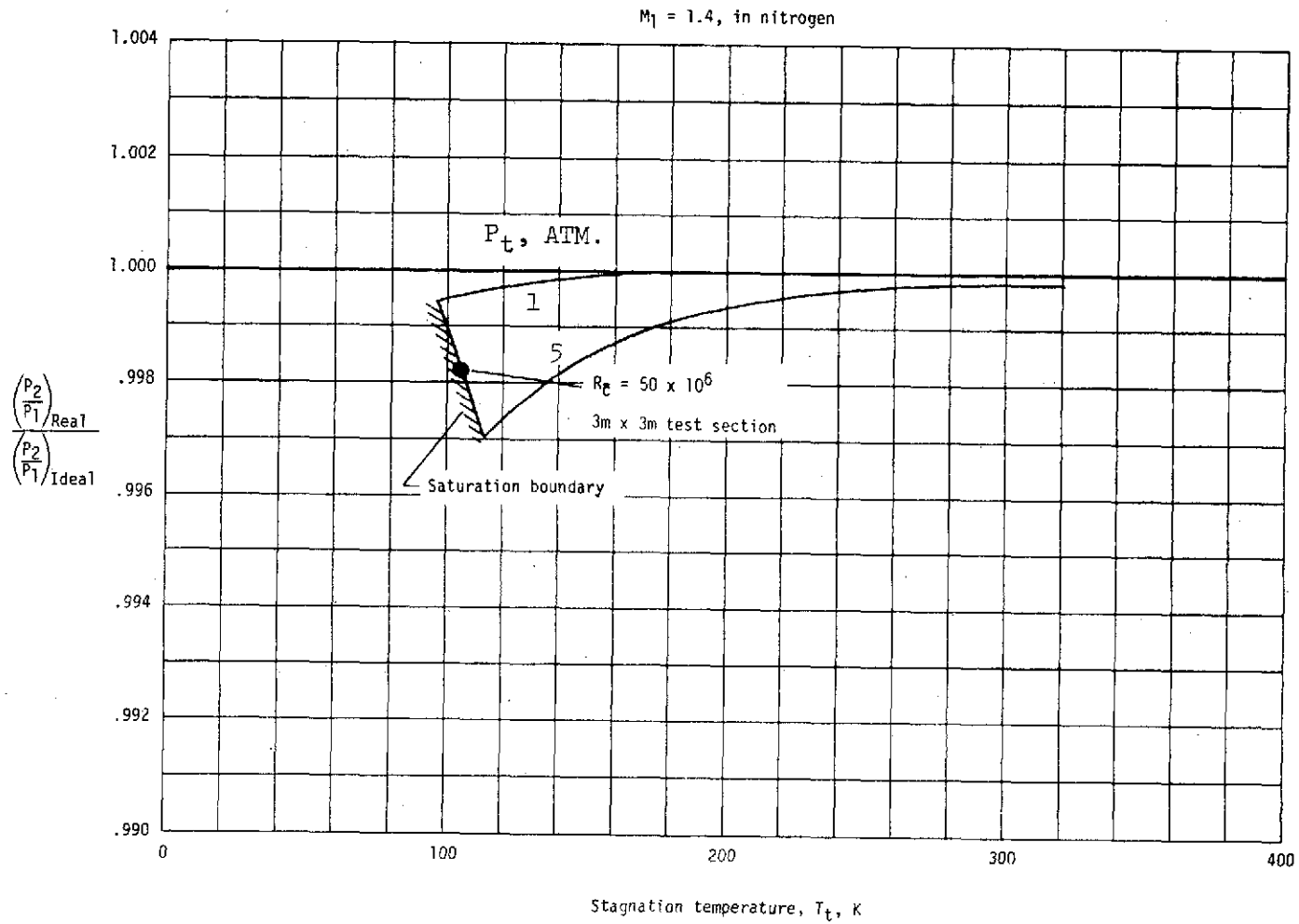

Figure 4.10 Ratio of real-gas to ideal-gas static pressure ratios across a normal shock as a function of stagnation temperature and pressure. Mach number ahead of the shock = 1.4.

5. Cryogenic Operation of Various Types of Tunnels.

Contents:

5.1 Introduction.

As far as can be seen at this time, the benefits of cryogenic operation can be realized with most types of tunnels with the obvious exception of the hypersonic tunnel. Brief comments will now be made concerning the application of the cryogenic concept to several types of tunnels.

5.2 The Cryogenic Ludwieg Tube Tunnel.

5.2.1 Theory of operation

The operating principle of what has come to be known as the Ludwieg tube tunnel was first suggested by Prof. Ludwieg in 1955. The Ludwieg tube tunnel in its simplest form consists of a long supply tube separated from a nozzle and test section by a diaphragm. When the diaphragm is broken a rearward-facing centered rarefaction fan propagates down the supply tube setting the gas in motion and lowering both the pressure and temperature of the gas.

In reference 22 several useful relationships describing flow conditions are presented for Ludwieg tube tunnels. These relations assume that the flow in the supply tube is one-dimensional and

isentropic, and that the test gas acts as a perfect gas.

Constant stagnation conditions exist at the entrance to the nozzle during the time required for the head of the incident wave to travel to the closed end of the supply tube, reflect, and return to the nozzle. This time is given by

$$t = \frac{2L}{a_s(1 + M_1)} \left[1 + \frac{\gamma - 1}{2} M_1\right]^{\frac{\gamma + 1}{2(\gamma - 1)}} \qquad \text{—— 5.1}$$

where

t = time of constant stagnation conditions

a_s = speed of sound at initial supply tube conditions

L = supply tube length

M_1 = Mach number of the gas leaving the supply tube during the steady run period

γ = ratio of specific heats

The stagnation conditions are given by

$$\frac{P_t}{P_s} = \frac{\left(1 + \frac{\gamma - 1}{2} M_1^2\right)^{\frac{\gamma}{\gamma - 1}}}{\left(1 + \frac{\gamma - 1}{2} M_1\right)^{\frac{2\gamma}{\gamma - 1}}} \qquad \text{—— 5.2}$$

and

$$\frac{T_t}{T_s} = \frac{1 + \frac{\gamma - 1}{2} M_1^2}{\left(1 + \frac{\gamma - 1}{2} M_1\right)^2} \qquad \text{—— 5.3}$$

where

P_t = stagnation pressure
T_t = stagnation temperature
} in the nozzle during the steady run period

P_s = initial supply tube pressure

T_s = initial supply tube temperature

Equations 5.1, 5.2, and 5.3 show that the period of steady flow and the stagnation conditions depend only on the initial storage pressure and temperature in the supply tube, the length of the tube, the ratio of specific heats of the test gas, and the Mach number in the supply tube. This Mach number is in turn a function of the ratio of supply tube cross-sectional area to the nozzle throat area.

If we assume the test gas to be an ideal diatomic gas, ($\gamma = 1.4$) the above equations become

$$t = \frac{2L}{a_s(1 + M_1)} \left(1 + 0.2\, M_1\right)^3 \qquad \text{—— 5.4}$$

$$\frac{P_t}{P_s} = \frac{\left(1 + 0.2\, M_1^2\right)^{3.5}}{\left(1 + 0.2\, M_1\right)^7} \qquad \text{—— 5.5}$$

and

$$\frac{T_t}{T_s} = \frac{1 + 0.2\, M_1^2}{\left(1 + 0.2\, M_1\right)^2} \qquad \text{—— 5.6}$$

5.2.2 Benefits of cryogenic operation

In order to illustrate the benefits of cryogenic operation of a Ludwieg tube tunnel, the above equations have been used to determine the time of constant stagnation conditions and the required storage temperature for a range of operating temperatures for a hypothetical Ludwieg tube tunnel using nitrogen as the test gas.

The following conditions are assumed:

3m (9.84 feet) square test section

$\bar{c}$ = 0.3m (0.984 foot)

M = 1.00

M_1 = 0.40 (hence $\frac{T_t}{T_s} = 0.885$, $\frac{P_t}{P_s} = 0.651$)

L = 500m (1640 feet)

P_t = 2.52 atm., hence P_s = 3.87 atm.

The lowest stagnation temperature is chosen so that $R_c = 50 \times 10^6$ and the saturation boundary is reached at a Mach number of 1.40. The results are given in the following table.

TABLE 5.1.

Ludwieg tube tunnel using nitrogen as the test gas.

T_s, K	T_t, K	t, sec	$R_c \times 10^{-6}$	$\frac{t}{t_{105K}}$	$\frac{R_c}{R_{c_{105K}}}$
118.7	105.0	4.04	50.0	1	1
239.0	211.5	2.85	18.1	.71	.36
293.2	259.4	2.57	13.7	.64	.27

The increase in both Reynolds number and the time of constant stagnation conditions as temperature is reduced clearly show the advantage of cryogenic operation. For example, for the same R_c and t as in the cryogenic Ludwieg tube tunnel, the ambient temperature tunnel would require a supply tube about 1.56 times as long and a test section about 3.65 times as large in linear dimension.

An analysis presented in reference 8 considers the benefits of cooling a transonic Ludwieg tube tunnel to 239K (-30°F) and predicts a potential savings of slightly over 30 percent on capital investment for a given Reynolds number. As can be seen in Table 5.1, a storage temperature of 239K does increase both R_c and t over ambient temperature conditions. However, the selected temperature of 239K apparently comes nowhere near to the realization of the full potential of cryogenic operation.

Operating with nitrogen as the test gas permits the use of slightly lower temperatures than operating with air due to the lower saturation temperature of nitrogen for a given pressure. However, the use of an air-nitrogen mixture might in many cases be a more practical choice of test gas. For example, one very simple method of charging the supply tube with cryogenic gas would be to inject liquid nitrogen directly into the supply tube with the usual compressed air so that the evaporated nitrogen becomes a part of the supply gas. Also, because of the efficiency of this direct method of cooling, the cost of cooling should be less than the cost of cooling by less direct methods such as the use of nitrogen-air heat exchangers.

The combined effect of the reduction of supply tube volume resulting from cryogenic operation and the use of the direct method of cooling would be to considerably reduce the recharging time. For example, for the same pressure, Mach number, Reynolds number, and run time, and with equal investment in compressors, a cryogenic Ludwieg tube tunnel using the direct method of cooling can make nearly 13 times as many runs as an ambient Ludwieg tube tunnel during the same period of time.

5.3 The Cryogenic Evans Clean Tunnel.

5.3.1 Theory of operation

The Evans Clean Tunnel (ECT) is under study in England as a possible high Reynolds number wind tunnel. In this type of intermittent wind tunnel, the settling chamber of the conventional tunnel is extended to form a long tube. Air is allowed to settle in this tube before the start of a run. During the run it is pushed through the test section by a piston moving along the tube. The air is then decelerated in a conventional diffuser and returned through a closed circuit to the upstream side of the piston. Opening a valve at the

end of the diffuser produces an expansion wave which, by suitable timing, cancels the compression wave due to the acceleration of the piston so that uniform flow is maintained during the travel of the piston along the tube. Thus virtually all of the air originally contained in the tube passes through the test section at constant stagnation pressure. A complete discussion of the principle of the ECT concept can be found in reference 7.

5.3.2 Benefits of cryogenic operation

The use of low temperatures in an ECT-driven tunnel results in significant increases in Reynolds number and run time. For sonic testing in a hypothetical ECT we can assume a normal (ambient) operating stagnation pressure of 3 atmospheres and stagnation temperature of 300K (80°F). If stagnation pressure is held constant, the stagnation temperature can be reduced to 107 K (-267°F) for testing in nitrogen while reaching the saturation boundary at a maximum local Mach number of 1.40. The reduction in temperature increases Reynolds number by a factor of 4.32 and increases run time by a factor of 1.71. Piston velocity is reduced by 42 percent.

An alternative approach to the exploitation of low temperatures with the ECT might be to achieve the same Reynolds number and run time as in the normal temperature ECT. In this case, the diameter of the tunnel would everywhere be reduced by 77 percent and the circuit length reduced by 42 percent, figures comparable with those for the cryogenic Ludwieg tube tunnel.

5.4 The Cryogenic Blowdown Tunnel.

The cryogenic mode of operation appears applicable to the blowdown tunnel. Prior to a run, the model would have to be pre-cooled to the desired operating temperature.

One possible method of testing would be to pass dry air

from a high pressure supply through a precooled metal heat exchanger having sufficient thermal inertia to insure the temperature of the air remains relatively constant in the test section during a run.

A second and more efficient method of operating a cryogenic blowdown tunnel would be to store air at ambient temperature T_s, precool the test section and model, and during a run hold a constant test temperature by injecting and evaporating liquid nitrogen in the region of the settling chamber. In this case the test-section mass flow is given by

$$\dot{m}_{t.s.} = \dot{m}_{AIR} + \dot{m}_{LN_2} \qquad \text{—— 5.7}$$

The energy balance in the mixing process requires that

$$\dot{m}_{AIR} C_p \Delta T = \dot{m}_{LN_2} \beta \qquad \text{—— 5.8}$$

where C_p = specific heat of air

$$\Delta T = T_s - T_t$$

and β = cooling capacity of LN_2 (see Fig. 8.3)

Solving equations 5.7 and 5.8 for $\dot{m}_{LN_2}$ gives

$$\dot{m}_{LN_2} = \frac{\dot{m}_{t.s.} C_p \Delta T}{\beta + C_p \Delta T} \qquad \text{—— 5.9}$$

In order to illustrate this mode of cryogenic operation of a blowdown tunnel, the above equations have been used to determine the mass-flow rates of both the air from storage and the liquid nitrogen used as coolant for a hypothetical blowdown tunnel over a range of operating temperatures. Reynolds number based on $\bar{c}$ has been

calculated for each temperature.

The following conditions are assumed

3m (9.84 feet) square test section

$\bar{c}$ = 0.3m (0.984 foot)

M = 1.00

P_t = 2.7 atm.

T_s = 288K

The lowest stagnation temperature is chosen so that $R_{\bar{c}} = 50 \times 10^6$ and the saturation boundary of the air-nitrogen mixture is reached at a Mach number of 1.40. The results are given in the following table.

Table 5.2.

Blowdown tunnel using air-nitrogen mixture as the test gas.

T_t, K	Mass flow rate, kg/sec			$R_{\bar{c}} \times 10^{-6}$	$\frac{R_{\bar{c}}}{R_{\bar{c}_{110K}}}$
	t.s.	AIR	LN_2		
110	9502	5276	4226	50.0	1
150	8042	5278	2764	31.6	.63
200	6935	5429	1506	21.0	.42
250	6192	5623	569	15.4	.31
288	5765	5765	——*	12.8	.26

*no cooling required

As can be seen, cryogenic operation results in a large increase in Reynolds number. However, the flow rate of liquid nitrogen is relatively high, comprising about 44 percent of the total mass flow through the test section at the lowest temperature.

As an example of some of the changes to tunnel design that would result from cryogenic operation, a comparison can be made between a normal-temperature blowdown tunnel and an equivalent fully cryogenic tunnel operating at the same Reynolds number, stagnation pressure (2.7 atmospheres) and Mach number (M = 1.0). The test section of the cryogenic tunnel would be only 25 percent of the size of that for the normal tunnel, and when operating from the same size air storage bottles the cryogenic tunnel could run over 17 times as long.

5.5 The Cryogenic Induced-Flow Tunnel.

The cryogenic mode of operation could also be used to advantage with a closed-circuit induced-flow tunnel. In order to maintain a constant test temperature, the temperature of the inducing gas must be cooled to match that of the tunnel circuit.

One method of testing in a cryogenic induced-flow tunnel with air would be to use the same scheme suggested for the cryogenic blowdown tunnel in which air would pass from the high pressure supply through a precooled metal heat exchanger. A second possible method for testing in air would be to evaporate suitable proportions of liquid oxygen and liquid nitrogen within the inducing airstream.

As was the case for the cryogenic blowdown tunnel, the most efficient method of cryogenic operation might well be to use an air-nitrogen mixture resulting from the injection and evaporation of liquid nitrogen in a mixing section between the high pressure air storage and the injector.

Assume that air is delivered to the mixing section at a temperature T_s where the proper amount of liquid nitrogen is combined with the air so that the air-nitrogen mixture reaches the injector at the operating temperature T_t. If the ratio of injector mass flow rate $\dot{m}_i$ to test-section mass flow rate $\dot{m}_{t.s.}$ is χ,

it can be shown in a manner identical to that used for the cryogenic blowdown tunnel that

$$\chi \dot{m}_{t.s.} = \dot{m}_i = \dot{m}_{AIR} + \dot{m}_{LN_2} \qquad \text{---- 5.10}$$

and that

$$\dot{m}_{LN_2} = \frac{\chi \dot{m}_{t.s.} C_p \Delta T}{\beta + C_p \Delta T} \qquad \text{---- 5.11}$$

If the same example were to be used for the injector tunnel as was used in the previous section for the blowdown tunnel, the mass flow rates of AIR and LN_2 would simply be multiplied by the factor χ. Based on results obtained in a pilot transonic injector tunnel recently built at the Langley Research Center, realistic values of χ for Mach one operation range from about 0.17 to 0.20. Thus, for $\chi = 0.2$, the injector mass flow rate would be 20 percent of the test-section mass flow rate and the mass flow rates of AIR and LN_2 required from storage would be only 20 percent of the values needed in the blowdown tunnel. The values of R_c would of course remain unchanged. Therefore, the comments concerning the benefits of cryogenic operation made for the blowdown tunnel apply also to the injector tunnel.

5.6 The Cryogenic Continuous-Flow Fan Driven Tunnel.

When run times greater than those available in intermittent tunnels are required for a particular testing procedure, some form of continuous or semi-continuous tunnel must be used. Also, where the amount of testing is large, the high productivity of a continuous-flow tunnel is essential even for those types of tests capable of being made in intermittent tunnels. As noted in Chapter 1, high

Reynolds number tunnels capable of continuous running at normal temperatures and moderate pressures are large, and thereby costly, and make heavy demands on power. Were economic considerations not dominant, such tunnel would have been chosen for the high Reynolds number application. Because of the large reductions in tunnel size (and thereby cost) and drive power made possibly by operating at cryogenic temperatures, a high Reynolds number continuous-flow fan-driven tunnel, with all of its attendant advantages, now becomes an economically feasible proposition.

As with any wind-tunnel concept, details of tunnel design and operating capability will vary greatly depending upon the main purpose for which a particular tunnel is built. For the purpose of this brief illustration, two possible continuous-flow fan-driven cryogenic tunnels are compared with their non-cryogenic counterparts at the same Reynolds number and Mach number in order to illustrate the impact of cryogenic operation on tunnel size and drive-power requirements.

Low-speed testing (M = 0.35).- At a stagnation pressure of 1 atmosphere, the cryogenic tunnel would be 20 percent of the size and require 2 percent of the drive power of a conventional tunnel.

Sonic testing (M = 1.0).- At a stagnation pressure of 3 atmospheres, the cryogenic tunnel would be 23 percent of the size and require 3 percent of the drive power of a conventional tunnel.

Some experimental work relating to the cryogenic continuous flow fan-driven tunnel is described in Chapters 6 and 7. The anticipated characteristics of large continuous-flow high Reynolds number transonic cryogenic tunnels are given in Chapter 8.

5.7 List of Symbols Used in Chapter 5.

Symbol	Meaning
a	speed of sound
$\bar{c}$	reference chord, 0.1 $\sqrt{\text{Test-section area}}$
C_p	specific heat at constant pressure
L	supply tube length
$\dot{m}$	mass-flow rate
M	free-stream Mach number
M_1	Mach number of gas leaving supply tube during steady run period
P	pressure
$R_{\bar{c}}$	Reynolds number based on $\bar{c}$
t	time of constant stagnation conditions
T	temperature, kelvin
β	cooling thermal capacity of liquid nitrogen
γ	ratio of specific heats
χ	$\dot{m}_i/\dot{m}_{t.s.}$

Subscripts

i	injector
s	initial supply tube conditions or storage conditions
t	stagnation conditions
$t.s.$	test section
AIR	air
LN_2	liquid nitrogen

6. The Low-Speed Cryogenic Tunnel.

Contents:

6.1 Introduction.

The reduction in tunnel cost which is implied by the reduction in tunnel size and power requirements with cryogenic operation coupled with the advantages of lower operating pressures, convenience, and high productivity, has prompted further consideration of the closed-circuit continuous-flow fan-driven cryogenic tunnel for the attainment of high Reynolds numbers. Two closed-circuit continuous-flow fan-driven cryogenic tunnels have been constructed at the NASA Langley Research Center in order to investigate practical aspects of the cryogenic concept.

The first tunnel was a very simple atmospheric low-speed tunnel designed to demonstrate in incompressible flow that cryogenic operation was feasible. Adaption of an existing low-speed tunnel began in November of 1971 with initial operation in January of 1972. Testing with the low-speed tunnel continued through August of 1972 at which time it was decided to extend the experimental work to transonic speeds. A description of the transonic cryogenic tunnel experiment is given in Chapter 7.

6.2 Description of the Low-Speed Tunnel and General Operating Characteristics.

The low-speed tunnel was a single-return fan-driven tunnel with a 17.8 cm × 27.9 cm (7" x 11") closed-throat test section. The atmospheric tunnel could be operated at Mach number from near zero to 0.2 over a temperature range from 333K (+140°F) to 80K (-316°F). The low-speed tunnel was adapted from an existing 1/24 - scale model of the Langley V/STOL tunnel and was therefore aerodynamically representative of modern low-speed tunnel practice.

A sketch of the low-speed tunnel circuit is shown in Figure 6.1. A photograph of the tunnel being insulated is shown in Figure 6.2 and a photograph of the insulated tunnel and test apparatus is shown in Figure 6.3. Materials of construction included wood, plywood, plexiglas, mild and stainless steels, aluminum, brass, copper, and fiberglas reinforced plastic. The fan blades were made of laminated wood.

Viewing ports were provided to allow inspection of key areas of the tunnel circuit including the test section, spray zones, corner vanes, screen section, and contraction section. The viewing ports consisted of either 3 or 4 layers of plexiglas separated by air gaps. Thermal insulation for the remainder of the circuit was a 7.6 cm to 10.2 cm (3" to 4") layer of expanded styrofoam applied to the outside of the tunnel structure with a 0.0127 cm (.005 inch) thick polyethylene vapor barrier on the outside. Some details of a typical section of insulation and a typical viewing port are shown in Figure 6.4.

The expanded styrofoam thermal insulation proved adequate and kept the outside of the tunnel warm and dry even in areas of minimum thickness (7.6 cm). The viewing ports as originally designed consisted of only two layers of plexiglas and would fog

over after a few minutes of tunnel operation at cryogenic temperatures. A second design added a third piece of plexiglas and allowed a continuous flow of ambient temperature nitrogen between the two outer layers. While this approach proved satisfactory for the smaller viewing ports, a very high nitrogen flow rate was needed to keep the larger viewing ports clear for even 5 or 10 minutes of cryogenic operation. The final design, illustrated in Figure 6.4, consisted of 4 layers of plexiglas separated by "air" gaps. This system, which was completely passive in that no ambient temperature nitrogen was used, allowed clear viewing even after as much as an hour of cryogenic operation except under very humid room air conditions when moisture would condense on the outer plexiglas surface.

Prior to cooling the tunnel it was necessary to remove any moisture from the tunnel circuit in order to avoid the formation of frost on the model and those parts of the tunnel which cooled down first such as the screens and turning vanes. Most of the moisture was removed during a pre-run purging of the tunnel at ambient temperature. The drive fan was used during the pre-run purge to keep a slight circulation in the tunnel while gaseous nitrogen was injected into the tunnel. The nitrogen gas displaced the oxygen, water vapor, and other gases which were exhausted along with the excess nitrogen gas to the atmosphere through a duct leading from the tunnel circuit. The test gas was therefore nitrogen. Any moisture remaining in the circuit was removed by freezing it out of the stream on a cryopanel located against the tunnel wall in the low-speed end of the return leg of the circuit. The cryopanel was a 0.28 square meter (3.0 square feet) sheet of copper to which was brazed a coil of 1.27 cm (0.5 inch) diameter copper tubing. By passing liquid nitrogen through the tubing, the temperature of the cryopanel was held near 77K (-320°F) which caused any moisture in the

tunnel circuit to condense and remain on the cryopanel as frost.

The tunnel was cooled and the heat of compression added to the stream by the drive fan was removed by spraying liquid nitrogen at about 77K (-320°F) directly into the tunnel circuit in either of the two locations shown in Figure 6.1. Complete evaporation of the liquid nitrogen was achieved down to the lowest temperature explored of 80K (-316°F).

The liquid nitrogen was injected into the tunnel circuit through very simple spray bars consisting of copper pipes with narrow slots as sketched in Figure 6.5. The liquid pressure was measured near the spray bars. The differential injection pressure ranged from near zero at the low flow rates to about 0.70 atmospheres at the high flow rates.

The rate of cooling of the tunnel circuit was such that, for example, a temperature of 116K (-250°F) could be stabilized within 10 minutes of the initiation of cooling from room temperature. The tunnel was operated at temperatures from 333K (+140°F) to 80K (-316°F). The lower temperature is very close to the saturation temperature of nitrogen of 77.4K (-320.4°F) at 1 atmosphere. At 80K the Reynolds number is increased by a factor of about 7 over that achieved at normal tunnel temperatures and the same Mach number. Approximately 40 hours of tunnel operation was at cryogenic temperatures, that is, below 172K (-150°F). At the reference station in the test section the test temperature was held to within about ± 1 K (± 2°F) by automatic on-off control of one or more of the nitrogen injection nozzles. Much closer temperature control was achieved by injecting a slight excess of liquid nitrogen and establishing temperature equilibrium at the desired test temperature by modulating the heat input from a simple wire-grid electrical heater which was built into the tunnel in the low-speed end of the return leg of the

circuit. Using this technique, test temperatures within about ± 0.2K (± 0.4°F) of the mean could be maintained.

The gas temperature in the test section was measured with a aspirated copper constantan thermocouple probe. The probe was mounted such that it could be traversed and sample along a horizontal line passing across the test section and through its centerline. The thermocouple and its recording meter were carefully calibrated at the tunnel site between room temperature and liquid nitrogen temperature and could resolve about 0.2K at liquid nitrogen temperature. With this system it was not possible to detect any temperature variation across the test section at any operating temperature.

The tunnel was instrumented to measure temperatures and pressures around the circuit, dew point (or frost point) of the test gas, oxygen content of the test gas, and drive motor speed and power.

6.3 Experimental Results.

6.3.1 Drive power and fan speed

The low-speed tunnel was powered by a water-jacketed fan motor which was mounted in a nacelle in the return leg of the circuit. The fan motor was rated at 10 horsepower but due to frequency limitations of the generating system which powered the fan motor, the maximum power was limited to about 2.46kW (3.3 horsepower).

No practical problems were encountered with the drive motor or fan blades. The theoretical variation of drive power with increase of Reynolds number above the value at room temperature for constant Mach number is shown in Figure 6.6 for three methods of increasing Reynolds number. Shown also are the measured power variations taken with nitrogen in the cryogenic tunnel at $M_\infty \approx 0.1$. The different coefficients of expansion of the materials used to build the low-speed tunnel caused gaps to open up around the tunnel circuit

as the operating temperature was reduced. At the lowest operating temperatures many of the gaps were as wide as 1.27 cm (0.5 inch). The additional circuit losses caused by these gaps are thought to have caused the measured values of drive power to be greater than the predicted values.

The velocities of the gas around the circuit are a function of test section Mach number and temperature. Fan rotational speed is roughly proportional to gas velocity, and at a particular Mach number the gas velocity is proportional to the speed of sound which in turn is proportional to the square-root of the gas temperature. The theoretical and measured variation of fan speed with M and temperature are shown in Figure 6.7. The fan speed varied roughly as predicted by theory, that is, proportional to M at constant temperature and proportional to the square root of temperature at constant Mach number. The higher than theoretically predicted fan speeds observed at lower temperatures might also have been caused by demands for higher values of drive power and fan pressure ratio caused by the gaps which opened up around the tunnel circuit at the lower operating temperatures.

6.3.2 Boundary layer experiment

An experiment was devised to demonstrate the changes of Reynolds number that accompany changes of conditions in the test section. Clearly an aerodynamic experiment was required in which there would be a change in some measurable aerodynamic parameter solely due to change of Reynolds number. Further, the change in the measured parameter should be reasonably sensitive to and vary predictably with Reynolds number. It was decided to install a simple boundary-layer experiment in which the variation of a measure of boundary layer thickness with Reynolds number would be compared with theory. It was decided to make measurements in a laminar boundary layer since

boundary layer thickness, δ, varies as $R_x^{-1/2}$ for a laminar boundary layer but only approximately as $R_x^{-1/5}$ for a turbulent boundary layer.

A small diameter pitot-tube (.0330 cm o.d. and 0.0165 cm i.d.) was mounted as a Preston tube against a flat plate in the test section. The pitot-tube was mounted at a fixed position 3.261 cm (1.284") from the rounded leading edge of the plate. The longitudinal location of the pitot-tube was such that it would lie in the laminar portion of the boundary layer over a wide range of conditions in the test section. A sketch of the experimental arrangement is shown in Figure 6.8.

In the tunnel, Reynolds number was varied by temperature or by M_∞. Changes in the ratio of the dynamic head at the pitot-tube to the free-stream dynamic head indicate changes in boundary layer thickness and Reynolds number. The zero pressure gradient form of the Pohlhausen laminar boundary layer velocity profile was adopted in order to allow a curve to be fitted to data taken with the tunnel running warm which eliminated the need to estimate effective values for x and y from the geometry of the plate and pitot tube. The form is

$$\frac{u}{u_\infty} = 2\,\frac{y}{\delta}\left[1 - (y/\delta)^2 + \frac{1}{2}\,(y/\delta)^3\right] \qquad \text{—— 6.1}$$

where y = height above surface

u = local velocity in boundary layer at height y

u_∞ = free-stream velocity

and δ = total thickness of boundary layer

$$= \frac{cx}{\sqrt{R_x}} \qquad \text{—— 6.2}$$

where c = constant

x = distance from surface leading edge

$$R_x = \frac{\rho u_\infty x}{\mu} \qquad \text{---- 6.3}$$

The whole of the tests were carried out at low Mach number, hence we may write

$$q/q_\infty = Q = \left(\frac{u}{u_\infty}\right)^2 \qquad \text{---- 6.4}$$

where q = dynamic head in boundary layer

q_∞ = free-stream dynamic head

From equation 6.1,

$$Q = 4(y/\delta)^2\left[1 - 2(y/\delta)^2 + (y/\delta)^3 + (y/\delta)^4 - (y/\delta)^5 + \frac{1}{4}(y/\delta)^6\right] \qquad \text{---- 6.5}$$

where from equation 6.2

$$\frac{y}{\delta} = \frac{y\sqrt{R_x}}{cx} = \frac{y}{c}\left(\frac{\rho M\, a}{\mu x}\right)^{1/2}$$

In this equation, y, c, x are constants. For constant test conditions of pressure and temperature, ρ, a, and μ are also constant. Hence we may write

$$\frac{y}{\delta} \propto \sqrt{M}$$

If the constant of proportionality is $\sqrt{\frac{k}{4}}$, where k is a new dimensionless constant, then equation 6.5 may be rewritten

$$Q = kM\left[1 - \frac{kM}{2} + \left(\frac{kM}{4}\right)^{1.5} + \left(\frac{kM}{4}\right)^{2} - \left(\frac{kM}{4}\right)^{2.5} + \frac{1}{4}\left(\frac{kM}{4}\right)^{3}\right] \quad \text{—— 6.6}$$

At low Mach numbers, such that $kM \ll 1$,

$$Q = kM \quad \text{—— 6.7}$$

allowing the constant k to be determined very simply from a measurement of the ratio of dynamic heads Q and Mach number. Since, from equation 6.7 the slope of the $Q - M$ curve at the origin is k, a value for k may be obtained conveniently from a measurement of the slope.

Test data is shown in Figure 6.9. The data taken at a stagnation temperature of 322K has a slope of $k = \left(\frac{dQ}{dM}\right)_{M=0} = 2.57$. The line through the test data at a stagnation temperature of 322K is calculated from equation 6.6 with this value of k.

From equations 6.2 and 6.5 it can be seen that for a fixed geometry of experiment the ratio q/q_∞ is simply a function of Reynolds number. Therefore there is a unique relationship between $Q = q/q_\infty$ and either R_x or unit Reynolds number, independent of test temperature and Mach number provided that the flow can be treated as incompressible. Values of unit Reynolds number are tabulated below with corresponding values of Q for the geometry of this experiment. A unit Reynolds number scale is shown as an alternate ordinate on Figure 6.9.

$\frac{\text{Reynolds no. per meter}}{10^6}$	1	2	3	4
$Q = q/q_\infty$	0.1182	0.2239	0.3186	0.4031

The Mach number required to achieve a particular Reynolds number reduces with temperature. This can be seen by re-writing equation 2.2 for flow at low Mach number where $P \rightarrow P_t$ and $T \rightarrow T_t$:

$$R = \frac{P_t M \ell}{\mu} \sqrt{\frac{m\gamma}{RT_t}}$$

For testing in a particular gas at constant P_t and T_t, unit Reynolds number

$$\frac{R}{\ell} \propto \frac{M}{\mu\sqrt{T_t}} \qquad \text{---- 6.8}$$

Viscosity, μ, varies almost linearly with temperature and it is clear therefore from equation 6.8 that in order to hold a fixed value of Reynolds number the test Mach number must be reduced with temperature. Further measurements were made with this simple equipment at test temperatures of 227.6K (-50°F), 144.3K (-200°F), and 95.9K (-287°F). At these temperatures, test Reynolds number is raised above the value of 322K, at the same Mach number, by the factors 1.569, 2.950, and 5.350 respectively. Therefore, to achieve the same Reynolds number (and the same boundary layer thickness and Q) the test Mach number must be reduced by the above factors. The curves on Figure 6.9 corresponding to the reduced-temperature test conditions were obtained in this way.

The experimental data at 227.6K is in good agreement with the theoretical curve, and the data at the two lower temperatures are in fair agreement. The experimental data was a confirmation of the magnitude of the theoretical predictions of the increase of Reynolds number with M_∞ at constant temperature, but, more importantly a first experimental confirmation of the increases

of Reynolds number with decreasing temperature at constant M_∞.

6.3.3 Strain-gage balance experiment

In order to determine if conventional techniques might be used to make force and moment measurements at cryogenic temperatures, a 11.4 cm (4.5") span sharp leading edge 74° delta-wing model was tested on an existing water-jacketed strain-gage balance in the cryogenic tunnel. Since the purpose of this test was to investigate any possible adverse effects of temperature on the measuring techniques rather than the effects of Reynolds number on the model, a sharp leading-edge 74° delta-wing model was chosen since it is known that, except for the usual effects of friction drag, the aerodynamic characteristics of this shape are relatively insensitive to Reynolds number. A sketch of the model is shown in Figure 6.10 and a photograph of the model, balance, and supporting sting is presented in Figure 6.11. The strain-gage elements of the balance were heated and insulated from the cryogenic environment by a water jacket through which was circulated water at approximately 294K (+70°F). A quadrant allowed model incidence to be changed from -4° to +22°. A sketch of the model support mechanism is shown in Figure 6.12.

Some of the aerodynamic test results are presented in Figure 6.13 as the variation of C_m, C_L, and C_D with α for various test conditions. As can be seen, there is good agreement between the data obtained at stagnation temperatures from 322K (+120°F) to 111K (-260°F). Based on the results of these tests there appear to be no fundamental or practical difficulties in obtaining force and moment data in a cryogenic tunnel using conventional strain-gage balance techniques.

6.4 Conclusions from the Low-Speed Tunnel Testing.

A summary of the conslusions is:

1. Cooling with liquid nitrogen is practical. Rapid cool-down rates may be achieved. Following purging of the tunnel circuit with dry nitrogen before cool-down, the gas stream in the test section remains clear and free from frost. Liquid nitrogen completely evaporates even at test temperatures close to the liquid temperature. The test temperature can be controlled with acceptable limits either manually or automatically. The temperature distribution in the test section is satisfactory.
2. Satisfactory insulation techniques exist. The outside of the tunnel may be held above the dew point of room air with a thickness of about 7.6 cm of styrofoam. Viewing ports are easily constructed and maintained clear.
3. A fan-driven tunnel is satisfactory at cryogenic temperatures. Drive power and fan speed vary with temperature in accordance with simple theory.
4. Pressure measurements may be made at cryogenic temperatures. Quite satisfactory results are obtained by locating the pressure transducer outside the tunnel at ambient temperature and connecting the transducer to the sensor in the circuit by a short length of tubing.
5. There is good agreement between theoretical predictions and experimental measurements of the development of laminar boundary layers at cryogenic temperatures.
6. Conventional strain-gage balances can be used for model testing. A satisfactory arrangement is to maintain the strain-gage balance at ambient temperatures by heating.

6.5 List of Symbols Used in Chapter 6.

Symbol	Meaning
a	speed of sound
C_D	drag coefficient, $\frac{\text{Drag}}{q_\infty S}$
C_L	lift coefficient, $\frac{\text{Lift}}{q_\infty S}$
C_m	pitching-moment coefficient, $\frac{\text{Pitching moment}}{q_\infty S\bar{c}}$
c	constant
$\bar{c}$	reference chord
k	constant
ℓ	linear dimension
M	free-stream Mach number
P	pressure
q	dynamic pressure
Q	q/q_∞
R	Reynolds number
$\mathfrak{R}$	universal gas constant
S	reference area
T	temperature
u	local velocity in boundary layer at height y
u_∞	free-stream velocity
x	distance from leading edge of flat plate
y	height above surface of flat plate
α	angle of incidence
γ	ratio of specific heats
δ	total thickness of boundary layer
μ	viscosity
ρ	density

Subscripts

t	stagnation conditions
x	based on x
∞	free-stream conditions

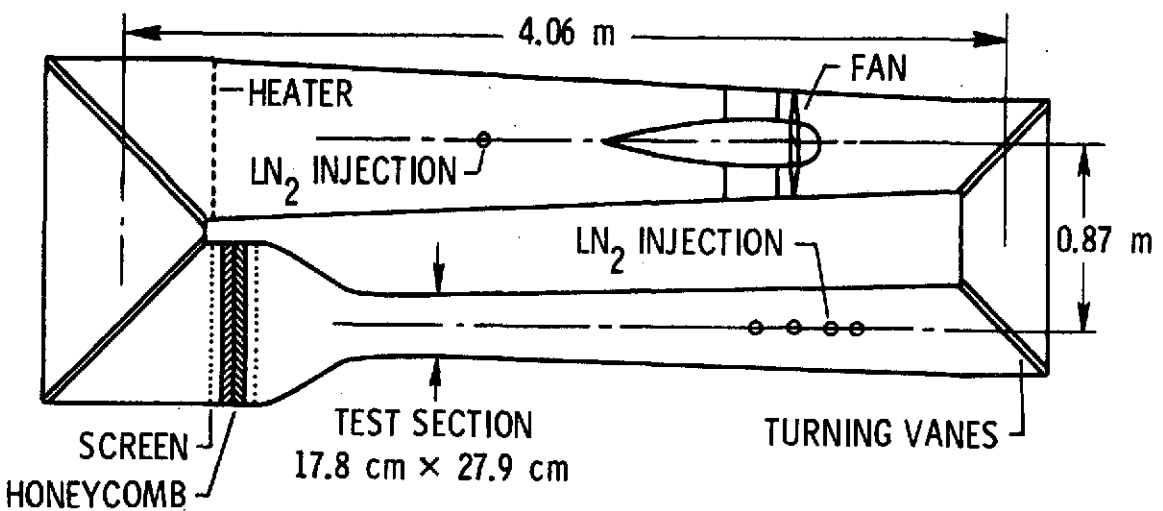

Figure 6.1 Low-speed cryogenic tunnel circuit.

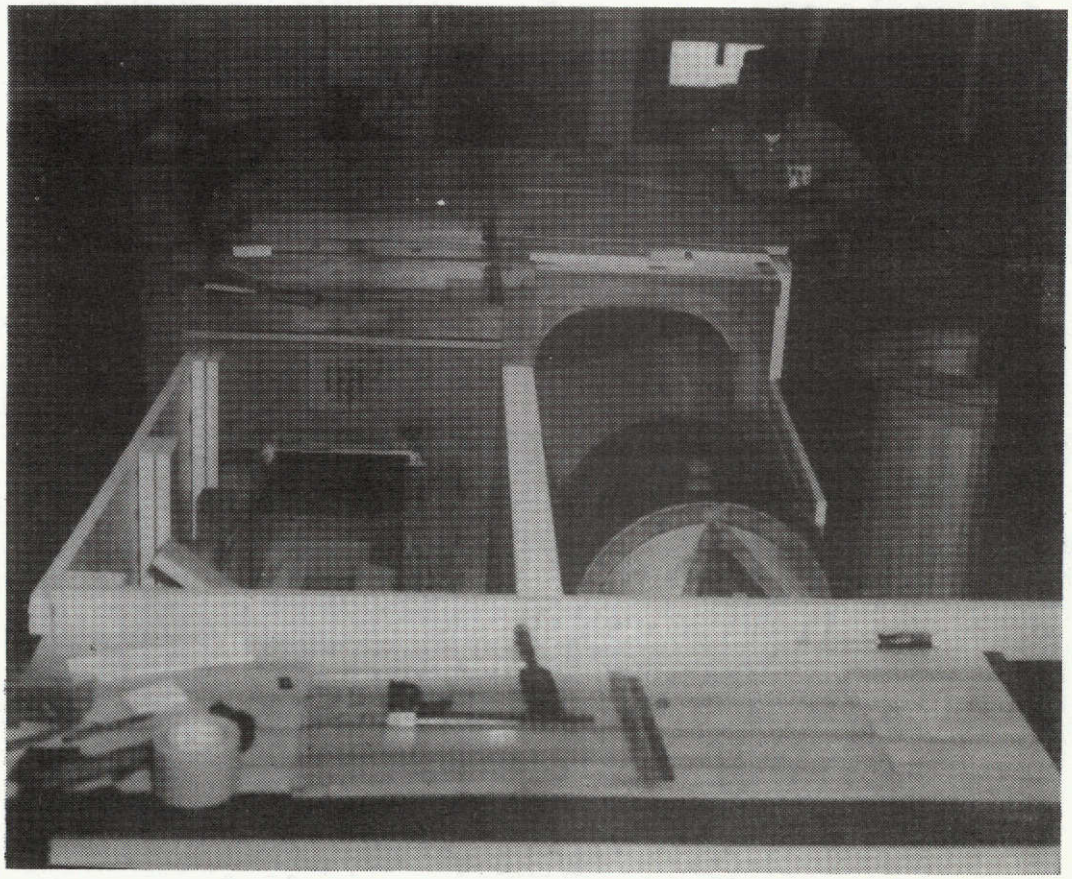

Figure 6.2 Low-speed tunnel being insulated.

Figure 6.3 Insulated low-speed tunnel and test apparatus.

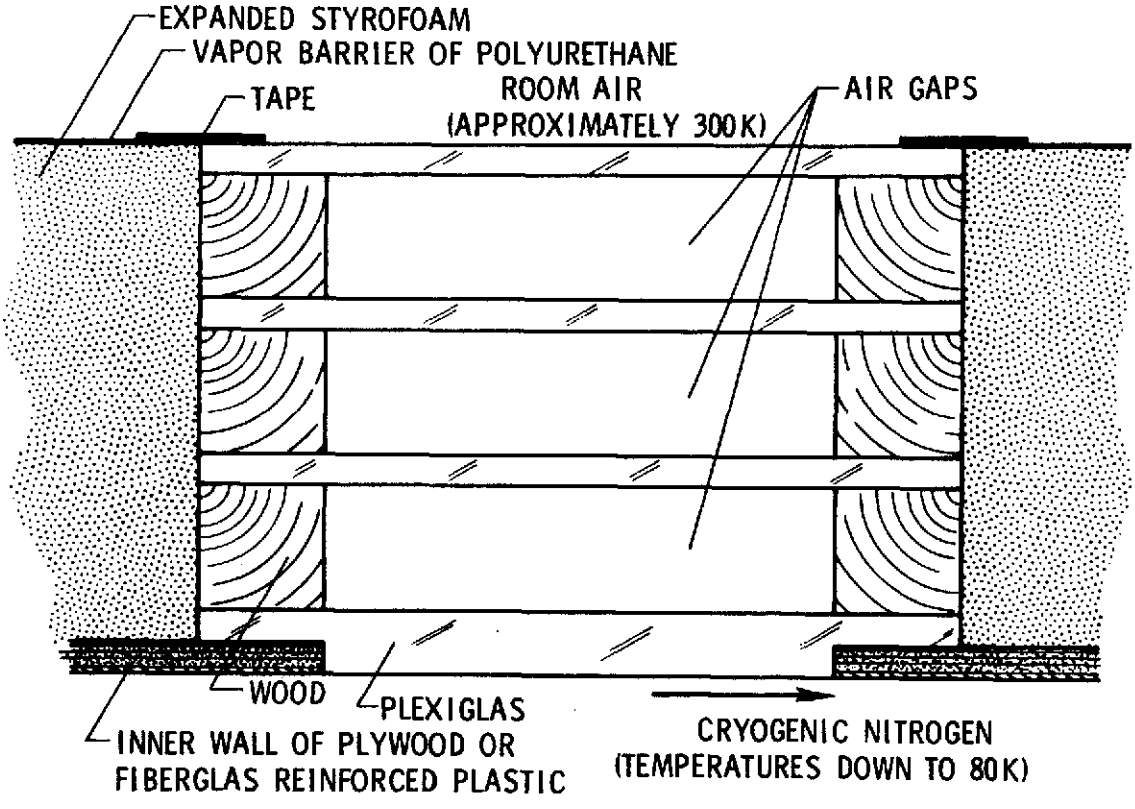

Figure 6.4 Sketch of typical section of insulation and viewing port.

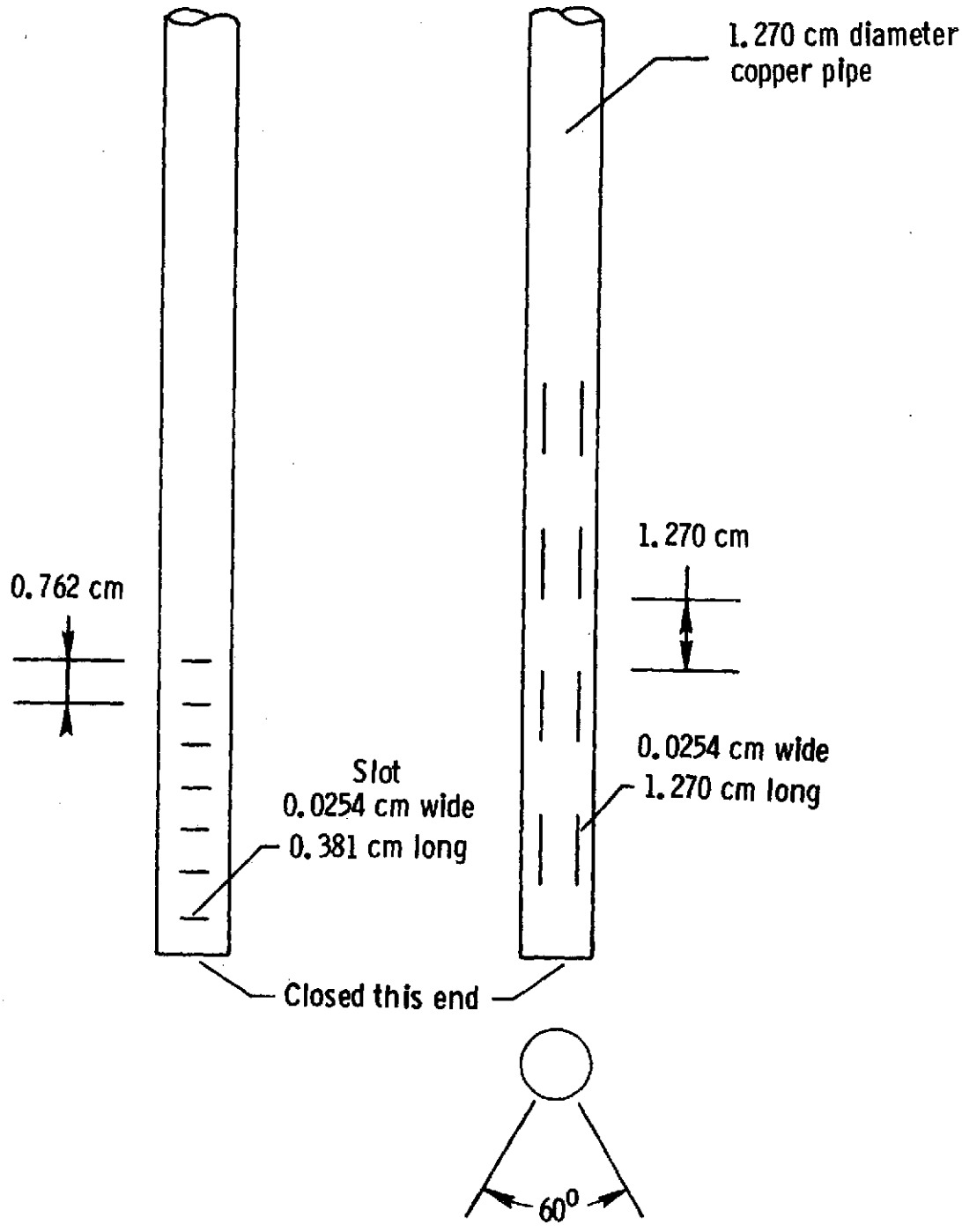

Figure 6.5 Liquid nitrogen injection spray bars.

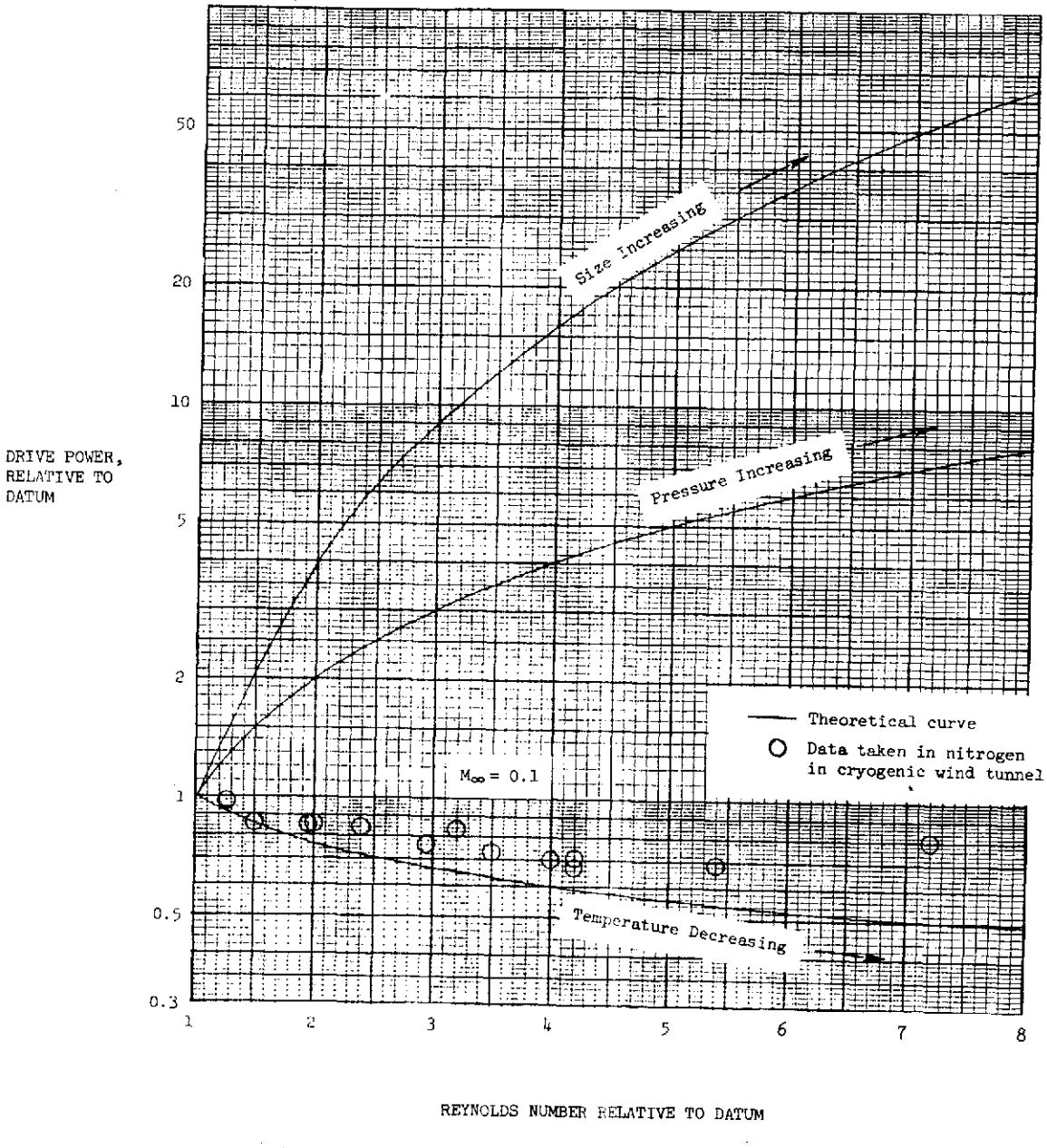

Figure 6.6 Theoretical variation of drive power for three methods of increasing Reynolds number and measured variation of drive power for low-speed cryogenic tunnel.

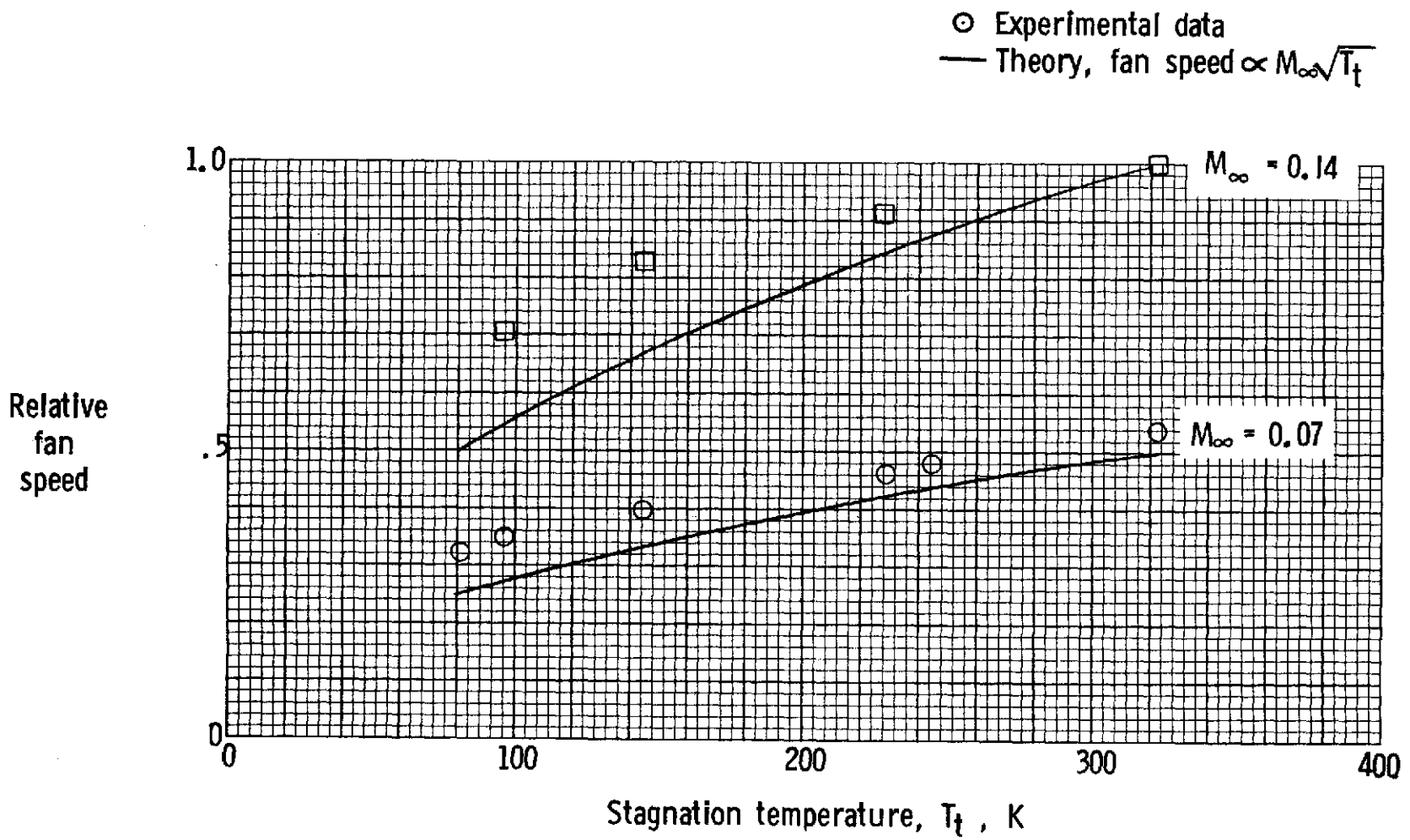

Figure 6.7 Theoretical and measured variation of fan speed relative to maximum fan speed with stagnation temperature in low-speed cryogenic tunnel.

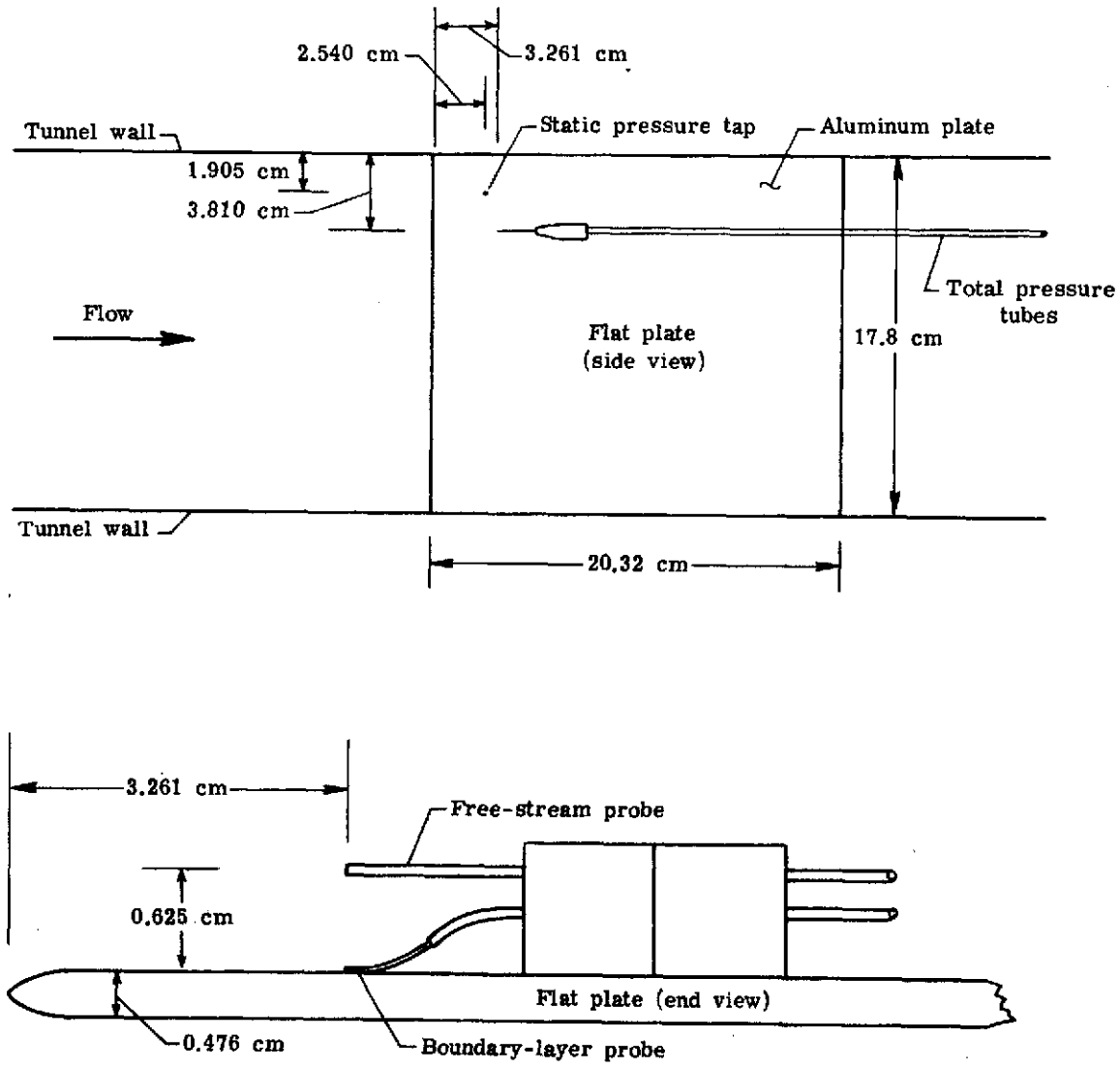

Figure 6.8 Sketch of plate and probes used in boundary-layer experiment.

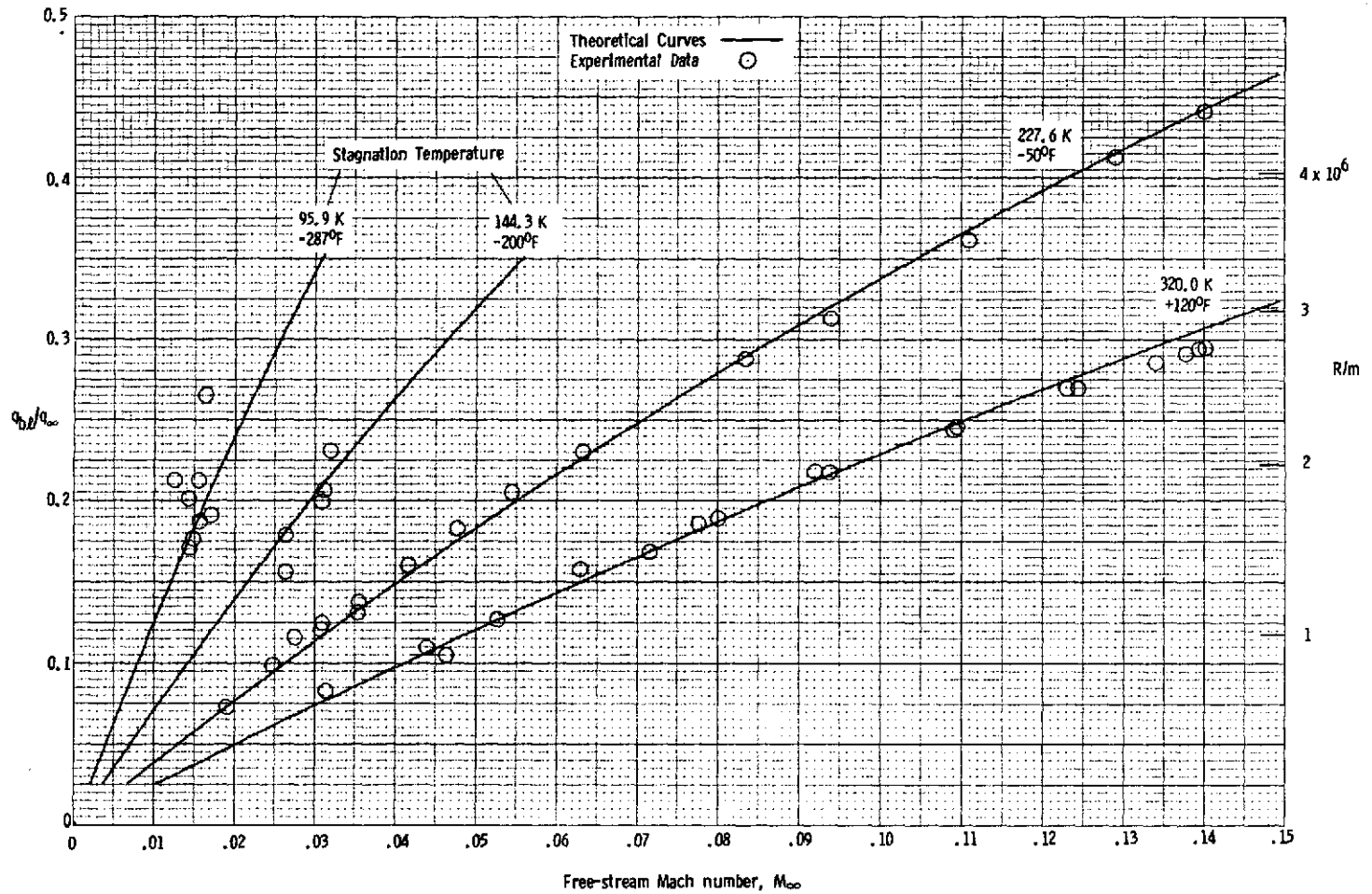

Figure 6.9 Theoretical and measured variation of the ratio of dynamic pressure in a laminar boundary layer to free-stream dynamic pressure as a function of Mach number and stagnation temperature.

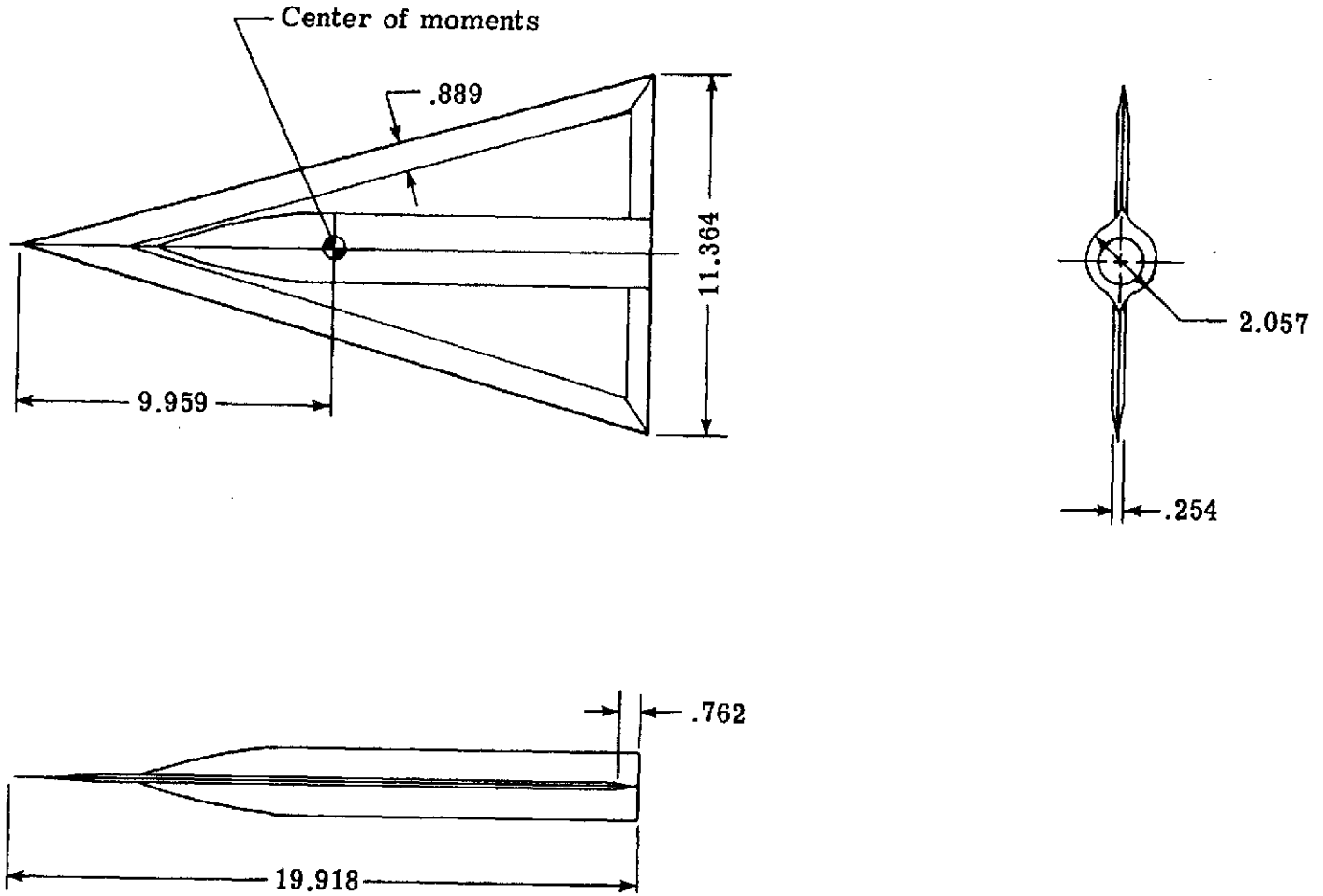

Figure 6.10 74° delta-wing model tested in low-speed cryogenic tunnel. Dimensions in centimeters.

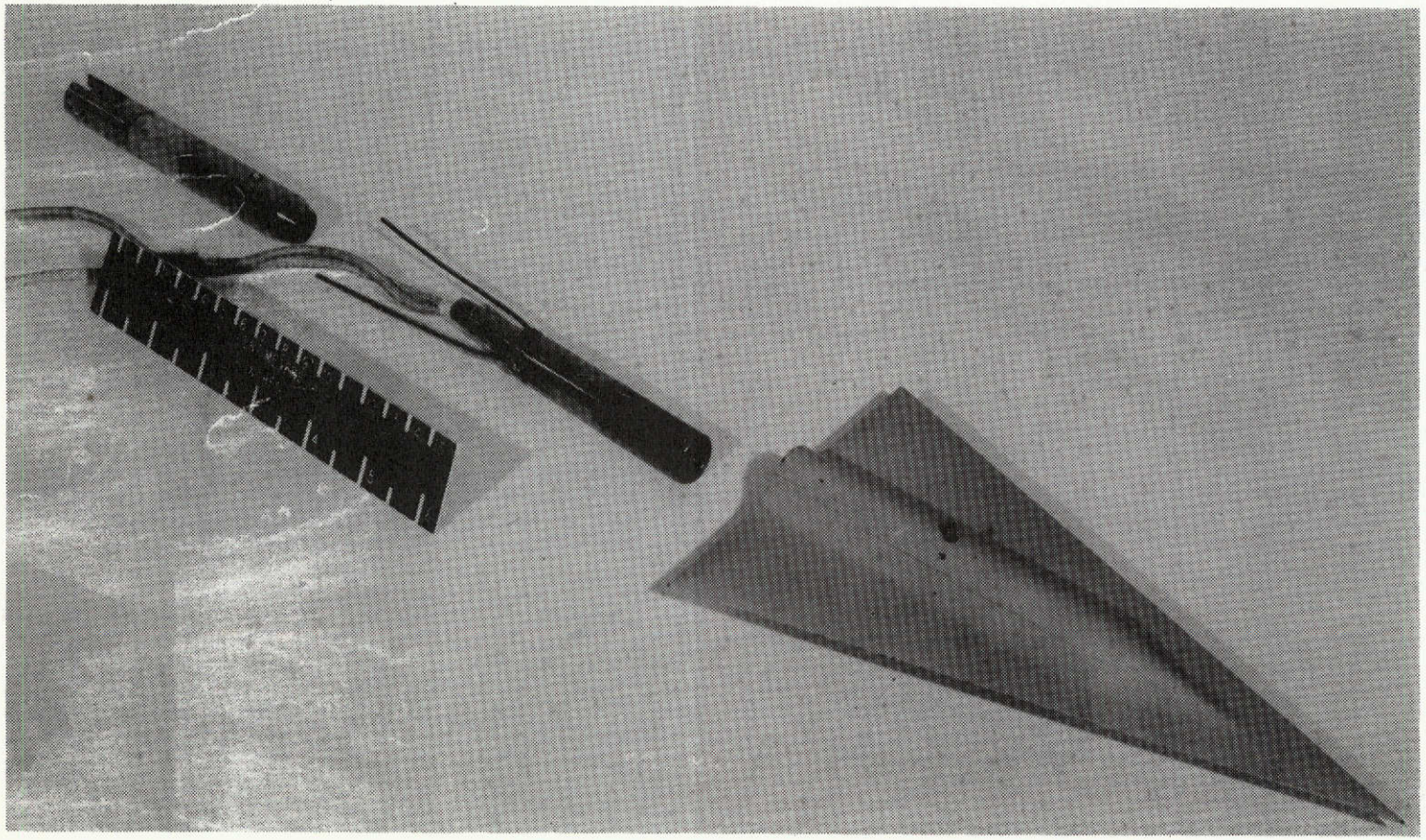

Figure 6.11 74° delta-wing model, strain-gage balance, and supporting sting.

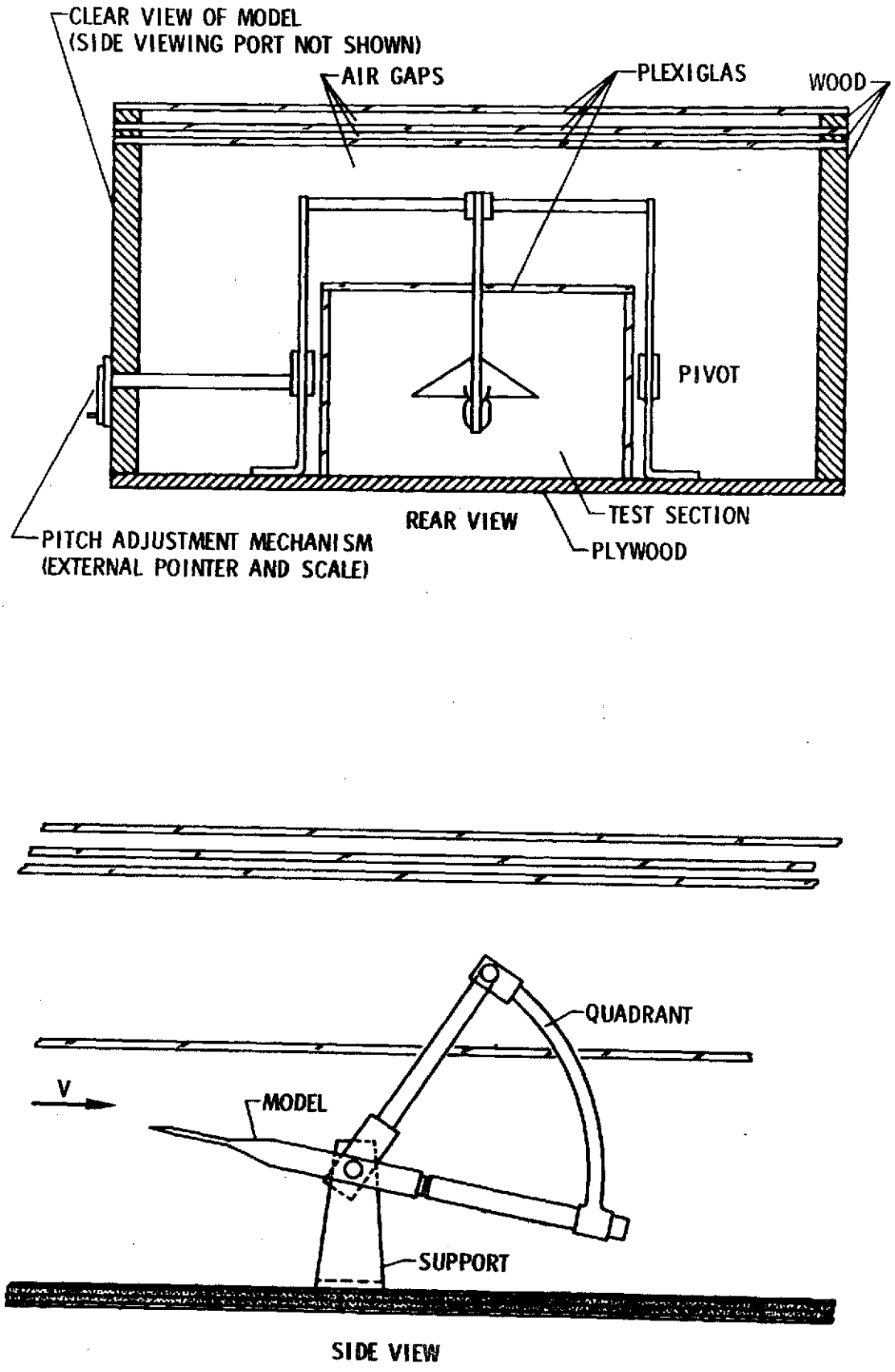

Figure 6.12 Model support mechanism used in low-speed cryogenic tunnel.

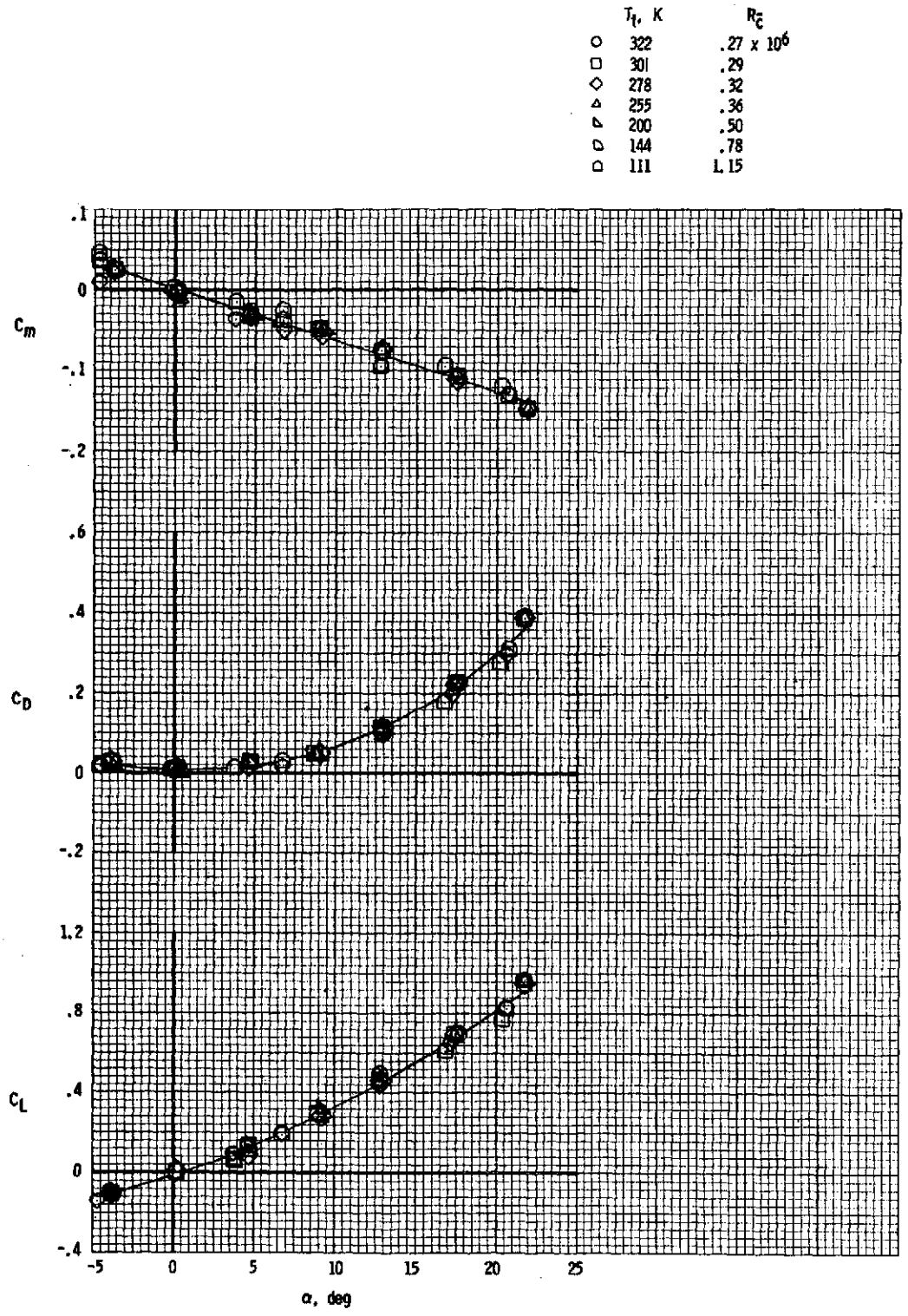

Figure 6.13 Aerodynamic data obtained in low-speed cryogenic tunnel on sharp-leading-edge 74° delta-wing model.

7. The Transonic Cryogenic Tunnel.

7.1 Introduction.

Following the completion of the low-speed cryogenic tunnel experiment in the summer of 1972, it was decided to extend the experimental work to transonic speeds. After some deliberation on how best to proceed, it was decided that a continuous-flow fan-driven pressure tunnel would provide the most flexible tool for the exploration of this application of cryogenic principles. The purpose of the transonic cryogenic pressure tunnel is to demonstrate in compressible flow that Reynolds number dependent aerodynamic phenomena behave in the same manner when a given Reynolds number is obtained by temperature as when obtained by pressure; to demonstrate at high power levels the method of cooling; to determine any limitations imposed by liquefaction of the test gas; to verify engineering concepts with a realistic tunnel configuration; and to provide operational experience. Design of the transonic tunnel began in December of 1972 with initial operation in September of 1973.

7.2 Description of the Transonic Tunnel and Ancillary Equipment.

The Pilot Transonic Cyrogenic Tunnel has been constructed at NASA Langley Research Center and is a single-return fan-driven tunnel with a slotted octagonal test section 34.3 cm (13.5") across flats. The tunnel can be operated at Mach numbers from near 0.05 to about 1.3 at stagnation pressures from slightly greater than 1 atmosphere to 5 atmospheres over a temperature range from 340K to about 77K (+152°F to about -320°F). The ranges of pressure and temperature provide the opportunity of investigating Reynolds number effects by temperature and pressure independently over almost a 5 to 1 range of Reynolds number.

A sketch of the tunnel circuit is shown in Figure 7.1 and a photograph of the tunnel taken during final assembly is shown in Figure 7.2. A more detailed description of the Transonic Tunnel is given in the sections which follow.

7.2.1 Materials of construction.

The tunnel pressure shell is constructed of 0.635 and 1.270 cm (0.25 and 0.50 inch) thick plates of 6061-T6 aluminum alloy. The flanges used to join the various sections of the tunnel were machined from plates of this same material. The bolts for the flanges are made from 2024-T4 aluminum alloy. These particular aluminum alloys were selected because they have good mechanical characteristics at cryogenic as well as ambient temperatures and could easily be fabricated using equipment and techniques available at Langley.

The flange joints, depending upon size, are sealed with either a flat gasket or a teflon coated hollow metal "o"-ring. Several different types of seals were tested at pressure under both ambient and cryogenic conditions to determine their suitability for use with the cryogenic tunnel. Because of its reusability, the flat

gasket seal, made from a mixture of teflon resin and pulverized glass fiber, was selected as the best seal overall. However, since gasket material was not available in widths sufficient to make gaskets for the largest flanges, a teflon coated hollow "o"-ring of 321 stainless steel is used at each of the three largest flanges. Sketches of typical flange joints are shown in Figure 7.3.

7.2.2 Tunnel support system

The tunnel supports shown in Figure 7.1 are constructed in two parts. The upper portion of each support, which might be cooled to very low temperatures, is made from 347 stainless steel. The lower portion, which is never subjected to low temperatures, is made of A-36 carbon steel.

The 3200kg (7050 lbm) tunnel is mounted on the four "A"-frame support stands shown in Figure 7.1, one of which is a "tunnel anchor" support designed so that the center of the fan hub keeps a fixed position relative to the drive motor. Thermal expansion and contraction of the tunnel results in a change in overall tunnel length of about 4.0cm (1.57") between extremes in operating temperature. Sliding pads at each of the tunnel support attachments allow free thermal expansion or contraction of the tunnel structure. The sliding surfaces consist of 2.54cm (1 inch) thick teflon sheets placed between the support attachments on the tunnel and the stainless steel blocks mounted on the upper portion of the carbon steel "A"-frame stands. Vertical and lateral movement at each joint is constrained by bolts passing through the tunnel support attachment and the teflon sheet into the "A"-frame. The tunnel support attachments are slotted in the longitudinal direction to allow free longitudinal expansion or contraction of the tunnel. A sketch of the tunnel anchor support is shown in Figure 7.4.

The object of the anchor support is to hold the centerline of the tunnel at this support in a fixed position relative to the ground in the presence of relatively large amounts of thermal expansion. The undersides of all of the tunnel support attachments, including those at the anchor point, are on the horizontal plane through the axis of the return leg of the tunnel. With symmetrical expansion the tunnel centerline is held at a fixed height above the ground. A fork on the tunnel underside at the anchor point, shown on Figure 7.4, additionally prevents lateral or axial movement of the tunnel at this station. In this way the axis at the anchor point is fixed relative to the ground and the tunnel expands and contracts symmetrically about this point on the axis. Since the fan and tunnel are both manufactured from aluminum, thermal expansion does not materially affect the tip clearance of the fan or generate any misalignment between the axis of the fan and the externally mounted drive motor. This support scheme has proved to be entirely adequate and no problems have been encountered.

7.2.3 Thermal insulation

Thermal insulation for most of the tunnel circuit consists of 12.7cm (5") of blown urethane foam applied to the outside of the tunnel structure with a fiberglas reinforced polyester vapor barrier on the outside. A sketch showing a typical section of the thermal insulation and the method used to insulate the flanges is presented in Figure 7.5. As can be seen in Figure 7.5 the urethane foam is not bonded directly to the aluminum tunnel wall but rather is separated from the wall by a shear layer consisting of two layers of fiberglas cloth. This allows the differential expansion between the aluminum and urethane foam to take place without causing the foam to fracture. In addition, the insulation is applied in two layers separated by a layer of fiberglas cloth. Again, the purpose of the fiberglas shear

layer within the insulation is to allow differential expansion to take place within the urethane foam insulation itself without fracture. This insulation has proved adequate and keeps the outside of the tunnel warm and dry under all operating conditions even during periods of high humidity.

7.2.4 Viewing and lighting ports

Seven ports are provided to allow illumination and visual inspection of the interior of the tunnel in the plenum and test-section areas and the nitrogen injection regions. A sketch of one of the ports showing details of construction is shown in Figure 7.6. Each of the ports consists of a 3.56cm (1.4") diameter glass window (VARIAN Model 954-5127) which is designed to take the maximum differential pressure of 4 atmospheres at cryogenic temperatures. To provide protection against possible window failure and to provide thermal insulation, two 0.953cm (0.375 inch) thick sheets of clear polycarbonate resin plastic (General Electric "Lexan"), separated by air gaps, are fitted securely over each glass window. Should these sheets of plastic also fail following failure of the glass window, additional protection is provided by a third sheet of plastic fitted as a blast shield to standoff supports on the port assembly such that the shield is not subjected to the tunnel pressure. The tunnel is capable of operating indefinitely at cryogenic temperatures and therefore it is necessary to purge with ambient temperature dry nitrogen between the layers of plastic in order to prevent dew or frost from forming on the outer surface.

It should be noted that there is no fundamental reason for using such small diameter ports. The small size of the present ports was chosen to limit to a harmless level the pressure rise which would occur in the building which houses the tunnel in the event of failure of a glass window with the tunnel operating at maximum pressure and minimum temperature.

The inside of the tunnel is illuminated by directing the collimated output of three small incandescent lamps into the tunnel through three of the ports. A layer of 0.635cm (0.25 inch) thick heat-absorbing glass is placed between the light source and the port to prevent any differential heating of the glass window.

7.2.5 Drive-fan system

The tunnel has a fixed geometry drive-fan system which consists of 7 pre-rotation vanes, and a 12-bladed fan followed by 15 anti-swirl vanes. The photograph presented as Figure 7.7 is a view looking upstream at the fan, and shows the section of the tunnel just downstream of the fan-section which contains the nacelle. The hollow nacelle was cast from 6061-T6 aluminum alloy and then machined on the outside to provide an aerodynamically smooth surface.

The drive fan is powered by a 2.2MW (3000 horsepower) water-cooled synchronous motor with variable frequency speed control. The motor, which is external to the tunnel, is capable of operating at speeds from 600 rpm to slightly less than 7200 rpm. However, at present, operation of the fan/motor system is restricted to speeds below 6200 rpm due to the excitation of resonance in the drive shaft between the motor and the fan at this speed.

7.2.6 Return-leg diffuser and turning vanes

The return-leg diffuser section is shown in the photograph presented as Figure 7.8. Shown in this photograph are two of the liquid nitrogen injection spray bars and two of the ports used for illuminating and viewing the spray bars. As can be seen, no attempt was made to fair the spray bars to reduce their drag. Also shown in Figure 7.8 is the tunnel section containing the 3rd and 4th corners. The turning-vane design shown here is typical of all four corners which have the same 15-vane arithmetic progression spacing design

which has been used successfully in the 8ft x 8ft Supersonic Tunnel at the Royal Aircraft Establishment, Bedford, and which is to be used in the 5 meter Low Speed Tunnel now under construction at RAE, Farnborough.

7.2.7 Screen section

The screen section is shown in the photograph presented as Figure 7.9. The screen design requirement was to provide a turbulence level in the test section of 0.1 percent. Each of the three screens is made from 0.0165cm (0.0065 inch) diameter monel wire woven with approximately 16 openings per centimeter (40 openings per inch). Also shown in Figure 7.9 is the temperature survey rig. This rig is located upstream of the screens and comprises eight arms and a center-support ring which are aerodynamically faired to reduce the possibility of the wake from the rig adversely affecting the flow quality in the test section. (The thermocouple elements were covered with tape when the photograph was taken.)

7.2.8 Contraction section

The contraction section of the transonic tunnel has a 12 to 1 contraction ratio. The contraction section was designed with a smooth distribution of wall curvature with low curvature at both the entrance and exit regions in order to avoid, if possible, boundary layer separation in these two critical regions. In consideration of good lateral velocity distribution, the test-section end of the contraction section was favored in the design to provide sufficient length for very low curvature in this region. The contraction section, shown during construction in the photograph presented as Figure 7.10, is designed so that the transition from the circular cross-section at the downstream end of the screens to the octagonal cross-section of the up-stream end of the test section follows exactly the prescribed longitudinal variation in cross-sectional area. Also, the design is

such that the streamlines near the walls cross only one weld in the critical high velocity region. The circumferential weld was hand finished so that the entire inner surface of the contraction section is aerodynamically smooth. The variation of contraction section area with longitudinal station is given in Table 7.1.

7.2.9 Test section

The slotted-wall octagonal test section is 34.32cm (13.511 inches) across flats and 85.73 cm (33.75 inches) long. The entire test section, including the longitudinal variation of open area, is modeled after the test section evolved for the Langley 16 Foot Transonic Tunnel before that tunnel was equipped with a plenum air removal system. Provision is made for changing the slot configuration and adjusting the wall divergence over a range from zero to 30 minutes of arc. Adjustable re-entry flaps at the downstream end of the slots allow control over the amount of diffuser suction. Some details of test-section design and the initial geometrical settings are shown on Figure 7.11, 7.12, and 7.13 and in Table 7.2. A photograph of the test-section is presented in Figure 7.14. With the initial test-section configuration the maximum test-section Mach number is 1.06. In order to operate above $M_\infty = 1.06$, the tunnel must be operated at pressures sufficiently high to allow gas to be exhausted from the plenum. This is achieved by passing gas from the plenum chamber through pressure regulating valves directly to the atmosphere. Under these conditions, test-section Mach numbers up to about 1.3 can be obtained.

7.2.10 Liquid nitrogen system

A schematic drawing of the liquid nitrogen system is shown in Figure 7.15. Liquid nitrogen is stored at atmospheric pressure in two vacuum insulated tanks having a total capacity of about 30,000 liters (8,000 U.S. gallons). When the tunnel is being operated at less

than about 2.5 atmospheres absolute pressure the liquid can be supplied to the tunnel simply by pressurizing the supply tank with the pressurizing coil shown in Figure 7.15. The liquid nitrogen pump must be used whenever the tunnel is operated at high pressures. When the pump is used, the supply tank is pressurized to about 1.7 atmospheres absolute pressure in order to maintain sufficient net positive suction head at the pump inlet to prevent cavitation. The pump has a capacity of about 500 liters per minute (150 U.S. gal per minute) with a delivery pressure of 9.3 atmospheres absolute, and is driven by a 22.4kW (30 horsepower) constant speed electric motor.

When the pump is used, the liquid nitrogen supply pressure is set and held constant by the pressure control valve, shown in Figure 7.15, which regulates the amount of liquid returned to the storage tank through the pressure-control return line.

The flow rate of liquid nitrogen into the tunnel circuit is regulated by pneumatically operated control valves located outside the tunnel at each of the three injection stations. These valves, which may be used either singly or in combination, can be controlled either manually or automatically. A helium filled constant-volume bulb thermometer located in the settling chamber serves as the temperature sensing element when the valves are being controlled automatically.

Since the transonic tunnel operates over wide ranges of pressure and Mach number it is necessary to allow for a wide range of liquid nitrogen flow rate. This is accomplished by designing the spray bar at each of the injection stations to cover a limited range of flow rates by the proper selection of the number as well as the size of the nozzles used on each spray bar. By operating various combinations of the three spray bars and by changing the liquid nitrogen supply pressure, liquid nitrogen flow rates from 1 to 400 liters per minute (0.25 to to 107 U.S. liquid gallons per minute) are realized.

Originally, ten nozzles having small orifice diameters were used on each of the spray bars at injection stations 2 and 3. These nozzles were prone to become blocked with foreign matter inadvertently (but perhaps inevitably) left in the liquid nitrogen supply system. The twenty original nozzles were replaced with eight nozzles having larger orifice diameters.

The two types of nozzles currently in use are shown in Figure 7.16. Both types are commercial nozzles designed to give a full-cone spray pattern and fine spray particles over a wide range of spraying pressure. Sketches in Figure 7.17 show the type and number of nozzles currently used at each of the injection stations. The flow capacity as a function of the differential pressure across the nozzle is also tabulated on Figure 7.17.

In its present configuration, the liquid nitrogen system has two principal deficiencies. The first of these is the rather lengthy time required to cool the LN_2 supply pipes. The minimum time required to cool the pipe between the LN_2 pump and the injection stations is determined by the rate at which the gas generated during the cooldown process can be vented to the atmosphere through the tunnel exhaust system without damage to turbine flow meters located in the liquid nitrogen supply pipes at each injection station. The minimum supply pipe cooldown time with the present system is 15 minutes. A recirculating loop supply system would greatly reduce this cooldown time and also simplify the control of liquid nitrogen flow rate by eliminating boiling in the pipe during tunnel operation which is also a problem with the present system at very low flow rates.

The second deficiency arises from the fact that a completely pneumatic control system is used with the flow-rate control valves. Automatic control of flow rate and hence tunnel operating

temperature is possible for only a very limited range of conditions due to the very long response time of the pneumatic system.

7.2.11 Nitrogen exhaust system

The system for exhausting gaseous nitrogen from the tunnel is shown schematically in Figure 7.15. Tunnel total pressure is adjusted by means of pneumatically operated control valves in exhaust pipes leading to the atmosphere from the low-speed section of the tunnel. In order to minimize flow disturbance, the exhaust pipes are taken from the low-speed section of 120° intervals just ahead of the 3rd set of turning vanes. The valves may be used either singly or in combination in order to provide fine control over a wide range of exhaust flow rates. A total pressure probe located downstream of the screens provides the reference pressure measurement when tunnel pressure is being controlled automatically.

As originally designed, the nitrogen exhaust from the tunnel vented directly to the atmosphere through pipes carried through the roof of the building housing the tunnel. A severe fogging problem existed with this original design during periods of high humidity and low wind speed. On several occasions it was necessary to suspend operations until there was a favorable change in the weather. A simple and completely effective solution to this problem has been found and consists of an exhaust driven ejector as shown in the sketch in Figure 7.18. The low pressure ejector induces ambient air which dilutes and warms the cold nitrogen exhaust gas. The resulting foggy mixture is propelled high into the air and dissipates completely. No measurements have yet been made to determine the ratio of induced ambient air to exhaust nitrogen gas. However, this simple exhaust ejector, which has an area ratio of about 5:1, induces sufficient ambient air and discharges the mixture so effectively that it has completely eliminated the fogging problem even under the most adverse weather conditions.

As noted in section 7.2.9, in order to operate above $M_\infty = 1.06$, the tunnel must be operated at pressures sufficiently high to allow gas to be exhausted from the plenum chamber to the atmosphere. Manually-controlled pneumatically-actuated valves in three pipes leading to the atmosphere from the plenum allow approximately one percent of the mass flow entering the test section to be exhausted when operating at $M_\infty = 1$ or greater. By using this method, test-section Mach numbers up to about 1.3 can be obtained. The plenum exhaust pipes lead from the plenum at 120° intervals through its upstream wall. The control valves may be used either singly or in combination.

7.2.12 Instrumentation

In addition to special instrumentation required for test-section calibration and special aerodynamic tests, the tunnel is instrumented to measure temperatures and pressures around the circuit, dew point (or frost point) of the test gas, oxygen content of the test gas, pressure of the LN_2 supply, LN_2 flow rate, mass flow rate of the gas exhausting from the stilling section and the plenum chamber, changes in tunnel linear dimension with temperature, fan speed, and torque at the drive motor shaft.

7.3 Operating Procedure.

Many of the operating procedures developed for the low-speed cryogenic tunnel are being used with the transonic tunnel. However, since the transonic tunnel was designed and built purposely for cryogenic operation, the detailed procedures used for purging, cooldown, and running differ from those developed for the low-speed tunnel. A description of the operating procedures currently being used with the transonic tunnel is given in the sections which follow.

7.3.1 Purging

Any moisture in the tunnel circuit is removed by purging with nitrogen gas. With the present liquid nitrogen supply system, described in section 7.2.10, sufficient purging gas is generated during the cooldown of the supply pipes. The gas is injected into the tunnel circuit through the liquid-nitrogen injection nozzles. During the pre-run purge, the tunnel fan is used to maintain circulation and provide sufficient heat to maintain the stream and wall temperatures above the dew (or frost) point of the gas in the tunnel. The nitrogen exhaust system valves at the third turning vanes are used to keep the tunnel at about 1.2 atmospheres absolute pressure during the pre-run purge. At the end of the 15 to 30 minute period required to cool the liquid nitrogen supply pipes and get liquid nitrogen to the injection nozzles, the dew point is usually very close to the lower limit of measurement of the dew-point monitoring system. This limit is about 200K ($-80^{\circ}F$). Cooldown of the tunnel then commences.

7.3.2 Cooldown

Following the pre-run purging process, the stream and tunnel are cooled to the desired operating temperature by injecting liquid nitrogen into the tunnel at the rate of about 75 liters per minute (about 20 U.S. gallons per minute) using injection station number 3 shown on Figure 7.15. The total pressure of the gas in the settling chamber is held near 1.2 atmospheres absolute and the drive fan is operated at a constant speed of about 700 rpm during the cooldown process. This low speed provides the necessary circulation in the tunnel during the cooldown process without adding a significant amount of heat to the stream. Under these conditions, cooling the tunnel and the stream from 300 K ($+80^{\circ}F$) to 110 K ($-262^{\circ}F$) requires, on average, 2450 liters (650 U.S. gallons) of LN_2 and takes about 30 minutes.

The required LN_2 flow rate as a function of cooldown time for cooling from 300 K to 110 K is shown on Figure 7.19 for extremes in cooldown efficiency. These curves were calculated with the method of reference 23, which is described in more detail in Chapter 8, section 8.3.3. Also shown on Figure 7.19 is the experimental data quoted above which indicates that a 30 minute cooldown time is of average efficiency. Since, in general, slower cooldown rates are probably more efficient, increasing the cooldown time should tend to reduce the LN_2 requirement toward the lower value of 1725 liters which was used for the lower curve on Figure 7.19.

7.3.3 Running

Following cooldown of the stream and tunnel to the desired operating temperature, test Mach number is set by adjustment of fan speed. The setting of Mach number is made while the tunnel is near 1.2 atmospheres absolute pressure. A small computer automatically provides the operators with a continually updated display of Mach number based on the ratio of total pressure measured downstream of the screens to static pressure measured in the plenum. Once Mach number is set, the desired operating total pressure is obtained by adjustment of nitrogen-exhaust control valves as described in section 7.2.11. While adjusting total pressure, the liquid nitrogen flow rate must also be adjusted to hold total temperature constant since the heat added by the fan is changing in direct proportion to pressure. Because of the interaction between the variables of fan speed, pressure, and LN_2 flow rate, and inadequacies in some automatic control systems, the tunnel controls are operated in a manual mode while setting the desired tunnel conditions. This procedure takes between 1 and 5 minutes with variation of operating pressure between 1.2 and 5 atmospheres absolute pressure.

The heat to be removed while running at constant test conditions consists of the heat conduction through the tunnel walls and the heat energy added to the tunnel circuit by the drive fan. The running LN_2 requirement has been calculated as a function of Mach number for the two extremes of total pressure for ambient and cryogenic operation. In calculating the heat conducted through the tunnel walls it was assumed that the inner surface of the tunnel was at a temperature equal to the stagnation temperature, T_t, that there was zero temperature gradient through the metal pressure shell, and that the outside surface temperature of the insulation was at 300K (+80°F). The heat added by the fan was calculated by the method described in Appendix II, section II.6. The tunnel power factor, η, was based on values measured in several large transonic tunnels at the Langley Research Center. η was assumed to vary only with Mach number. The values of η which were used for these calculations are as follows:

M_∞	0.2 to 1.0	1.1	1.2
η	0.20	0.22	0.25

The estimated LN_2 requirements are shown on Figure 7.20. It is interesting to note that at a given pressure the required nitrogen flow rate is not a strong function of temperature. This arises from the fact that while the power required to drive the tunnel increases with temperature, the cooling capacity of the liquid nitrogen also increases with temperature. Also shown are several measured values of LN_2 flow made during preliminary operation of the tunnel. Due to faults with the LN_2 supply system and flow-rate meters, there is considerable scatter in the experimental data. However, there is general agreement between the estimated and measured flow rates.

7.3.4 Warmup and re-oxygenation

Following cryogenic operation, the tunnel is warmed, depressurized, and re-oxygenated so that model changes may be made at ambient conditions.

The warming of the tunnel is accomplished by stopping the flow of LN_2 and continuing to operate the drive fan. The time required to warm the tunnel is a function of the temperature range through which the tunnel is warmed and the total pressure and Mach number maintained during the warming process.

As an example, the theoretical warm-up time as a function of Mach number and pressure for warming the tunnel from 110K ($-262^{\circ}F$) to 300K ($+80^{\circ}F$) is shown on Figure 7.21.

Also shown on Figure 7.21 is an experimentally determined value of warm-up time obtained during preliminary operation of the tunnel. As can be seen, there is reasonably good agreement between the theory and experiment.

When the tunnel is warmed, and with the fan still running, the valves which are normally used to exhaust nitrogen from the plenum chamber and the settling region are opened. This results in an influx of ambient air into the tunnel through the plenum chamber, with corresponding efflux through the settling chamber vents, the plenum chamber holding slightly below atmospheric pressure while the settling region holds a pressure slightly above atmospheric. This pumping action brings the oxygen level in the tunnel to 20 percent by volume within one or two minutes depending upon the Mach number. The fan is then stopped with the exhaust valves open, leaving the tunnel warm, depressurized, and re-oxygenated.

7.4 Experimental Results.

Two types of experimental data are being obtained from the transonic cryogenic tunnel. The first type relates to the operation

and performance of the tunnel itself. The data for the most part consists of the usual tunnel calibration information but with particular emphasis being placed on identifying any problems related either to the method of cooling or to the wide range of operating temperature.

The second type of experimental data is primarily aimed at determining the validity and the practicality of the cryogenic concept in compressible flow. For this second type of data, a two-dimensional airfoil pressure model is being tested over a range of Mach number and Reynolds number in such a way as to allow comparison to be made between pressure distribution data obtained at ambient temperatures and data obtained at cryogenic temperatures at the same values of Mach number and Reynolds number.

Some of the results of initial tunnel operation have been reported in reference 24. The results reported in reference 24 along with additional results of the preliminary tunnel calibration and two-dimensional airfoil tests are given in the sections which follow.

7.4.1 Test-section Mach number distribution

The test section Mach number distribution has been determined over a wide range of test conditions. Static pressure orifices located along the tunnel wall and along a tunnel centerline probe are used to determine the static pressure distribution. A pitot tube located downstream of the screens is used to measure stagnation pressure. As noted in Chapter 4, for stagnation pressures up to about 5 atmospheres the isentropic expansion relations calculated from the real-gas properties of nitrogen differ by no more than about 0.2 percent from the corresponding relations calculated from ideal diatomic gas properties and ideal gas equations. However, since the pressure measuring instrumentation being used is capable of resolving such differences, the appropriate real-gas relation is

used to determine Mach number from the stagnation to static pressure ratio. The nominal test-section Mach number is calculated from the ratio of stagnation pressure measured just downstream of the screens to static pressure measured in the plenum chamber.

The initial calibration of the tunnel indicates nearly identical tunnel wall and tunnel centerline Mach number distributions for all test conditions. In addition, there are no detectable differences between Mach number distributions at ambient and cryogenic temperatures. An example of the tunnel wall and tunnel centerline Mach number distribution is shown in Figure 7.22. Examples of the wall Mach number distribution over a range of Mach number is shown in Figure 7.23. Since the purpose of these tests was only to validate the cryogenic concept, no attempt has yet been made to improve the distributions by changes to slot geometry, wall divergence, or re-entry flap position.

7.4.2 Transverse temperature distribution

Since the heat of compression of the fan is removed by spraying liquid nitrogen directly into the tunnel circuit, there was some concern about the uniformity of the resulting temperature distribution, particularly at the power levels required for transonic testing where the mass flow rate of liquid nitrogen is in the order of one percent of the test section mass flow rate. Therefore, it was decided to measure the transverse temperature distribution in the tunnel over a wide range of operating conditions in order to determine if there were any problems of uniformity of temperature distribution related to the method of cooling.

The temperature survey rig described in section 7.2.7 and shown in the photograph presented as Figure 7.9 was used to determine the transverse temperature distribution just ahead of the screens. Six examples of the transverse temperature distribution are shown in

Figure 7.24. These distributions, all obtained at a test-section free-stream Mach number of 0.85, are typical of the data which have been obtained over the entire tunnel operating envelope. With each distribution is shown the mean value (arithmetic average) of temperature and standard deviation (measure of dispersion around the mean). As can be seen, there is a relatively uniform temperature distribution even at cryogenic temperatures where the tunnel is being operated within a few degrees of the test-section free-stream saturation conditions. It is expected that the screens and contraction section has a beneficial effect on temperature distribution such that the distribution in the test section is even more uniform than the distribution measured upstream of the screens.

7.4.3 Drive power and fan speed

During the initial calibration and aerodynamic testing, measurements were to be made of both the drive-shaft torque and speed in order to allow comparisons to be made between predicted and measured values of drive power and fan speed with temperature, pressure, and Mach number. Problems with the torque measurements (unrelated to cryogenic operation) preclude for the present any accurate determination of drive power. However, based on power supplied to the drive motor, it appears that the drive power varies roughly as predicted by theory, namely, for constant pressure and Mach number, power varies directly with the speed of sound, that is, as $T^{0.5}$.

Satisfactory measurements were made of fan speed. On Figure 7.25 is shown the theoretical variation of fan speed with temperature together with experimental values obtained at a test-section free-stream Mach number of 0.85 and at stagnation pressures of about 4.95 atmospheres. The Reynolds number in the test section varied from about 62×10^6 per meter (19×10^6 per foot) at the highest stagnation temperature, 326.7K, to 327×10^6 per meter

(99×10^6 per foot) at the lowest temperature, 99.5K. As can be seen, the fan speed actually decreases somewhat faster with decreasing temperature than predicted by the simple theory (speed $\propto T^{0.5}$), thus indicating perhaps a beneficial effect of the greatly increased Reynolds number on tunnel or fan efficiencies at the lower operating temperatures.

In an attempt to determine if the faster than predicted decrease in fan speed was indeed due to an increase in Reynolds number, additional fan speed data obtained at various Mach numbers was plotted as shown on Figure 7.26. This figure covers only the limited cryogenic temperature range over which these particular tests were made. The fan speed at cryogenic temperature was referenced to the corresponding fan speed at ambient temperature for each Mach number. All of the ambient temperature fan speed data was obtained at stagnation pressures near 4.95 atmospheres. Two sets of data are shown at cryogenic temperatures. The fan speeds at cryogenic temperatures used to calculate the data shown by the flagged symbols was obtained at stagnation pressures near 1.2 atmospheres. The flagged symbols therefore represent nearly constant Reynolds number between the ambient and cryogenic temperature conditions. The fan speeds at cryogenic temperatures used to calculate the data shown by the unflagged symbols was obtained at stagnation pressures near 4.95 atmospheres. These data, therefore, represent a fourfold increase in Reynolds number between ambient and cryogenic temperature conditions.

As can be seen from the data, the relative fan speed for the constant Reynolds number conditions generally decreases with temperature slightly less than predicted by theory. However, the relative fan speed for the increased Reynolds number conditions decreases slightly faster than predicted by theory. Therefore, the faster decrease in fan speed with decreasing temperature shown on

7.25 does in fact represent a true Reynolds number effect, indicating perhaps both improved fan performance and reduced skin friction around the tunnel circuit with increasing Reynolds number.

The data of Figure 7.26 indicates that for constant Reynolds number conditions, fan speed in this particular tunnel varies approximately as $T^{0.487}$. For the constant pressure condition, where Reynolds number is increasing as temperature is reduced, fan speed varies approximately as $T^{0.543}$.

7.4.4 Two-dimensional airfoil tests

Based on the real-gas studies described in Chapter 4, there is little doubt that Reynolds number obtained by reducing temperature should be fully equivalent to Reynolds number obtained by increasing size or by increasing pressure. However, in order also to provide experimental verification of this equivalence, an experiment was sought in which there would be a change in some easily measured aerodynamic parameter solely due to change of Reynolds number. The measurement of the pressure distribution of a two-dimensional airfoil was selected as a suitable experiment since the pressure distribution is easily measured and, as noted in Chapter 1, section 1.1, is sensitive to Reynolds number at high subsonic and transonic speeds.

A modified NACA 0012-64 airfoil having a 13.72cm (5.40") chord was used for the two-dimensional airfoil pressure tests. A sketch of the model showing the orifice locations and a table of the airfoil coordinates are shown on Figure 7.27. The airfoil spanned the octagonal test section and was fastened to the walls in such a way that incidence could be varied. An airfoil somewhat larger than would normally be tested in this size tunnel was selected in order to allow for more accurate model construction, a reasonable number of pressure orifices, and higher chord Reynolds number. The fact that the relatively low chord to tunnel-height ratio may result in wall

induced interference was of no particular concern since the tests were being made only to determine if the airfoil pressure distribution was in any way modified by real-gas effects associated with testing at cryogenic temperatures. The pressure distribution data should therefore be looked at from the point of view of agreement or lack of agreement between data obtained at ambient and cryogenic conditions and the results used only as an indication of the validity of the cryogenic concept.

In order to allow any possible temperature effects on the boundary-layer development, the airfoil was tested with free transition. In order to eliminate any effect of changing dynamic pressure on model shape or incidence, for many tests the symmetrical airfoil was tested at zero incidence.

A comparison of the pressure distribution for ambient and cryogenic temperature tests at free-stream Mach numbers of 0.75 and 0.85 are shown in Figure 7.28. For this comparison, the same chord Reynolds number was obtained at each temperature and constant Mach number by an appropriate adjustment of pressure with temperature. As can be seen, there is excellent agreement at both Mach numbers between the pressure distributions obtained at ambient and cryogenic conditions. This is encouraging because additional tests which have been made over wide ranges of Reynolds number and Mach number have established that the pressure distribution for this airfoil is sensitive to changes in Reynolds number as well as Mach number.

The distribution at $M_\infty = 0.85$ is of perhaps greater significance since the pressure distribution shows the flow to be supersonic over a large portion of the airfoil, reaching a local Mach number of about 1.22 just ahead of the strong recompression shock. This type of flow, typical of supercritical flows, should be extremely sensitive to any anomalous behavior of the test gas should such

behavior arise due to operation at cryogenic temperatures. The almost perfect agreement in the pressure distributions provides experimental confirmation that the test gas behaves in the manner of a perfect gas as predicted by the real-gas studies described in Chapter 4, and that Reynolds number obtained by reducing temperature is equivalent to Reynolds number obtained by increasing pressure in compressible flow.

As noted in Chapter 4, for most tests at moderate operating pressures there should be negligible difference even at cryogenic temperatures between the "real" and "ideal" pressure ratios required for isentropic expansion to a given Mach number. Therefore, the computer used in the setting of test Mach number was programed to calculate Mach number in the usual way from measured pressures and the ideal isentropic equation with γ taken to be constant at 1.4. However, the program used to reduce the pressure distribution data uses the real-gas equations to calculate the test Mach number from the measured stagnation to static pressure ratio. The Mach number as set using ideal-gas relations and the Mach number as calculated using real-gas relations agree to within better than 0.2 percent. Additionally, since the pressure distribution for this airfoil is very sensitive to Mach number, particularly near $M_\infty = 0.85$, the distribution would reflect any error in setting Mach number. The agreement between the distributions provides further confirmation that no anomalous real-gas behavior is present at cryogenic temperatures.

7.4.5 Testing beyond the saturation boundary

Supersaturation is experienced in hypersonic tunnels with no apparent effect on test data. However, Daum (see reference 25) shows that the permissible supersaturation is a function of pressure and supersaturation is only possible at pressures much lower than used in this tunnel.

As described in Chapter 4, the saturation boundary is well defined and any possible effect of liquefaction of the test gas can easily be avoided provided that the maximum local Mach number on the model is known. A significant increase in test Reynolds number is possible if the saturation boundary may be crossed in these localized regions. For example, if the test temperature for sonic testing is selected to avoid the saturation boundary based on free-stream Mach number, the test Reynolds number is about 15 percent greater than can be achieved at the same stagnation pressure had the test temperature been selected to avoid the saturation boundary based on a maximum local Mach number of 1.4. In order to determine if such an increase in test Reynolds number could safely be realized, an experiment was needed to investigate the feasibility of testing under conditions of local supersaturation.

The pressure distribution of an airfoil having a strong recompression shock should provide a sensitive indicator of condensation, which would first be expected to occur in the low pressure region ahead of the shock. Therefore, the two-dimensional airfoil pressure model described in the previous section was also used in a series of supersaturation tests.

The test conditions were chosen to provide two sets of pressure distribution data at a constant Mach number and Reynolds number. The airfoil was first tested under conditions such that the free-stream was at or near the saturation boundary. Under such conditions much of the flow over the airfoil was supersaturated. The model was then tested at the same Mach number and Reynolds number but under stagnation pressure and temperature conditions chosen to keep the flow everywhere well away from the saturation boundary. A comparison of the pressure distributions obtained under these two conditions should then provide some evidence as to whether advantage might be

taken of the increase in test Reynolds number with locally supersaturated flow.

The pressure distributions shown in Figure 7.29 were obtained with the airfoil at zero incidence at $M_\infty = 0.85$ with $R_c = 27 \times 10^6$. As can be seen there is no significant difference in the two distributions even though one was obtained while operating at the free-stream saturation boundary resulting in over 7 degrees of supersaturation at the minimum pressure point on the airfoil.

A similar set of data was acquired during tests of the airfoil at 3° incidence. The pressure distributions shown in Figure 7.30 were obtained at $M_\infty = 0.75$ with $R_c = 24 \times 10^6$. Again there is no significant difference in the two distributions.

Based on these results, it is apparent that under some conditions several degrees of local supersaturation have no effect on the pressure distribution over an airfoil. Condensation is a function of the time the flow remains in a supersaturated condition as well as the degree of supersaturation. Thus, the results obtained in this relatively small tunnel may not be applicable to larger tunnels where, for the same test conditions, the flow will be in a supersaturated condition for a longer time while passing over the larger model. However, it should be noted that the 13.72 cm (5.40") chord of the two-dimensional airfoil used for these tests is of about the same length as the mean chords of three-dimensional models tested in tunnels having test sections 1.37m x 1.37m (4.5 ft x 4.5 ft). It is possible therefore, that several degrees of supersaturation would have no adverse effect on the test results obtained in a large cryogenic tunnel on models having chords not much greater than this model.

There will be considerable simplification in the selection of test temperature if further study shows that the minimum operating

temperature can in all cases be based on free-stream Mach number rather than maximum local Mach number. This simplification would be of particular advantage for those tests where local values of C_p are not known, as is the case, for example, in many force tests.

The feasibility of testing beyond the free-stream saturation boundary was not investigated during these tests. Testing under such conditions should be investigated since large increases in test Reynolds number may be realized for even a few degrees of supersaturation due to the large changes in Reynolds number with temperature near the saturation boundary, typically about 1.7 percent change in Reynolds number per degree K change in stagnation temperature.

7.4.6 Test-section noise measurements

The background noise in the test section is of concern since excessive noise levels can prevent the proper simulation of the unsteady aerodynamic parameters usually of interest in dynamic tests, and in addition, may affect certain static or steady-state parameters being measured. Because of the large reduction in both drive power and pressure as temperature is reduced, it was expected that background noise would be reduced when a given Reynolds number was obtained at cryogenic temperatures rather than at ambient temperature. Therefore noise measurements have been made in the test section over a range of test conditions in order to determine the effect of cryogenic operation on noise.

The test section noise levels are presented in terms of the broadband (10Hz to 20 kHz) sound pressure level, L_p, with the reference pressure taken to be 20 $\mu N/m^2$ (2.9×10^{-9} pounds per square inch). The measurements were made during the testing of the two-dimensional airfoil at 3° incidence and $M_\infty = 0.80$ by a microphone which was mounted flush with the inner surface of the test section wall just above the airfoil. The noise levels are not strictly

background noise because of the presence of the airfoil. The data, therefore, should not be used as an indication of the minimum background noise in the test section but rather should be used comparatively to indicate the general effect of cryogenic operation on noise level. The sound pressure level data are presented in Figure 7.31 as a function of chord Reynolds number, R_c. Next to each plotted point are the corresponding values of stagnation pressure and temperature. As can be seen, at a constant Reynolds number of about 8.5×10^6, the combined effect of reducing temperature and pressure results in a reduction of the sound pressure level by 10 dB from the level measured at high pressure and ambient temperature. Data also was taken at a nearly constant pressure and shows Reynolds number increased by either a factor of 3 or 4.6, depending on the reduction in temperature, with only a 1 dB increase in the broadband sound pressure level.

Extensive analysis of the test-section noise data has not as yet been made. However, based on the limited amount of available data, significant reductions in noise level will be obtained at cryogenic temperature.

7.5 Conclusions from the Transonic Tunnel Testing.

Many of the conclusions of the low-speed testing were confirmed during the operation and testing in the transonic tunnel. Additional conclusions from the transonic tunnel are as follows:

1. A transonic cryogenic pressure tunnel is simple to operate.
2. Purging, cooldown, and warmup times are acceptable and can be predicted with good accuracy.
3. Liquid nitrogen requirements for cooldown and running can be predicted with good accuracy.
4. Cooling with liquid nitrogen is practical at the power levels required for transonic testing. Test temperature is easily controlled and good temperature distribution obtained by

using a simple nitrogen injection system.

5. Test-section noise level is reduced when a given Reynolds number is obtained by operating at cryogenic temperatures.
6. In compressible flow, Reynolds number dependent aerodynamic phenomena behave in the same manner when Reynolds number is changed by temperature as when changed by pressure. Identical pressure distributions were obtained on a two-dimensional airfoil having a strong recompression shock when tested at ambient and cryogenic stagnation temperatures with stagnation pressure adjusted to maintain a constant Reynolds number.
7. Several degrees of local supersaturation have been obtained with no detectable effect on the pressure distribution over an airfoil.

7.6 List of Symbols Used in Chapter 7.

Symbol	Meaning
C_p	pressure coefficient, $C_p = \frac{P - P_\infty}{q_\infty}$
c	chord of two-dimensional airfoil
x	linear dimension along airfoil chord line
L_p	sound pressure level, dB (reference 20 $\mu N/m^2$)
M_L	local Mach number
M_∞	free-stream Mach number
P	pressure
q	dynamic head
R_c	Reynolds number based on c
T	temperature
α	angle of incidence
η	tunnel power factor
σ	standard deviation

Subscripts

t	stagnation conditions
max	maximum value
∞	freestream conditions

Table 7.1 Design Dimensions of the Transonic Tunnel Contraction Section.

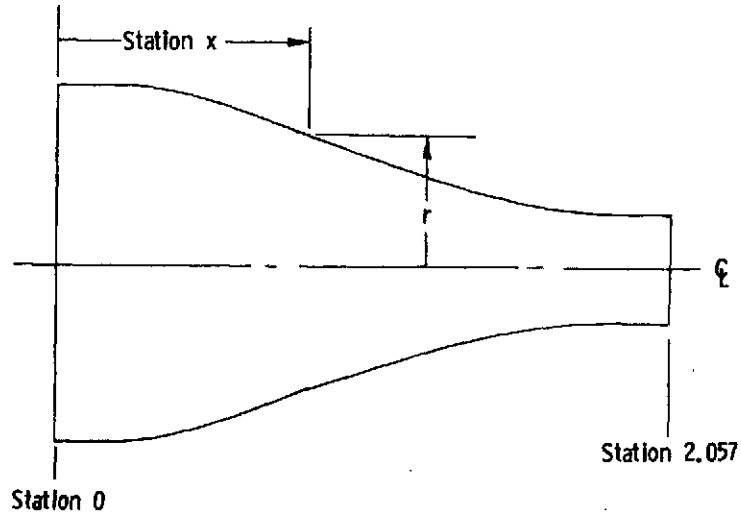

Longitudinal station x, m	Area, m^2	Equivalent-circle radius, r, m
0.000	1.167	0.610
.111	1.165	.609
.204	1.156	.607
.309	1.144	.603
.405	1.090	.589
.496	1.013	.568
.581	.922	.541
.657	.831	.514
.730	.744	.486
.802	.661	.459
.873	.583	.431
.941	.511	.403
1.009	.445	.377
1.078	.386	.351

Longitudinal station x, m	Area, m^2	Equivalent-circle radius, r, m
1.143	0.344	0.326
1.210	.288	.303
1.278	.248	.281
1.345	.213	.260
1.414	.183	.241
1.481	.158	.225
1.550	.140	.211
1.620	.126	.200
1.691	.115	.192
1.763	.108	.185
1.834	.102	.181
1.908	.100	.178
1.982	.098	.177
2.057	.098	.176

Table 7.2 Transonic Tunnel Test-Section Slot Geometry.

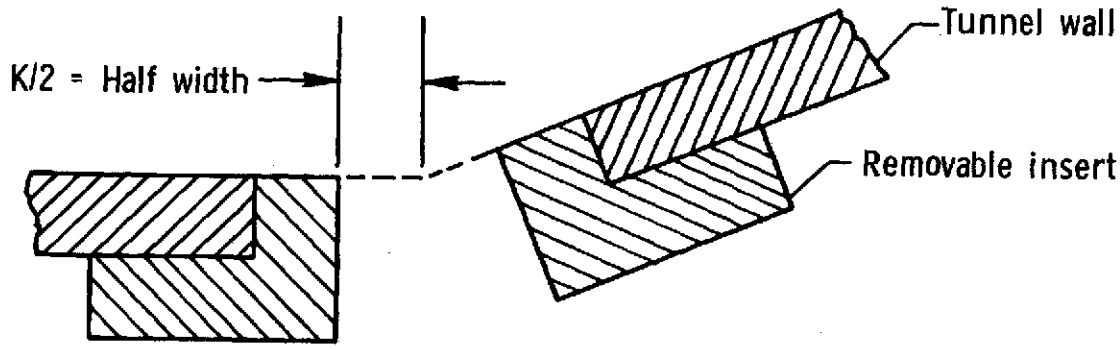

Cross section at station S
(See figure 7.11 for definition of S)

Station S, cm	K/2, cm
17.145	0
18.250	0
19.357	.0274
20.462	.0516
21.569	.0706
22.674	.0876
23.782	.1013
24.886	.1133
25.994	.1242
27.099	.1328
28.207	.1402
29.312	.1476
30.419	.1529
31.524	.1585
32.631	.1631
33.736	.1679
34.844	.1704
35.949	.1737
37.056	.1770
38.161	.1798

Station S, cm	K/2, cm
39.268	.1826
40.373	.1854
41.481	↓
42.586	.1887
43.693	.1913
44.798	.1976
45.905	.2027
47.010	.2195
48.118	.2433
49.223	.2731
50.328	.3117
51.435	.3541
52.540	.4011
53.647	.4516
54.752	.5034
55.860	.5530
56.965	.6055
58.072	.6513
59.177	.6988
60.284	.7468

Station S, cm	K/2, cm
61.389	.7915
62.497	.8324
63.602	.8679
64.707	.8997
65.814	.9263
66.921	.9495
68.026	.9347
↓	↓
↓	↓
102.870	↓

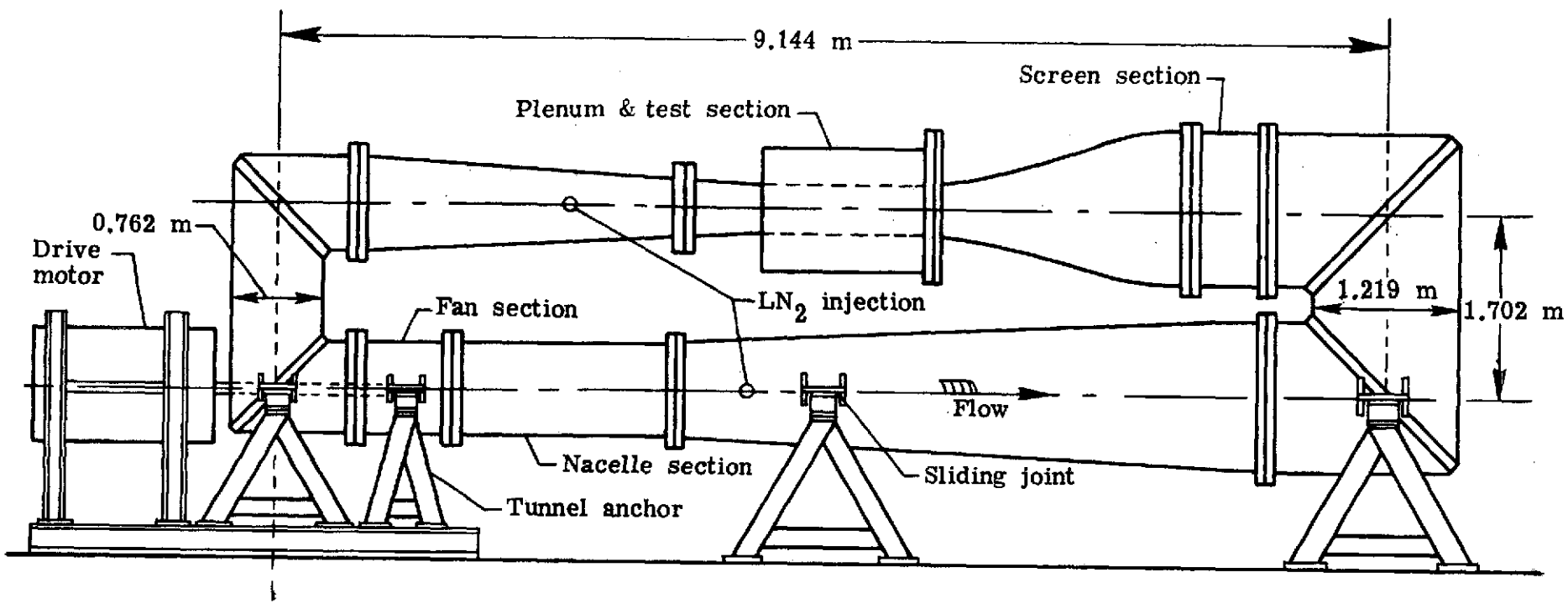

Figure 7.1 Layout of transonic cryogenic tunnel circuit.

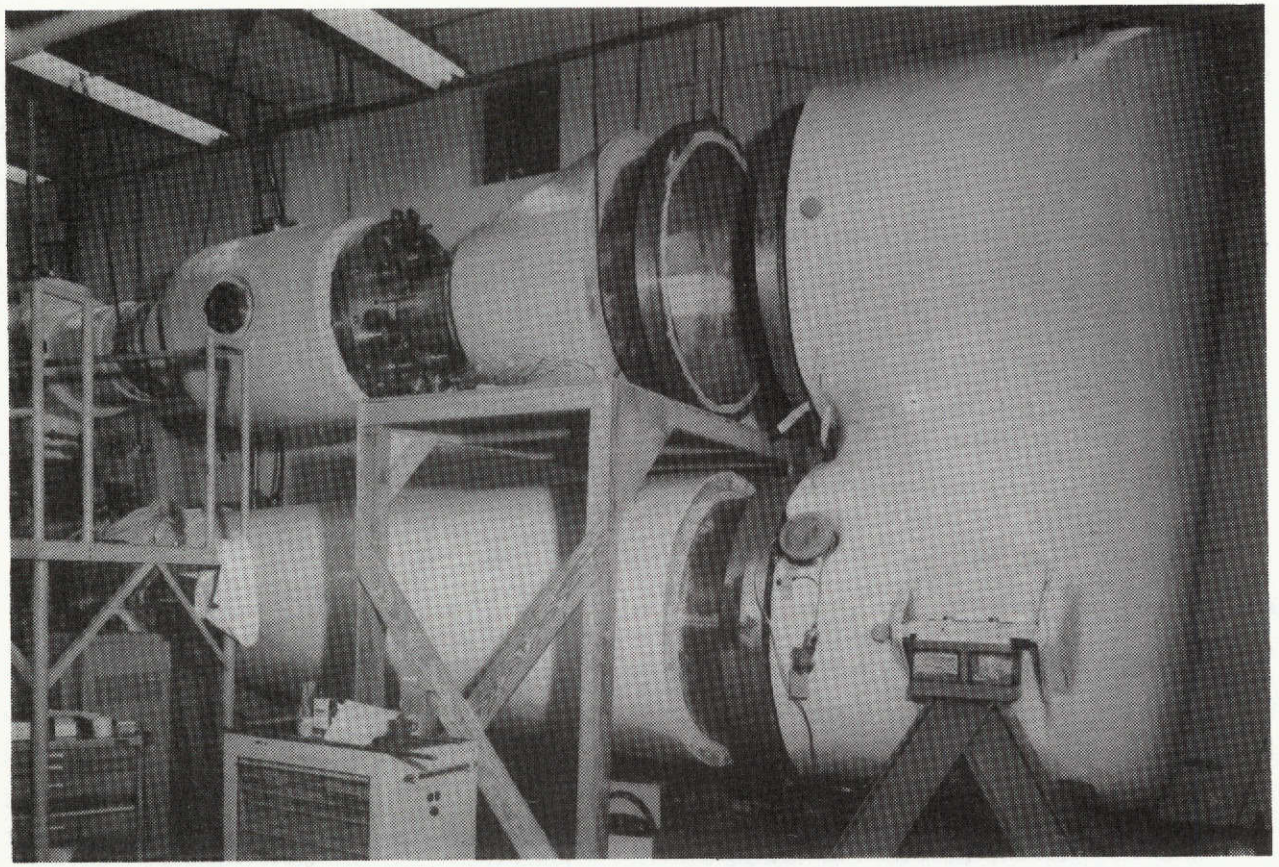

Figure 7.2 Transonic cryogenic tunnel during final assembly.

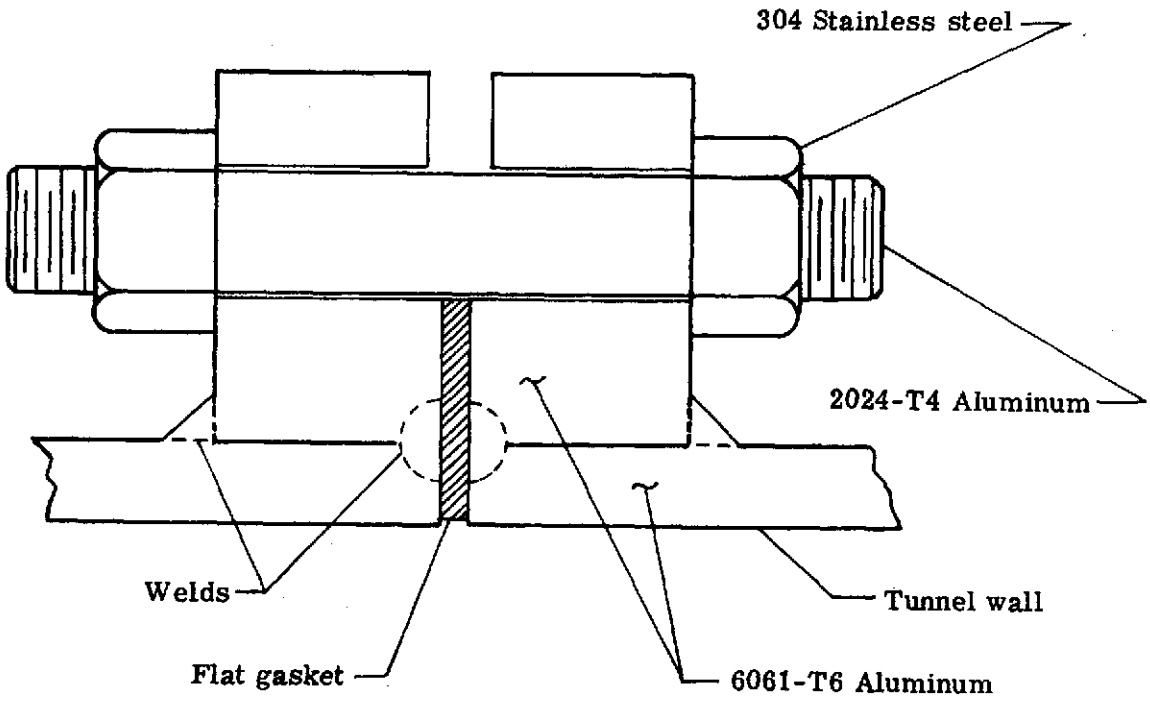

a) Typical small flange joint with flat gasket seal

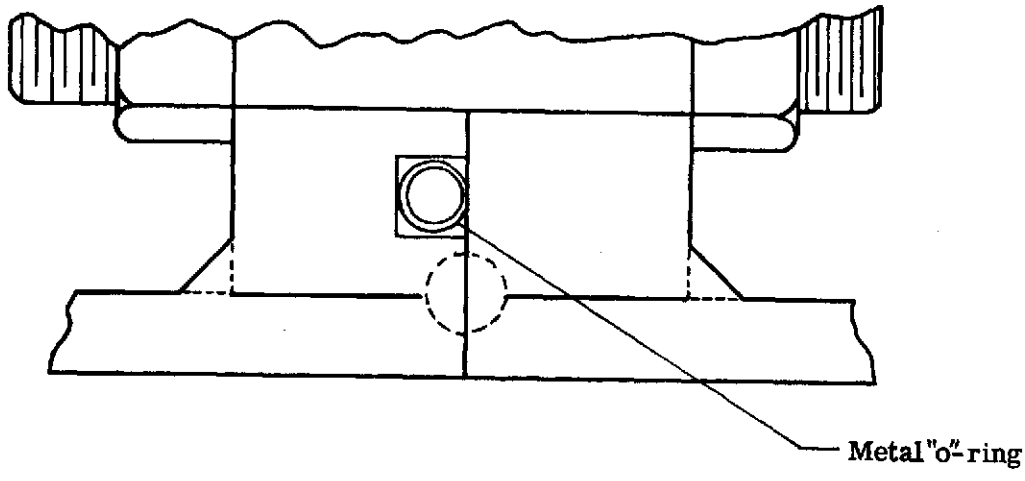

b) Typical large flange joint with teflon coated metal "o"-ring seal

Figure 7.3 Typical flange joints showing details of seals.

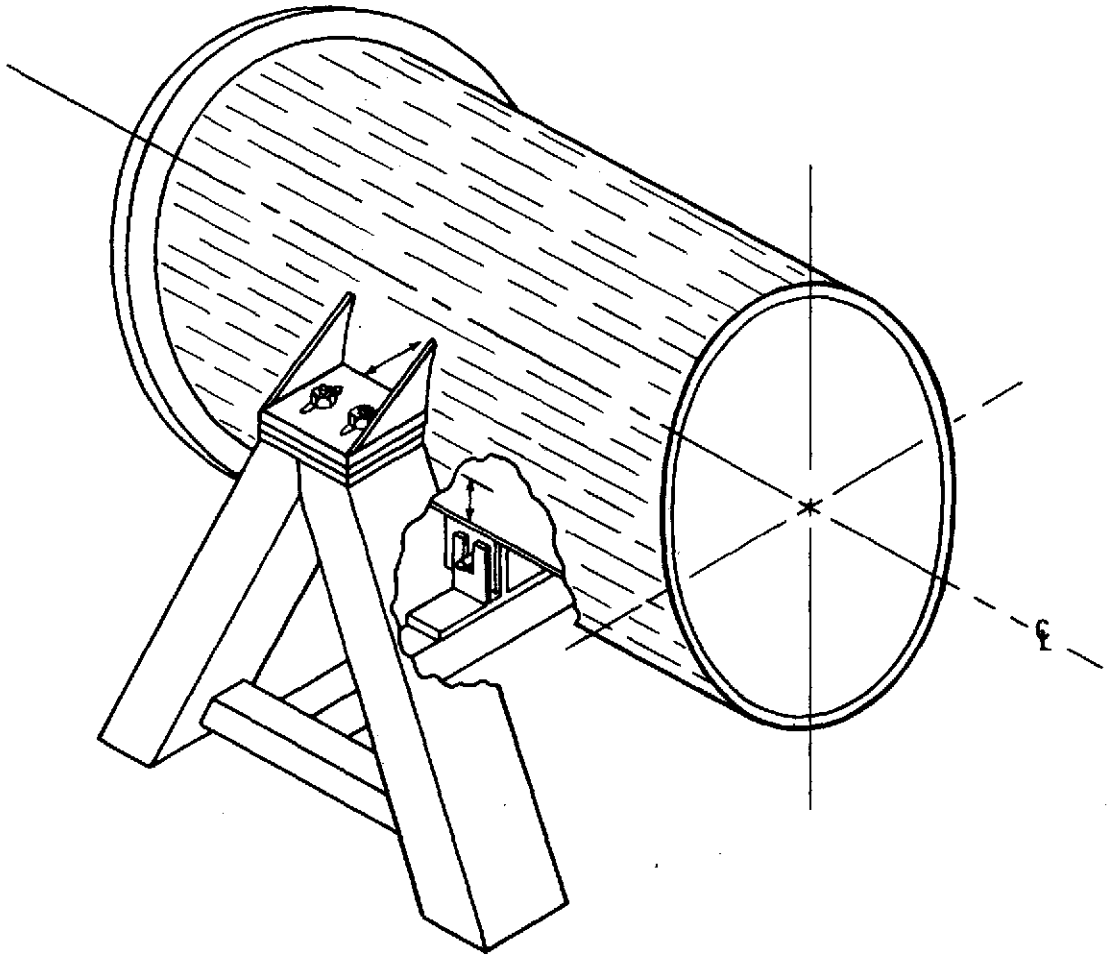

Figure 7.4 Transonic cryogenic tunnel anchor support.

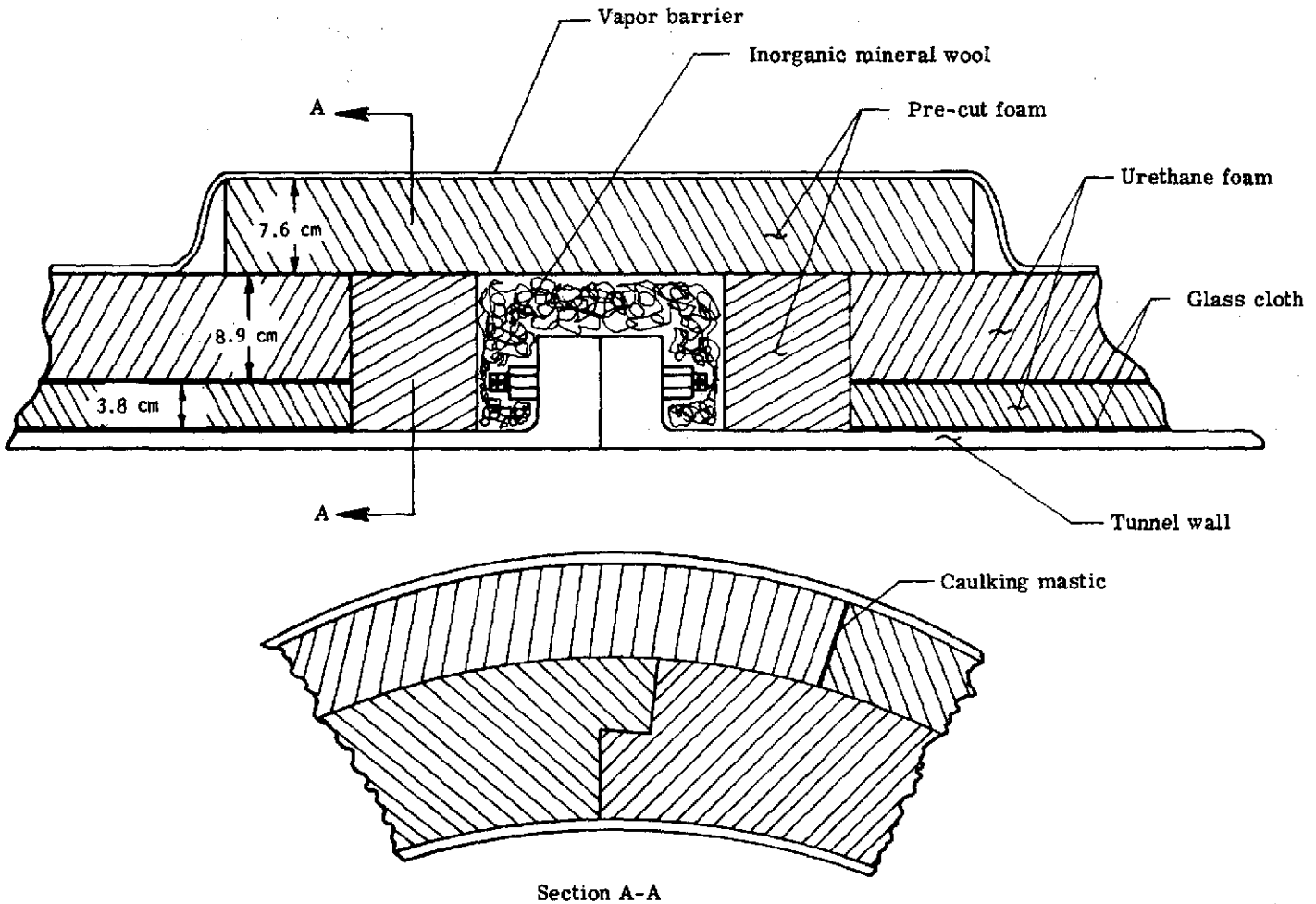

Figure 7.5 Details of insulation used on transonic cryogenic tunnel.

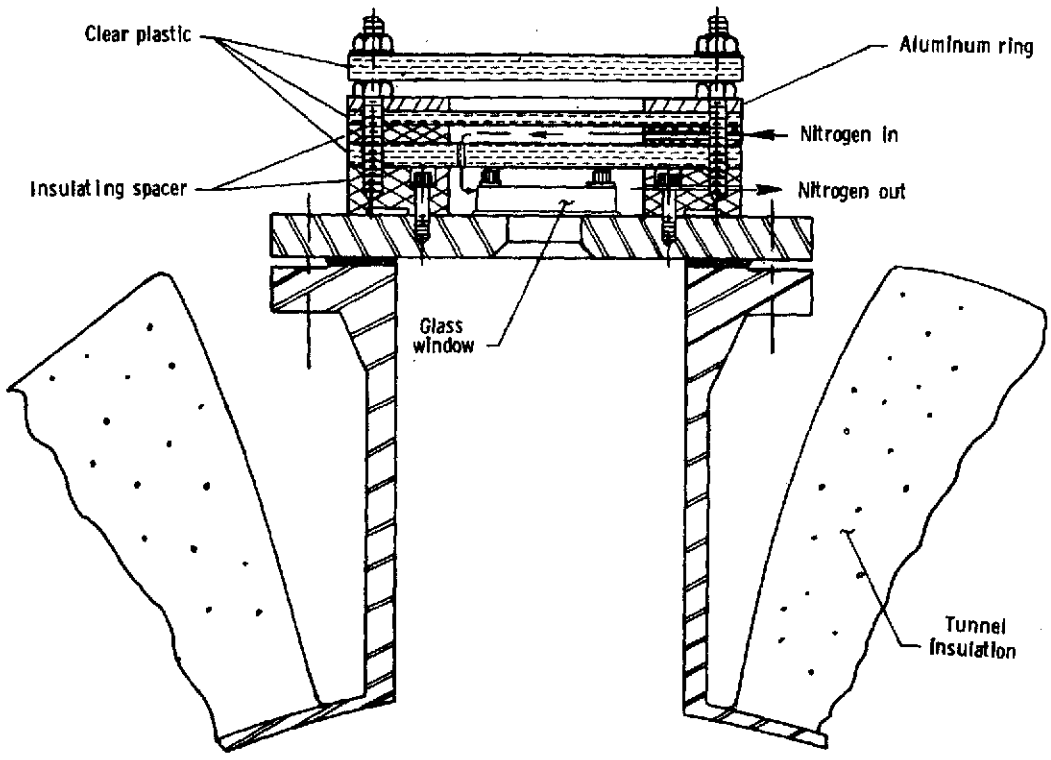

Figure 7.6 Transonic cryogenic tunnel port.

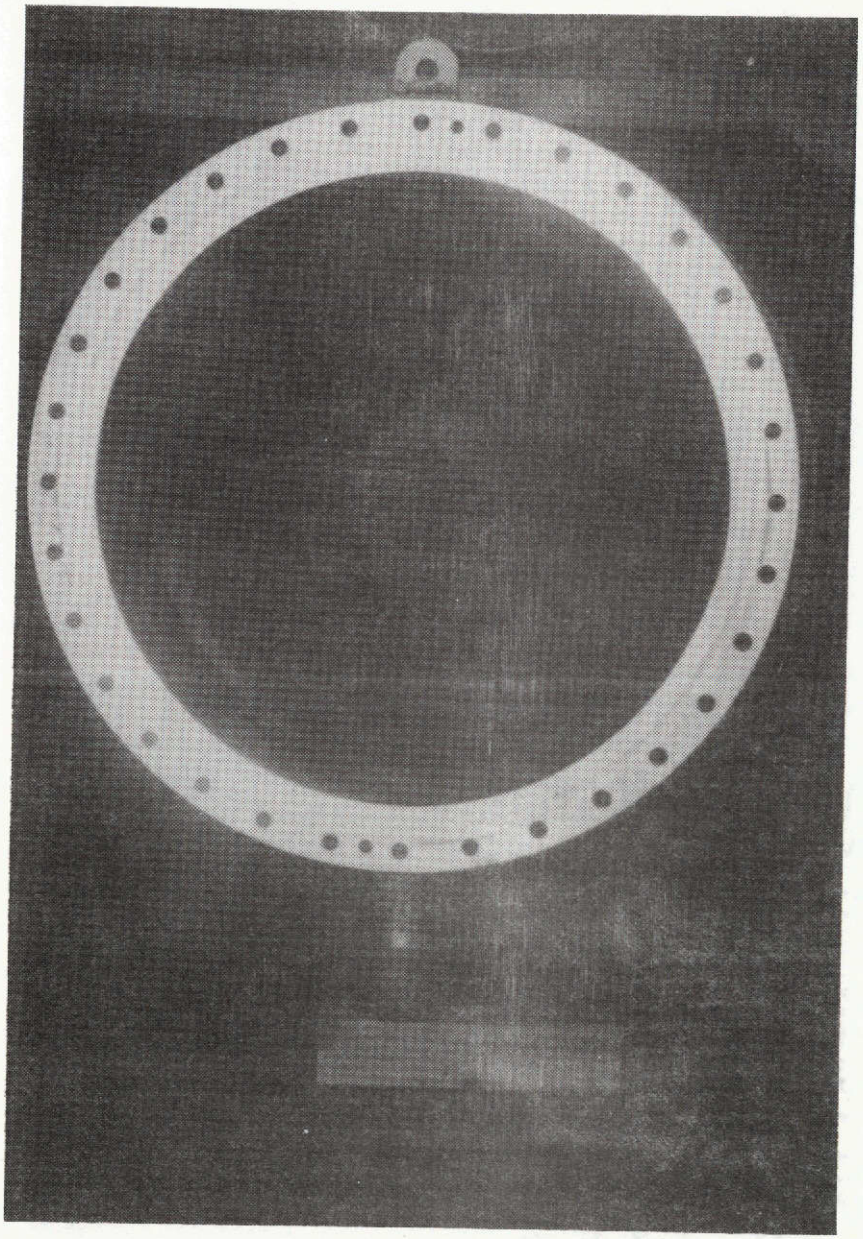

Figure 7.7 View looking upstream showing the nacelle section and fan section.

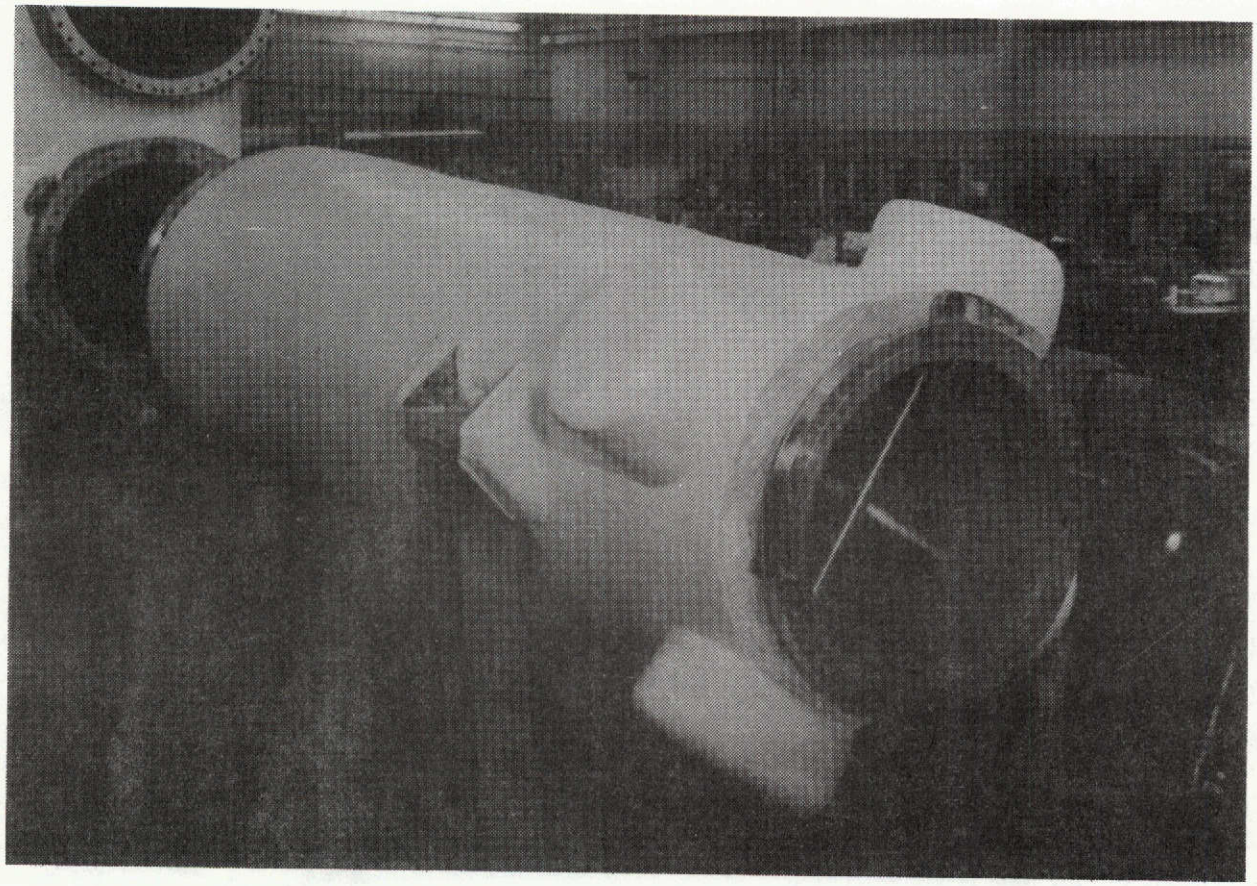

Figure 7.8 Return-leg diffuser and 3rd and 4th corners.

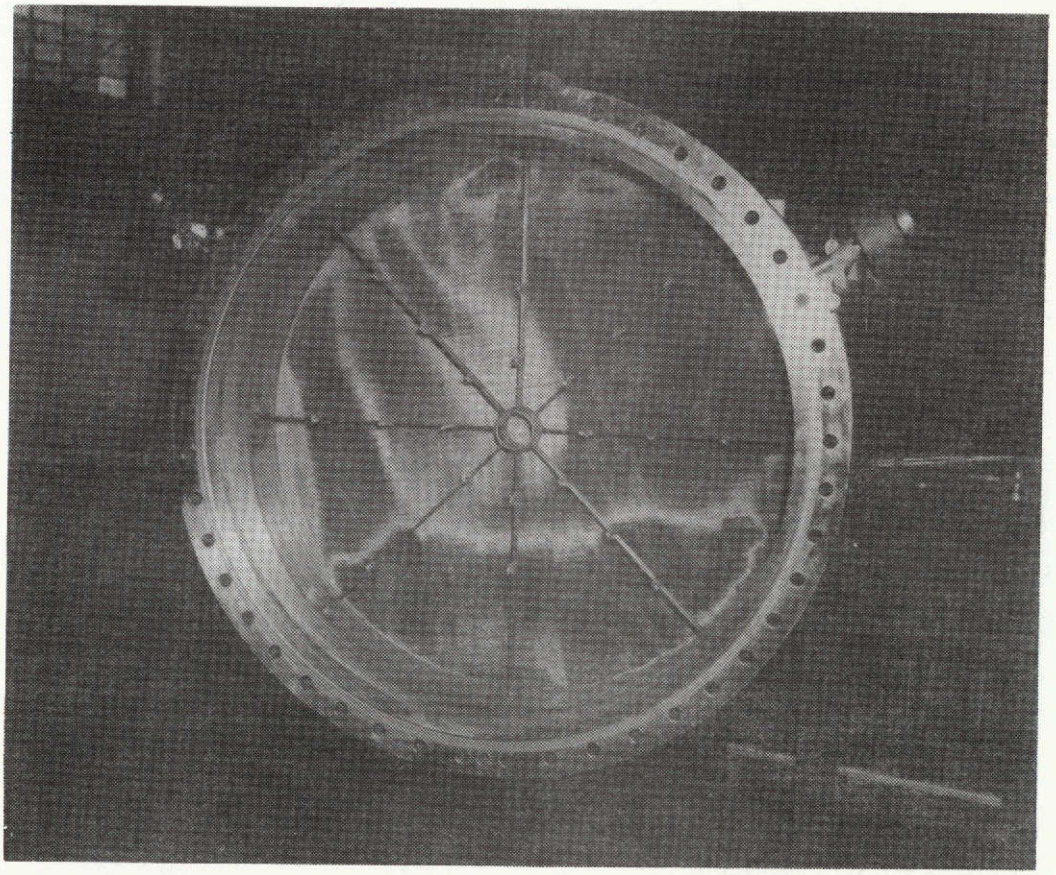

Figure 7.9 Screen section showing the temperature survey rig.

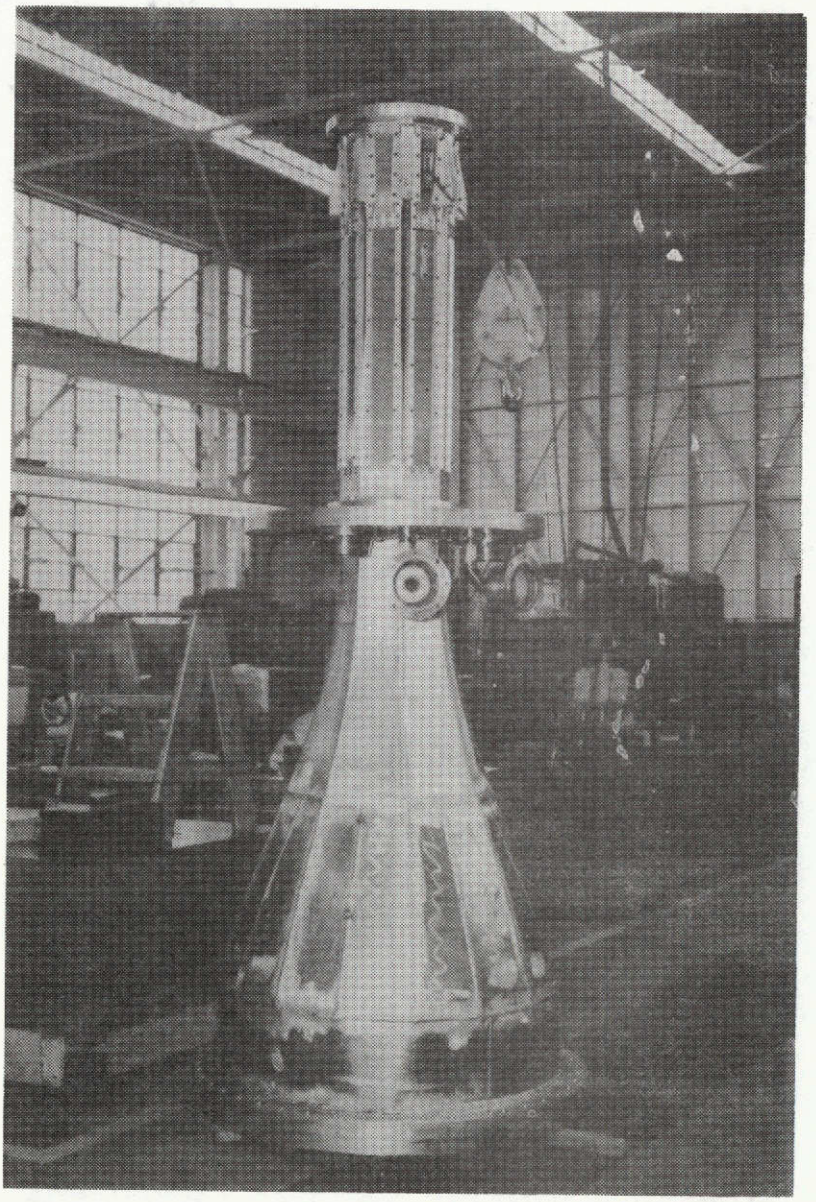

Figure 7.10 Contraction section and test section.

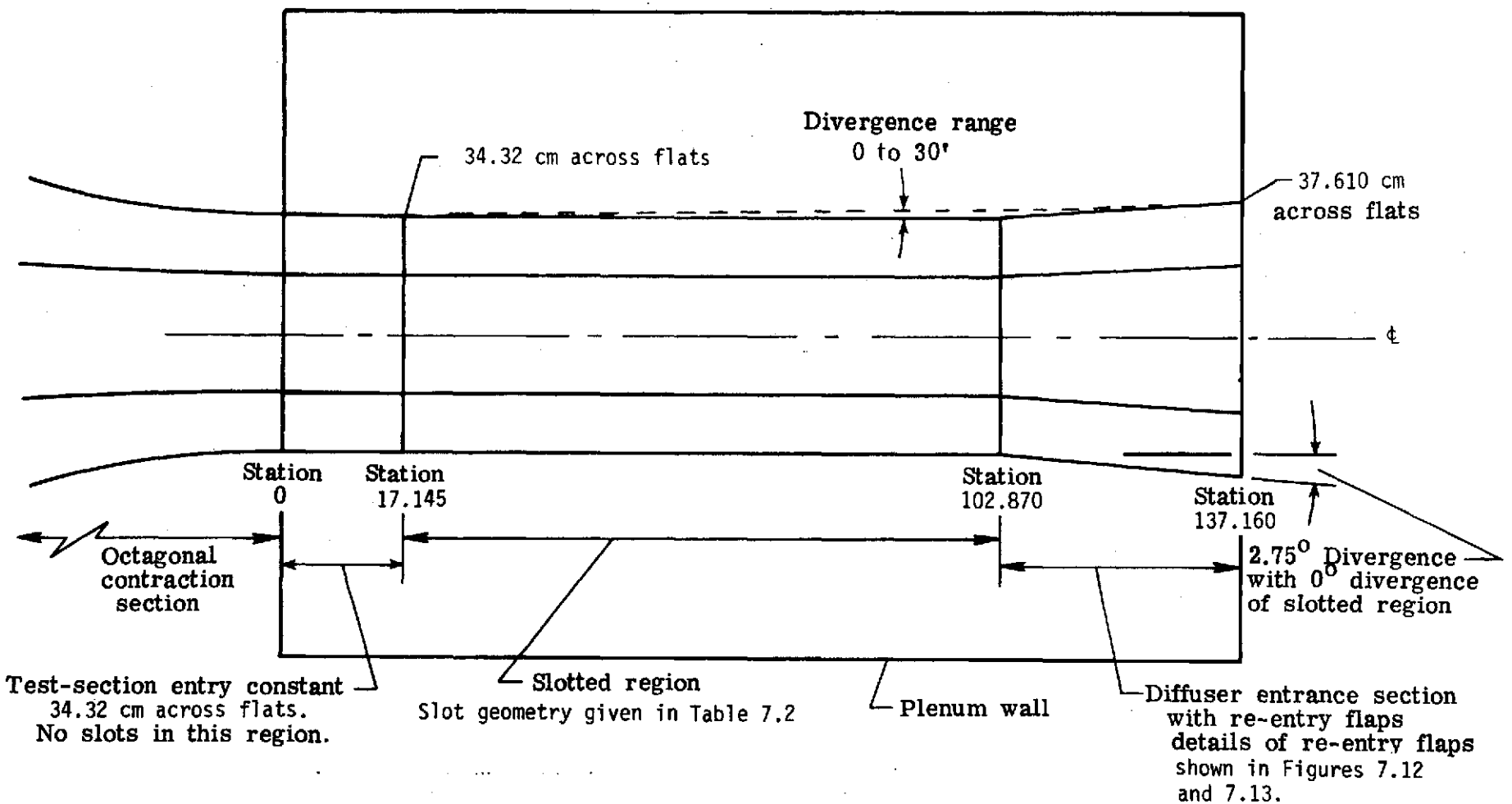

Figure 7.11 Layout of test section. Station given in centimeters.

Wall Divergence set at 5' for initial tests.

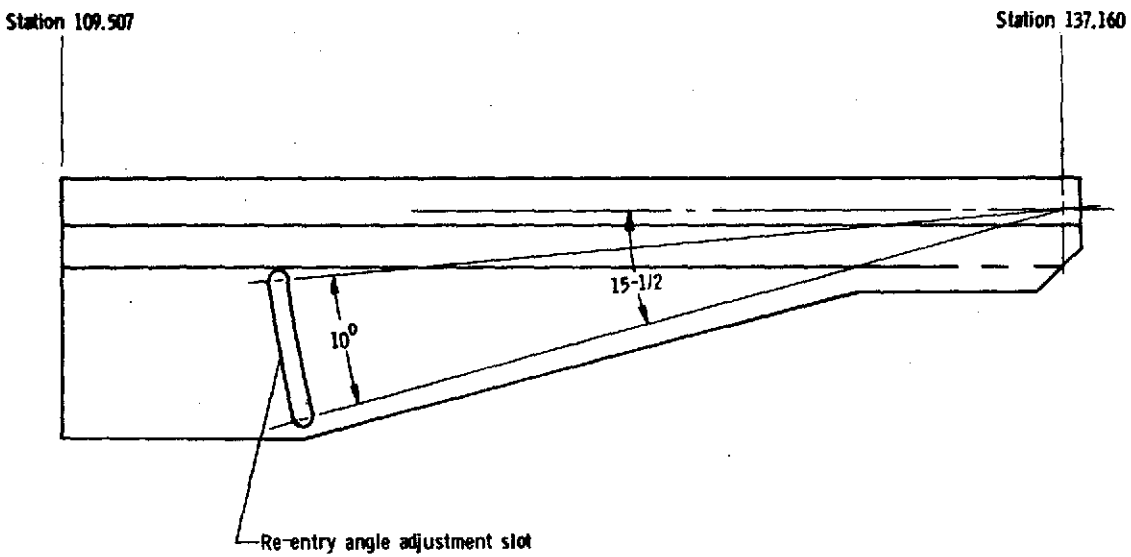

Side view of side plate

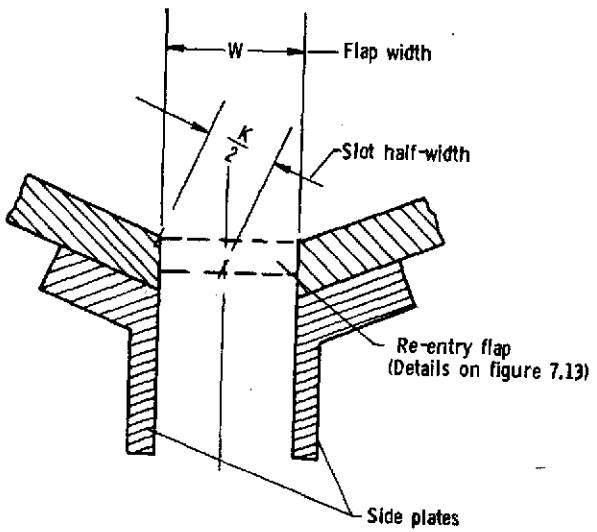

S, cm	K/2, cm
109.507	1.472
110.338	1.489
111.719	1.516
116.144	1.605
120.569	1.693
124.993	1.781
129.418	1.869
137.160	2.023

Figure 7.12 Details of re-entry slot design.

Re-entry flap set at 7° for initial tests.

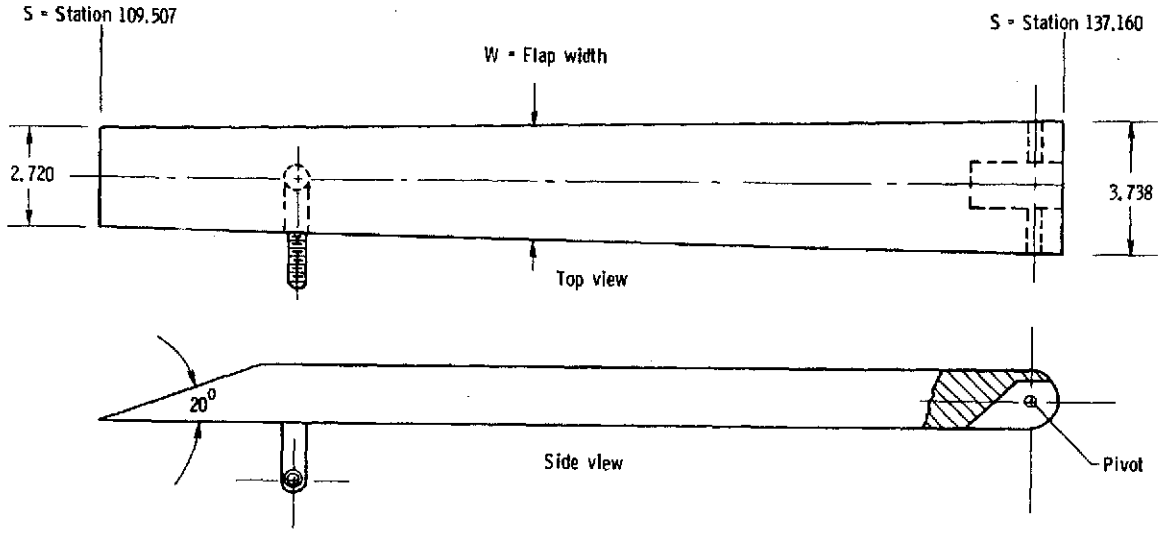

S, cm	W, cm
109.507	2.720
110.338	2.751
111.719	2.802
116.144	2.967
120.569	3.128
124.993	3.291
129.418	3.453
137.160	3.738

Figure 7.13 Details of re-entry flap design.

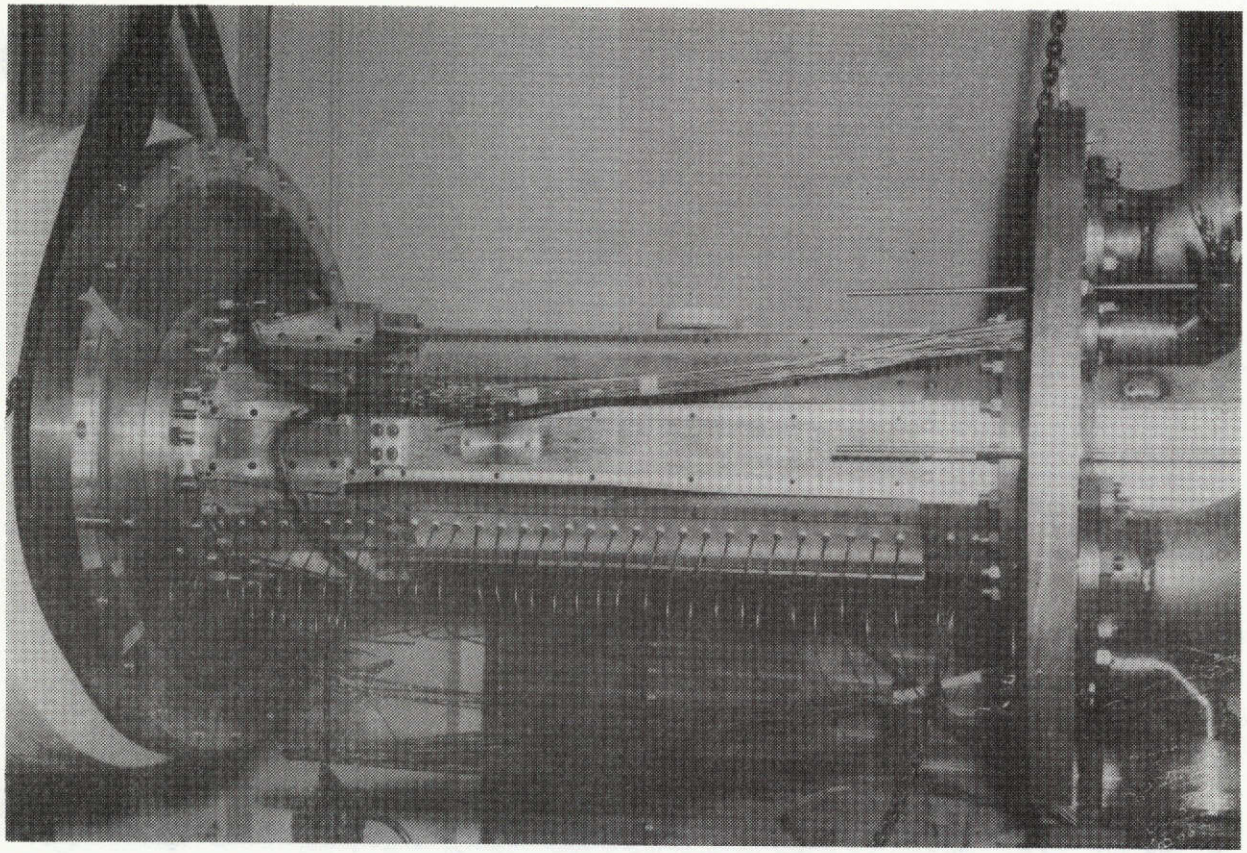

Figure 7.14 Transonic cryogenic tunnel test section.

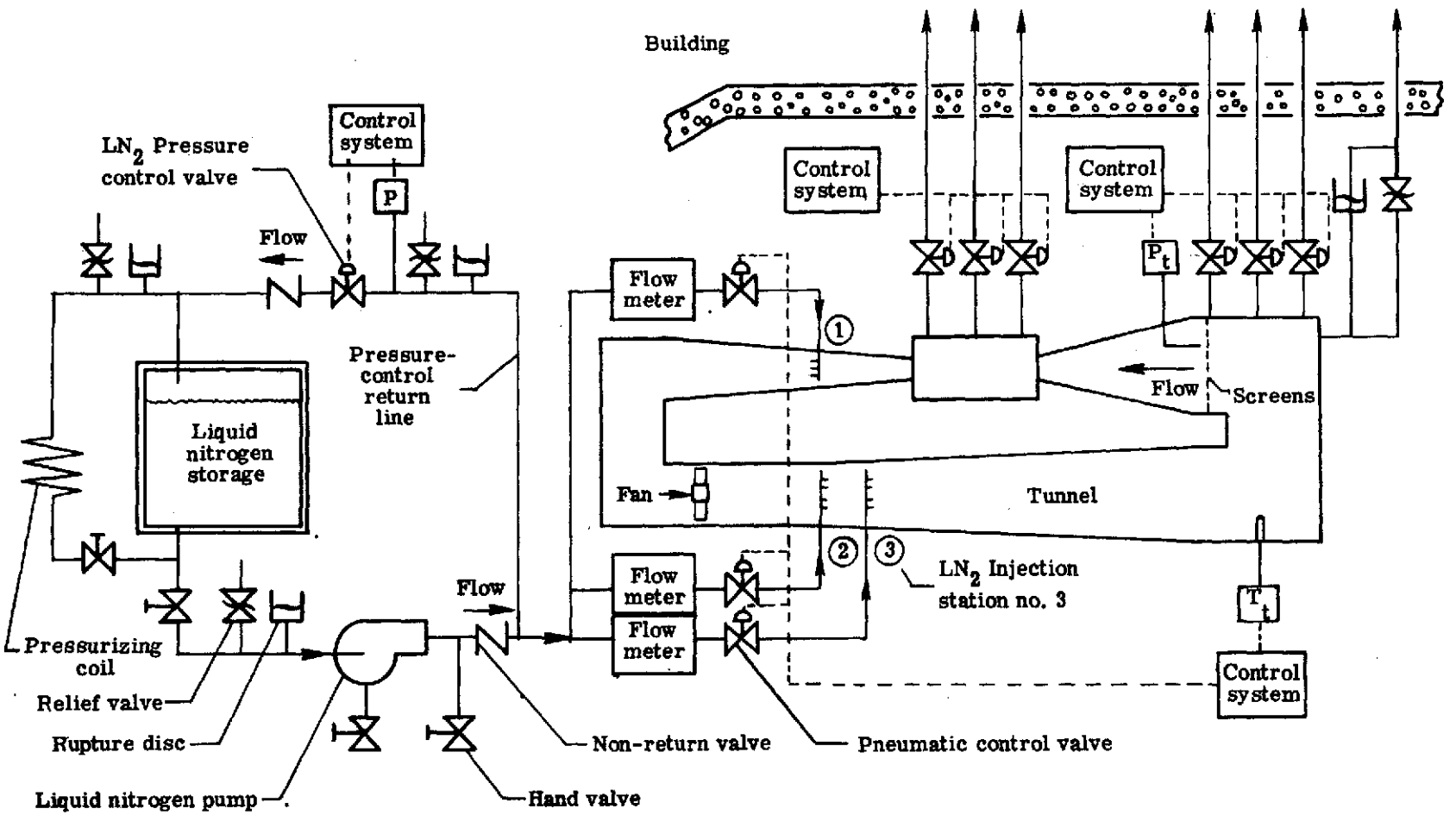

Figure 7.15 Schematic drawing of the liquid nitrogen system and nitrogen exhaust system.

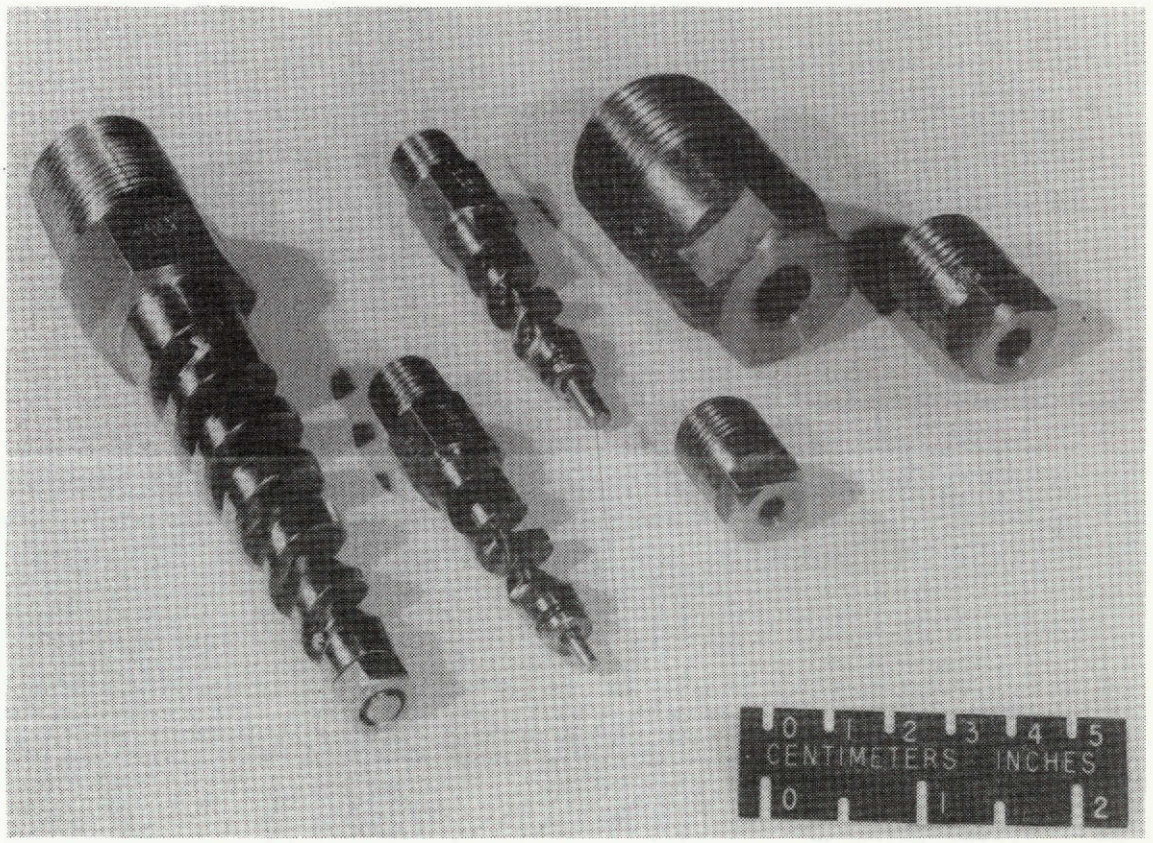

Figure 7.16 Liquid-nitrogen injection nozzles.

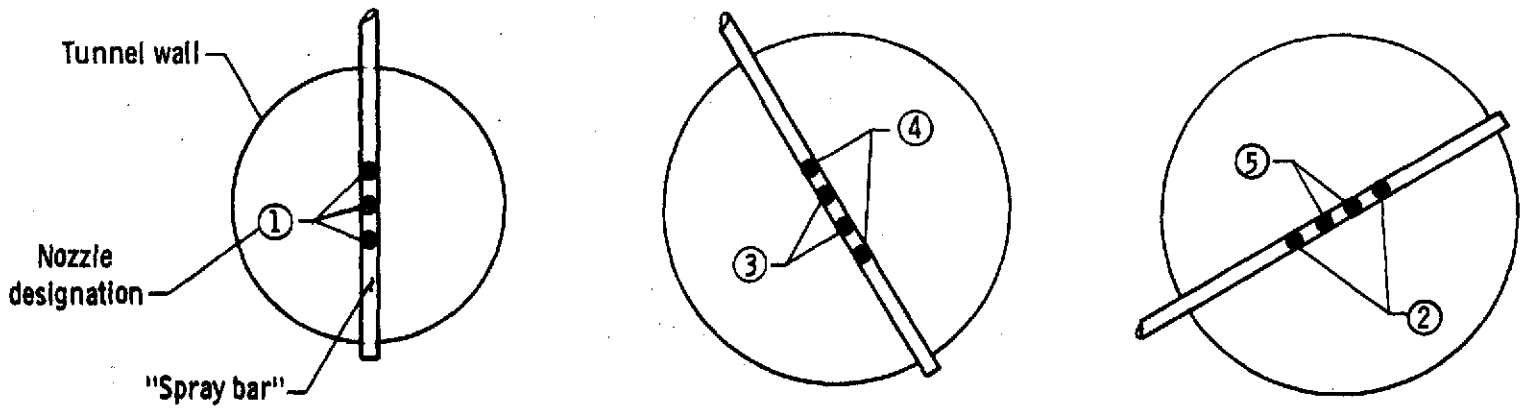

Nozzle designation	Manufacturers model number	Liquid nitrogen flow rate liter per minute at stated differential pressure								
		0.5 atm	1 atm	2 atm	3 atm	4 atm	5 atm	6 atm	7 atm	8 atm
1†	1HH12	51.4	72.5	98.2	118.4	135.2	149.6	163.0	175.7	187.5
2	1/2HHSS4.0	13.9	20.0	27.8	33.5	38.3	42.8	46.8	50.4	53.7
3	3/8HHSS9.5	3.41	4.97	6.74	8.00	9.14	10.15	11.04	11.92	12.68
4	AA6FC	2.49	3.83	5.56	6.74	7.88	8.59	9.27	9.72	10.20
5	B16FC	19.0	27.0	38.3	46.8	53.9	60.3	66.1	71.2	76.0

†Nozzles 1, 2, and 3 were manufactured by Spraying Systems Co., Wheaton, Ill., U.S.A.
Nozzles 4 and 5 were manufactured by Bete Fog Nozzle, Inc., Greenfield, Mass., U.S.A.

Figure 7.17 Sketches of the three liquid nitrogen spray bars with tabulated flow capacity for each type nozzle.

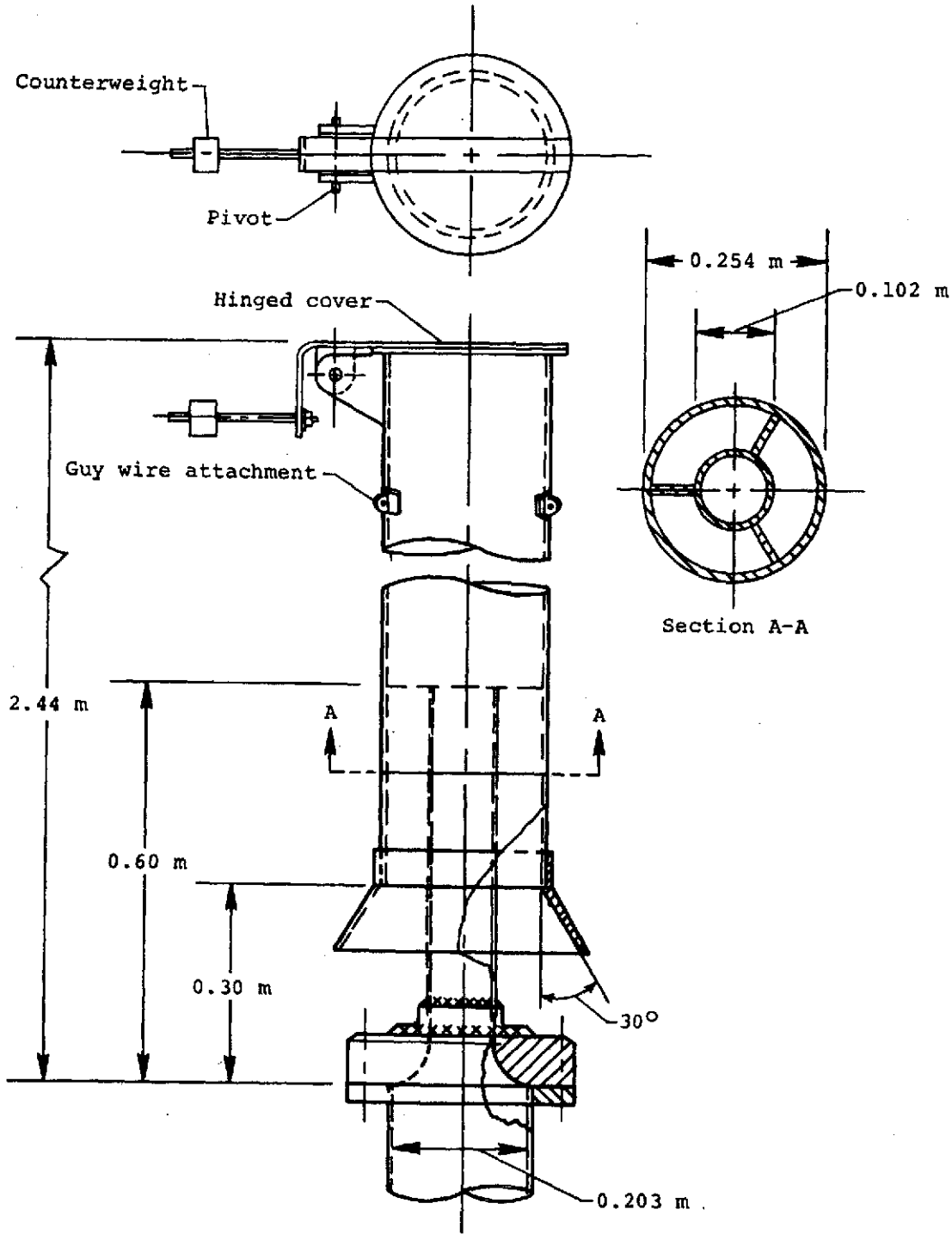

Figure 7.18 Tunnel exhaust ejector.

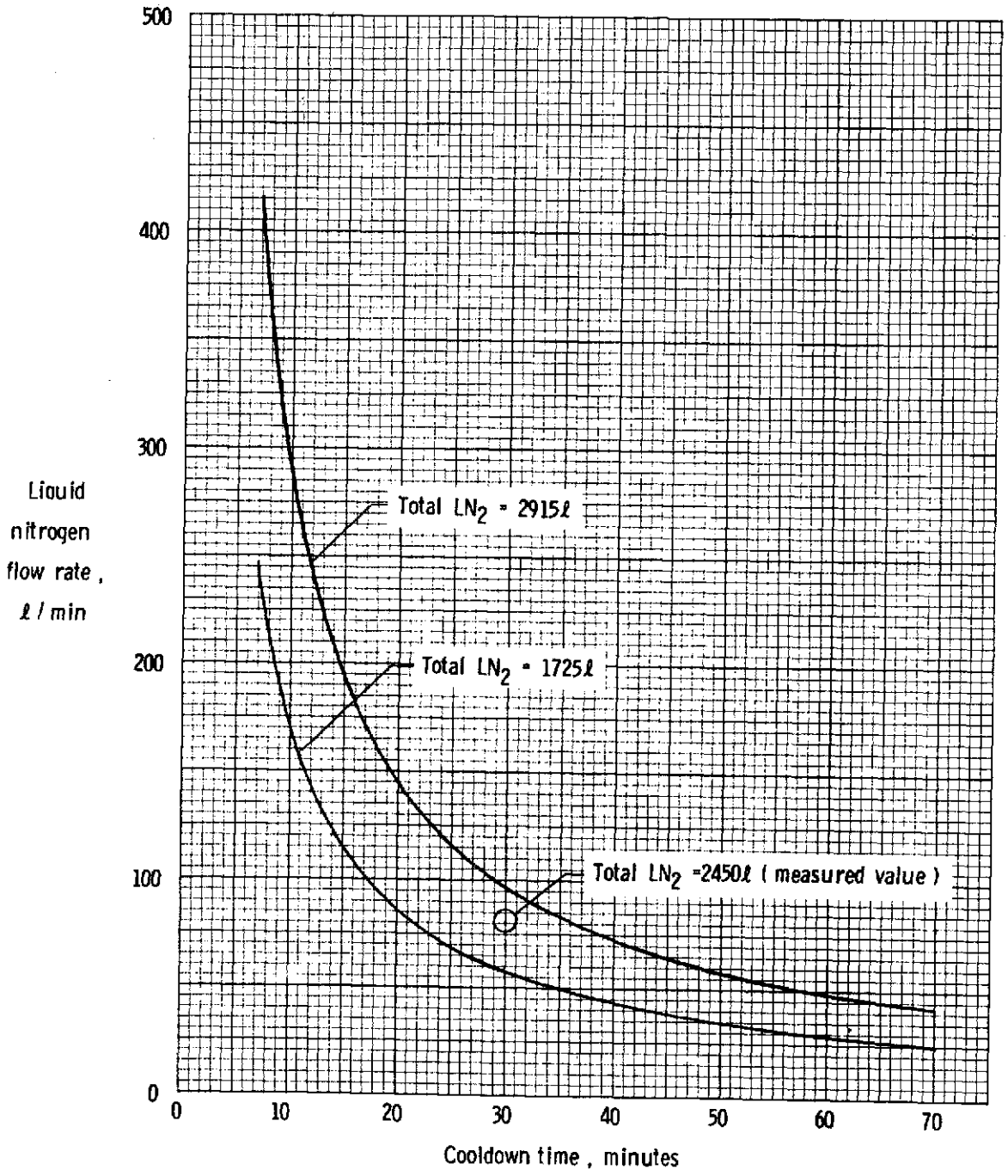

Figure 7.19 Required liquid nitrogen flow rate as a function of cooldown time for cooling the transonic tunnel from 300K to 110K.

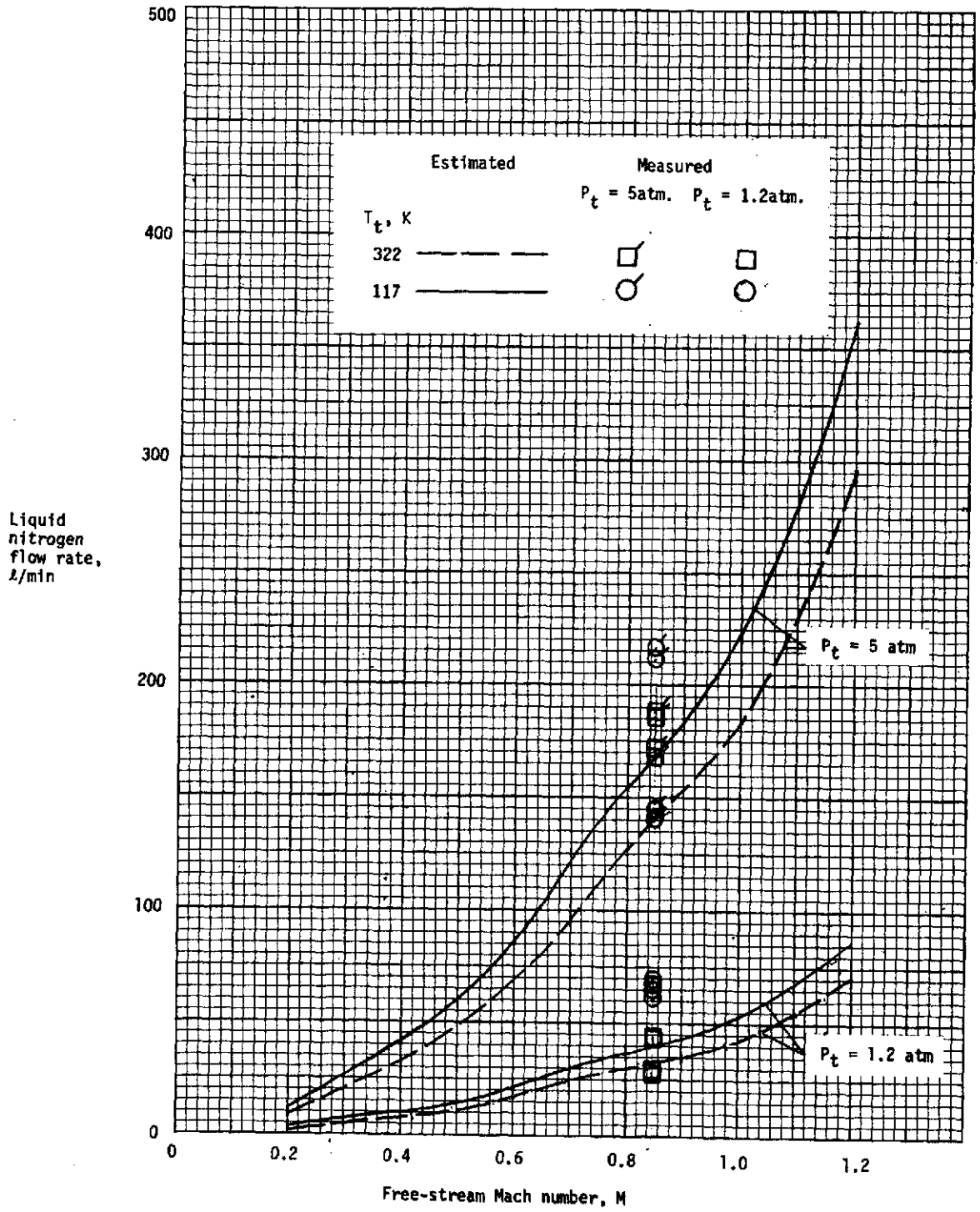

Figure 7.20 Required liquid nitrogen flow rate as a function of test Mach number, pressure, and temperature.

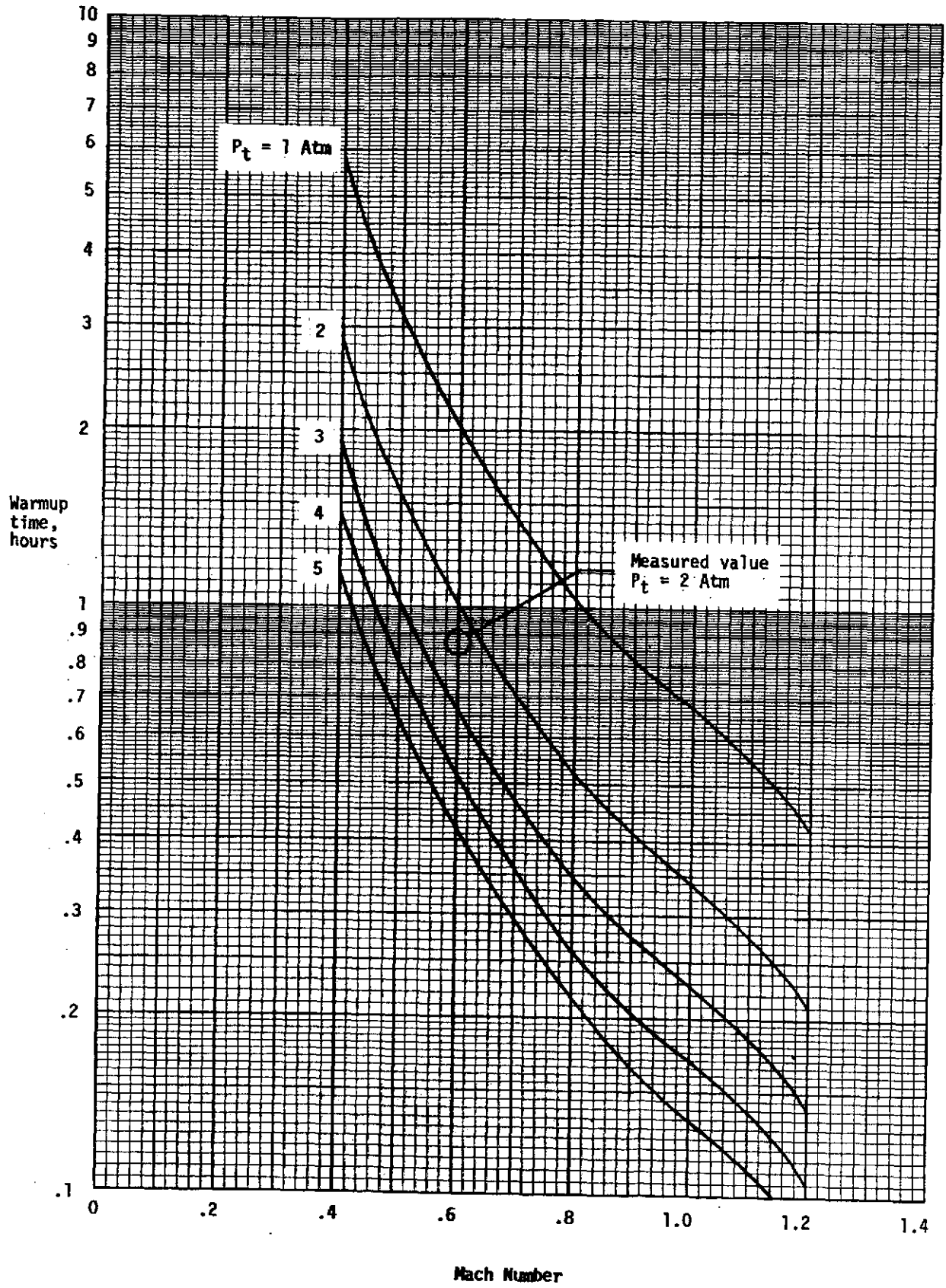

Figure 7.21 Warm-up time as a function of Mach number and pressure for warming the transonic tunnel from 110K to 300K.

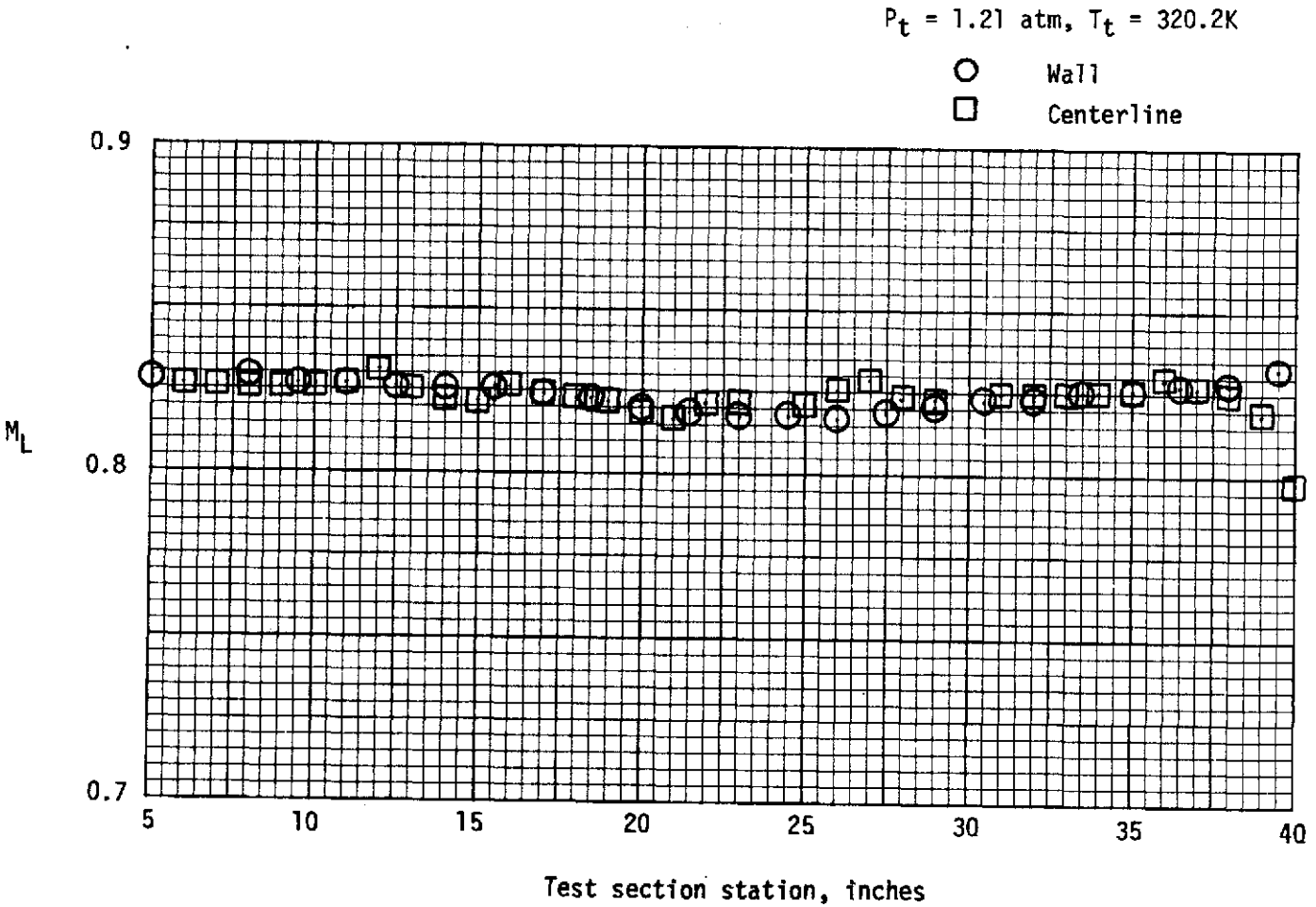

Figure 7.22 Examples of test-section wall and centerline Mach number distribution at $M_\infty \approx 0.825$.

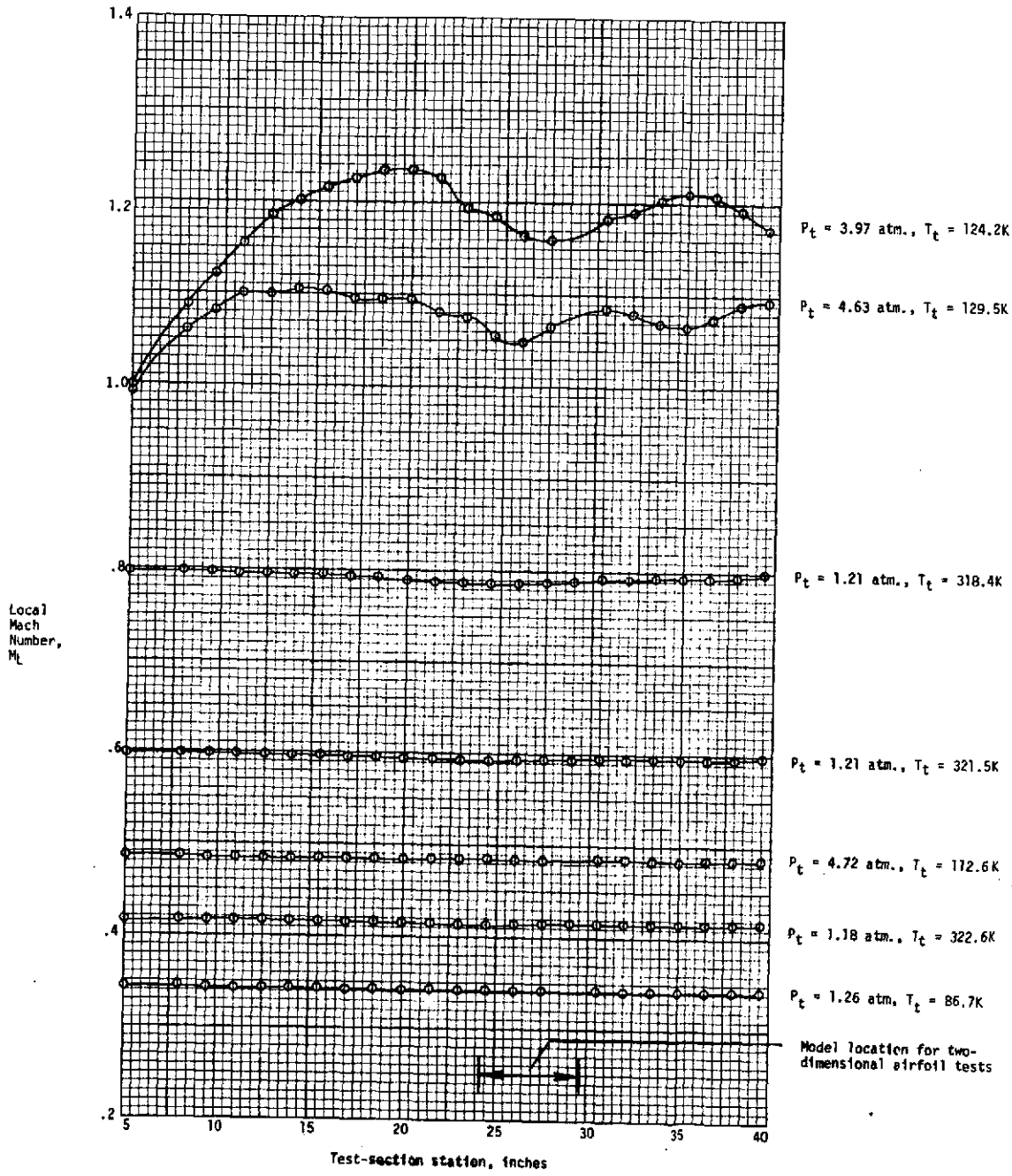

Figure 7.23 Examples of test-section wall Mach number distribution for several values of Mach number.

$M_\infty = 0.85$.

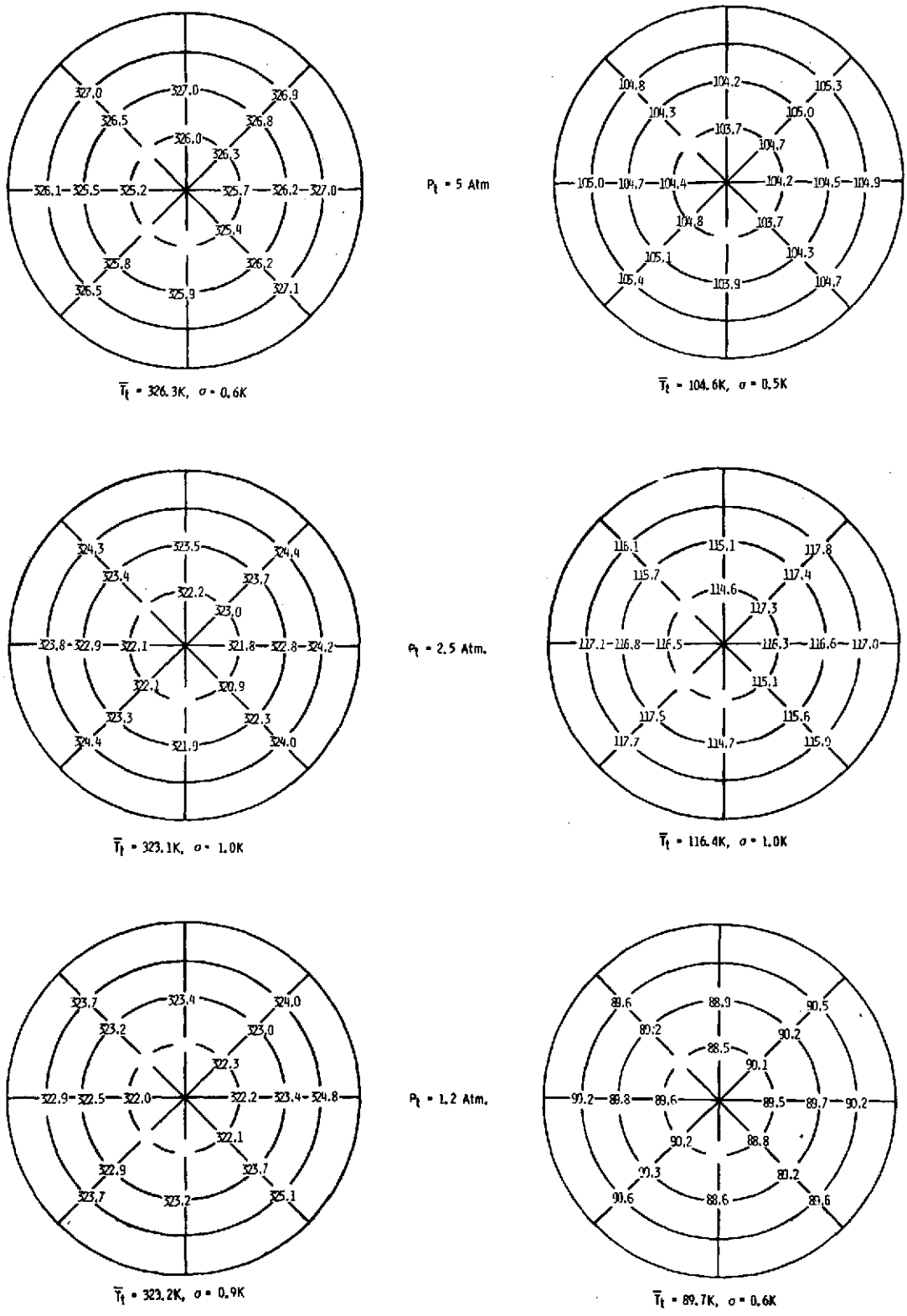

Figure 7.24 Examples of transverse temperature distribution in the transonic cryogenic tunnel. Measurements made upstream of the screens.

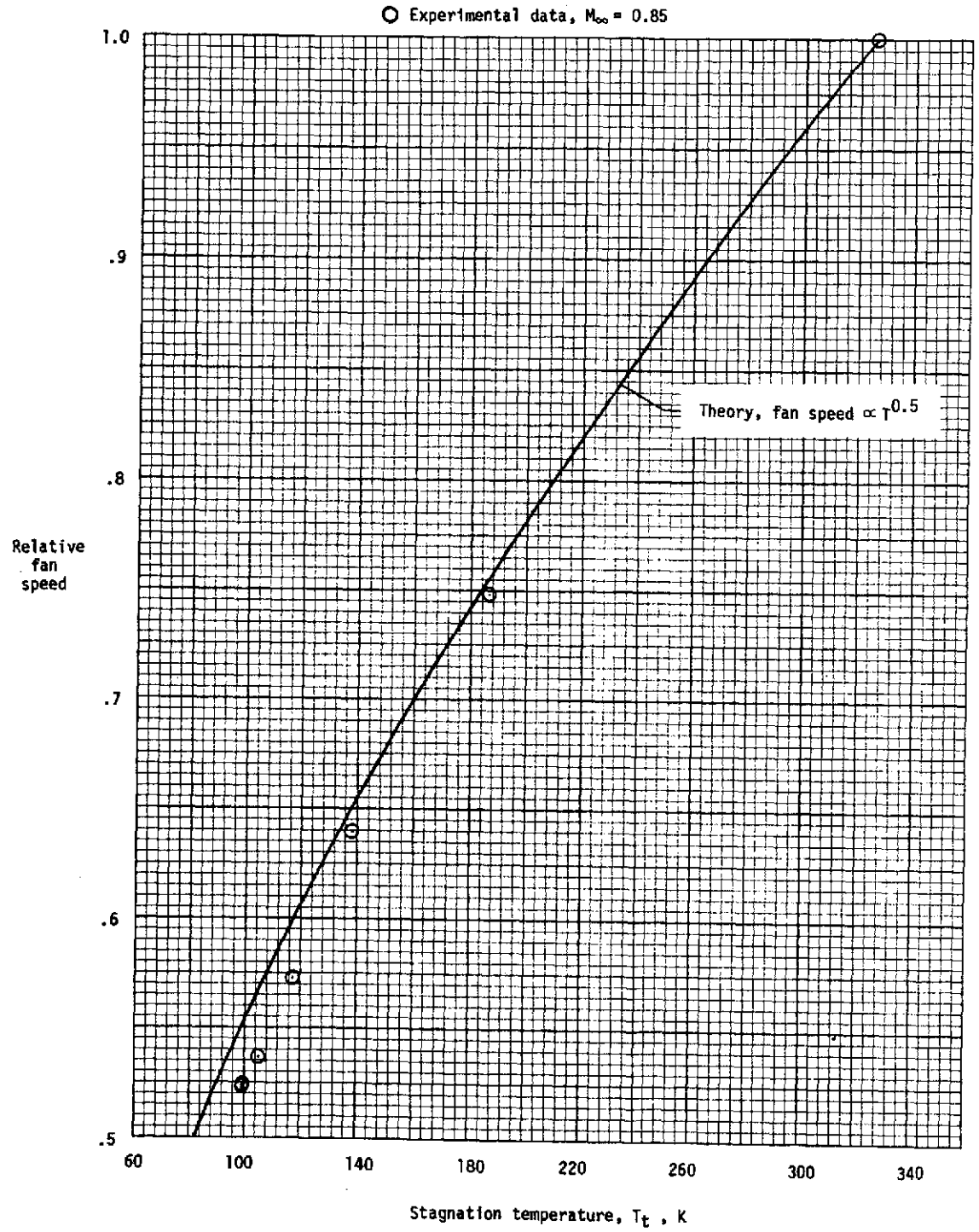

Figure 7.25 Theoretical and measured variation of fan speed relative to maximum fan speed with stagnation temperature at M_∞ = 0.85.

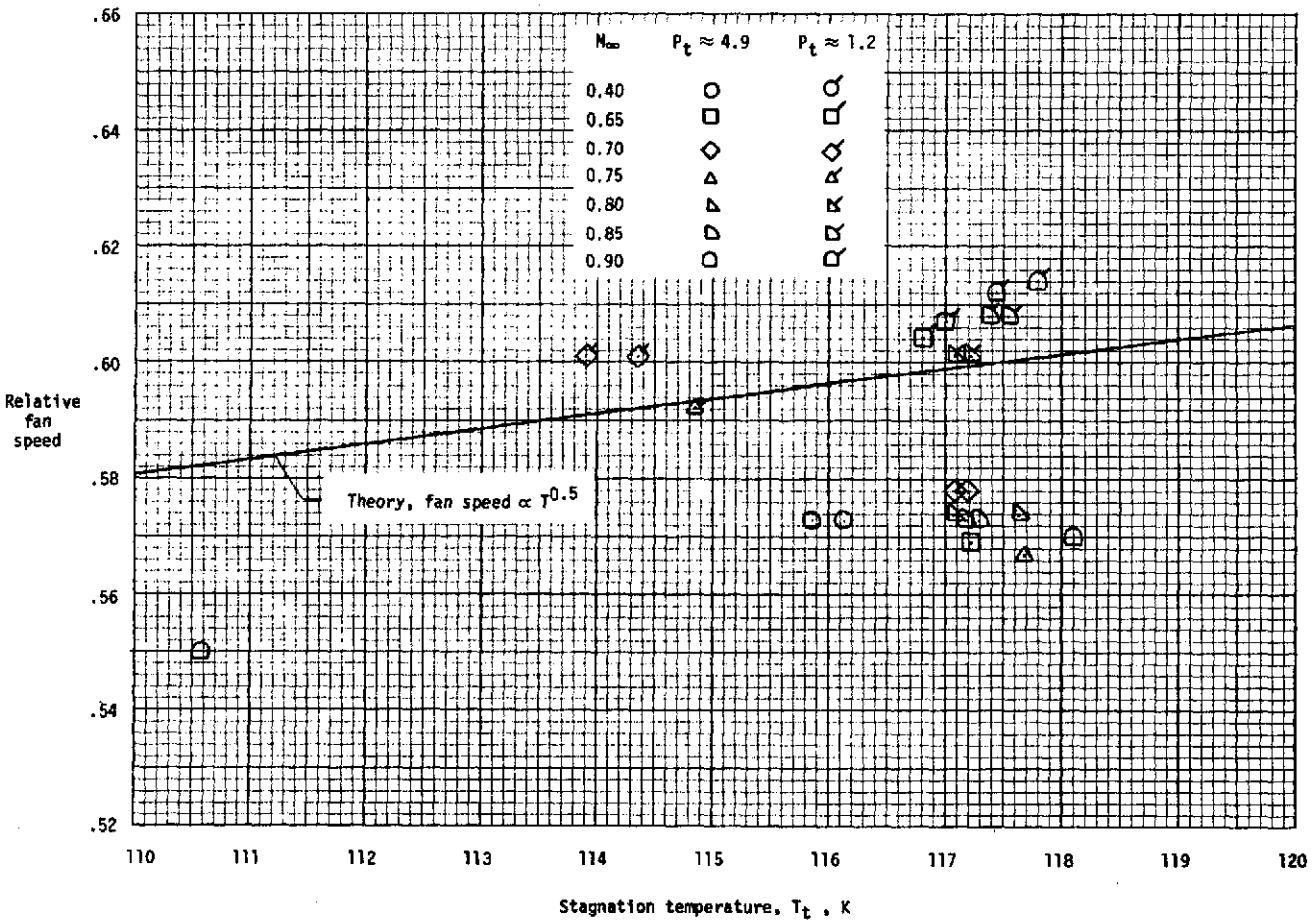

Figure 7.26 Theoretical and measured variation of fan speed relative to maximum fan speed with stagnation temperature for several values of Mach number.

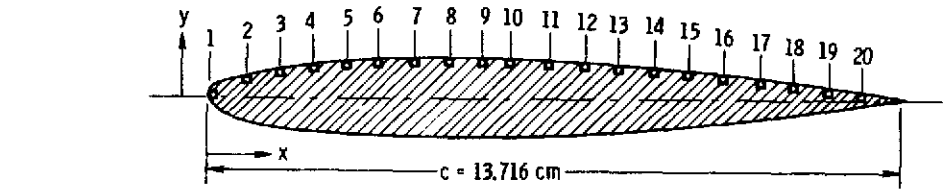

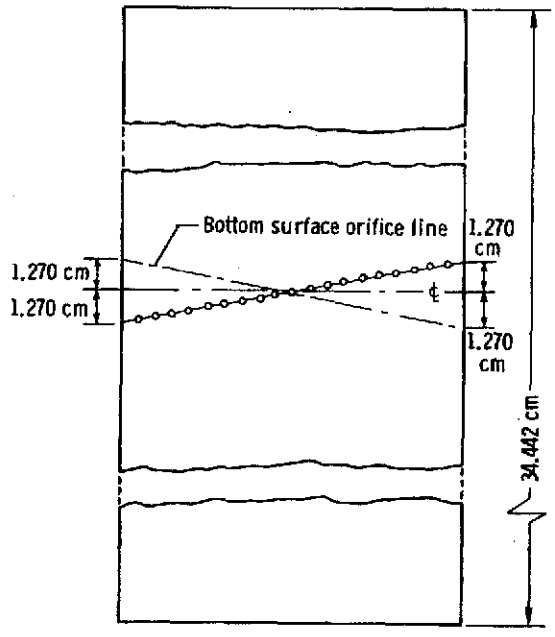

Airfoil coordinates	
x	y
0	0
0.175	± 0.249
.348	± 0.335
.699	± 0.447
1.046	± 0.523
1.372	± 0.582
2.062	± 0.668
2.743	± 0.726
4.115	± 0.800
5.486	± 0.823
6.858	± 0.800
8.230	± 0.729
9.601	± 0.615
10.973	± 0.455
12.344	± 0.257
13.030	± 0.140
13.716	± 0.015

Orifice locations		
Orifice number	Orifice station x, cm	$\frac{x}{c}$
1	0	0
2	0.698	0.0509
3	1.372	.1000
4	2.062	.1504
5	2.743	.2000
6	3.429	.2500
7	4.115	.3000
8	4.801	.3500
9	5.486	.4000
10	6.172	.4500
11	6.858	.5000
12	7.544	.5500
13	8.230	.6000
14	8.915	.6500
15	9.601	.7000
16	10.287	.7500
17	10.973	.8000
18	11.659	.8500
19	12.344	.9000
20	13.030	.9500

Figure 7.27 Two-dimensional airfoil model showing airfoil coordinates and orifice locations.

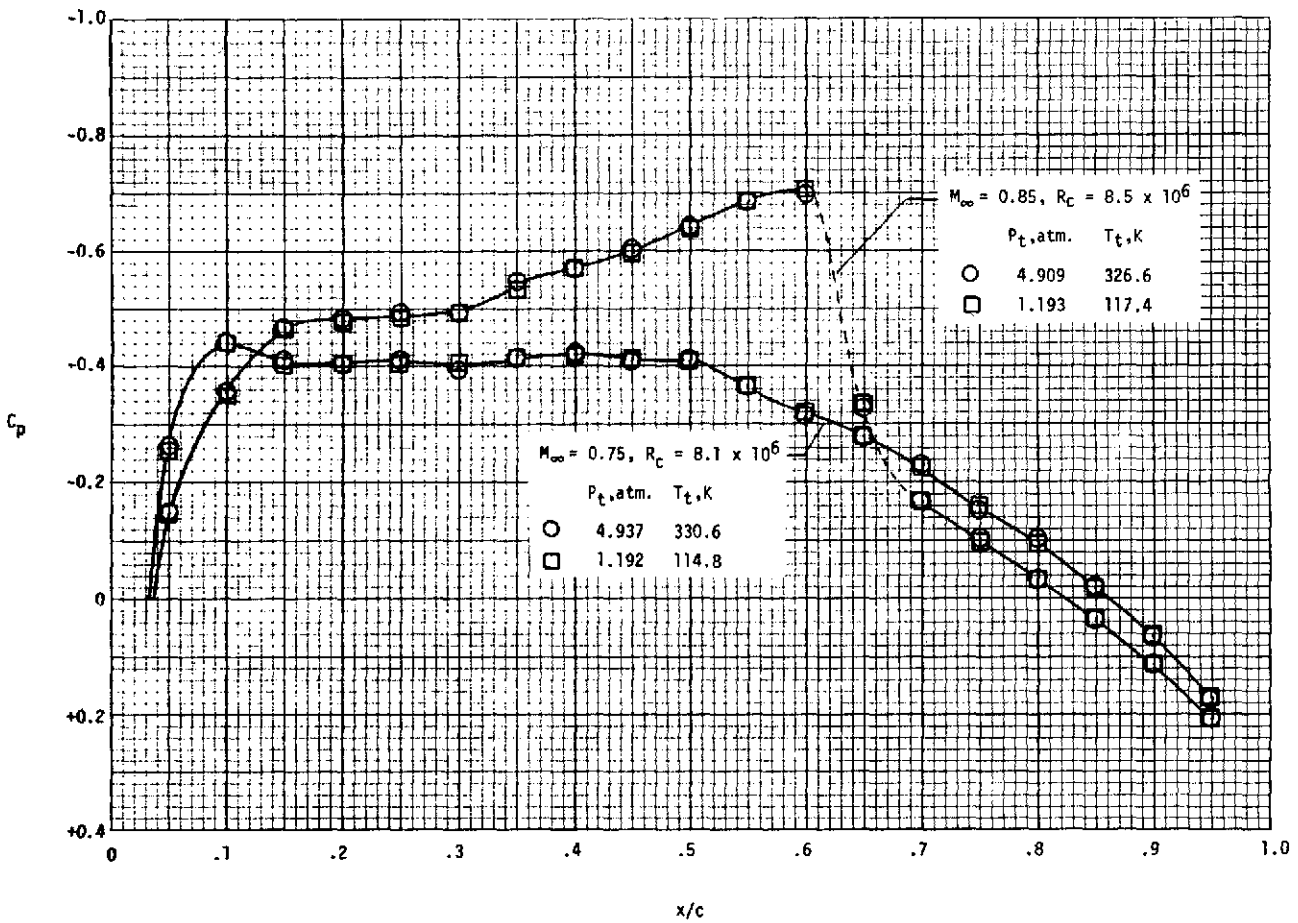

Figure 7.28 Comparison of pressure distributions on two-dimensional airfoil for ambient and cryogenic temperature conditions at free-stream Mach numbers of 0.75 and 0.85.

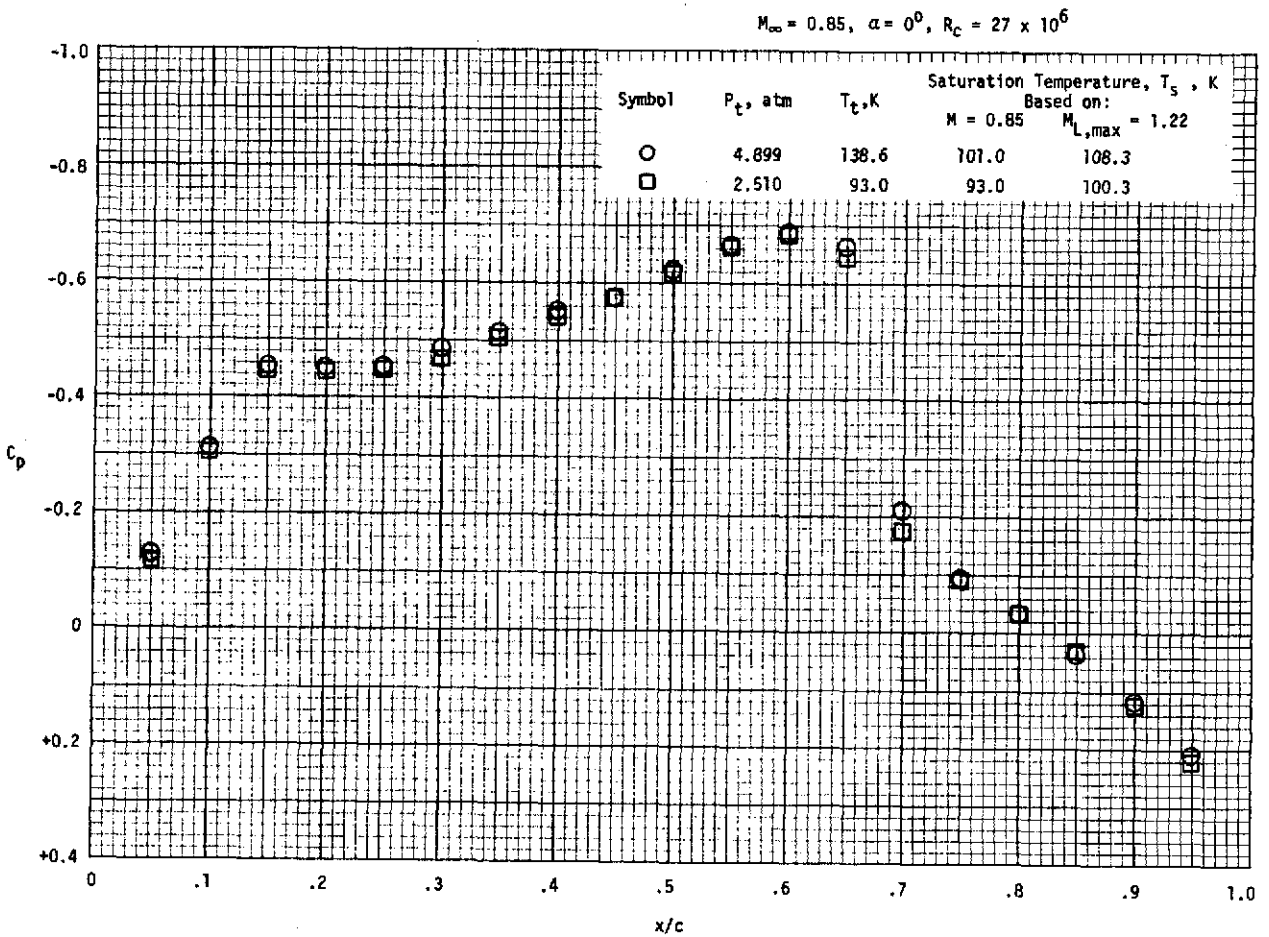

Figure 7.29 Comparison of pressure distributions on two-dimensional airfoil at $M_\infty = 0.85$ and zero incidence showing the effect of testing under conditions where portions of the flow are beyond the local saturation boundary.

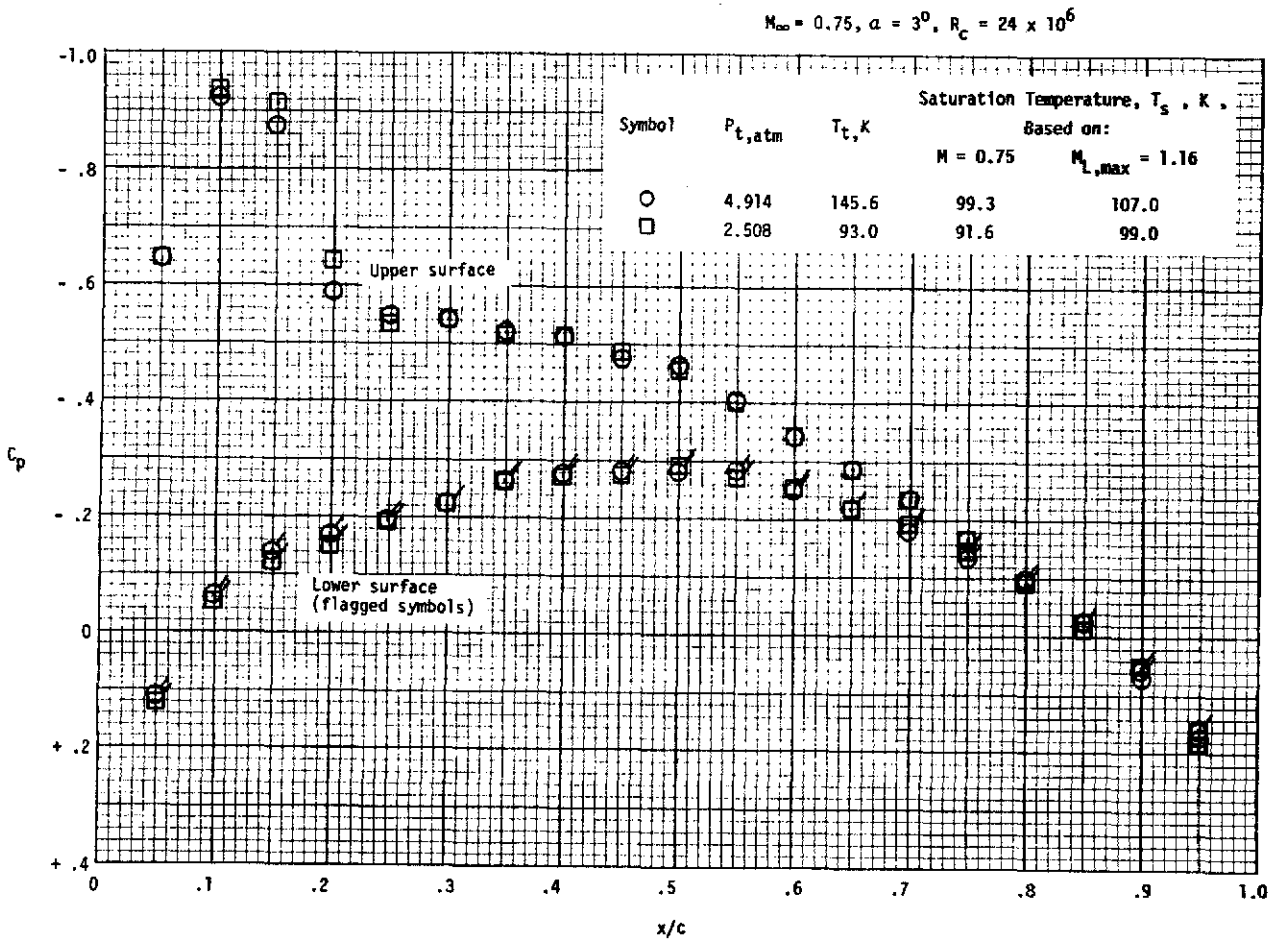

Figure 7.30 Comparison of pressure distributions on two-dimensional airfoil at $M_\infty = 0.75$ and 3^0 incidence showing the effect of testing under conditions where portions of the flow are beyond the local saturation boundary.

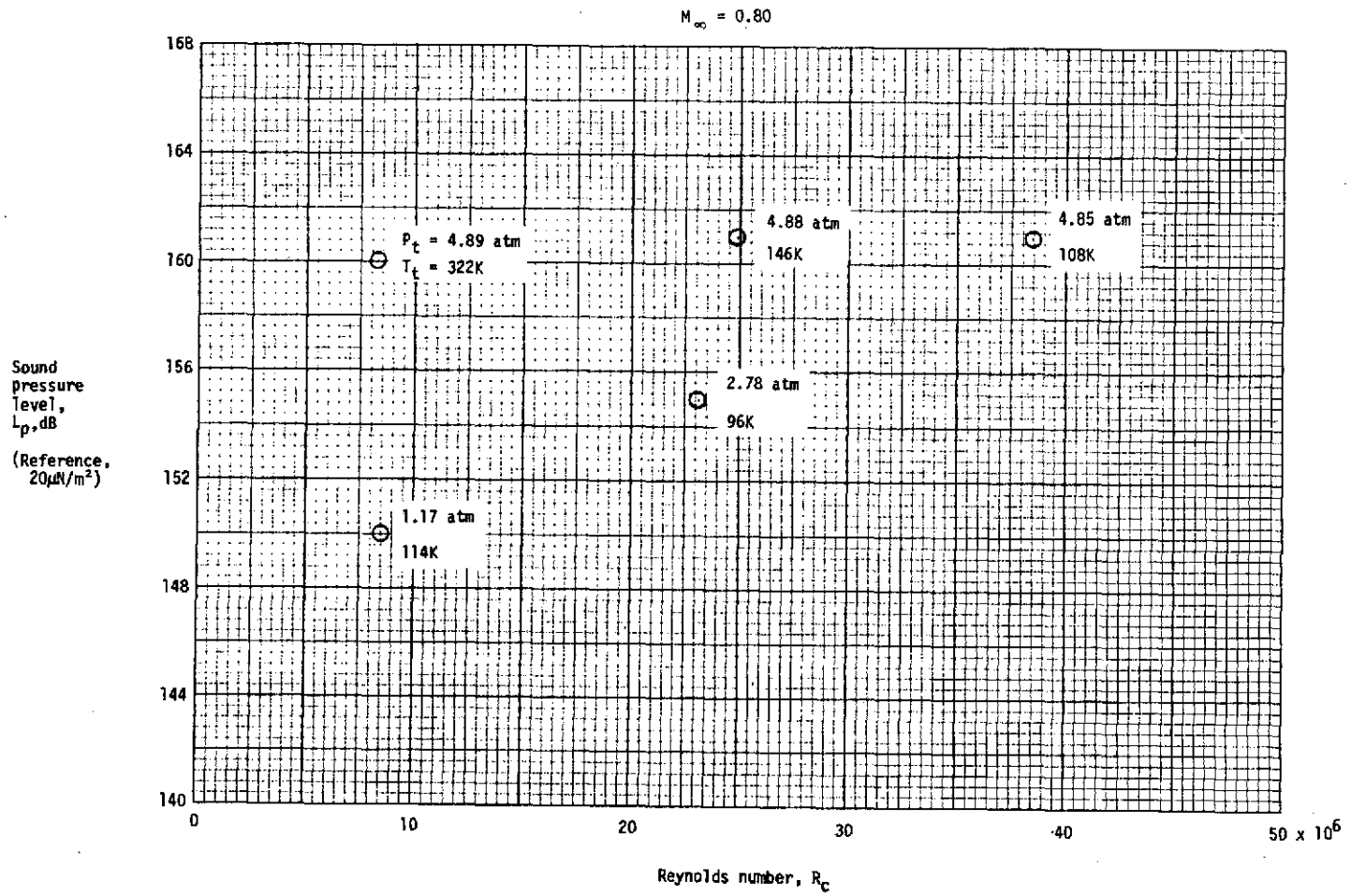

Figure 7.31 Broadband sound pressure level in the test section as a function of Reynolds number for various combinations of temperature and pressure at M_∞ = 0.80.

8. Anticipated Characteristics of Continuous-Flow High Reynolds Number Cryogenic Tunnels.

Contents:

8.1 Introduction.

As noted in Chapter 1, it is widely recognized both in the United States and in Europe that there is an urgent need for wind tunnels capable of testing models at near full-scale Reynolds number. Because of the large power requirements of transonic tunnels, economic forces have dictated the use of relatively small transonic tunnels. With ever increasing aircraft size, existing transonic tunnels are becoming even more inadequate in test Reynolds number capability. As previously noted, the cryogenic concept is applicable over a wide range of Mach number. However, a high Reynolds number transonic tunnel is at present generally considered to be one of the most urgent needs. Therefore, in this section, performance charts, anticipated design features, and anticipated operational characteristics are presented for continuous-flow fan-driven closed-circuit pressure tunnels capable of transonic operation at cryogenic temperatures. Although the information was produced specifically for low-speed and transonic fan-driven tunnels, much of the material is general in nature and is therefore applicable to supersonic cryogenic fan-driven tunnels as well as to non-fan-driven tunnels such as those described in Chapter 5.

8.2 Performance Charts.

Performance charts for continuous-flow cryogenic tunnels using nitrogen as the test gas have been prepared and published in reference 26. These charts show the variation of Reynolds number and drive power with test section size and stagnation pressure for free-stream Mach numbers of 0.35, 0.70, 1.00, and 1.20. The charts for free-stream Mach numbers of 0.35 and 1.00 are presented herein in order to illustrate the use of the charts and to illustrate by way of detailed examples the reduction in size and drive power made possible by operation at cryogenic temperatures.

8.2.1 Basic assumptions

Reynolds Number

Reynolds number is based on mean aerodynamic chord $\bar{c}$, where $\bar{c}$ is taken to be one-tenth of the square root of the test-section area. The Reynolds number calculations were based on the real-gas properties of the test gas. However, certain simplifying assumptions were made so that the majority of the calculations could be made on a relatively small digital computer. The errors introduced by the simplifying assumptions were generally less than two tenths of one-percent and are believed to be entirely negligible.

Minimum Stagnation Temperature

As previously discussed, the values of minimum stagnation temperatures were dictated by consideration of avoiding liquefaction of the test gas under the local conditions of temperature and pressure determined by isentropic expansion to an assumed maximum local Mach number, $M_{L,max}$. Three values were assumed:

(a) $M_{L,max}$ = Free-stream Mach number, M_∞

(b) $M_{L,max}$ = Typical maximum local Mach number (see Fig. 3.3)

(c) $M_{L,max}$ = High maximum local Mach number (see Fig. 3.3)

The minimum stagnation temperatures dictated by these assumed restrictions on $M_{L,max}$ can be found from the curves presented in Figure 4.1.

Drive Power

Drive power was calculated from the equation

$$\text{Drive power} = \frac{qVA\eta}{\eta'}$$

where q is the dynamic pressure in the test section, V is the velocity in the test section, A is the cross-sectional area of the test section, η the tunnel power factor (see Chapter 2, section 2.2.4), and η' is the efficiency of the drive motor. The values of η and η' used for these calculations are based on measured values in some typical transonic tunnels at the Langley Research Center. The values used in the following examples are

M_∞	η	η'
0.35	0.150	0.59
1.00	.130	.90

The performance charts for free-stream Mach numbers of 0.35 and 1.00 are presented in Figures 8.1 and 8.2 respectively.

Tabulated values of minimum stagnation temperature and other conditions relating to the performance charts are given in Tables 8.1 and 8.2 presented at the end of this chapter.

8.2.2 Examples of use of performance charts

Low-speed Testing ($M_\infty = 0.35$)

The charts for a Mach number of 0.35 are presented in Figure 8.1. For subsonic wind-tunnel research, operation at less than full-scale Reynolds numbers often appears adequate, as suggested, for example, in reference 27. For the purposes of this example, therefore, it is assumed that a fairly modest Reynolds number of 15×10^6 based on $\bar{c}$ is desired in a 3 m (9.84 feet) square test section. The maximum local Mach number on the model is assumed to be equal to the "Typical" maximum value of 0.88 (see Fig. 3.4). At these local conditions the gas-liquid saturation boundary is just reached. In Figure 8.1b the value of a 3 m test section intersects $R_{\bar{c}} = 15 \times 10^6$ to indicate operation at a stagnation pressure of about 1.16 atmospheres for a drive power of 1.37 MW (1830 horsepower). At these test conditions, Table 8.1 indicates operation with nitrogen at a stagnation temperature of about 85.9 K (-305°F). In comparison it should be noted that a conventional tunnel operating at 300 K ($+80^\circ$F) and at the same stagnation pressure, 1.16 atmospheres, and the same Reynolds number, $R_{\bar{c}} = 15 \times 10^6$, would require a 17.4 m (57.2 feet) test section with a drive power of about 88 MW (118,000 horsepower). Alternately, in a conventional tunnel operating at 300 K with the same size test section (3 m, 9.8 feet), the same Reynolds number would require operation at a stagnation pressure of 6.8 atmospheres with a drive power of about 15 MW (20,000 horsepower).

Sonic Testing ($M_\infty = 1.00$)

The performance charts for a Mach number of 1.00 are given in Figure 8.2. For the purposes of this example it is assumed that a Reynolds number of 40×10^6 based on $\bar{c}$ is desired in a 3 m (9.8 feet) square test section. The maximum local Mach number on the model

is assumed to correspond to the "Typical" maximum value of 1.40 (see Fig. 3.3). It can be seen from Figure 8.2b that a stagnation pressure of about 1.93 atmospheres is required in a cryogenic tunnel with a drive power of about 17 MW (23,000 horsepower). At these test conditions, Table 8.2 indicates operation with nitrogen at a stagnation temperature of about 102 K (-276°F).

While a stagnation temperature of 300 K is typical of low-speed testing, most conventional fan-driven transonic pressure tunnels operate at higher temperatures so that smaller heat exchangers can be used in the circuit for cooling. Thus a stagnation temperature of 322 K (+120°F) is now assumed for a conventional pressure tunnel to compare with the cryogenic pressure tunnel. At the same stagnation pressure, 1.93 atmospheres, and the same Reynolds number, $R_c = 40 \times 10^6$, a conventional tunnel operating at 322 K would require a 15.2 m (49.9 feet) test section with a drive power of about 808 MW (1,080,000 horsepower). Alternately, with a stagnation temperature of 322 K and a 3 m test-section, a Reynolds number of 40×10^6 would require a stagnation pressure of about 9.9 atmospheres and a drive power of about 160 MW (214,000 horsepower).

From the foregoing examples, it is apparent that operating at cryogenic temperature can significantly decrease the size or operating pressure and drive power requirements such that the capital cost of a high Reynolds number continuous-flow fan-driven tunnel becomes acceptable. This claim is supported by the existence of many fan-driven transonic tunnels absorbing powers greater than those required by the cryogenic tunnel. The operating costs of a cryogenic tunnel, including the cost of liquid nitrogen to cool down and hold the tunnel cool during a run, are considered in section 8.3.3.

8.3 Anticipated Design Features and Operational Characteristics.

The material presented in this section is based largely on experience gained with the low-speed and transonic cryogenic tunnels previously described, and on studies made in connection with the design of a large cryogenic tunnel. The techniques described are not necessarily the best that can be devised, but are included in order to show that workable techniques now exist and that a cryogenic tunnel is feasible at this time. There is much still to be learned, and during the design studies relating to large cryogenic tunnels, new and better techniques and procedures will undoubtedly materialize.

8.3.1 The tunnel circuit

Choice of Structural Material

As reported in reference 28, some common structural materials such as carbon steel have severely reduced impact strength at low temperatures. It is anticipated, therefore, that the cryogenic tunnel circuit would be fabricated from materials such as 9-percent nickel steel or 5058 aluminum alloy that have acceptable structural properties down to the temperature of boiling liquid nitrogen at 1 atmosphere, 77.4 K (-320.4°F). Many different aspects must be considered in deciding on the material of construction. For example, the cool down requirements are approximately 30% less for a tunnel constructed of 9-percent nickel steel compared to a tunnel constructed of aluminum alloy.

Provision must be made for an increased range of thermal expansion depending upon the choice of structural material. The worst case might be operation of the whole of the tunnel pressure vessel at the minimum temperature of the test gas stream. The change of linear dimension for a 9-percent nickel steel cryogenic tunnel being operated over a temperature range from a normal operating

temperature for fan-driven transonic tunnels of 322 K (120°F) to the minimum temperature of about 77 K (-320°F) would be about 3 times the change of linear dimension for a conventional carbon steel tunnel subjected to a temperature change from a low winter ambient of 255 K (0°F) to a normal operating temperature of 322 K. Studies made for large cryogenic tunnels indicate that conventional techniques can be used in dealing with the increased thermal expansion. In support of this view, it is noted that no problems due to thermal expansion have been encountered with the pilot transonic tunnel described in Chapter 7, section 7.2. This tunnel, which is a nominal 10 m (33 feet) long, changes length by about 4.0 cm (1.57") when the temperature of the tunnel is changed from 334 K (+152°F) to 86K (-305°F).

Thermal Insulation

Of the many types of insulation which might be used for a cryogenic tunnel, the expanded foams are perhaps best suited. They are low in initial cost, can be foamed in place or applied in pre-cut shapes, and they require no rigid vacuum jacket. Although expanded foams have a higher thermal conductivity than some other insulations, the use of the more effective and costly types of insulation is rarely justified for large ground-based systems operating at liquid nitrogen temperatures.

The optimum type and location of thermal insulation will vary with the size of the tunnel and the way a particular tunnel will be used. One method which would be suitable for relatively small tunnels would be to place the entire tunnel circuit in an insulated room or building. The main advantages of this technique are that it is simple and allows easy access to the interior and exterior of the tunnel for inspection or modification. However, for larger tunnels the increase in surface area of the building as the size of the tunnel increases may result in unacceptable liquid nitrogen usage if the

tunnel and building are kept at cryogenic temperatures for extended periods.

A relatively thin layer of insulation might be applied to the inside of a tunnel circuit in the low velocity regions in order to reduce the mass of the tunnel structure to be cooled. Internal insulation would be particularly advantageous for the type of testing which would require several cooldown and warmup operations each day since both cooldown and warmup times as well as liquid nitrogen consumption are reduced. An additional nontrivial advantage of certain types of internal insulation would be a reduction in noise within the tunnel circuit. In particular, the inner surface of the plenum surrounding the transonic test section is an ideal location for a combination thermal insulation-sound absorbing material. Also, valve and/or compressor noise could be considerably attenuated in tunnels using either passive or active plenum air removal systems if the pipes were lined on the inside with a suitable insulating-sound absorbing material.

Although the use of internal insulation offers the advantage of reduced cooldown and warmup times and costs and reduced circuit noise, there are several disadvantages to internal insulation which must also be considered. One disadvantage is that the size of the pressure shell must be increased if the insulation is internal rather than external. Another disadvantage is related to the desire, if not the requirement, to periodically inspect the tunnel pressure shell. If only a thin layer of internal insulation is used to reduce the cooldown and warmup times, it may be necessary to have additional external insulation to reduce the heat conduction through the tunnel walls to acceptable levels for tests requiring very long periods at cryogenic temperatures. Inspection of the tunnel pressure shell would be difficult in the areas where insulation was on both sides

of the tunnel shell. Another disadvantage to internal insulation in a fan-driven tunnel is the possibility of damage to the fan or other parts of the tunnel as a consequence of some insulation breaking away.

Fan Design

An analysis has been made by Goodyer which indicates that the aerodynamic matching of the drive fan with a wind tunnel operating over a range of temperatures into the cryogenic range is no more involved than for a conventional tunnel. The analysis is presented in reference 26.

8.3.2 Liquid nitrogen injection

Experience with the low-speed and transonic tunnels has demonstrated that simple and straightforward liquid nitrogen injection systems work well. Specifically, neither the location of the injector nozzles nor the detail design of the nozzles appear to be critical with respect to temperature control or distribution, within the bounds of current experience. The two injector locations which have been used, namely downstream of the test section and downstream of the fan, work equally well. The different types of nozzles which have been used seem to work equally well and all produced satisfactory temperature distributions regardless of the spray pattern at the nozzle.

The required liquid nitrogen supply pressure will be dictated by the tunnel operating pressure and by the particular injection scheme used. Experience with the transonic tunnel described in Chapter 7 , section 7.2 , indicates equally good temperature distribution for a particular set of test conditions with either four relatively large nozzles working at a few tenths of an atmosphere differential pressure or twenty small nozzles working at 5 atmospheres differential pressure.

Large nozzles are less prone to become blocked than smaller nozzles and a low-pressure liquid nitrogen supply system is less expensive than a high-pressure system. Therefore a low-pressure liquid nitrogen supply with a few relatively large nozzles is the preferred injection scheme.

If a tunnel is to be operated over wide ranges of Mach number and pressure, it may be necessary, as was the case with the pilot transonic tunnel, to have control over separate banks of nozzles in order to have proper control over the wide range of liquid nitrogen flow rate.

Where possible, a recirculating loop liquid nitrogen supply system should be used since, as noted in Chapter 7, section 7.2.10, such a system reduces supply pipe cooldown time and simplifies the control of liquid nitrogen flow rate by eliminating boiling in the supply pipe during tunnel operation.

8.3.3 Liquid nitrogen requirements

Cool-down Requirements

The amount of liquid nitrogen required to cool-down a cryogenic tunnel to its operating condition is a function of the cool-down procedure as well as the insulation and structural characteristics of the tunnel.

Under the idealized assumptions of zero heat conduction through the tunnel insulation and zero heat added to the stream by the fan during the cool-down process, the amount of liquid nitrogen required for cooling the tunnel structure is a minimum when the tunnel is cooled slowly and in such a way that the nitrogen gas leaves the tunnel circuit at a temperature equal to that of the warmest part of the structure being cooled. Again, with the same assumptions of zero heat conduction through the tunnel insulation and zero heat

added by the fan, and with the additional assumption that all of the liquid nitrogen does, in fact, vaporize, the amount of liquid nitrogen required for cool-down is a maximum when only the latent heat of vaporization is used and the nitrogen gas leaves the tunnel circuit at the saturation temperature.

Let σ represent the mass of LN_2 required to cool a unit mass of material through a given temperature range. An analysis using the method of reference 23 gave $\sigma_{min} = 0.26$ and $\sigma_{max} = 0.40$ for cooling a steel structure from 300 K (+80°F) to 100 K (-280°F).

Cooling through this large temperature range would not necessarily be a regular occurrence since under some circumstances the tunnel circuit could be allowed to remain cold between runs. Under these conditions, the heat to be removed before each run would equal the heat gained by the tunnel structure and test gas by conduction through the insulation. By proper design the heat conduction through the insulation can be kept to an acceptably low level.

Cool-down experience with the transonic cryogenic tunnel described in Chapter 7, section 7.3.2, indicates that the liquid nitrogen required for cool-down is adequately predicted by the method of reference 23. This tunnel is made of aluminum alloy with 12.7 cm (5 inches) of urethane foam applied on the outside as thermal insulation. For aluminum σ_{min} and σ_{max} are 0.44 and 0.74 respectively for cooling from 300 K to 110 K. The experimental value determined from the total amount of LN_2 used during a 30 minute cooldown of the approximately 3200 kg (7050 lbm) structure over the same temperature range is $\sigma = 0.62$.

Running Requirements

The heat to be removed while the tunnel is running consists of the heat conduction through the walls of the tunnel and the heat energy added to the tunnel circuit by the drive fan. As previously

noted, the heat conduction can be made relatively small by using reasonable thicknesses of insulation either inside or outside the tunnel structure.

The conditions assumed for the two examples previously given to illustrate the use of the tunnel design charts will now be used to illustrate the amount of liquid nitrogen required to remove the heat added to the tunnel circuit by the drive fan and by conduction through the tunnel walls.

The following assumptions are made:

square test section	3 m (9.84 feet)
tunnel surface area	5400 m^2 (58,125 ft^2)
thermal conductivity of insulation	0.0329 $\frac{W}{m^2 - {}^oK/m}$
	$\left(0.0190 \frac{Btu}{hr - ft^2 - {}^oF/ft}\right)$
insulation thickness	20 cm (7.9 inches)

It is assumed that the inner surface of the tunnel is at a temperature equal to the stagnation temperature, T_t, that there is zero temperature gradient through the metal pressure shell, and that the outside surface temperature is 300 K (+80°F).

It is also assumed that the cooling thermal capacity of the nitrogen is equal to the latent heat together with the sensible heat of the gas phase between the saturation temperature and T_t. The cooling thermal capacity for nitrogen has been calculated based on the above assumptions and is given in Figure 8.3 for a range of final gas conditions.

Low-Speed Testing ($M_\infty = 0.35$, $R_c = 15 \times 10^6$).

The earlier example gave a drive power of requirement of 1.37 MW (1830 horsepower) and a value of T_t of 85.9 K (-305°F). Under these conditions, the liquid nitrogen requirement is

6.55 kg/sec (14.44 lbm/sec) to remove heat added by fan

.94 kg/sec (2.08 lbm/sec) to remove heat conducted through walls

For this low-speed example, the liquid nitrogen required to remove the heat conducted through the walls amounts to about 12.6 percent of the total running requirement.

The total nitrogen requirement of 7.49 kg/sec (16.52 lbm/sec) would cost about 28¢/second based on the 1974 cost of liquid nitrogen in the U.S.A. of $0.0375/kg ($34/short ton).

Sonic Testing ($M_\infty = 1.00$, $R_c = 40 \times 10^6$)

This example gave a power requirement of 17 MW (23,000 horsepower) and T_t = 102 K (-276°F). Under these conditions the liquid nitrogen requirement is

77.23 kg/sec (170.27 lbm/sec) to remove heat added by fan

0.81 kg/sec (1.78 lbm/sec) to remove heat conducted through walls

For this sonic example, the liquid nitrogen required to remove the heat conducted through the walls amounts to about 1 percent of the total running requirement.

The total nitrogen requirement of 78.04 kg/sec (172.05 lbm/sec) would cost about $2.92/sec.

8.3.4 Nitrogen exhaust system

In order to hold stagnation pressure constant, the excess nitrogen gas, which amounts to about 1 percent of the test-section mass flow at sonic speeds, must be discharged from the tunnel circuit. If discharged directly from a large tunnel into the atmosphere there would be potential problems associated with fogging, discharge noise, and possible freezing and asphyxiation of personnel and wildlife. Before being discharged, therefore, the excess nitrogen gas should be

oxygenated and warmed to a safe level. Based on the results obtained with the pilot transonic tunnel described in Chapter 7, both oxygenation and warming can be achieved by discharging the nitrogen as the driver gas in an ejector which induces ambient air. The resultant mixture would be discharged through a muffler in order to reduce the noise associated with the discharge to an acceptable level. In the case of transonic testing at sufficiently high values of stagnation pressure the major portion of the discharge might be taken from the test section plenum chamber, but in other cases it might be taken from the low-speed section of the circuit.

8.3.5 The balance and model

It would be desirable to make changes on the model or to rectify faults in the balance without bringing the gas in the tunnel or the tunnel structure up to room temperature. For this purpose, the model and sting could be mechanically removed from the test section into an airlock for warming. The strain-gage balance and pressure transducers probably would be calibrated at room temperature and kept at room temperature by heating while in use in the cryogenic wind tunnel.

Complete elimination of model support interference and compromise of model shape which are inherent in conventional model-support schemes can be achieved by the use of magnetic model suspension and balance systems as described, for example, in reference 29. The demonstrated ease and rapidity with which the orientation of the model may be changed with the magnetic suspension system while keeping the model in the center of the test section will facilitate the rapid acquisition of aerodynamic data which may be a necessary feature of any high Reynolds number tunnel. In addition, the retrieval of the model from the test section of a cryogenic tunnel for model configuration changes would be a simple operation with a magnetic suspension and

balance system.

The use of magnetic-suspension systems with wind tunnel test sections greater than about 30 cm (2 feet) in diameter has, up until now, been generally discounted due to the mass of the electromagnetic coils and the problems of removing the heat generated in such coils. However, researchers at the University of Virginia have recently demonstrated a magnetic-suspension and balance system using superconducting coils which makes possible the consideration of magnetic-suspension and balance systems for large cryogenic tunnels. Thus, magnetic-suspension and balance systems appear particularly well suited for the proper exploitation and preservation over the model of the high quality flows which will be, as noted in reference 1, a necessary feature of high Reynolds number facilities.

8.3.6 Operating envelopes

In addition to the advantages of reduced dynamic pressures and reduced drive-power requirements, the cryogenic tunnel concept offers some unique operating envelopes. For a given model orientation, any aerodynamic coefficient, C, is a function of Mach number, M, a function of the dynamic pressure, q, and a function of Reynolds number, R.

$$C = f(M, q, R)$$

The ability to operate a cryogenic tunnel at constant pressure over a range of temperature allows tests to be made over a range of Reynolds number while holding dynamic pressure and Mach number constant. If the tunnel is also capable of operating over a range of pressure, tests can be made over a range of dynamic pressure while holding Mach number constant and also Reynolds number constant by suitable adjustment of temperature. With the ability to vary Mach

number, tests can be made over a range of Mach number while holding Reynolds number and dynamic pressure constant by suitable adjustments to stagnation pressure and temperature. Thus, in a cryogenic tunnel with independent control of the three variables temperature, pressure, and Mach number it is possible to determine independently the effect of the three parameters Reynolds number, dynamic pressure, and Mach number on the aerodynamic characteristics of the model.

Expressed in terms of partial derivatives, this testing ability, which is unique to the pressurized cryogenic tunnel, allows the determination of the pure partial derivatives,

$$\frac{\partial C}{\partial R} , \frac{\partial C}{\partial q} , \text{ and } \frac{\partial C}{\partial M}$$

In order to illustrate how this is accomplished, envelopes for several modes of operation are presented for a 3-meter cryogenic transonic pressure tunnel. The main purpose of the envelopes is to illustrate the various modes of operation. However, the size of the tunnel as well as the ranges of temperature, pressure, and Mach number have been selected with some care in order to represent the anticipated characteristics of a future high Reynolds number transonic tunnel.

Constant Mach Number Mode

A typical operating envelope showing the ranges of q and R available for sonic testing is presented in Figure 8.4. The envelope is bounded by the maximum temperature boundary (taken in this example to be 350 K), the minimum temperature boundary (chosen to avoid saturation with $M_{L,max} = 1.40$), the maximum pressure boundary (4.0 atmospheres), the minimum pressure boundary (0.2 atmosphere), and a boundary determined by an assumed maximum available fan drive power (45 MW (60,300 horsepower)). The arrows indicate typical paths

which might be used in determining $\frac{\partial C}{\partial R}$ and $\frac{\partial C}{\partial q}$. With such an operating capability, it is possible, for example, to determine at a constant Mach number the true effect of Reynolds number on the aerodynamic characteristics of the model, $\frac{\partial C}{\partial R}$, without having the results influenced by changes of model shape due to changing dynamic pressure as is the case in a conventional pressure tunnel. This capability is of particular importance, for example, in research on critical shock boundary layer interaction effects. As indicated by the envelope, pure aeroelastic studies can be made and various combinations of R and q can be established to accurately represent the variations in flight of aeroelastic deformation and changes of Reynolds number with altitude. Similar envelopes are of course available for other Mach numbers.

Constant Reynolds Number Mode

A typical operating envelope is presented in Figure 8.5 which shows the range of q and M which are available when testing at a constant Reynolds number of 40×10^6. The same maximum temperature limits, maximum and minimum pressure limits, and fan drive power limits have been assumed as above. The minimum temperatures were never less than those consistent with avoiding saturation under local conditions where the maximum local Mach number corresponded to the "Typical" local Mach number curve of Figure 3.3. The arrows indicate typical paths which might be used to determine $\frac{\partial C}{\partial q}$ and $\frac{\partial C}{\partial M}$. The derivative $\frac{\partial C}{\partial q}$ has been discussed above. The unique capability associated with $\frac{\partial C}{\partial M}$ allows true Mach number effects to be obtained by eliminating the usual problem introduced by changes of Reynolds number or aeroelastic effects.

Constant Dynamic Pressure Mode

Although the three derivatives were illustrated by the above envelopes, an additional form of the envelope is illustrated in

Figure 8.6 which shows the range of R and M available at a constant dynamic pressure of 100 kN/m^2 (2088.5 lb/ft^2). The arrows indicate typical paths which might be used in determining $\frac{\partial C}{\partial R}$ and $\frac{\partial C}{\partial M}$. With such an operating capability, it is possible to determine, for example, drag rise with Mach number, $\frac{\partial C_D}{\partial M}$ without having the results influenced in any way by Reynolds number or aeroelastic effects.

8.4 List of Symbols Used in Chapter 8.

Symbol	Meaning
A	test-section area
$\bar{c}$	reference chord, 0.1 $\sqrt{A}$
C	any aerodynamic coefficient
M_∞	free-stream Mach number
$M_{L,max}$	maximum local Mach number
P	pressure
q	dynamic pressure
R	Reynolds number
$R_{\bar{c}}$	Reynolds number based on $\bar{c}$
T	temperature
V	velocity
η	power factor
σ	mass of LN_2 needed to cool unit mass of material through given temperature range

Subscripts

max	maximum value
min	minimum value
D	drag
t	stagnation conditions

Table 8.1 – ASSUMED OPERATING CONDITIONS RELATED TO A CRYOGENIC NITROGEN TUNNEL AT A FREE-STREAM MACH NUMBER OF .35

STAGNATION PRESSURE, P_t, ATM.	MINIMUM STAGNATION TEMPERATURE, T_t, Min, K	REYNOLDS NUMBER PER METER, MILLIONS	REYNOLDS NUMBER FACTOR (A)	DYNAMIC PRESSURE q, kN/M^2	FREE-STREAM STATIC PRESSURE, P_∞, ATM.	FREE-STREAM STATIC TEMPERATURE, T_∞, K	COMPRESSIBILITY FACTOR UNDER FREE-STREAM CONDITIONS, Z_∞	RATIO OF SPECIFIC HEATS UNDER FREE-STREAM CONDITIONS, γ_∞
MAXIMUM LOCAL MACH NUMBER = .35								
1.00	78.5	49.3	6.5	8.0	.92	76.6	.958	1.452
1.25	80.5	59.4	6.5	10.0	1.15	78.6	.951	1.462
1.50	82.2	69.2	6.2	12.0	1.38	80.2	.944	1.472
1.75	83.6	78.7	6.2	14.0	1.61	81.6	.938	1.481
2.00	85.0	87.8	6.0	16.0	1.84	83.0	.932	1.490
2.50	87.3	105.6	5.8	20.0	2.30	85.2	.920	1.508
3.00	89.3	122.6	5.6	23.9	2.76	87.2	.910	1.526
3.50	91.0	139.2	5.4	27.9	3.22	88.8	.900	1.543
4.00	92.6	155.1	5.3	31.9	3.68	90.4	.891	1.560
5.00	95.4	185.7	5.1	39.9	4.59	93.1	.874	1.593
MAXIMUM LOCAL MACH NUMBER = .88								
1.00	84.6	44.0	5.8	8.0	.92	82.6	.967	1.442
1.25	86.6	53.1	5.8	10.0	1.15	84.5	.961	1.450
1.50	88.3	61.9	5.5	12.0	1.38	86.2	.956	1.458
1.75	89.8	70.4	5.5	14.0	1.61	87.7	.951	1.465
2.00	91.2	78.7	5.3	16.0	1.84	89.0	.946	1.473
2.50	93.5	94.8	5.1	20.0	2.30	91.3	.937	1.487
3.00	95.5	110.2	5.0	23.9	2.76	93.2	.928	1.501
3.50	97.3	125.1	4.8	27.9	3.22	95.0	.920	1.515
4.00	98.9	139.6	4.7	31.9	3.68	96.5	.913	1.529
5.00	101.7	167.4	4.5	39.9	4.59	99.3	.899	1.555
MAXIMUM LOCAL MACH NUMBER = 1.42								
1.00	96.2	36.2	4.8	8.0	.92	93.9	.978	1.428
1.25	98.2	43.9	4.8	10.0	1.15	95.9	.974	1.434
1.50	100.0	51.3	4.6	12.0	1.38	97.6	.970	1.439
1.75	101.6	58.4	4.6	14.0	1.61	99.2	.967	1.445
2.00	102.9	65.5	4.4	16.0	1.84	100.4	.963	1.450
2.50	105.4	79.0	4.3	20.0	2.30	102.9	.957	1.460
3.00	107.4	92.1	4.2	23.9	2.76	104.8	.951	1.470
3.50	109.3	104.7	4.0	27.9	3.22	106.7	.946	1.479
4.00	110.9	117.1	4.0	31.9	3.68	108.2	.940	1.488
5.00	113.8	140.7	3.8	39.9	4.59	111.1	.930	1.507

(A) REYNOLDS NUMBER OBTAINED AT MINIMUM STAGNATION TEMPERATURE DIVIDED BY REYNOLDS NUMBER OBTAINED AT TYPICAL STAGNATION TEMPERATURE OF 300 K(+ 80°F)

Table 8.2 - ASSUMED OPERATING CONDITIONS RELATED TO A CRYOGENIC NITROGEN TUNNEL AT A FREE-STREAM MACH NUMBER OF 1.00

STAGNATION PRESSURE, P_t, ATM.	MINIMUM STAGNATION TEMPERATURE, T_t, Min, K	REYNOLDS NUMBER PER METER, MILLIONS	REYNOLDS NUMBER FACTOR (A)	DYNAMIC PRESSURE q, kN/M^2	FREE-STREAM STATIC PRESSURE, P_∞, ATM.	FREE-STREAM STATIC TEMPERATURE, T_∞, K	COMPRESSIBILITY FACTOR UNDER FREE-STREAM CONDITIONS, Z_∞	RATIO OF SPECIFIC HEATS UNDER FREE-STREAM CONDITIONS, γ_∞
MAXIMUM LOCAL MACH NUMBER = 1.00								
1.00	86.7	88.4	6.6	37.5	.53	72.3	.972	1.434
1.25	88.8	106.6	6.3	46.8	.66	74.0	.967	1.441
1.50	90.5	124.4	6.1	56.2	.79	75.4	.962	1.447
1.75	92.0	141.7	5.9	65.6	.92	76.7	.958	1.453
2.00	93.4	158.4	5.8	74.9	1.06	77.8	.954	1.458
2.50	95.7	191.1	5.6	93.7	1.32	79.8	.946	1.470
3.00	97.7	222.4	5.5	112.4	1.59	81.4	.938	1.481
3.50	99.6	252.3	5.3	131.1	1.85	83.0	.932	1.491
4.00	101.2	281.7	5.2	149.9	2.11	84.3	.925	1.501
5.00	104.0	338.5	5.0	187.3	2.64	86.7	.912	1.522
MAXIMUM LOCAL MACH NUMBER = 1.40								
1.00	95.7	76.0	5.7	37.5	.53	79.7	.979	1.426
1.25	97.8	92.0	5.4	46.8	.66	81.5	.976	1.431
1.50	99.5	107.5	5.3	56.2	.79	82.9	.972	1.435
1.75	101.1	122.6	5.1	65.6	.92	84.2	.969	1.440
2.00	102.5	137.3	5.0	74.9	1.06	85.4	.966	1.444
2.50	104.9	165.8	4.9	93.7	1.32	87.4	.960	1.453
3.00	107.0	193.3	4.8	112.4	1.59	89.1	.954	1.461
3.50	108.8	220.0	4.6	131.1	1.85	90.7	.949	1.469
4.00	110.4	245.9	4.5	149.9	2.11	92.0	.944	1.477
5.00	113.3	295.9	4.4	187.3	2.64	94.4	.934	1.492
MAXIMUM LOCAL MACH NUMBER = 1.70								
1.00	104.2	66.8	5.0	37.5	.53	86.8	.984	1.420
1.25	106.4	81.0	4.8	46.8	.66	88.7	.981	1.424
1.50	108.2	94.8	4.7	56.2	.79	90.2	.978	1.427
1.75	109.7	108.4	4.5	65.6	.92	91.4	.976	1.431
2.00	111.2	121.4	4.5	74.9	1.06	92.7	.973	1.434
2.50	113.7	146.8	4.3	93.7	1.32	94.8	.969	1.441
3.00	115.8	171.4	4.2	112.4	1.59	96.5	.964	1.448
3.50	117.7	195.2	4.1	131.1	1.85	98.1	.960	1.454
4.00	119.4	218.3	4.0	149.9	2.11	99.5	.956	1.460
5.00	122.3	263.3	3.9	187.3	2.64	101.9	.949	1.472

(A) REYNOLDS NUMBER OBTAINED AT MINIMUM STAGNATION TEMPERATURE DIVIDED BY REYNOLDS NUMBER OBTAINED AT TYPICAL STAGNATION TEMPERATURE OF 322 K (+120° F)

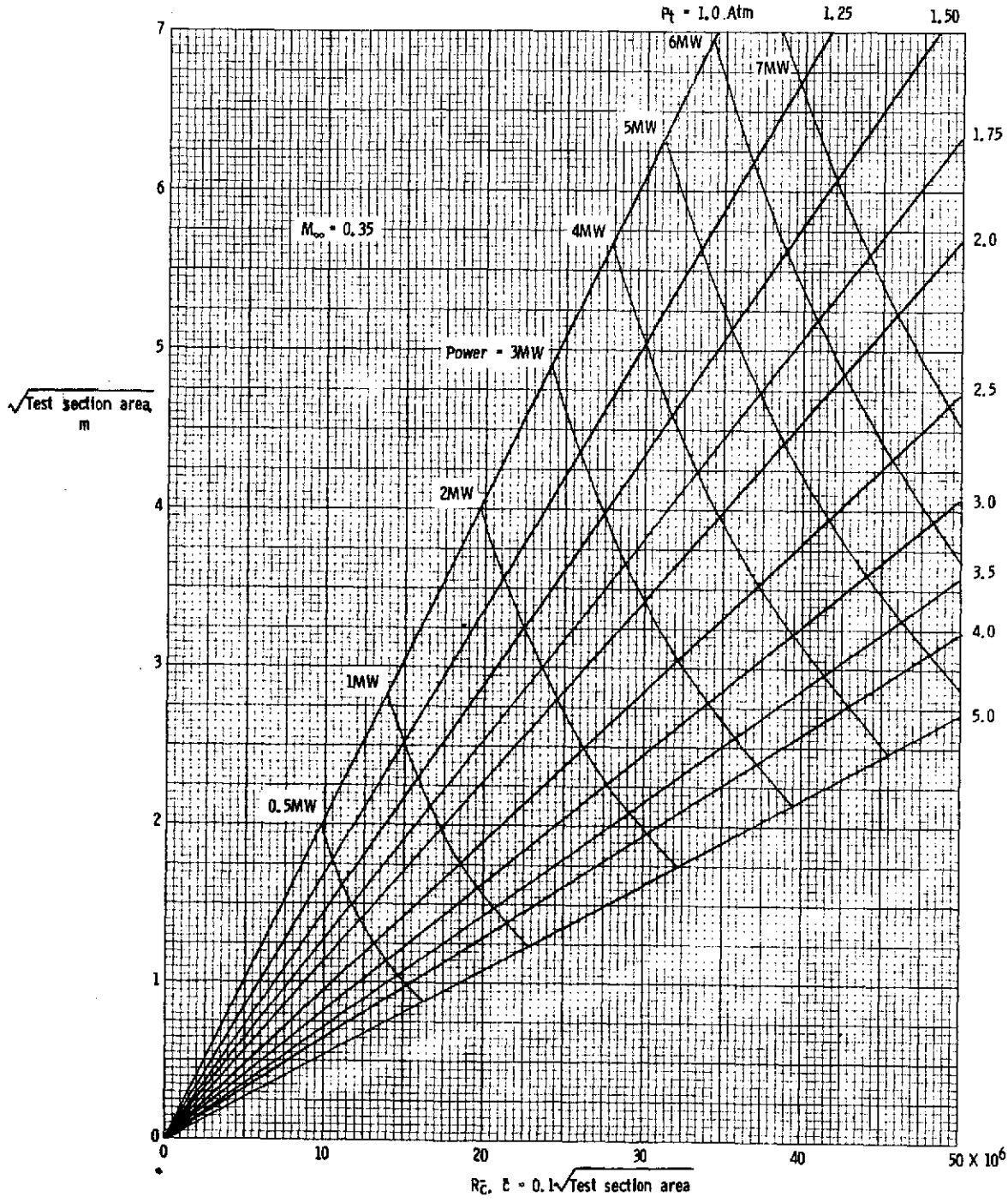

(a) $M_{L,max} = 0.35$

Figure 8.1 Performance chart for cryogenic nitrogen tunnel showing relationship between tunnel size, stagnation pressure, drive power, and Reynolds number for a free-stream Mach number of 0.35.

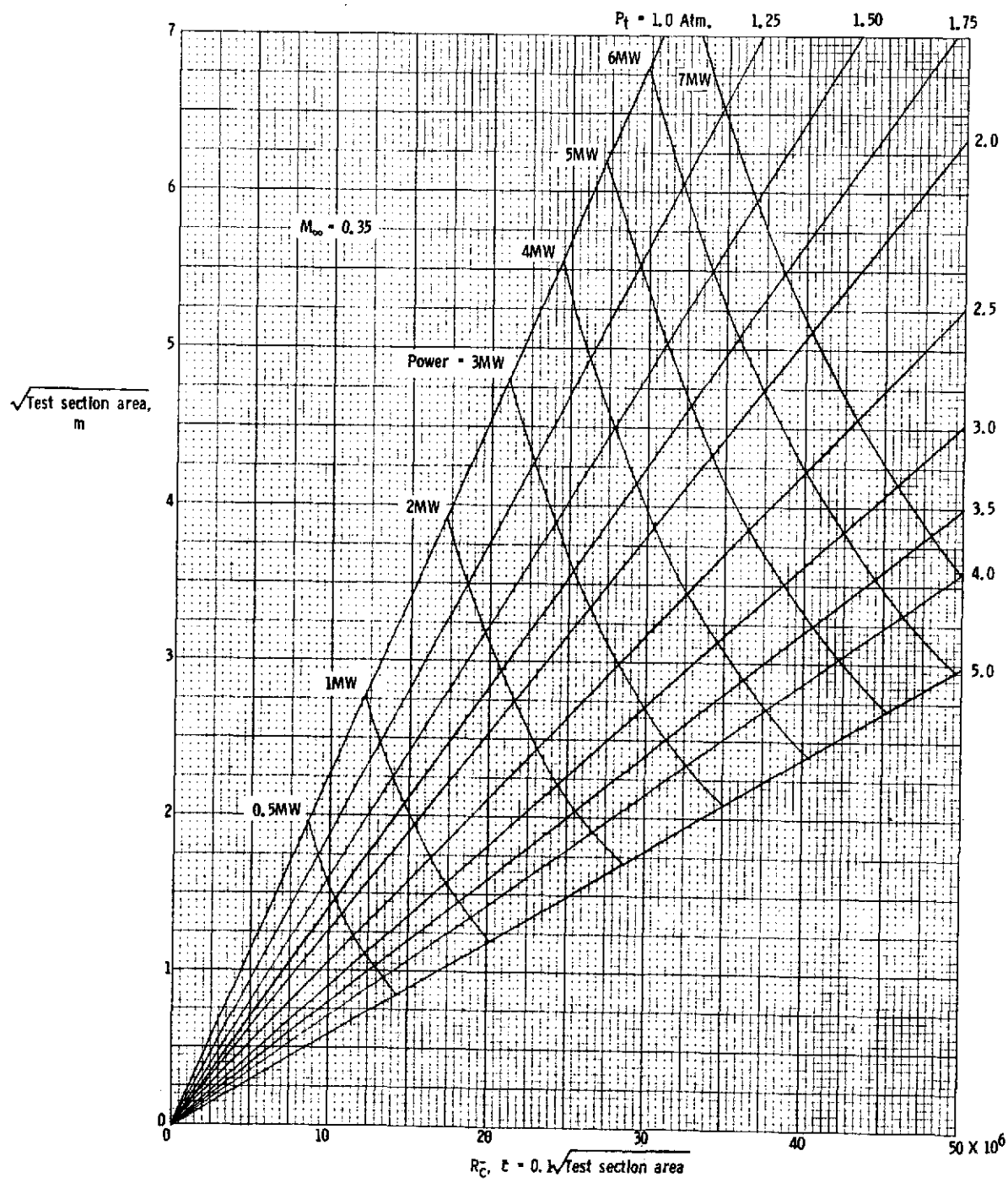

(b) $M_{L,max} = 0.88$

Figure 8.1 Continued.

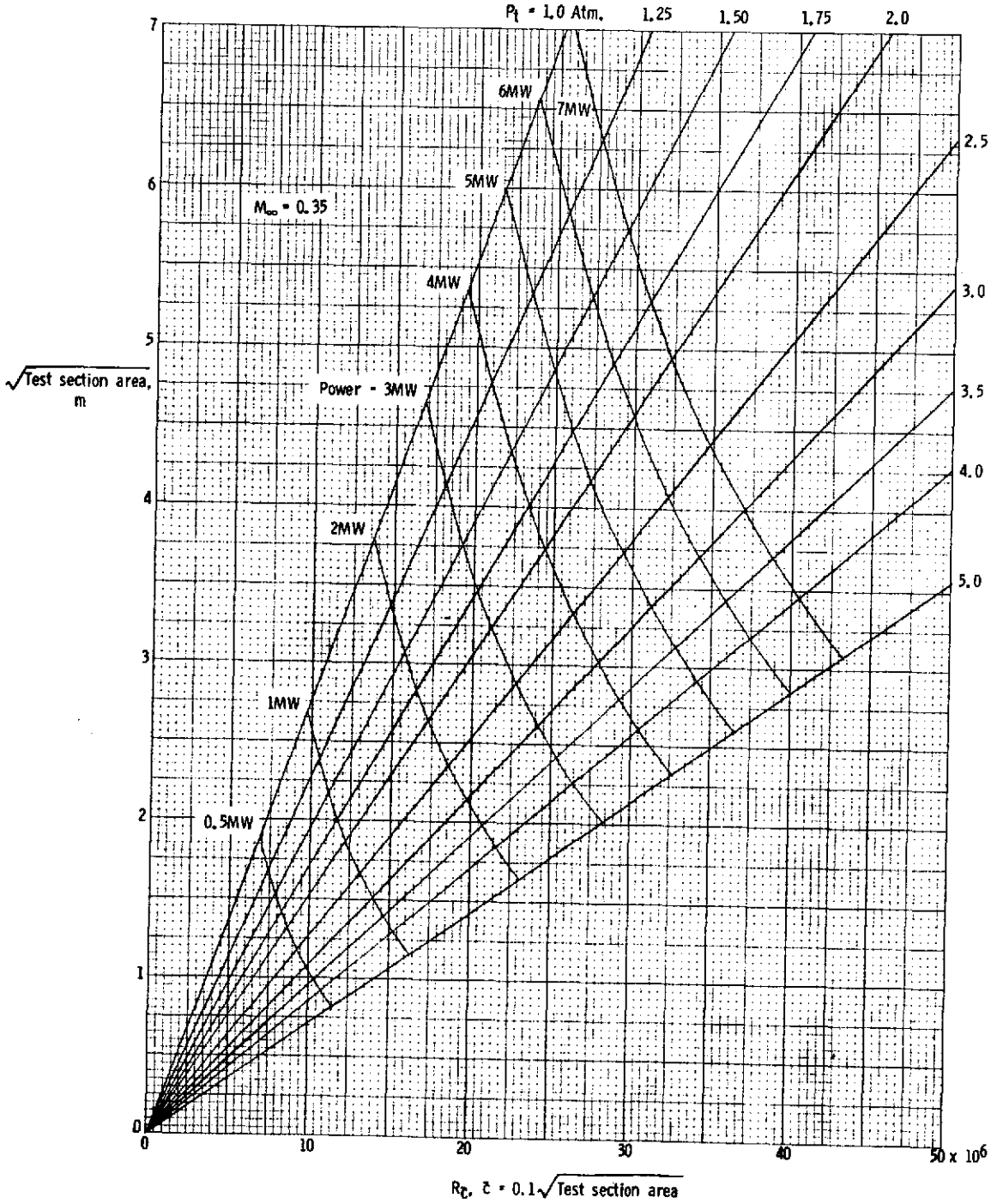

(c) $M_{L,max}$ = 1.42

Figure 8.1 Concluded.

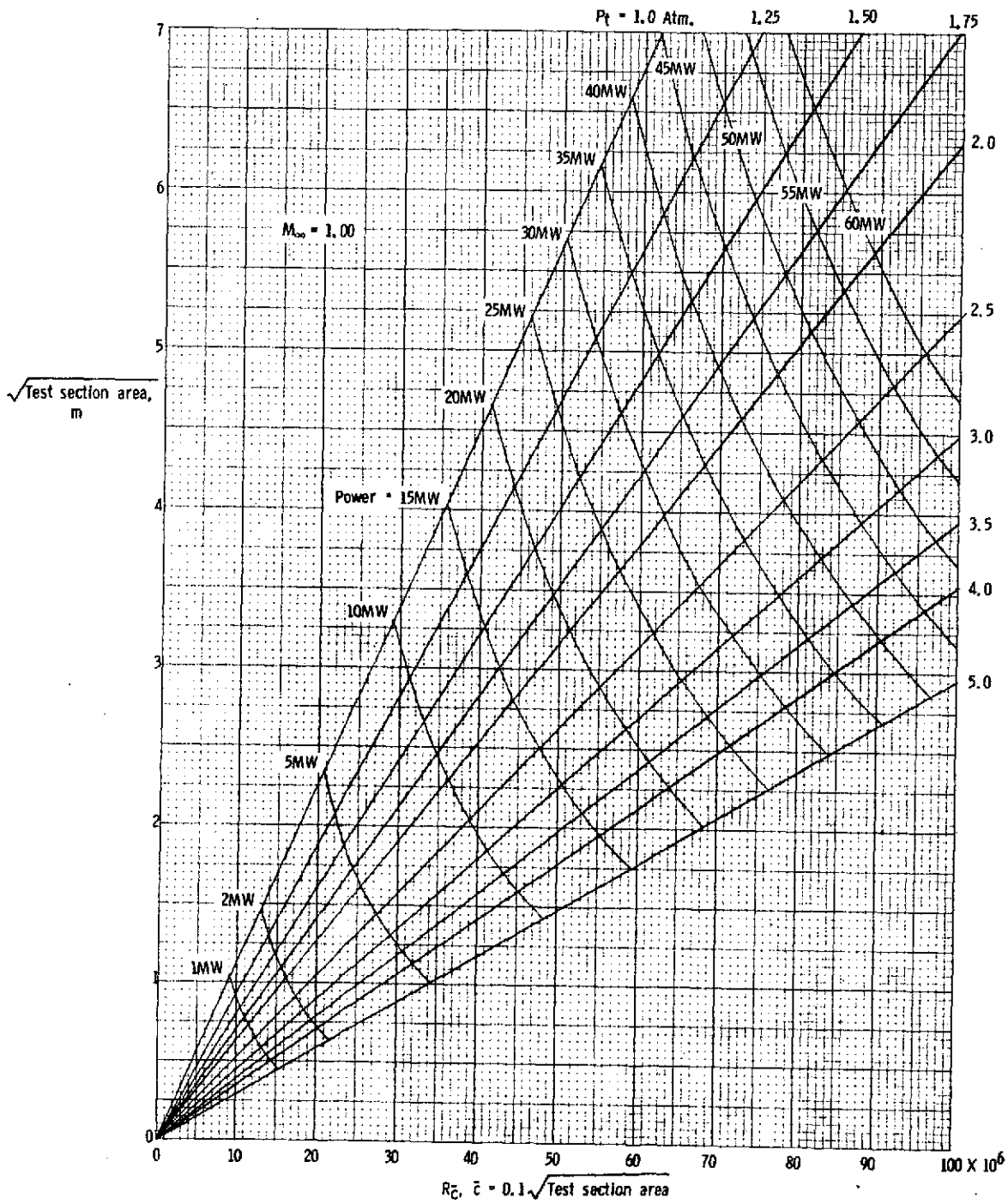

(a) $M_{L,max}$ = 1.00

Figure 8.2 Performance chart for cryogenic nitrogen tunnel showing relationship between tunnel size, stagnation pressure drive power, and Reynolds number for a free-stream Mach number of 1.00.

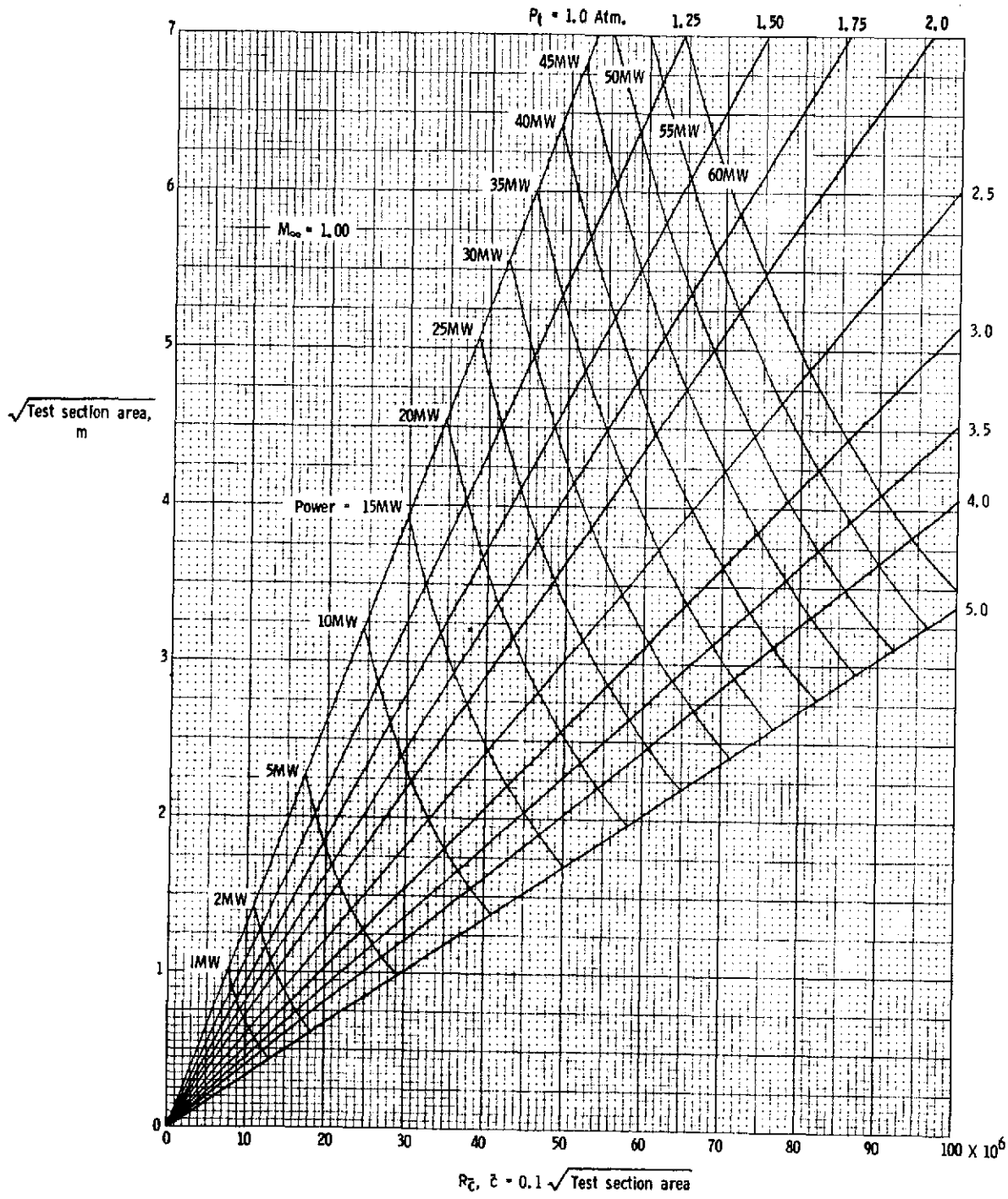

(b) $M_{L,max}$ = 1.40

Figure 8.2 Continued.

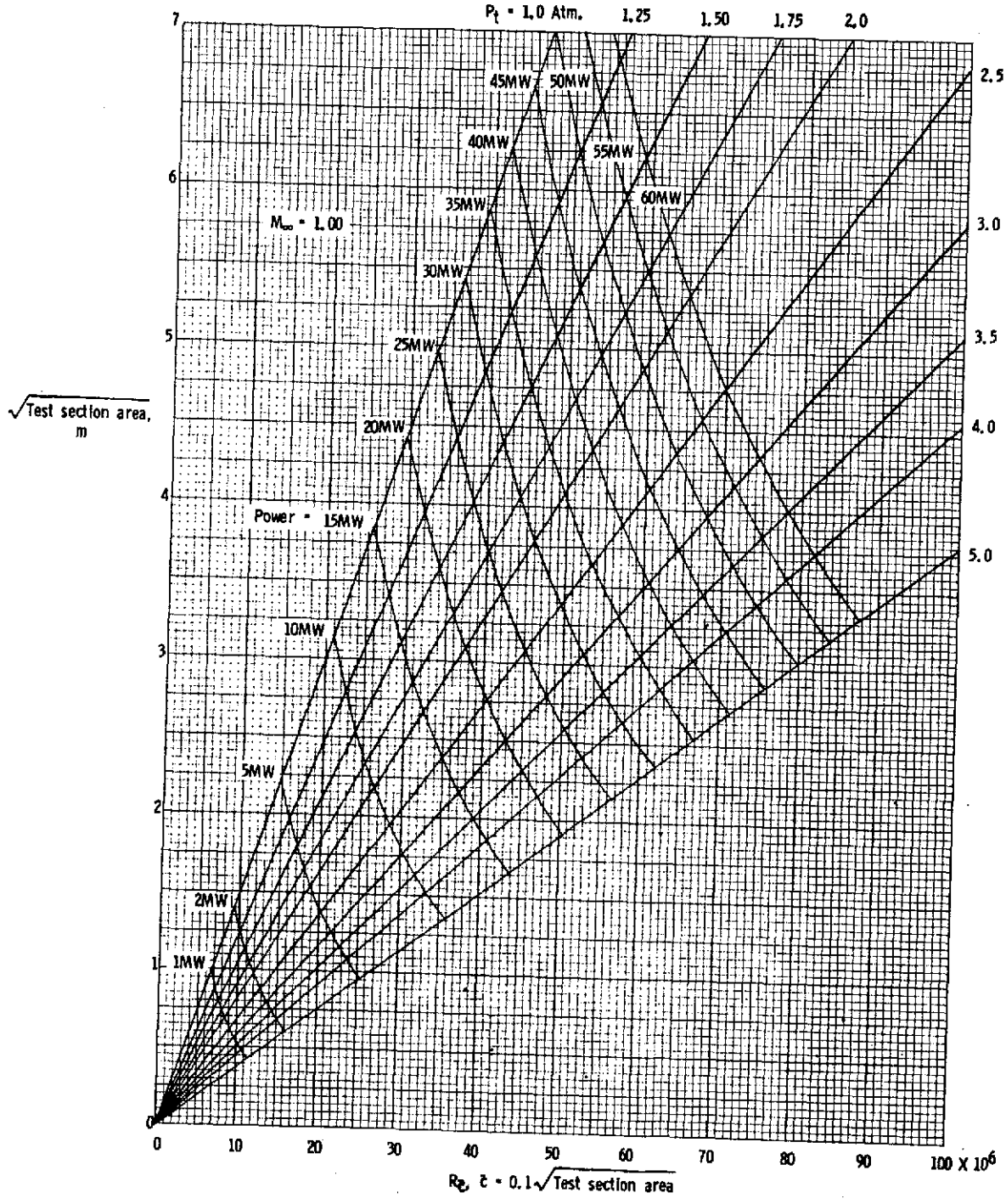

(c) $M_{L,max} = 1.70$

Figure 8.2 Concluded.

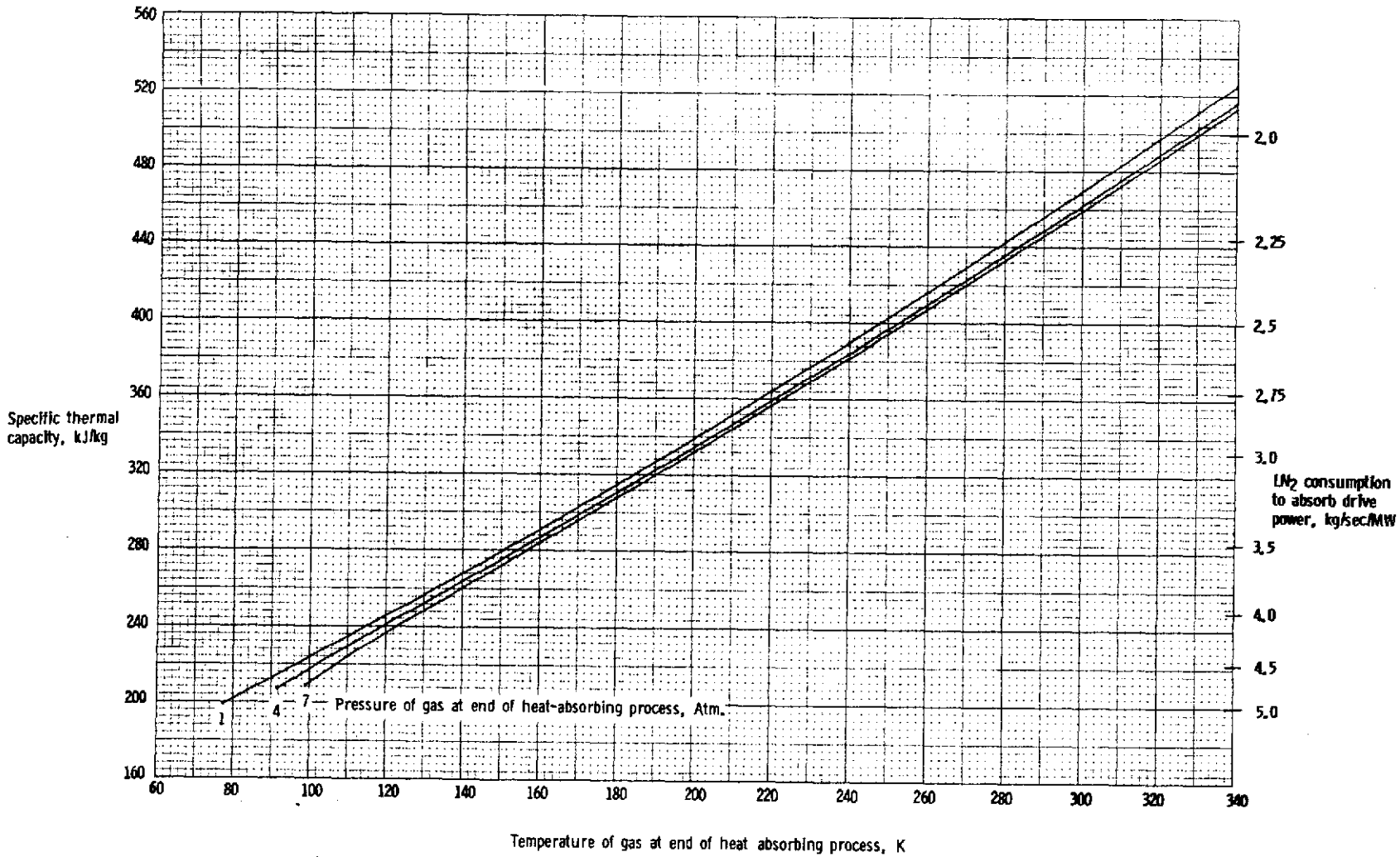

Figure 8.3 Heat absorbing capacity of liquid nitrogen. Liquid initially at a pressure of one atmosphere and a temperature of 77.347K.

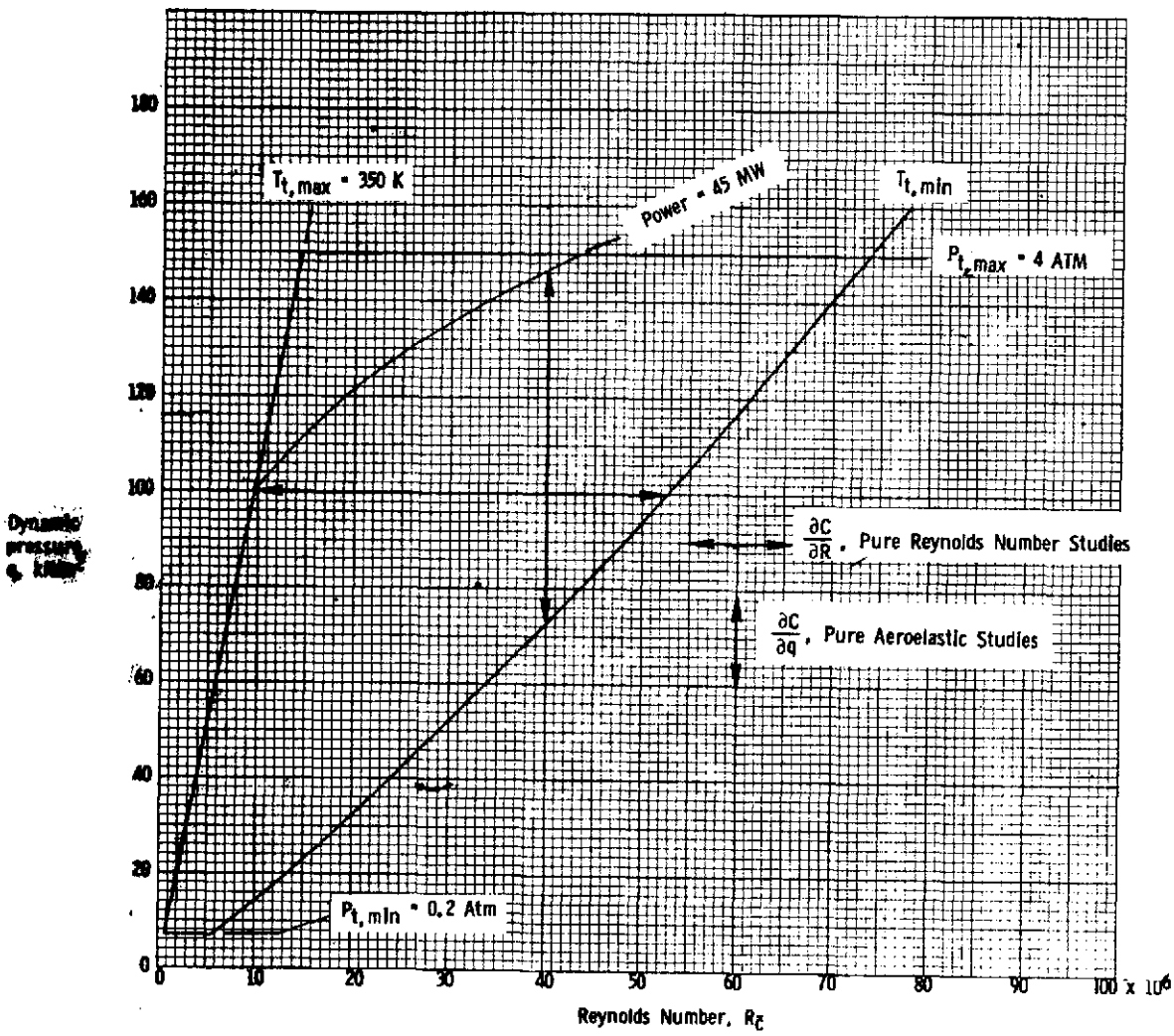

Figure 8.4 Constant Mach number operating envelope for a cryogenic nitrogen tunnel having a 3m x 3m test section. M_∞ = 1.00.

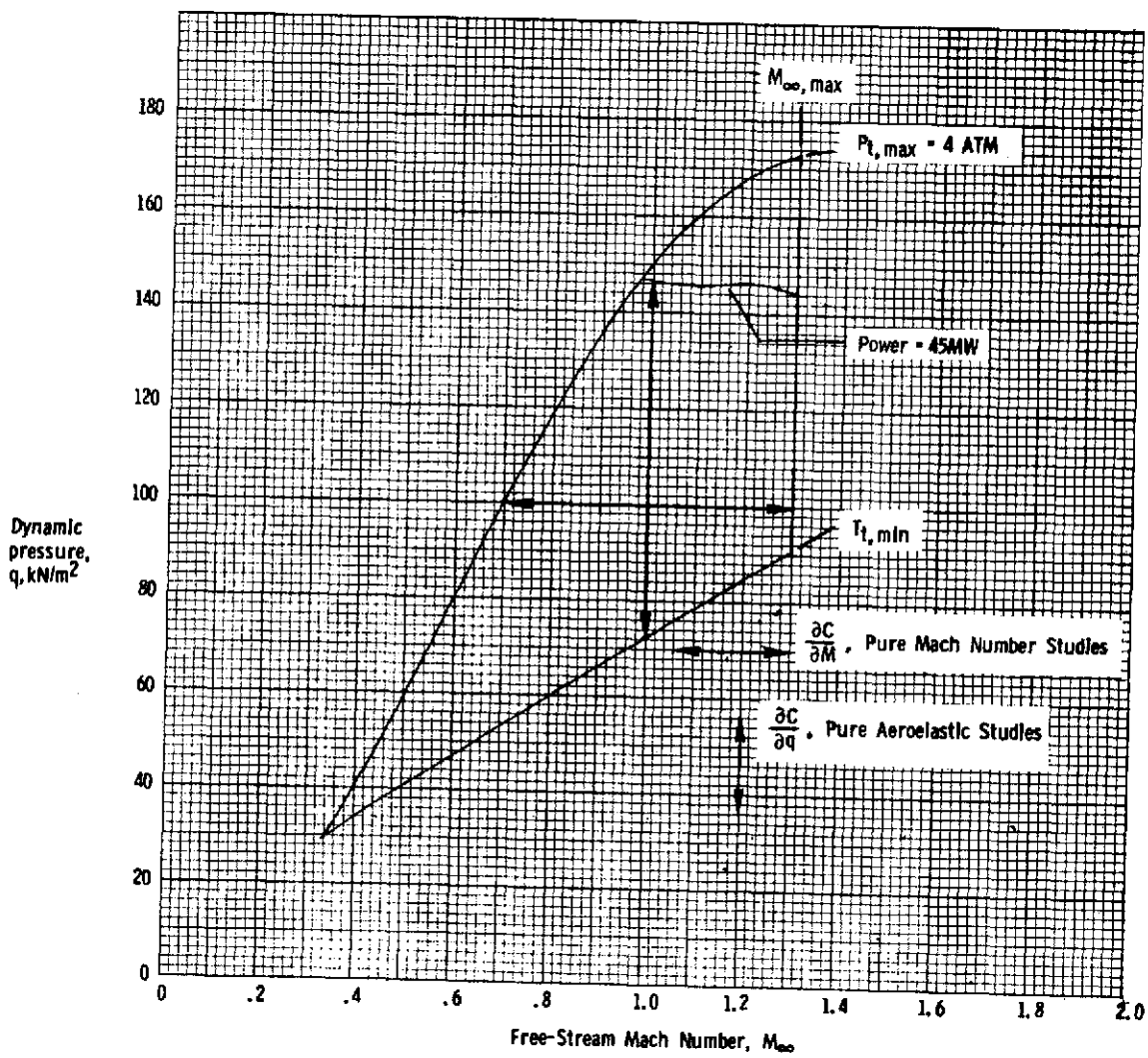

Figure 8.5 Constant Reynolds number operating envelope for a cryogenic nitrogen tunnel having a 3m x 3m test section. $R_{\bar{c}} = 40 \times 10^6$.

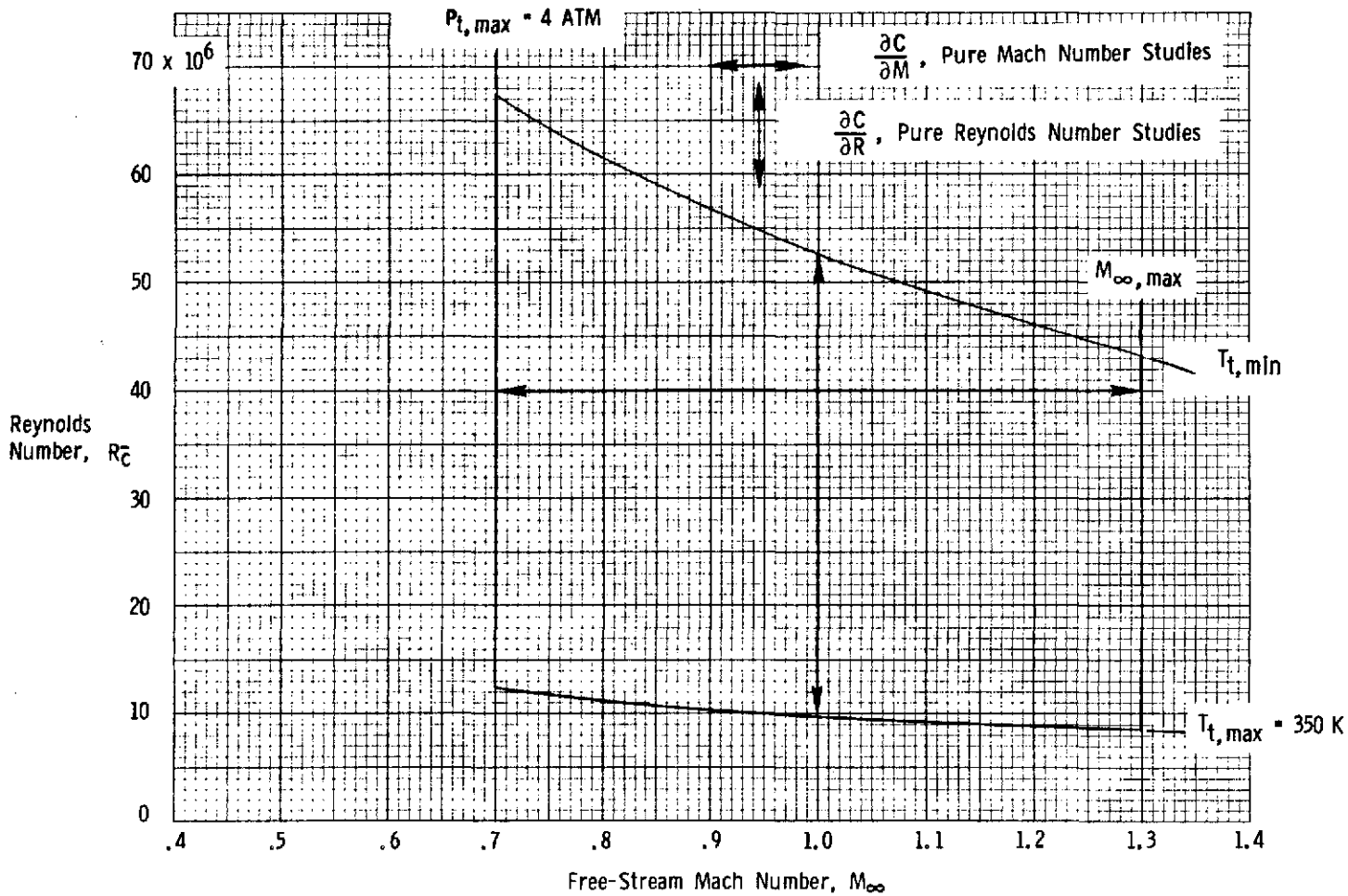

Figure 8.6 Constant dynamic pressure operating envelope for a cryogenic nitrogen tunnel having a 3m x 3m test section. q = 100 kN/m^2.

9. Conclusions.

The major conclusions to be drawn from the theoretical and experimental research related to the operation of wind tunnels at cryogenic temperatures are as follows:

A. General conclusions.

1. Cryogenic subsonic, transonic, and supersonic wind tunnels offer significant increases in test Reynolds number without increase in aerodynamic loads. For example, in an atmospheric cryogenic wind tunnel, Reynolds number may be increased by a factor of 7 at low subsonic speeds and by a factor of 5 at sonic speeds with no increase in dynamic pressure.

2. Once a tunnel size and the required Reynolds number have been established, the use of cryogenic operating temperatures greatly reduces the required tunnel stagnation pressure and therefore greatly reduces both the dynamic pressure and tunnel drive power.

3. In a cryogenic tunnel with independent control of the three parameters, temperature, pressure, and Mach number, it is possible to determine independently the effect of the three parameters, Reynolds number, aeroelastic distortion, and Mach number on the aerodynamic characteristics of the model. Various combinations of Reynolds number and dynamic pressure can be established to accurately represent flight variations of aeroelastic deformation with altitude changes.

4. Whereas most types of tunnels could operate with advantage at cryogenic temperatures, the continuous-flow fan-driven tunnel is particularly well suited to take full advantage of operating at cryogenic temperatures. Constructional and operational techniques are available, and costs appear to be acceptable.

B. Conclusions from the real-gas studies.

1. The saturation boundary is well defined and therefore any possible effects of liquefaction of the test gas can easily be avoided provided that the maximum local Mach number on the model is known.

2. The use of real values of the ratio of specific heats in the ideal isentropic equations gives results which are generally in error by an unacceptable amount. Both the thermal and the caloric imperfections must be taken into account.

3. For stagnation pressures up to about 5 atmospheres, the isentropic expansion and the normal shock relations calculated from the real-gas properties of nitrogen differ by a maximum of about 0.4-percent (depending on test conditions) from the corresponding relations calculated from ideal diatomic gas properties and ideal gas equations.

4. For most purposes it would be satisfactory to adopt ideal gas equations in the analysis of wind-tunnel test data taken in a cryogenic nitrogen wind tunnel at any stagnation pressure up to about 5 atmospheres.

C. Conclusions from the low-speed and transonic tunnel testing.

1. Cooling by injecting liquid nitrogen directly into the tunnel circuit is practical. Liquid nitrogen completely evaporates even at test temperatures close to the liquid temperature. Test temperature is easily controlled and good temperature distribution obtained by using a simple nitrogen injection system.

2. A cryogenic tunnel is simple to operate.

3. Purging, cooldown, and warmup times are acceptable and can be predicted with good accuracy.

4. Liquid nitrogen requirements for cooldown and running can be predicted with good accuracy.

5. Conventional strain-gage balances can be used for model testing. A satisfactory arrangement is to maintain the strain-gage balance at ambient temperatures by heating.

6. There is good agreement between theoretical predictions and experimental measurements of the development of laminar boundary layers at cryogenic temperatures.

7. Test-section noise level is reduced when a given Reynolds number is obtained by operating at cryogenic temperatures.

8. In compressible flow, Reynolds number dependent aerodynamic phenomena behave in the same manner when Reynolds number is changed by temperatures as when changed by pressure. Identical pressure distributions were obtained on a two-dimensional airfoil having a strong recompression shock

when tested at ambient and cryogenic stagnation temperatures with stagnation pressure adjusted to maintain a constant Reynolds number.

9. Several degrees of local supersaturation have been obtained with no detectable effect on the pressure distribution over an airfoil.

10. References.

1. Heppe, R. O., O'Laughlin, B. D., and Celniker, L. "New Aeronautical Facilities - We Need Them Now." Astronaut. Aeron., vol. 6, no. 3, March 1968, pp. 42-54.

2. Poisson-Quinton, P. "From Wind Tunnel to Flight, the Role of the Laboratory in Aerospace Design." Jour. of Aircraft, vol. 5, no. 3, May - June 1968, pp. 193 - 214.

3. The AGARD Fluid Dynamics Panel HiRT Group, Dietz, R. O., Chairman "AGARD Study of High Reynolds Number Wind Tunnel Requirements for the North Atlantic Treaty Organization Nations." Proceedings of AGARD Conference on Facilities and Techniques for Aerodynamic Testing at Transonic Speeds and High Reynolds Number. AGARD-CP-83-71, August 1971, Paper no. 32.

4. Baals, D. D., and Stokes, G. M. "A Facility Concept for High Reynolds Number Testing at Transonic Speeds." Proceedings of AGARD Conference on Facilities and Techniques for Aerodynamic Testing at Transonic Speeds and High Reynolds Number. AGARD-CP-83-71, August 1971, Paper no. 28.

5. Evans, J.Y.G., and Taylor, C. R. "Some Factors Relevant to the Simulation of Full-Scale Flows in Model Tests and to the Specification of New High-Reynolds-Number Transonic Tunnels." Proceedings of AGARD Conference on Facilities and Techniques for Aerodynamic Testing at Transonic Speeds and High Reynolds Number. AGARD-CP-83-71, August 1971, Paper no. 31.

6. Igoe, W. B., and Baals, D. D. "Reynolds Number Requirements for Valid Testing at Transonic Speeds." Proceedings of AGARD Conference on Facilities and Techniques for Aerodynamic Testing at Transonic Speeds for High Reynolds Number. AGARD-CP-83-71, August 1971, Paper no. 5.

7. Evans, J. Y. G. "A Scheme for a Quiet Transonic Flow Suitable for Model Testing at High Reynolds Number." Proceedings of AGARD Conference on Facilities and Techniques for Aerodynamic Testing at Transonic Speeds and High Reynolds Number. AGARD-CP-83-71, August 1971, Paper no. 35.

8. Whitfield, J. D., Schueler, C. J., and Starr, R. F. "High Reynolds Number Wind Tunnels-Blowdown on Ludwieg Tube?" Proceedings of AGARD Conference on Facilities and Techniques for Aerodynamic Testing at Transonic Speeds and High Reynolds Number. AGARD-CP-83-71, August 1971, Paper no. 29.

9. Pozniak, O. M. "Investigation Into the Use of Freon 12 as a Working Medium in a High-Speed Wind-Tunnel." The College of Aeronautics, Cranfield, Note No. 72.

10. Treon, S. L., Hofstetter, W. R., and Abbott, F. T., Jr. "On the Use of Freon-12 for Increasing Reynolds Number in Wind-Tunnel Testing of Three-Dimensional Aircraft Models at Subcritical and Supercritical Mach Numbers." Proceedings of AGARD Conference on Facilities and Techniques for Aerodynamic Testing at Transonic Speeds and High Reynolds Number. AGARD-CP-83-71, August 1971, Paper no. 27.

11. Smelt, R. "Power Economy in High Speed Wind Tunnels by Choice of Working Fluid and Temperature." Report No. Aero. 2081, Royal Aircraft Establishment, Farnborough, England, August 1945.

12. Rush, C. K. "A Low Temperature Centrifugal Compressor Test Rig." National Research Council of Canada, Ottawa Low Temperature Lab. MD-48; NRC-7776, November 1963.

13. Goodyer, M. J. A verbal proposal on 25th October 1971 by Dr. M. J. Godyer of the Department of Aeronautics and Astronautics, University of Southampton, while at NASA Langley Research Center as Post Doctoral Resident Research Associate.

14. Chapman, D. R. "Some Possibilities of Using Gas Mixtures Other Than Air in Aerodynamic Research." NACA TR-1259, 1956.

15. Pankhurst, R. C., and Holder, D. W. "Wind-Tunnel Technique." Pitman and Son, Ltd., 1965.

16. Jacobsen, R. T. "The Thermodynamic Properties of Nitrogen from 65 to 2000K with Pressures to 10,000 atm." Ph. D. Thesis, Washington State University, 1972.

17. Hilsenrath, J.,et al. "Tables of Thermal Properties of Gases." National Bureau of Standards Circular 564, November 1955.

18. Ruhemann, M. "The Separation of Gases." Oxford University Press, 1940.

19. Dodge, B. F., and Davis, H. N. "Vapor Pressure of Liquid Oxygen and Nitrogen." Jour. Am. Chem. Soc., vol. 49, March 1927, pp. 610-620.

20. Goodyer, M. J., and Kilgore, R. A. "High-Reynolds-Number Cryogenic Wind Tunnel." AIAA Journal, vol. 11, no. 5, May 1973, pp. 613-619. Presented as AIAA Paper No. 72-995 at the AIAA 7th Aerodynamic Testing Conference, Palo Alto, Calif., September 13-15, 1972.

21. McCarty, R. D. Private communication from Mr. R. D. McCarty of National Bureau of Standards (Boulder) of an unpublished program for the thermodynamic and transport properties of nitrogen. March 1973.

22. Davis, J. W. "A Shock Tube Technique for Producing Subsonic, Transonic, and Supersonic Flows with Extremely High Reynolds Numbers." Presented as AIAA Paper No. 68-18 at the AIAA 6th Aerospace Sciences Meeting, New York, N.Y. January 22-24, 1968.

23. Jacobs, R. B. "Liquid Requirements for Cool-Down of Cryogenic Equipment." Advances in Cryogenic Engineering, vol. 8, Plenum Press, 1963.

24. Kilgore, R. A., Adcock, J. B., and Ray, E. J. "Flight Simulation Characteristics of the Langley High Reynolds Number Cryogenic Transonic Tunnel." Presented as AIAA Paper No. 74-80 at the AIAA 12th Aerospace Sciences Meeting, Washington, D. C., January 30 - February 1, 1974.

25. Daum, F. L. "Air Condensation in a Hypersonic Wind Tunnel." AIAA Journal, vol. 1, no. 5, May 1963, pp. 1043-1046.

26. Kilgore, R. A., Goodyer, M. J., Adcock, J. B., and Davenport, E. E. "The Cryogenic Wind Tunnel Concept for High Reynolds Number Testing." NASA LWP-1075, September 1972. (Proposed NASA Technical Note)

27. Jones, J. L. "Problems of Flow Simulation in Wind Tunnels." Presented as AIAA Paper No. 69-660 at the AIAA Fluid and Plasma Dynamics Conference, San Francisco, Calif., June 16-18, 1969.

28. Barron, R. "Cryogenic Systems." McGraw-Hill Book Co., Inc., 1966.

29. Department of Aeronautics and Astronautics, University of Southampton "The Second International Symposium of Magnetic Balance and Suspension Systems." Southampton, England, July 1971.

30. Cornette, E. S., and Stokes. G. M. Private communication, NASA Langley Research Center, November 1973.

Appendix I.

Properties of Nitrogen at Cryogenic Temperatures

Contents:

I.1 Introduction.

As noted in Chapter 8, section 8.2.1 certain simplifying assumptions were made so that most of the calculations of Reynolds number could be made on a relatively small digital computer. Some of the simplifying assumptions had to do with the way in which the properties of nitrogen were calculated at cryogenic temperatures. For example, very precise values of the compressibility factor, Z, can be obtained over the temperature range from 65 to 2000 K at pressures up to 10,000 atmospheres from the National Bureau of Standards computer program of reference 21. However, the equation which covers these wide ranges of temperature and pressure has many more terms than are required to cover the limited range of temperature and pressure of interest in the study of a cryogenic wind tunnel. Therefore, a less complicated equation has been fitted to allow its use in a small digital computer. The same situation is true in the case of both the ratio of specific heats, γ, and the viscosity of nitrogen, μ, where relatively simple equations are used to cover only the limited ranges of temperature and pressure of interest. No particular effort was made to optimize the form of the equations. In general the forms are those which tended to linearize and therefore

reduce the number of terms required to provide an adequate fit.

The equation for vapor pressure is taken from reference 16 without modification since it is relatively simple as presented.

I.2 Compressibility Factor, Z.

For the ranges of temperature and pressure of interest, the values of compressibility factor, Z, were calculated using the program of reference 21 and were fitted with an equation of the form

$$Z = \frac{P}{\rho R T} = 1 + BP + CP^2 \qquad \text{I.1}$$

where

P = pressure, atmospheres

(1 atm. = 1.01325×10^5 N/m^2)

T = temperature, K ($K = {}^{\circ}C + 273.15$)

ρ = density

R = gas constant for nitrogen

and B and C are constants given by

$$\ln(-B) = \sum_{i=0}^{4} b_i T^i$$

$$\ln(-C) = \sum_{i=0}^{4} c_i T^i$$

where the values of b_i and c_i are as follows:

$b_o = 1.370$

$b_1 = -8.773 \times 10^{-2}$

$b_2 = 4.703 \times 10^{-4}$

$b_3 = -1.386 \times 10^{-6}$

$b_4 = 1.462 \times 10^{-9}$

$c_o = 5.521$

$c_1 = -1.986 \times 10^{-1}$

$c_2 = 7.817 \times 10^{-4}$

$c_3 = -1.258 \times 10^{-6}$

$c_4 = 5.333 \times 10^{-10}$

The values of Z calculated from equation I.1 agree with the values calculated using the program of reference 21 generally within 0.05 percent for pressures from near zero to 7 atmospheres and temperatures from saturation to 350 K.

The compressibility factor, Z, for nitrogen as a function of pressure for various value of temperature was calculated using equation I.1 and is presented graphically for pressures from 0.25 to 7 atmospheres in Figure I.1a and for pressures from 0.1 to 1.5 atmospheres in Figure I.1b.

I.3 Ratio of Specific Heats, γ.

The ratios of specific heats were calculated from the tabulated data of reference 16 and were plotted, faired, and fitted with an equation of the form

$$\gamma = \frac{C_p}{C_v} = A + BP + CP^2 \qquad \text{I.2}$$

where

C_p = specific heat at constant pressure

C_v = specific heat of constant volume

P = pressure, atmospheres

A = 1.400

and B and C are constants given by

$$\ln B = \sum_{i=0}^{4} b_i T^i$$

$$\ln C = \sum_{i=0}^{1} c_i T^i$$

where T = temperature, K

and the values of b_i and c_i are as follows:

$b_o = 1.86799$ $\qquad c_o = -1.25126$

$b_1 = -9.52187 \times 10^{-2}$ $\qquad c_1 = -4.969 \times 10^{-2}$

$b_2 = 5.14638 \times 10^{-4}$

$b_3 = -1.35950 \times 10^{-6}$

$b_4 = 1.31676 \times 10^{-9}$

For most purposes the values of γ calculated from equation I.2 are adequate for pressures from near zero to 7 atmospheres and temperatures from saturation to 350 K. The values of γ calculated from equation I.2 agree with the values calculated from the data of reference 16 generally within 0.03 percent over the entire range of temperatures from saturation to 350 K for pressures of 4 atmospheres or less. The greatest differences exist for conditions of high pressure and low temperature. For example, the value of γ calculated from equation I.1 is about 0.3 percent less than the value calculated from the data of reference 16 at 7 atmospheres and 110 K.

The ratio of specific heats, γ, for nitrogen as a function of pressure for various values of temperature was calculated using equation I.2 and is presented graphically for pressures from 0.25 to 7 atmospheres in Figure I.2a and for pressures from 0.1 to 1.5 atmospheres in Figure I.2b.

I.4 Vapor Pressure.

The vapor pressure equation presented below is taken directly from reference 16. The equation covers the range from the triple point to the critical point and is of the form

$$\ln (P) = N_1/T + N_2 + N_3 T + N_4 (T_c - T)^{1.95} + N_5 T^3$$

$$+ N_6 T^4 + N_7 T^5 + N_8 T^6 + N_9 \ln(T) \qquad \text{I.3}$$

where T_c = 126.20 K, the critical point temperature, T is the saturation temperature, and P is the vapor pressure in atmospheres. The coefficients for this equation are given in the following table:

Coefficient	Numerical Value	Coefficient	Numerical Value
N_1	$0.8394409444 \times 10^{4}$	N_6	$-0.5944544662 \times 10^{-5}$
N_2	$-0.1890045259 \times 10^{4}$	N_7	$0.2715433932 \times 10^{-7}$
N_3	$-0.7282229165 \times 10^{1}$	N_8	$-0.4879535904 \times 10^{-10}$
N_4	$0.1022850966 \times 10^{-1}$	N_9	$0.5095360824 \times 10^{3}$
N_5	$0.5556063825 \times 10^{-3}$		

The vapor pressure equation I.3 is accurate to within ± 0.01 K between the triple point and the critical point.

The vapor pressure, P, for nitrogen as a function of saturation temperature, T, is presented graphically in Figure I.3 from the triple point to the critical point.

I.5 Viscosity, μ.

Values of the dynamic viscosity of nitrogen, μ, were calculated from the National Bureau of Standards computer program. The dimensions of μ are newton-second per square meter (N-s/m^2).

These values were then fitted with an equation of the form

$$\mu = \sum_{i=0}^{2} \mu_i T^i \qquad \text{I.4}$$

where T = temperature, K

and where the values of μ_i are given by

$$\mu_i = \sum_{j=0}^{2} \mu_{ij} P^j$$

where P = pressure, atmospheres

and the values of μ_{ij} are as follows:

$\mu_{00} = -2.86896 \times 10^{-7}$	$\mu_{10} = 7.55226 \times 10^{-8}$	$\mu_{20} = -4.89417 \times 10^{-11}$
$\mu_{01} = 1.23678 \times 10^{-7}$	$\mu_{11} = -6.10964 \times 10^{-10}$	$\mu_{21} = 9.51640 \times 10^{-13}$
$\mu_{02} = 1.29862 \times 10^{-9}$	$\mu_{12} = -1.22089 \times 10^{-11}$	$\mu_{22} = 2.52130 \times 10^{-14}$

The values of μ calculated from equation I.4 agree with the values calculated using the program of reference 21 generally within 0.2 percent for pressures from zero to 20 atmospheres and temperatures from saturation to 350 K.

The coefficient of viscosity, μ, for nitrogen as a function of temperature for various values of pressure was calculated using equation I.4 and is presented graphically in Figure I.4 for temperatures from saturation to about 340 K and pressures from zero to 10 atmospheres.

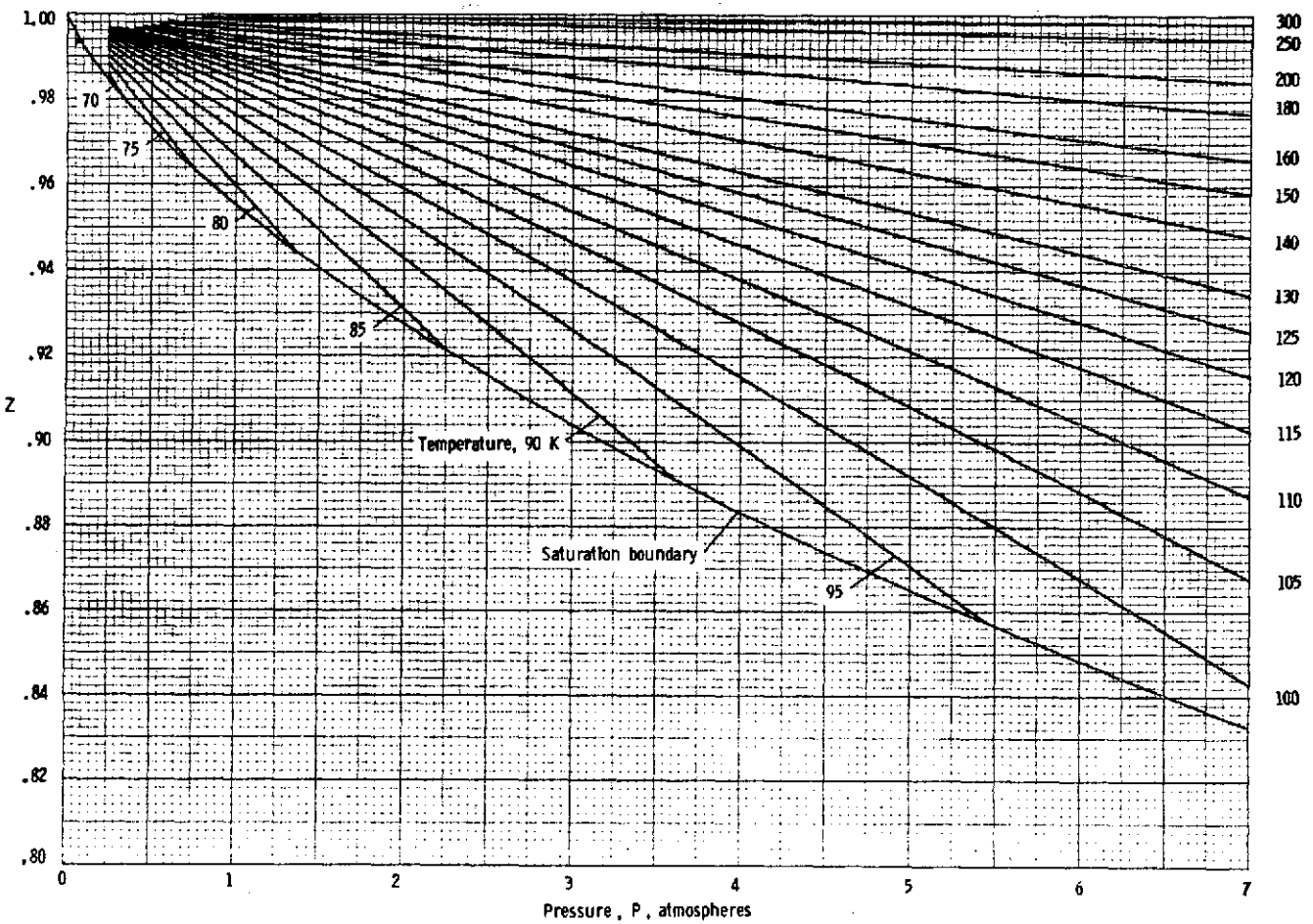

(a) Pressures from 0.25 to 7 atmospheres.

Figure I.1 Compressibility factor, $Z = PV/\mathcal{R}T$, for nitrogen as a function of pressure and temperature.

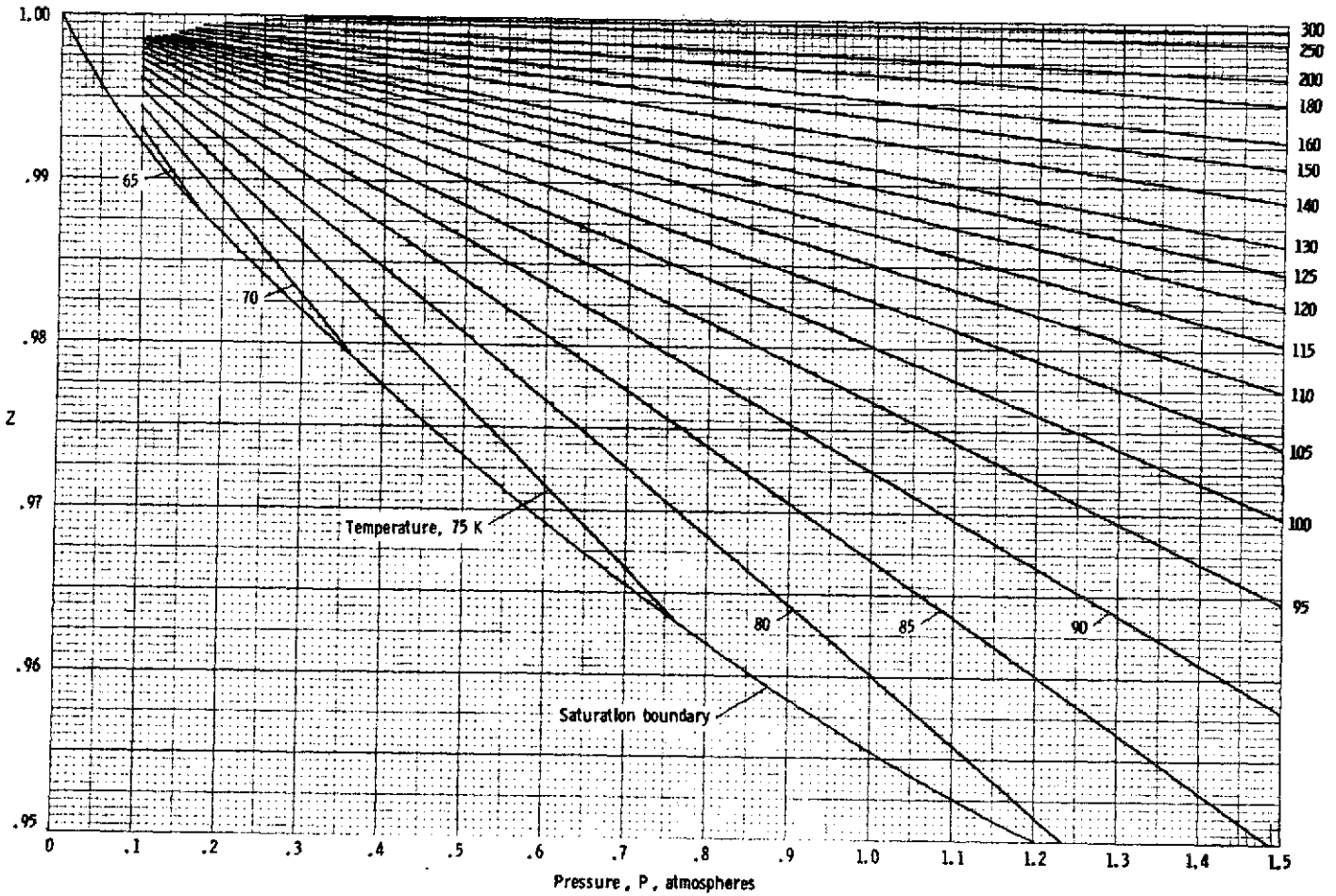

(b) Pressures from 0.1 to 1.5 atmospheres.

Figure I.1 Concluded.

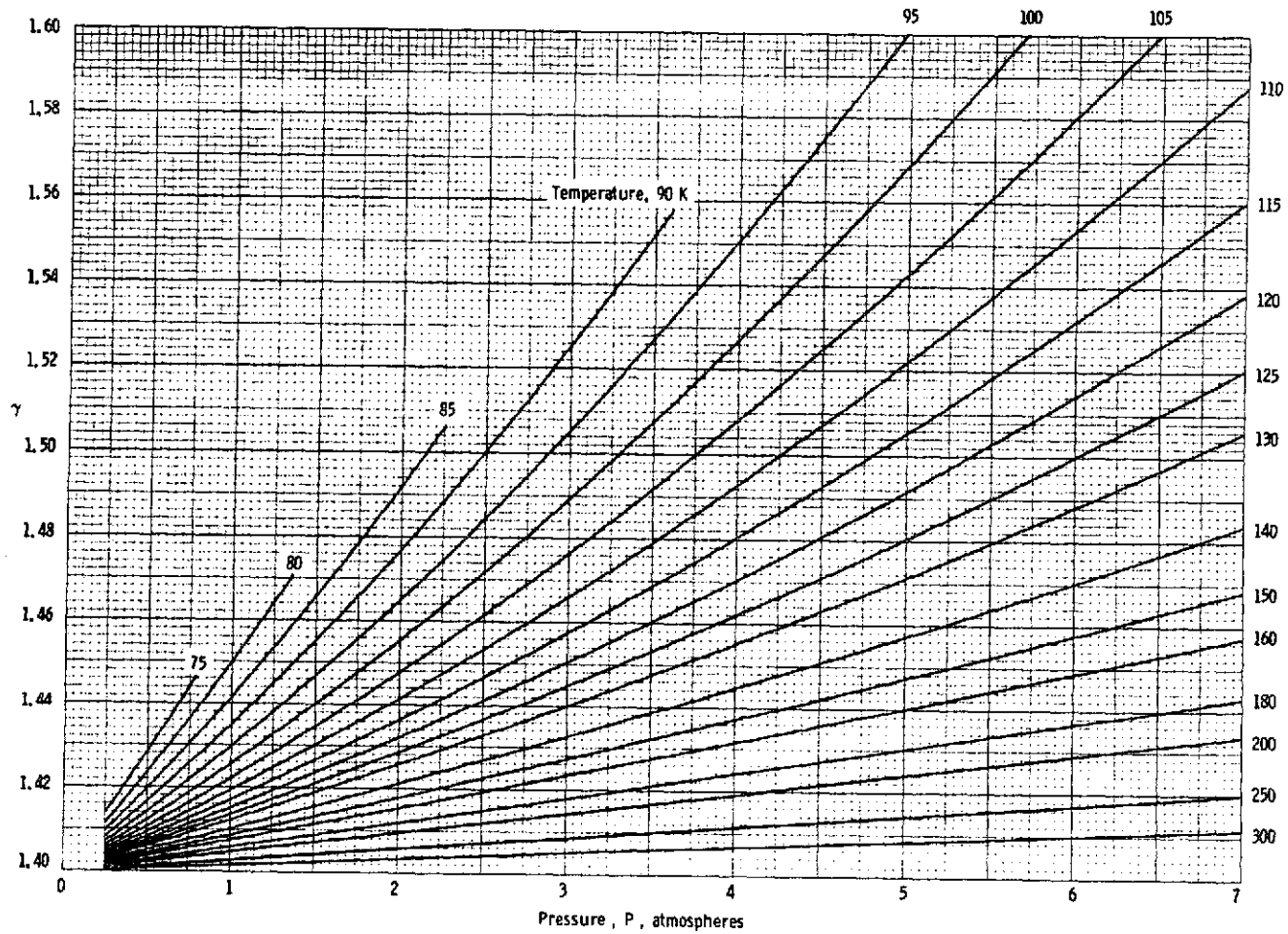

(a) Pressures from 0.25 to 7 atmospheres.

Figure I.2 Ratio of specific heats, $\gamma = C_p/C_v$, for nitrogen as a function of pressure and temperature.

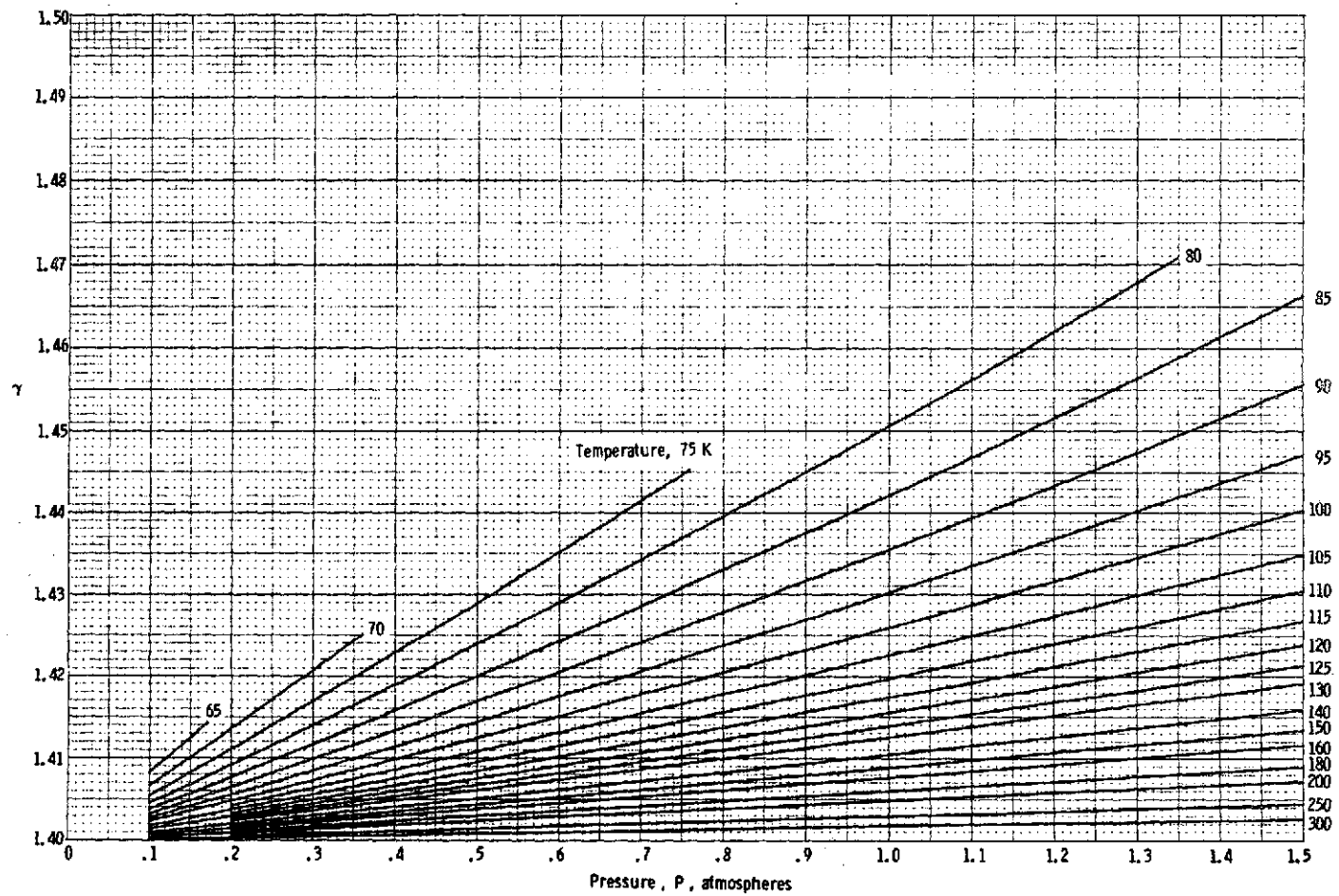

(b) Pressures from 0.1 to 1.5 atmospheres.

Figure I.2 Concluded.

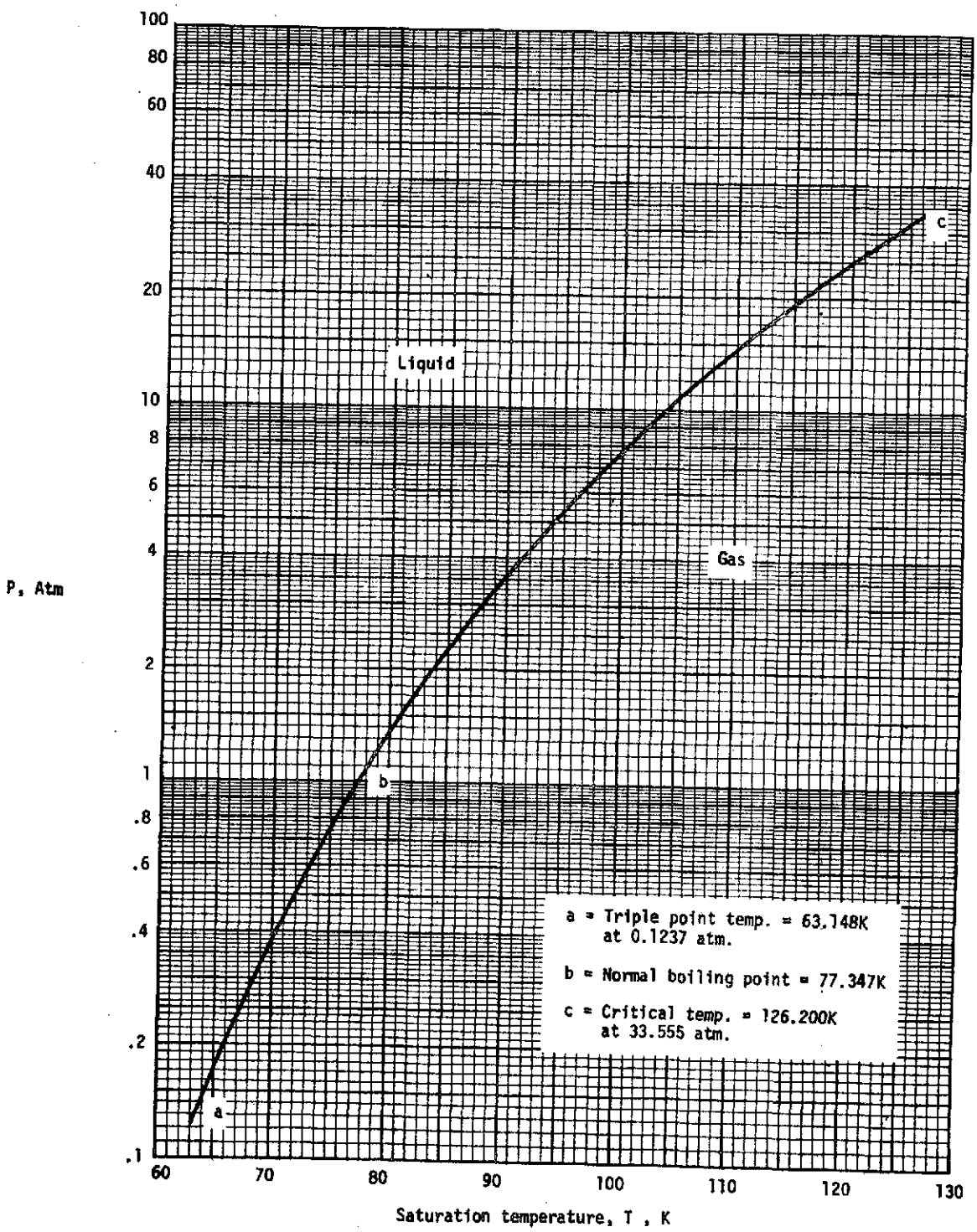

Figure I.3 Vapor pressure, P, for nitrogen as a function of saturation temperature, T.

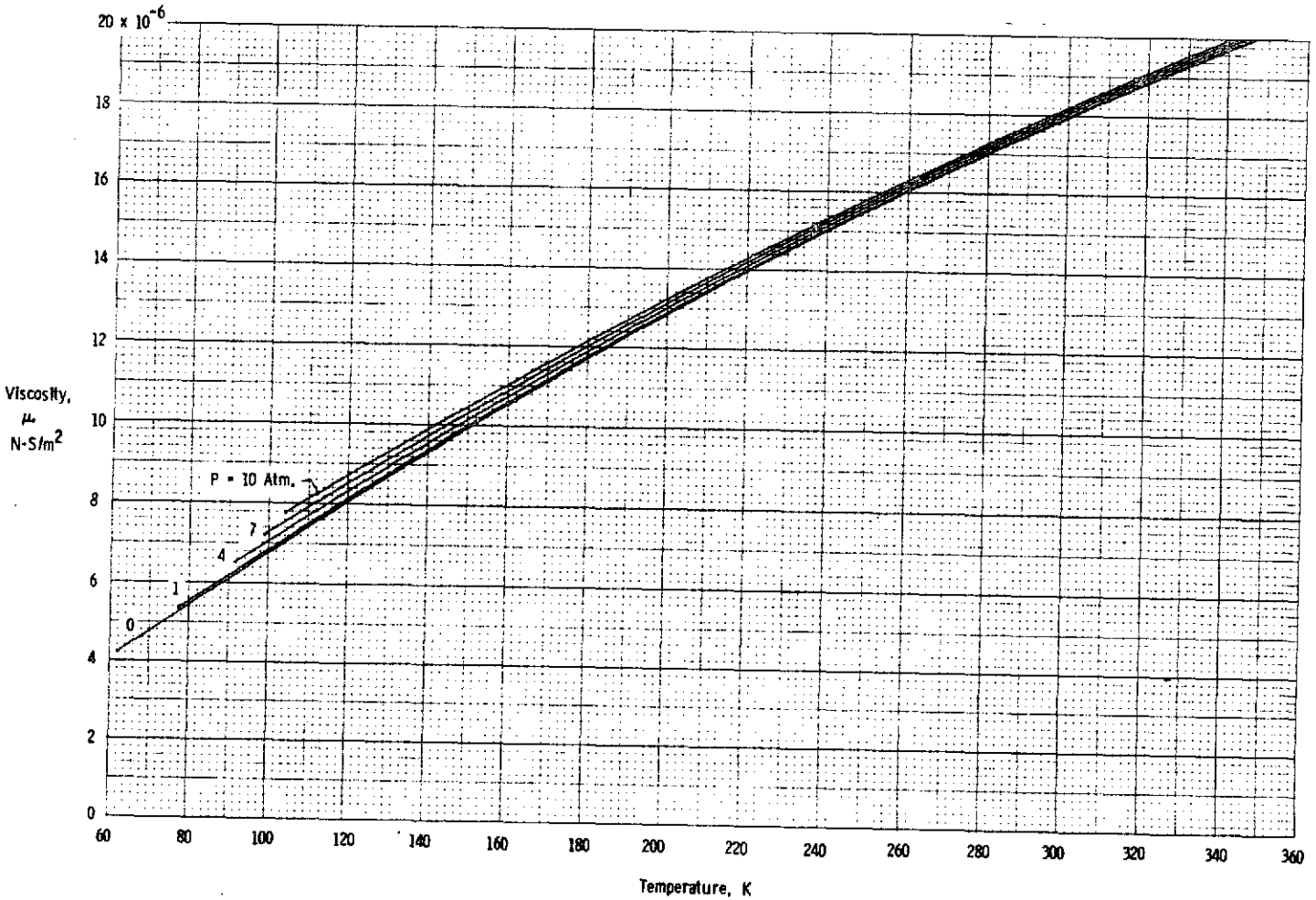

Figure I.4 Dynamic viscosity, μ , for nitrogen as a function of temperature and pressure.

Appendix II. Energy Requirements at Ambient and Cryogenic Conditions for Various Types of Wind Tunnels

In this appendix the total energy requirements of several types of wind tunnels are calculated for ambient and cryogenic operating temperatures under conditions of constant Mach number, Reynolds number, and total pressure in order to allow comparisons to be made in terms of total energy consumption.

Contents:

II.1 Introduction.

The cryogenic operation of various types of tunnels was considered in Chapter 5 where many of the advantages of cryogenic operation were noted. In an age where the conservation of energy is assuming an increasing importance, the total energy consumption during a given test is an important consideration in the evaluation of a tunnel concept. Therefore, in this appendix, the total energy requirements for several types of wind tunnels are calculated for ambient and cryogenic operating temperatures, all operating at the same Mach number, Reynolds number, and pressure, in order to allow comparisons to be made between cryogenic and ambient temperature operation in terms of total energy consumption.

The total energy requirement for each type of tunnel is determined from the total power that would be required to operate the tunnel continuously whether or not the tunnel is designed for continuous operation. For cryogenic operation, the energy required for initial cooldown of the tunnel structure and the energy required to overcome the heat conduction through the tunnel walls has been neglected.

The following conditions are assumed for all tunnels:

$M_\infty = 1.00$

$R_{\bar{c}} = 50 \times 10^6$

$\bar{c} = 0.1\sqrt{\text{Test-section area}}$

$P_t = 2.52$ atmospheres

For ambient temperature operation with the tunnel cooled by a water-air heat exchanger, a stagnation temperature T_t of 300K ($80^\circ F$) is assumed. The resultant size of test section is 13.3m (43.64 feet) square.

For cryogenic temperature operation and cooling with liquid nitrogen, a stagnation temperature T_t of 105K ($-271^\circ F$) is assumed. The resultant size of test section is 3m (9.84 feet) square. For the tunnels where cooling is accomplished by the mixing of liquid nitrogen and air, it is also assumed that the cooling thermal capacity of nitrogen is equal to the latent heat together with the sensible heat of the gas phase between the saturation temperature and the final temperature of the air-nitrogen mixture.

II.2 Ludwieg Tube Tunnel.

The theory of operation of the simplest form of Ludwieg tube tunnel is given in Chapter 5, section 5.2.1.

II.2.1 The power equivalent of LN_2 used for cryogenic operation

It is assumed that for cryogenic operation air can be delivered from the compressors to the supply tube at a temperature T_d of 300 K ($80^{\circ}F$). The proper amount of liquid nitrogen is then combined with the air so that the air-nitrogen mixture reaches the desired supply tube temperature T_s.

The energy balance in the mixing process requires that

$$\dot{m}_{Air}\, C_p \Delta T = \dot{m}_{LN_2} \beta \qquad \text{—— II.1}$$

where $\dot{m}_{Air}$ = mass flow rate of air from compressor

C_p = specific heat of air at constant pressure

$\Delta T = T_d - T_s$

$\dot{m}_{LN_2}$ = mass flow rate of LN_2 for cooling

and

β = cooling capacity of LN_2 (see Fig. 8.3)

The rate of consumption of air and LN_2 must equal the test-section mass flow rate, $\dot{m}_{t.s.}$. Therefore,

$$\dot{m}_{t.s.} = \dot{m}_{Air} + \dot{m}_{LN_2} \qquad \text{—— II.2}$$

Solving equations II.1 and II.2 for $\dot{m}_{LN_2}$ gives

$$\dot{m}_{LN_2} = \frac{\dot{m}_{t.s.} C_p \Delta T}{\beta + C_p \Delta T} \qquad \text{II.3}$$

If ε represents the energy required to produce a unit mass of LN_2, the power equivalent of the LN_2 used to cool the air delivered to the supply tube is

$$\text{Power}_{LN_2} = \varepsilon \dot{m}_{LN_2} \qquad \text{II.4}$$

The value of ε as determined from reference 28, is about 3.49 MJ/kg (3.49 MW/kg/sec or 2124 horsepower/lbm/sec).

II.2.2 Power required by compressor plant

It is assumed that ambient air is taken into the compressor at a temperature of 293K (68°F) and a pressure $P_a = 1$ atmosphere. Neglecting for the moment any pipe or valve losses, the minimum pressure ratio across the compressor is then the simple average of the initial pressure in the supply tube before a run P_s and the pressure in the tube at the end of a run P_f divided by P_a.

$$\text{Pressure ratio} = 0.5 \, (P_s + P_f)/P_a \qquad \text{II.5}$$

At the end of a run, after the expansion wave has reflected from the closed end of the supply tube and traveled back to the test section, the pressure in the supply tube is below P_t by about $P_s - P_t$. Therefore,

$$P_f \approx P_s - 2 \, (P_s - P_t) \qquad \text{II.6}$$

Substitution of P_f from Equation II.6 into Equation II.5 gives the simple relation

$$\text{Pressure ratio} = P_t/P_a$$

In order to allow for pipe and valve losses this pressure ratio is increased by a factor of 1.2 in the following calculations. Thus,

$$\text{Compressor pressure ratio} = 1.2\ P_t/P_a$$

From this pressure ratio an ideal temperature rise $\Delta T'$ is calculated assuming isentropic compression. Assuming that a compressor such as the centrifugal or axial-flow type is to be used, then using the isentropic efficiency η_c of the machine the actual temperature rise ΔT is $\Delta T'/\eta_c$.

The energy input to the compressor per unit time is then

$$\dot{m}_{Air}\ C_p \Delta T = \dot{m}_{Air}\ C_p \Delta T'/\eta_c \qquad \text{II.8}$$

For these calculations the isentropic efficiency of the compressor is assumed to be 90%.

Assuming a motor efficiency of 90%, the power input to the compressor drive motor is then

$$\text{Power}_{motor} = \frac{\dot{m}_{Air}\ C_p \Delta T}{0.9} \qquad \text{II.9}$$

II.2.3 Calculations

Based on the design of a proposed Ludwieg tube tunnel described in reference 3, the supply tube Mach number for these calculations is taken to be 0.4. Equations 5.5 and 5.6 were then used to find the initial supply tube conditions. Equations II.3 through II.9 were used to determine the total power requirement for the two values of total temperature.

The results of these calculations for the Ludwieg tube tunnel are presented in the following table.

Table II.1.

Ludwieg-tube tunnel, $M_\infty = 1.0$, $R_c = 50 \times 10^6$, $P_t = 2.52$ atm.

T_t, K	T_o, K	Test-section size, m	Mass flow rate, $\dot{m}$, kg/sec			Power, MW		
			t.s.	Air	LN_2	Air compressor	LN_2 production	Total
300	339	13.3	103,600	103,600	—	14,256	—	14,256
105	119	3.0	9,090	5,030	4,060	692	14,166	14,858

II.3 Evans Clean Tunnel.

The method of operation of the Evans Clean Tunnel is given in Chapter 5, section 5.3.1.

II.3.1 The power equivalent of LN_2 used for cryogenic operation

The method of recharging the tunnel between runs which is assumed here is described in section II.3.2. It is assumed that the compressor inlet temperature is equal to T_t and that all of the heat of compression when operating at cryogenic temperatures must be removed by the evaporation of liquid nitrogen. This could be accomplished either by using a LN_2-air heat exchanger or by injecting liquid nitrogen directly into the tunnel. In the latter case the total pressure would rise unless some gas were vented to atmosphere. Under the operating conditions assumed there is at most a 10% difference in the LN_2 requirements of the two modes of cooling. Therefore, for this example, the heat-exchanger mode is selected as the method of cooling at cryogenic temperatures since this is the simpler mode of operation. Under these conditions the specific thermal capacity of LN_2, β, is taken to be 200 kJ/kg.

II.3.2 Power required for compressore plant

It is assumed that the tunnel is normally recharged between runs by closing the valve at the diffuser exit and pumping air from the return circuit into the primary piston tube downstream of the piston. In a tunnel design described in reference 7 the primary piston tube is assumed to be pressurized to 1.10 P_t and the return circuit pressurized to 0.86 P_t before a run. The primary piston is driven by driving pistons. The air swallowed by the driving cylinders during a run amounts to 14.5 percent of the air stored in the primary tube. Assuming equal volumes for the primary piston tube and return circuit and recalling that virtually all of the air originally in the primary piston tube is either discharged through the test section or flows into the driving cylinders, the driving cylinders, in effect, increase the total volume of the tunnel by about 7.25 percent. The pressure everywhere in the circuit after a run is therefore approximately

$$\frac{0.5(1.1\ P_t + 0.86\ P_t)}{1.07} = 0.916\ P_t$$

The average intake pressure to the compressor is therefore taken to be

$$P_i = 0.5\ (0.916\ P_t + 0.86\ P_t) = 0.888\ P_t$$

The average discharge pressure from the compressor is taken to be

$$P_d = 0.5\ (0.916\ P_t + 1.1\ P_t) = 1.008\ P_t$$

The required average pressure ratio is therefore

$$\text{Pressure ratio} = \frac{P_d}{P_i} = \frac{1.008\ P_t}{0.888\ P_t} = 1.135$$

In order to allow for pipe and valve losses this pressure ratio is increased by a factor of 1.2. Thus, for these calculations,

$$\text{Pressure ratio} = 1.362$$

The energy input to the compressor is then calculated in the same manner as for the Ludwieg tube tunnel using equation II.9 and assuming the mass flow rate through the compressor equals the sum of the flow rates through the test section and into the driver tubes.

II.3.3 Calculations

The results of these calculations for the Evans Clean Tunnel are presented in the following table.

TABLE II.2

Evans Clean Tunnel, $M_\infty = 1.0$, $R_c = 50 \times 10^6$, $P_t = 2.52$ atm.

T_t, K	Test section size, m	Mass flow rate, $\dot{m}$, kg/sec			Power, MW		
		t.s.	Air	LN_2	Air compressor	LN_2 production	Total
300	13.3	103,600	121,880	—	4,239	—	4,239
105	3.0	9,090	10,690	599	133	2,091	2,224

II.4 Blowdown Tunnel.

II.4.1 The power equivalent of LN_2 used for cooling

The equation for the flow rate of LN_2 required for a continuous-flow blowdown tunnel is identical to that used for the Ludwieg tube tunnel, equation II.3

$$\dot{m}_{LN_2} = \frac{\dot{m}_{t.s.} C_p \Delta T}{\beta + C_p \Delta T}$$

where, for the blowdown tunnel

$$\Delta T = T_d - T_t$$

As was the case for the Ludwieg tube tunnel, the power equivalent of the LN_2 used to cool the air from compressor delivery conditions to the desired stagnation temperature T_t is given by

$$\text{Power}_{LN_2} = \varepsilon \dot{m}_{LN_2}$$

II.4.2 Power required for compressor plant

The compressor plant power is calculated in the same manner as for the Ludwieg tube tunnel using equation II.9 where again the required pressure ratio is taken as $1.2\ P_t/P_a$, where the factor of 1.2 is used to allow for pipe and valve losses.

II.4.3 Calculations

The results of the calculations are presented in the following table.

TABLE II.3

Blowdown tunnel, $M_\infty = 1.0$, $R_c = 50 \times 10^6$, $P_t = 2.52$ atm.

T_t, K	Test section size, m	Mass flow rate, $\dot{m}$, kg/sec			Power, MW		
		t.s.	Air	LN_2	Air compressor	LN_2 production	Total
300	13.3	103,600	103,600	—	14,273	—	14,273
105	3.0	9,090	4,750	4,340	654	15,146	15,800

II.5 Induced-Flow Tunnel.

II.5.1 The power equivalent of LN_2 used for cooling

If the ratio of injector mass flow rate, $\dot{m}_i$, to test-section mass flow rate, $\dot{m}_{t.s.}$, is χ, then

$$\chi \dot{m}_{t.s.} = \dot{m}_i = \dot{m}_{Air} + \dot{m}_{LN_2}$$

The equation for $\dot{m}_{LN_2}$ is thus identical to equation II.3 except for the factor χ,

$$\dot{m}_{LN_2} = \frac{\chi \dot{m}_{t.s.} C_p \Delta T}{\beta + C_p \Delta T}$$

where, for the induced flow tunnel

$$\Delta T = T_d - T_t$$

The power equivalent of the LN_2 used to cool the air is again given by

$$\text{Power}_{LN_2} = \epsilon \dot{m}_{LN_2}$$

II.5.2 Power required for compressor plant

If the ratio of injector to test-section mass flow rate is χ, the rate at which air must be supplied by the compressor is

$$\dot{m}_{Air} = \chi \dot{m}_{t.s.} - \dot{m}_{LN_2}$$

For the following analysis, χ is taken to be 0.2 for testing at $M_\infty = 1.0$, a value based on experience at the Langley Research Center (reference 30) with a transonic injector tunnel operating with an injector Mach number of 1.14 and a blowing pressure of 1.5 times the stagnation pressure P_t. Allowing an additional factor of 1.2 for pipe and valve losses, the required compressor pressure ratio is $1.8\ P_t/P_a$.

The compressor plant power is again calculated using Equation II.9.

II.5.3 Calculations

The results of the calculations are presented in the following table.

TABLE II.4

Injector tunnel, $M_\infty = 1.0$, $R_c = 50 \times 10^6$, $P_t = 2.52$ atm.

T_t, K	Test section size, m	Mass flow rate, $\dot{m}$, kg/sec				Power, MW		
		t.s.	i	Air	LN_2	Air compressor	LN_2 production	Total
300	13.3	103,600	20,720	20,720	—	4,148	—	4,148
105	3.0	9,090	1,818	950	868	190	3,029	3,219

II.6 Continuous-Flow Fan-Driven Tunnel.

II.6.1 Ambient temperature operation

The power which must be supplied to the fan-drive motor is given by the following expression:

$$\text{Fan power} = \frac{qVA\eta}{\eta'} \qquad \text{II.10}$$

where q = free-stream dynamic pressure

V = free-stream velocity

A = test-section area

and η = tunnel power factor (see Chapter 2, Section 2.2.4)

η' = efficiency of drive motor

Based on measured values in several transonic tunnels at the Langley Research Center, values of $\eta = 0.130$ and $\eta' = 0.90$ are assumed. The drive power for the ambient temperature fan-driven tunnel is calibrated from Equation II.10 to be 777 MW (1,042,200 horsepower).

II.6.2 Cryogenic temperature operation

The drive power for the cryogenic fan-driven tunnel is calculated from Equation II.10 to be 22.9 MW (30,750 horsepower).

The portion of the main-drive fan power added to the stream is assumed to be

$$\text{Power to stream} = qVA\eta \qquad \text{II.11}$$

which is calculated to be 20.6 MW (27,640 horsepower).

Let β be the cooling capacity of the LN_2 used to remove

the heat added to the stream by the main-drive fan. The mass flow rate of LN_2 required to remove the heat of compression is the product of main-drive fan power added to the stream times β^{-1}. From equation II.11

$$\dot{m}_{LN_2} = qVA\eta\beta^{-1}$$

If ε represents the energy required to produce a unit mass of LN_2 the power equivalent of LN_2 used to remove the heat of compression is

$$\text{Power}_{LN_2} = \varepsilon \dot{m}_{LN_2} = \varepsilon\, qVA\eta\beta^{-1} \qquad \text{II.12}$$

The power equivalent of the LN_2 required to remove the heat of compression is calculated to be

$$\text{Power}_{LN_2} = 318 \text{ MW}$$

The results of the calculations are presented in the following table.

TABLE II.5

Continuous-flow fan driven tunnel, $M_\infty = 1.0$, $R_c = 50 \times 10^6$, $P_t = 2.52$ atm.

T_t, K	Test section size, m	Mass flow rate, $\dot{m}$, kg/sec		Power, MW		
		t.s.	LN_2	Drive motor	LN_2 production	Total
300	13.3	103,600	—	777	—	777
105	3.0	9,090	91	23	318	341

II.7 Comparisons.

The total energy required for a particular wind tunnel test will be the product of the total power required to operate the tunnel and the time required for the test. Thus, assuming a given test will require the same amount of testing time regardless of the type of tunnel, the ratio of total power requirement for two tunnels is also the ratio of total energy requirement.

The total power requirements for the various tunnels are listed in the following table along with the ratio of the total energy requirement at 105 K to the total energy requirement at 300 K.

TABLE II.6

Energy ratios for various tunnels, $M_\infty = 1.0$, $R_c = 50 \times 10^6$, $P_t = 2.52$ atm.

Type of tunnel	Total power, MW		$\frac{\text{Energy}(T_t=105K)}{\text{Energy}(T_t=300K)}$	$\frac{\text{Energy}(T_t=300K)}{\text{Energy, fan-cryo. tunnel}}$
	T_t = 300K	T_t = 105K		
Ludwieg tube	14,256	14,858	1.042	41.81
Evans Clean Tunnel	4,239	2,224	.525	12.43
Blowdown	14,273	15,800	1.107	41.86
Injector	4,148	3,219	.776	12.16
Fan driven	777	341	.439	2.28

Comparing the total energy requirements for cryogenic operation with those for ambient temperature operation it is seen that cryogenic operation can result in significant reductions in total demands for energy. However, for the Ludwieg tube driven tunnel and the blowdown tunnel, both of which discharge all of the test-section mass flow directly to atmosphere, there is a slight increase in total energy consumption at cryogenic temperatures.

From the point of view of minimum demands for energy, the fan-driven tunnel is clearly superior to the other types considered here, especially at cryogenic temperatures. If a high level of productivity is an important requirement, the fan-driven tunnel is also a clear choice because of its potentiality for continuous operation.

Relative to the fan-driven cryogenic tunnel, the other types require from about 2.3 to 42 times the total energy to do equal amounts of testing. In actual practice other factors will have a significant influence on the total energy required for a given test. For example, with intermittent tunnel operation there is usually a larger percentage of wasted energy during the starting and stopping operations than with a continuous flow tunnel. Also, the details of the high pressure air storage systems normally used with the blowdown and injector tunnels have a major influence on the energy required for the compressor plant. For example, the pressure ratio assumed for both the blowdown and Ludwieg-tube driven tunnels was 1.2 P_t/P_a or 3.024. Had these tunnels been supplied from a 40 atmosphere storage supply such as that proposed in reference 3 for use with similar tunnels, the average pressure ratio would have been 20 and the energy requirement would be higher by a factor of about 2.7 assuming the use of a 3-stage compressor with perfect intercooling. Since storage at high pressure has advantages with respect to reduced storage volume and drying of the stored air, air storage systems are, in fact, usually designed for 40 atmospheres or higher. A 240 atmosphere air storage supply currently being installed at the Langley Research Center was for a time being considered as the supply for an ambient temperature injector-driven transonic tunnel having a 2.5m x 3m test section. Had such a supply been used for these examples,

the demands on energy due to the pumping requirements would have been higher by a factor of about 4.2 assuming an average pressure ratio of 120 and the use of a 5-stage compressor. Thus, from the point of view of actual operation, this analysis has been made in such a way as to favor those tunnels which normally operate from high pressure air storage.

The preceding analysis is on a basis, among other things, of the same stagnation pressure for all tunnels. There are varied opinions on suitable pressures for use in high Reynolds number tunnels, and it is not claimed that the value chosen for use in these comparisons is the correct value. However, economies in power (and probably in capital investment) are always possible by the choice of increased test pressure. The economies derived for one tunnel would be about the same as those for any other. Therefore, while the absolute values of power shown in Table II.6 would change with pressure, the relative powers and the energy ratios would not change.

II.8 List of Symbols Used in Appendix II.

Symbol	Meaning
A	test-section area
$\bar{c}$	reference chord, $0.1\sqrt{A}$
C_p	specific heat at constant pressure
$\dot{m}$	mass-flow rate
M_∞	free-stream Mach number
P	pressure
q	free-stream dynamic pressure
$R_{\bar{c}}$	Reynolds number based on $\bar{c}$
T	temperature
V	free-stream velocity
β	cooling thermal capacity of liquid nitrogen

ε	energy required to produce unit mass of LN_2
η	tunnel power factor
η_c	isentropic efficiency
η'	efficiency of drive motor
χ	$\dot{m}_i/\dot{m}_{t.s.}$

Subscripts

a	atmospheric
d	discharge
f	final condition
i	intake or injector
s	initial condition
t	total condition
t.s.	test section
Air	air
LN_2	liquid nitrogen